

Measurement and Modeling of Fugitive Dust from Off-Road DoD Activities

SERDP RC-1767

Final Report

Submitted to:

Strategic Environmental Research and Development Program (SERDP)

September 4, 2015

Version 3

December 8, 2017

By

Rangeland Resources & Systems Research Unit
Center for Agricultural Resources Research, Plains Area
Agricultural Research Service
United States Department of Agriculture
2150 Centre Ave., Bldg. D, Suite 200
Ft. Collins, CO 80526

Principle Investigators:

Drs. John Tatarko, Michael Wojcik, and Ronaldo Maghirang

John.Tatarko@ars.usda.gov

Report Authors:

Larry Wagner, Michael Wojcik, Fred Fox, John Tatarko, and Ronaldo Maghirang

Table of Contents

Table of Contents	ii
List of Figures	v
List of Tables	x
List of Acronyms	xvii
Keywords	xix
Acknowledgements	xx
RC-1767 Abstract	1
Objectives	5
Background	6
Off Road Trafficking	8
Materials and Methods.....	8
General Approach	8
Field Trafficking Experiments.....	8
Site and Vehicle Selections.....	8
Site Preparation.....	13
Field Experiments	15
Soil Characterization.....	20
Field Data Collected	24
Wind Tunnel Trays	25
Portable In-Situ Wind Erosion Laboratory (PI-SWERL).....	25
Bulk Density and Soil Water Content.....	28
Aggregate Size Distribution (ASD)	28
Random Roughness (RR)	28
Soil Attached Biomass and Vegetation Cover.....	29
Results and Discussion	31
Field Experiments	31
Tracked Vehicle Trafficking Effects on Vegetative Cover	33
Wheeled Vehicle Trafficking Effects on Vegetative Cover	38
Vegetation Cover Loss vs. Trafficking Pass Level Relationships	44
Vegetative Cover Measurements on Wind Tunnel Trays.....	46

Tracked Vehicle Trafficking Effects on Soil Attached (Standing) Vegetation Biomass ..	51
Wheeled Vehicle Trafficking Effects on Soil Attached (Standing) Vegetation Biomass .	56
Soil Attached Vegetation Biomass Loss vs. Trafficking Pass Level.....	63
Surface Soil Aggregate Size Distribution (ASD)	65
Random Roughness	71
Soil Bulk Density	78
Wind Tunnel Testing of PM10 Emissions.....	89
Non-abrader Wind Tunnel Tests.....	89
Abrader Wind Tunnel Tests.....	98
PI-SWERL Measurements and Comparison with Wind Tunnel Data.....	108
Development of a Trafficking Compaction Process Model	113
Potential use of WEPS for Off-Road Military Trafficking Scenarios	116
SWEEP use for Off-Road Military Trafficking Scenarios	117
Recovery from Trafficking	122
Summary	143
Conclusions.....	147
Off-Road Trafficking	147
Future Research	148
Compact Eye safe Lidar System (CELiS)	150
Materials and Methods.....	150
CELiS Development	150
Description of CELiS.....	151
CELiS Retrieval Code.....	151
CELiS Calibration and Testing.....	154
CELiS: Accomplishments Under SERDP Funding.....	164
What did it lead to?	165
CELiS Future Related Research Needs	166
Appendices.....	174
Appendix A: Field Sampling/Transportation/Laboratory Protocols.....	174
Wind Tunnel Tray Field Sampling/Transportation Protocol	174
Wind Tunnel Experimental Setup.....	175
Wind Tunnel Tray Test Preparation	180

Wind Tunnel Tray LEM Testing Procedure	181
Wind Tunnel Tray Sand Abrader Testing Procedure	183
Wind Tunnel Data Analysis.....	184
PI-SWERL Instrument Description	185
Appendix B: CELiS Design Schematics and Photos	188
Appendix C: Comparison of Technologies for Fence Line Monitoring.....	196
Appendix D: CELiS QA/QC Procedures.....	209
Appendix E: List of Scientific/Technical Publications.....	211
Conference Proceedings.....	211
Posters	211
Patent.....	212
Journal Articles	212
Theses	212
Additional Peer-reviewed Manuscripts.....	212

List of Figures

Figure 1. M1A1 Abrams tank (left) and HMMWV (right) used at Ft. Riley, KS.	12
Figure 2. M1A1 tank (left) and up-armored HMMWV (right) used at Ft. Benning, GA.....	12
Figure 3. HMMWV (left) and 5-ton Fire Truck (right) used at Yakima Training Center, WA. .	13
Figure 4. Up-armored HMMWV (left) and M88-A1 Tank Retriever (right) used at White Sands Missile Range, NM.	13
Figure 5. Mowing (left) and rake used (right) at Ft. Riley, KS site prior to conducting trafficking experiments.	14
Figure 6. Example of figure-8 traffic patterns on the landscape at Yakima Training Center, WA.	14
Figure 7. Figure-8 plot with relative sampling locations identified where CC = Center Cross, SS = Straight Section, CI = Curve Inside track, and CO = Curve Outside track, L0 (not shown) = un-trafficked location inside figure-8.....	17
Figure 8. Location of additional sampling zones within curved trafficking region, where RI = Ridge Inside, RO = Ridge Outside, DI = Deposition Inside, DO = Deposition Outside from an M1A1 trafficked plot at Ft. Riley after at least 5 trafficking passes (picture of M1A1 tracked vehicle at Ft. Riley).....	17
Figure 9. Distribution of soil texture classes among all experiment sites included a loamy sand, two sandy loams, a loam, a silt loam and a silty clay loam (red dots).....	21
Figure 10. Map of areas where wind erosion is likely to occur on cropland in the United States.	22
Figure 11. Wind tunnel tray sample extracted from the Yakima Training Center, WA site.	25
Figure 12. Portable In-Situ Wind Erosion Research Laboratory (PI-SWERL).....	26
Figure 13. PI-SWERL setup in the field at Yakima Training Center, WA for collecting data. .	27
Figure 14. Using a pin meter to take transect surface elevation data across tracks at WSMR.....	29
Figure 15. Soil attached biomass sampling method used at all sites.	30
Figure 16. Beaded string method used for measuring surface cover at all sites.	30
Figure 17. Figure-8 plot of curved traffic regions (left) and straight trafficked regions (right) for both the HMMWV (top) after 50 passes and the M1A1 tank (bottom) after one pass at Ft. Riley, KS.	32
Figure 18. Field vegetation cover after specified trafficking pass levels for tracked vehicles for all specified sites-soils. Bars represent the mean of the measured values and the error bars represent the maximum and minimum measured values. CI is curve inside, CO is curve outside, and SS is the straight section sampling location. Sites are FB = Fort Benning, GA; FR = Fort Riley, KS; WS = White Sands Missile Range, NM; and YK = Yakima Training Center, WA. Soils are LS = loamy sand, SiCL = silty clay loam, SiL = silt loam, SL = sandy loam, and L = loam.....	37
Figure 19. Field vegetation cover after specified trafficking pass levels for wheeled (HMMWV) vehicles for all specified sites-soils. Bars represent the mean of the measured values and the error	

bars represent the maximum and minimum measured values. CI is curve inside, CO is curve outside, and SS is the straight section sampling location. Sites are FB = Fort Benning, GA; FR = Fort Riley, KS; WS = White Sands Missile Range, NM; and YK = Yakima Training Center, WA. Soils are LS = loamy sand, SiCL = silty clay loam, SiL = silt loam, SL = sandy loam, and L = loam.	43
Figure 20. Field vegetation cover after specified trafficking pass levels for wheeled (Fire Truck) vehicle on specified soil/site. Bars represent the mean of the measured values and the error bars represent the maximum and minimum measured values. CI is curve inside, CO is curve outside, and SS is the straight section sampling location. Site designation is YK = Yakima Training Center, WA. Soil is SL = sandy loam.	44
Figure 21. Comparisons between figure-8 plot (solid line) and wind tunnel tray (dashed line) vegetation cover data for tracked vehicles. CI is curve inside, CO is curve outside, and SS is the straight section sampling location. Sites are FB = Fort Benning, GA; FR = Fort Riley, KS; and WS = White Sands Missile Range, NM. Soils are LS = loamy sand, SiCL = silty clay loam, SiL = silt loam, SL = sandy loam, and L = loam.	49
Figure 22. Comparisons between figure-8 plot (solid line) and wind tunnel tray (dashed line) vegetation cover data for wheeled (HMMWV) vehicles. CI is curve inside, CO is curve outside, and SS is the straight section sampling location. Sites are FB = Fort Benning, GA; FR = Fort Riley, KS; and WS = White Sands Missile Range, NM. Soils are LS = loamy sand, SiCL = silty clay loam, SiL = silt loam, SL = sandy loam, and L = loam.	50
Figure 23. Comparisons between figure-8 plot (solid line) and wind tunnel tray (dashed line) vegetation cover data for wheeled (Fire Truck) vehicle. CI is curve inside, CO is curve outside, and SS is the straight section sampling location. Site is YK = Yakima Training Center, WA. Soil is SL = sandy loam.	51
Figure 24. Soil attached vegetation biomass after specified trafficking pass levels for tracked vehicles for all specified soils/sites. Bars represent the mean of the measured values and the error bars represent the maximum and minimum measured values. CI is curve inside, CO is curve outside, and SS is the straight section sampling location. Sites are FB = Fort Benning, GA; FR = Fort Riley, KS; WS = White Sands Missile Range, NM; and YK = Yakima Training Center, WA. Soils are LS = loamy sand, SiCL = silty clay loam, SiL = silt loam, SL = sandy loam, and L = loam.	56
Figure 25. Soil attached vegetation biomass after specified trafficking pass levels for wheeled (HMMWV) vehicles for all specified sites-soils. Bars represent the mean of the measured values and the error bars represent the maximum and minimum measured values. CC is center cross, CI is curve inside, CO is curve outside, and SS is the straight section sampling location. Sites are FB = Fort Benning, GA; FR = Fort Riley, KS; WS = White Sands Missile Range, NM; YK = Yakima Training Center, WA. Soils are LS = loamy sand, SiCL = silty clay loam, SiL = silt loam, SL = sandy loam, and L = loam.	62

Figure 26. Soil attached vegetation biomass after specified trafficking pass levels for wheeled (Fire Truck) vehicle for the specified site-soil. Bars represent the mean of the measured values and the error bars represent the maximum and minimum measured values. CC is center cross, CI is curve inside, CO is curve outside, and SS is the straight section sampling location. Site is YK = Yakima Training Center, WA. Soil is SL = sandy loam. 63

Figure 27. Wheeled vehicles response to pass level on Erodible Fraction, GMD (geometric mean diameter), and GSD (geometric standard deviation). Means with the same letter are not significant ($p < 0.05$) between passes for each soil and vehicle type (see **Table 2**). FTB = Fort Benning, GA; FTR = Fort Riley, KS; YTC = Yakima Training Center, WA and WSMR = White Sands Missile Range, NM..... 68

Figure 28. Tracked vehicle response to pass level on Erodible Fraction, GMD (geometric mean diameter), and GSD (geometric standard deviation) within sampling location. Means with the same letter are not significant ($p < 0.05$) between passes for each soil and vehicle type (see Table 2). Note, no tracked vehicles were run at YTC. CT is the curve track sampling location, CR is the curve ridge sampling location, and SST is the straight section track sampling location. FTB = Fort Benning, GA; FTR = Fort Riley, KS and WSMR = White Sands Missile Range, NM. 70

Figure 29. PM10 emission values obtained from PI-SWERL at 2000 rpm setting for all sampling locations on all soils for the tracked vehicles. Bars represent the mean of the measured values and the error bars represent the maximum and minimum measured values. CC is center cross, CI is curve inside, CO is curve outside, DI is deposition inside, DO is deposition outside, and SS is the straight section sampling location. Sites are FB = Fort Benning, GA; FR = Fort Riley, KS and WS = White Sands Missile Range, NM. Soils are LS = loamy sand, SiCL = silty clay loam, SiL = silt loam, SL = sandy loam, and L = loam..... 108

Figure 30. PM10 emission values obtained from PI-SWERL at 2000 rpm setting for all sampling locations on all soils for the wheeled vehicles (HMMWV). Bars represent the mean of the measured values and the error bars represent the maximum and minimum measured values. CC is center cross, CI is curve inside, CO is curve outside, DI is deposition inside, DO is deposition outside, and SS is the straight section sampling location. Sites are FB = Fort Benning, GA; FR = Fort Riley, KS and WS = White Sands Missile Range, NM. Soils are LS = loamy sand, SiCL = silty clay loam, SiL = silt loam, SL = sandy loam, and L = loam. 109

Figure 31. PM10 emission values obtained from PI-SWERL at 2000 rpm setting for all sampling locations on the Yakima soil for the heavy wheeled vehicle (Fire Truck). Bars represent the mean of the measured values and the error bars represent the maximum and minimum measured values. CC is center cross, CI is curve inside, CO is curve outside, DI is deposition inside, DO is deposition outside, and SS is the straight section sampling location. Site is YK = Yakima Training Center, WA. Soil is SL = sandy loam. 110

Figure 32. Normalized bulk density due to tracked vehicle trafficking passes. CC is center cross, CI is curve inside, CO is curve outside, and SS is the straight section sampling location. Sites are FB = Fort Benning, GA; FR = Fort Riley, KS and WS = White Sands Missile Range, NM.

Soils are LS = loamy sand, SiCL = silty clay loam, SiL = silt loam, SL = sandy loam, and L = loam.....	114
Figure 33. Normalized bulk density due to HMMWV wheeled vehicle trafficking passes. CC is center cross, CI is curve inside, CO is curve outside, and SS is the straight section sampling location. Sites are FB = Fort Benning, GA; FR = Fort Riley, KS and WS = White Sands Missile Range, NM. Soils are LS = loamy sand, SiCL = silty clay loam, SiL = silt loam, SL = sandy loam, and L = loam.	115
Figure 34. Normalized bulk density due to Fire Truck wheeled vehicle trafficking passes. CC is center cross, CI is curve inside, CO is curve outside, and SS is the straight section sampling location. Site is YK = Yakima Training Center, WA. Soil is SL = sandy loam.....	116
Figure 35. Single-event Wind Erosion Evaluation Program (SWEEP) Run example results....	121
Figure 36. Single-event Wind Erosion Evaluation Program (SWEEP) Threshold Run example results screen.....	122
Figure 37. Google Earth images of the Ft. Riley trafficking sites taken on Sep. 21, 2012 (upper photo) and on Aug. 11, 2014 (lower photo).....	125
Figure 38. Snow covered figure-8 plot at Ft. Riley in early 2011(left photo) and later in April 2011 (right photo).	126
Figure 39. Google Earth image of the Ft. Benning, GA experimental site that was taken on Dec. 18, 2012, about 6 months after the trafficking experiments were conducted.	127
Figure 40. Google Earth image of the Ft. Benning, GA experimental site that was taken on Dec. 10, 2014, about 2 ½ years after the trafficking experiments were conducted.	128
Figure 41. Google Earth images of the Yakima Training Center, WA experimental site taken on July 9, 2013 (left photo) and May 6, 2015 (right photo), about one year and nearly 3 years respectively, after the trafficking experiments were conducted.	130
Figure 42. Google Earth images (left photo is sandy loam soil site and right photo is loam soil site) of the two locations at the White Sands Missile Range site taken on May 27, 2016, about 1 ½ years after the multi-trafficking experiments were conducted.	133
Figure 43. WSMR track vehicle tracks in curved section of figure-8 plot after trafficking in Jan. 2014 (upper photo) and ~10 months later (lower photo).	134
Figure 44. A figure-8 plot created by the tracked vehicle contains numerous small burrows and animal trails (upper photo) and a flagged HMMWV wheeled vehicle figure-8 location (lower photo), both ~10 months after conducting the multi-trafficking experiments at WSMR.....	135
Figure 45. A HMMWV wheeled vehicle created figure-8 on the loam soil site immediately following the conclusion of the multi-trafficking experiments in Jan. 2014 (upper photo) and another HMMWV wheeled vehicle figure-8 plot ~10 months later that was being flagged (lower photo).	136
Figure 46. Straight trafficked section on loam soil of figure-8 plot after tracked vehicle trafficking at WSMR (upper photo) and the resulting heavily vegetated straight away and cross-over sections 10 months later (lower photo).....	137

Figure 47. Comparison of vegetation mass levels for tracked vehicle trafficked conditions under curved and straight regions and un-trafficked regions (Control) for all sites. Sampling dates were in Aug. 2011 at Ft. Riley, KS and Nov. 2014 at White Sands Missile Range, NM. CI is curve inside, CO is curve outside, and SS is the straight section sampling location. Sites are FR = Fort Riley and WS = White Sands. Soils are SiCL = silty clay loam, SiL = silt loam, and SL = sandy loam.....	139
Figure 48. Comparison of vegetation mass levels for wheeled (HMMWV) vehicle trafficked conditions under curved and straight regions and un-trafficked regions (Control) for all sites. Sampling dates were in Aug. 2011 at Ft. Riley KS in Jul. 2013 at Yakima Training Center, WA and in Nov. 2014 at White Sands Missile Range. NM. Sites are FB = Fort Benning, GA; FR = Fort Riley, KS; WS = White Sands Missile Range, NM, and YK = Yakima Training Center, WA. CC is center cross, CI is curve inside, CO is curve outside, and SS is the straight section sampling location. Sites are FB = Fort Benning, FR = Fort Riley, WS = White Sands, and YK = Yakima. Soils are SiCL = silty clay loam, SiL = silt loam, SL = sandy loam, and L = loam. ..	141
Figure 49. Comparison of vegetation mass levels for wheeled (Fire Truck) vehicle trafficked conditions under curved (CI,CO) and straight (SS) regions and un-trafficked regions (Control) for all sites. Sampling date was in Jul. 2013 at Yakima Training Center, WA. YK = Yakima Training Center, WA and SL = sandy loam.	142
Figure 50. Plan view of CELiS located adjacent to fence line.	151
Figure 51. Approach for CELiS Retrieval of PM Concentrations. OPC: optical particle counter. DC: direct current. GFF: geometric form factor.....	153
Figure 52. Approach for CELiS Retrieval of PM Concentrations.....	154
Figure 53. Process flow diagram of CELiS range resolved PM algorithm.....	156
Figure 54. Dugway Proving Ground particulate chambers.....	157
Figure 55. CELiS installed inside a Dugway Proving Ground test trailer and in position for use at the JABT. The left picture is the complete CELiS system placed on a hydraulic lift inside the trailer. The right picture is CELiS hoisted into position.....	158
Figure 56. Range corrected data for SAMPLE (top) and CELiS (bottom) with relative amplitude on a common scale. These data are shown as waterfall plots with range on the vertical axis and time on the horizontal axis.....	159
Figure 57. Top plot, linear fit of PM ₁₀ vs Aerosol Backscatter. Bottom cluster of plots, PM ₁ , PM _{2.5} , PM ₅ , PM ₁₀ , PM ₁₅ and TSP vs total aerosol backscatter. Note the linear trend across all PSDs.....	162
Figure 58. Total backscatter ($\beta_a(R)+\beta_m$) for SAMPLE and CELiS.	163
Figure 59. Range resolved PM ₁₀ for SAMPLE and CELiS.....	164
Figure 60. A comparison of the lidar-derived PM ₁₀ data (blue) and the original calibration data (black).	164

List of Tables

Table 1. Site characteristics and sampling/re-sampling dates for each trafficking experiment site.	9
Table 2. Vehicles used for trafficking at each experimental site on the specified dates.	10
Table 3. Relevant specifications of vehicles used at experimental sites.	11
Table 4. Number of passes conducted per trafficking set by each vehicle at each site.	15
Table 5. Description of all sampling locations on the figure-8 plots.	18
Table 6. Location sampling zone of each data sample collected from each figure-8 plot (see Table 5 for sampling location definitions).	19
Table 7. Soil particle size distribution for the trafficking experiment locations.	23
Table 8. Average soil chemical and physical properties for the study sites.	24
Table 9. Overall ANOVA type III table of vegetation cover for tracked vehicles (Sum Sq = sum of squares; Mean Sq = mean of squares; NumDF = numerator degrees of freedom; DenDF = denominator degrees of freedom; F.value = F statistic ratio value; Pr(>F) = Probability p value associated with F statistic).	33
Table 10. Vegetation cover (%) least square means (lsmean) for tracked vehicles by soil and sampling location. CI is curve inside, CO is curve outside, and SS is straight section. Soil code designates the site and soil where sites are FB = Fort Benning, FR = Fort Riley, and WS = White Sands and soils are LS = loamy sand, SiCL = silty clay loam, SiL = silt loam, SL = sandy loam, and L = loam. SE = standard error of the mean, df = degrees of freedom, lower.CL = lower confidence level (95%), and upper .CL = upper confidence level (95%).	34
Table 11. Vegetation cover (%) least square means (lsmean) for tracked vehicles by trafficking pass across all soils. SE = standard error of the mean, df = degrees of freedom, lower.CL = lower confidence level (95%), and upper .CL = upper confidence level (95%).	35
Table 12. Field vegetation cover comparisons among trafficking pass levels and sampling locations by soil for tracked vehicles.	36
Table 13. Overall ANOVA type III table of vegetation cover for wheeled (HMMWV) vehicles (Sum Sq = sum of squares; Mean Sq = mean of squares; NumDF = numerator degrees of freedom; DenDF = denominator degrees of freedom; F.value = F statistic ratio value; PR(>F) = Probability p value associated with F statistic).	38
Table 14. Vegetation cover (%) least square means (lsmeans) for wheeled vehicles (HMMWV) by soil and sampling location. SE = standard error of the mean, df = degrees of freedom, lower.CL = lower confidence level (95%), and upper.CL = upper confidence level (95%).	39
Table 15. Vegetation cover (%) least square means (lsmean) for wheeled vehicles (HMMWV) by trafficking pass. SE = standard error of the mean, df = degrees of freedom, lower.CL = lower confidence level (95%), and upper .CL = upper confidence level (95%).	40
Table 16. Vegetation cover (%) least square means (lsmean) for wheeled vehicle (Fire Truck) by sampling location. SE = standard error of the mean, df = degrees of freedom, lower.CL = lower confidence level (95%), and upper .CL = upper confidence level (95%).	41

Table 17. Field vegetation cover comparisons among trafficking pass levels and sampling locations for wheeled vehicles.	42
Table 18. Fitted first order vegetation cover decay function parameters for the curved (CI, CO) and straight trafficked (SS) regions for all vehicles at all sites.	45
Table 19. Wind tunnel tray vegetation cover comparisons among trafficking pass levels and sampling locations for tracked vehicles.	46
Table 20. Wind tunnel tray vegetation cover comparisons among trafficking pass levels and sampling locations for wheeled vehicles.	47
Table 21. Overall ANOVA type III table of soil attached vegetation biomass for tracked vehicles. Sum Sq = sum of squares; Mean Sq = mean of squares; NumDF = numerator degrees of freedom; DenDF = denominator degrees of freedom; F.value = F statistic ratio value; PR(>F) = Probability p value associated with F statistic.	52
Table 22. Soil attached vegetation biomass (g m^{-2}) least square means (lsmeans) for tracked vehicles by soil and sampling location. SE = standard error of the mean, df = degrees of freedom, lower.CL = lower confidence level (95%), and upper .CL = upper confidence level (95%).	53
Table 23. Soil attached vegetation biomass (g m^{-2}) least square means (lsmeans) for tracked vehicles by trafficking pass across all soils. SE = standard error of the mean, df = degrees of freedom, lower.CL = lower confidence level (95%), and upper.CL = upper confidence level (95%).	54
Table 24. Soil attached vegetation biomass comparisons among trafficking pass levels and sampling locations by soil for tracked vehicles.	55
Table 25. Overall ANOVA type III table of soil attached vegetation biomass for wheeled vehicles (HMMWV). Sum Sq = sum of squares; Mean Sq = mean of squares; NumDF = numerator degrees of freedom; DenDF = denominator degrees of freedom; F.value = F statistic ratio value; PR(>F) = Probability p value associated with F statistic.	57
Table 26. Soil attached vegetation biomass (g m^{-2}) least square means (lsmeans) for wheeled vehicles (HMMWV) by soil and sampling location. SE = standard error of the mean, df = degrees of freedom, lower.CL = lower confidence level (95%), and upper .CL = upper confidence level (95%).	58
Table 27. Soil attached vegetation biomass (g m^{-2}) least square means (lsmeans) for wheeled vehicles (HMMWV) by trafficking pass across all soils. SE = standard error of the mean, df = degrees of freedom, lower.CL = lower confidence level (95%), and upper .CL = upper confidence level (95%).	59
Table 28. Overall ANOVA type III table of soil attached vegetation biomass for heavy wheeled vehicle (Fire Truck). Sum Sq = sum of squares; Mean Sq = mean of squares; NumDF = numerator degrees of freedom; DenDF = denominator degrees of freedom; F.value = F statistic ratio value; PR(>F) = Probability p value associated with F statistic.	59
Table 29. Soil attached vegetation biomass (g m^{-2}) least square means (lsmeans) for heavy wheeled vehicle (Fire Truck) by sampling location. SE = standard error of the mean, df =	

degrees of freedom, lower.CL = lower confidence level (95%), and upper .CL = upper confidence level (95%).	60
Table 30. Soil attached vegetation biomass (g m^{-2}) comparisons among trafficking pass levels and sampling locations by soil for wheeled vehicles.	61
Table 31. Fitted first order soil attached biomass decay function parameters for the curved (CI,CO) and straight trafficked (SS) regions for all vehicles at all sites.	64
Table 32. Significance of difference between location for tracked and wheeled vehicles for measured aggregate parameters at each study site.	66
Table 33. Predictive models of aggregate parameters based on soil properties and vehicle passes.	71
Table 34. Overall ANOVA type III table of random roughness values for tracked vehicles (Sum Sq = sum of squares; Mean Sq = mean of squares; NumDF = numerator degrees of freedom; DenDF = denominator degrees of freedom; F.value = F statistic ratio value; PR(>F) = Probability p value associated with F statistic).	72
Table 35. Random roughness (mm) least square means (lsmean) for tracked vehicles by soil and sampling location. CI is curve inside, CO is curve outside, and SS is straight section. Soil code designates the site and soil where sites are FB = Fort Benning, FR = Fort Riley, and WS = White Sands and soils are LS = loamy sand, SiCL = silty clay loam, SiL = silt loam, SL = sandy loam, and L = loam. SE = standard error of the mean, df = degrees of freedom, lower.CL = lower confidence level (95%), and upper .CL = upper confidence level (95%).	73
Table 36. Random roughness (mm) least square means (lsmean) for tracked vehicles by trafficking pass across all soils. SE = standard error of the mean, df = degrees of freedom, lower.CL = lower confidence level (95%), and upper .CL = upper confidence level (95%).	74
Table 37. Overall ANOVA type III table of random roughness values for wheeled (HMMWV) vehicles (Sum Sq = sum of squares; Mean Sq = mean of squares; NumDF = numerator degrees of freedom; DenDF = denominator degrees of freedom; F.value = F statistic ratio value; PR(>F) = Probability p value associated with F statistic).	74
Table 38. Random roughness (mm) least square means (lsmean) for wheeled (HMMWV) vehicles by soil and sampling location. CI is curve inside, CO is curve outside, and SS is straight section. Soil code designates the site and soil where sites are FB = Fort Benning, FR = Fort Riley, and WS = White Sands and soils are LS = loamy sand, SiCL = silty clay loam, SiL = silt loam, SL = sandy loam, and L = loam. SE = standard error of the mean, df = degrees of freedom, lower.CL = lower confidence level (95%), and upper .CL = upper confidence level (95%).	76
Table 39. Random roughness (mm) least square means (lsmean) for wheeled (HMMWV) vehicles by trafficking pass across all soils. SE = standard error of the mean, df = degrees of freedom, lower.CL = lower confidence level (95%), and upper .CL = upper confidence level (95%).	77

Table 40. Overall ANOVA type III table of random roughness values for heavy wheeled (Fire Truck) vehicle (Sum Sq = sum of squares; Mean Sq = mean of squares; NumDF = numerator degrees of freedom; DenDF = denominator degrees of freedom; F.value = F statistic ratio value; PR(>F) = Probability p value associated with F statistic).	77
Table 41. Random roughness (mm) least square means (lsmean) for heavy wheeled (Fire Truck) vehicle by trafficking pass across all soils. SE = standard error of the mean, df = degrees of freedom, lower.CL = lower confidence level (95%), and upper .CL = upper confidence level (95%).....	78
Table 42. Overall ANOVA type III table of soil bulk density (0-15cm depth) for tracked vehicles. Sum Sq = sum of squares; Mean Sq = mean of squares; NumDF = numerator degrees of freedom; DenDF = denominator degrees of freedom; F.value = F statistic ratio value; PR(>F) = Probability p value associated with F statistic.	79
Table 43. Soil bulk density (0-15 cm depth) (mg m^{-3}) least square (lsmean) for tracked vehicles by soil and sampling location. SE = standard error of the mean, df = degrees of freedom, lower.CL = lower confidence level (95%), and upper .CL = upper confidence level (95%).	80
Table 44. Soil bulk density (0-15 cm depth) (mg m^{-3}) least square means (lsmean) for tracked vehicles by trafficking pass across all soils. SE = standard error of the mean, df = degrees of freedom, lower.CL = lower confidence level (95%), and upper .CL = upper confidence level (95%).....	81
Table 45. Bulk density comparisons at 0-15 cm depth among trafficking pass levels and sampling locations for tracked vehicles.	82
Table 46. Overall ANOVA type III table of soil bulk density (0-15cm depth) for wheeled vehicles (HMMWV). Sum Sq = sum of squares; Mean Sq = mean of squares; NumDF = numerator degrees of freedom; DenDF = denominator degrees of freedom; F.value = F statistic ratio value; PR(>F) = Probability p value associated with F statistic.	83
Table 47. Soil bulk density (0-15 cm depth) (mg m^{-3}) least square means (lsmean) for wheeled vehicles (HMMWV) by soil and sampling location. SE = standard error of the mean, df = degrees of freedom, lower.CL = lower confidence level (95%), and upper .CL = upper confidence level (95%).	84
Table 48. Soil bulk density (0-15 cm depth) (mg m^{-3}) least square means (lsmean) for wheeled vehicles (HMMWV) by trafficking pass across all soils. SE = standard error of the mean, df = degrees of freedom, lower.CL = lower confidence level (95%), and upper .CL = upper confidence level (95%).	85
Table 49. Soil bulk density (0-15 cm depth) (mg m^{-3}) least square means (lsmean) for wheeled vehicle (Fire Truck) by sampling location. SE = standard error of the mean, df = degrees of freedom, lower.CL = lower confidence level (95%), and upper .CL = upper confidence level (95%).....	86
Table 50. Bulk density comparisons at 0-15 cm depth among trafficking pass levels and sampling locations for wheeled vehicles.	87

Table 51. General relationship of soil bulk density to root growth based on soil texture (source: USDA-NRCS, 2014).*	88
Table 52. Overall ANOVA type III table of wind tunnel non-abrader PM10 (mg m^{-2}) dust emissions (log transformed) for tracked vehicles. Sum Sq = sum of squares; Mean Sq = mean of squares; NumDF = numerator degrees of freedom; DenDF = denominator degrees of freedom; F.value = F statistic ratio value; PR(>F) = Probability p value associated with F statistic.	89
Table 53. Wind tunnel (log transformed) non-abrader PM10 (mg m^{-2}) least square means (lsmeans log transformed) for tracked vehicles by soil and sampling location. SE = standard error of the mean, df = degrees of freedom, lower.CL = lower confidence level (95%), and upper .CL = upper confidence level (95%).	90
Table 54. Wind tunnel (log transformed) non-abrader PM10 (mg m^{-2}) least square means (log transformed) for tracked vehicles by trafficking pass across all soils. SE = standard error of the mean, df = degrees of freedom, lower.CL = lower confidence level (95%), and upper .CL = upper confidence level (95%).	91
Table 55. Non-abrader PM10 emission (mg m^{-2}) comparisons among trafficking pass levels and sampling locations (tracked vehicles).	92
Table 56. Overall ANOVA type III table of wind tunnel non-abrader PM10 (mg m^{-2}) dust emissions (log transformed) for wheeled vehicles (HMMWV). Sum Sq = sum of squares; Mean Sq = mean of squares; NumDF = numerator degrees of freedom; DenDF = denominator degrees of freedom; F.value = F statistic ratio value; PR(>F) = Probability p value associated with F statistic.	93
Table 57. Overall ANOVA type III table of wind tunnel non-abrader PM10 (mg m^{-2}) dust emissions (log transformed) for heavy wheeled vehicle (Fire Truck). Sum Sq = sum of squares; Mean Sq = mean of squares; NumDF = numerator degrees of freedom; DenDF = denominator degrees of freedom; F.value = F statistic ratio value; PR(>F) = Probability p value associated with F statistic.	93
Table 58. Wind tunnel (log transformed) non-abrader PM10 (mg m^{-2}) least square means (log transformed) for wheeled vehicles (HMMWV) by soil and sampling location. SE = standard error of the mean, df = degrees of freedom, lower.CL = lower confidence level (95%), and upper .CL = upper confidence level (95%).	94
Table 59. Wind tunnel (log transformed) non-abrader PM10 (mg m^{-2}) least square means (log transformed) for wheeled vehicles (HMMWV) by trafficking pass across all soils. SE = standard error of the mean, df = degrees of freedom, lower.CL = lower confidence level (95%), and upper.CL = upper confidence level (95%).	95
Table 60. Wind tunnel (log transformed) non-abrader PM10 (mg m^{-2}) least square means (lsmeans) (log transformed) for heavy wheeled vehicle (Fire Truck) by trafficking pass across all soils. SE = standard error of the mean, df = degrees of freedom, lower.CL = lower confidence level (95%), and upper.CL = upper confidence level (95%).	96

Table 61. Non-abrader PM10 emission (mg m^{-2}) comparisons among trafficking pass levels and sampling locations (wheeled vehicles).	97
Table 62. Overall ANOVA type III table of wind tunnel abrader PM10 (mg m^{-2}) dust emissions (log transformed) for tracked vehicles. Sum Sq = sum of squares; Mean Sq = mean of squares; NumDF = numerator degrees of freedom; DenDF = denominator degrees of freedom; F.value = F statistic ratio value; PR(>F) = Probability p value associated with F statistic.	99
Table 63. Wind tunnel (log transformed) abrader PM10 (mg m^{-2}) least square means (lsmean) (log transformed) for tracked vehicles by soil and sampling location. SE = standard error of the mean, df = degrees of freedom, lower.CL = lower confidence level (95%), and upper .CL = upper confidence level (95%).	100
Table 64. Wind tunnel (log transformed) abrader PM10 (mg m^{-2}) least square means (lsmean) (log transformed) for tracked vehicles by trafficking pass across all soils. SE = standard error of the mean, df = degrees of freedom, lower.CL = lower confidence level (95%), and upper .CL = upper confidence level (95%).	101
Table 65. Abrader PM10 emission (mg m^{-2}) comparisons among trafficking pass levels and sampling locations (tracked vehicles).	102
Table 66. Overall ANOVA type III table of wind tunnel abrader PM10 (mg m^{-2}) dust emissions (log transformed) for wheeled vehicles (HMMWV). Sum Sq = sum of squares; Mean Sq = mean of squares; NumDF = numerator degrees of freedom; DenDF = denominator degrees of freedom; F.value = F statistic ratio value; PR(>F) = Probability p value associated with F statistic.	103
Table 67. Overall ANOVA type III table of wind tunnel abrader PM10 (mg m^{-2}) dust emissions (log transformed) for heavy wheeled vehicle (Fire Truck). Sum Sq = sum of squares; Mean Sq = mean of squares; NumDF = numerator degrees of freedom; DenDF = denominator degrees of freedom; F.value = F statistic ratio value; PR(>F) = Probability p value associated with F statistic.	103
Table 68. Wind tunnel (log transformed) abrader PM10 (mg m^{-2}) least square means (lsmean) (log transformed) for wheeled vehicles (HMMWV) by soil and sampling location. SE = standard error of the mean, df = degrees of freedom, lower.CL = lower confidence level (95%), and upper .CL = upper confidence level (95%).	104
Table 69. Wind tunnel (log transformed) abrader PM10 (mg m^{-2}) least square means (lsmean) (log transformed) for wheeled vehicles (HMMWV) by trafficking pass. SE = standard error of the mean, df = degrees of freedom, lower.CL = lower confidence level (95%), and upper .CL = upper confidence level (95%).	105
Table 70. Wind tunnel (log transformed) abrader PM10 (mg m^{-2}) least square means (lsmean) (log transformed) for heavy wheeled vehicle (Fire Truck) by sampling location. SE = standard error of the mean, df = degrees of freedom, lower.CL = lower confidence level (95%), and upper .CL = upper confidence level (95%).	106
Table 71. Abrader PM10 emission (mg m^{-2}) comparisons among trafficking pass levels and sampling locations (wheeled vehicles).	107

Table 72. Military vehicles' trafficking average ridge dimensions and impact widths for individual tracks measured at White Sands Missile Range, NM.....	119
Table 73. Fort Riley monthly precipitation and freeze/thaw cycles between sampling dates in October and November, 2010 and August of 2011 (~310 days).	124
Table 74. Fort Benning, GA monthly precipitation and freeze/thaw cycles after the sampling date in July 2012 through June of 2013 (365 days).....	129
Table 75. Yakima Training Center, WA monthly precipitation and freeze/thaw cycles between sampling dates in Aug 2012 and July of 2013 (~360 days).....	131
Table 76. WSMR monthly precipitation and freeze/thaw cycles between sampling dates in January and November of 2014 (~310 days).....	132
Table 77. Vegetation mass (mg m^{-2}) least square means (lsmean) for tracked vehicles by sampling location. CO is curve outside, and SS is straight section. Pass = the number of trafficking passes conducted, SE = standard error of the mean, df = degrees of freedom, lower.CL = lower confidence level (95%), and upper .CL = upper confidence level (95%).	138
Table 78. Vegetation mass (mg m^{-2}) least square means (lsmean) for wheeled (HMMWV) vehicles by sampling location. CO is curve outside, and SS is straight section. Pass = the number of trafficking passes conducted, SE = standard error of the mean, df = degrees of freedom, lower.CL = lower confidence level (95%), and upper .CL = upper confidence level (95%).	140
Table 79. Vegetation mass (mg m^{-2}) least square means (lsmean) for a wheeled (Fire Truck) vehicle by sampling location. CO is curve outside, and SS is straight section. Pass = the number of trafficking passes conducted, SE = standard error of the mean, df = degrees of freedom, lower.CL = lower confidence level (95%), and upper .CL = upper confidence level (95%).	142

List of Acronyms

ASD	Aggregate Size Distribution
CaCO ₃	Calcium Carbonate – a measured soil property
CC	Center Cross sampling location within figure-8 pattern
CEC	Cation Exchange Capacity – a measured soil property
CELiS	Compact Eye safe Lidar System
CI	Curve Inside track sampling location within figure-8 pattern
CO	Curve Outside track sampling location within figure-8 pattern
CONOPS	Concept of Operations
D	Used in statistical analyses to discern bulk density/moisture content sample depths
CR	Curve Ridge track sampling location within the figure-8 pattern where inside and outside curve are considered the same
CT	Curve Ridge track sampling location within the figure-8 pattern where inside and outside curve are considered the same
DAS	Dry Aggregate Stability
DenDF	Denominator Degrees of Freedom – computed in ANOVA statistical analysis
df	Degrees of Freedom calculation from statistical analysis package
DI	Deposition Inside region outside of inside curved track within figure-8 pattern
DO	Deposition Outside region outside of outside curved track within figure-8 pattern
DoD	Department of Defense
DRI	Desert Research Institute
EDL	Energy Dynamics Laboratory
EPA	Environmental Protection Agency
Factor	Independent factors and interactions used in statistical analysis
FB, FTB	Fort Benning, Georgia (Rowan Hill area)
FB-LS	SoilCode symbol for Loamy Sand soil at Ft. Benning, GA
FPGA	Field Programmable Gate Array (a configurable integrated circuit)
FR, FTR	Fort Riley, Kansas
FR-SiCL	SoilCode symbol for Silty Clay Loam soil at Ft. Riley, KS
FR-SiL	SoilCode symbol for Silt Loam soil at Ft. Riley, KS
FW	Front Wheeled drive vehicle (6-wheel drive fire truck used in experiments)
F.value	F statistic ratio value – computed in ANOVA statistical analysis
group	Grouping letters from statistical analysis package denoting significant differences
GMD	Geometric mean diameter (lognormal distribution parameter)
GSD	Geometric standard deviation (lognormal distribution parameter)
HMMWV	High Mobility Multipurpose Wheeled Vehicle
Humvee	Alias for HMMWV
ITAM	Integrated Training Area Management
JBAT	Joint Ambient Breeze Tunnel
L or LOC	Used in statistical analyses to discern sample locations within figure-8 plots
LEM	Loose Erodible Material
LO	Location of initial (pre-trafficked) samples taken within figure-8 plots at Ft. Riley
lower.CL	Lower Confidence Interval value (95%) from statistical analysis package

lsmean	Least squares mean from statistical analysis
Mean Sq	Mean of Squares – computed in ANOVA statistical analysis
msep	Mean squared error of prediction (statistical term)
M1A1	An Abrams military tank model number
M88-A1	A military tank retriever model number
NAAQS	National Ambient Air Quality Standards
NRCS	USDA- Natural Resources Conservation Service
NumDF	Numerator Degrees of Freedom – computed in ANOVA statistical analysis
OM	Soil Organic Matter – a measured soil property
OR	Oriented (ridge) Roughness
p0,p1,p2,p3	Trafficking pass levels conducted on figure-8 pots (0-initial condition, 1-first level of passes, 2-second level of passes and 3-third level of passes)
P or Pass	Used in statistical analyses to discern difference in number of trafficking passes
PI-SWERL	Portable In-Situ Wind Erosion Laboratory
PM	Particulate Matter
PM2.5	Particulate Matter with equivalent aerodynamic diameter less than 2.5 μ m
PM10	Particulate Matter with equivalent aerodynamic diameter less than 10 μ m
Pr(>F)	Probability p value associated with F statistic – computed in ANOVA statistical analysis
QAPP	Quality Assurance Project Plan
QA/QC	Quality Assurance/Quality Control
QMP	Quality Management Plan
R	The “R” statistical analysis package
Rep	Replicated samples collected – Used in statistical analysis
RF	Radio Frequency
RI	Ridge Inside region, outside of inside curved track within figure-8 pattern
RO	Ridge Outside region outside of outside curved track within figure-8 pattern
RR	Random Roughness
S	Seasons - Used in statistical analysis to discern difference in seasons
SAS	“Statistical Analysis System” statistical analysis package
SE	Standard Error term from statistical analysis package
SERDP	Strategic Environment Research and Development Program
SDL	Space Dynamics Laboratory
Signif.	Significance code – computed in ANOVA statistical analysis
SoilCode	Used in statistical analyses to discern differences in soils/sites
SoN	Statement of Need
Sum Sq	Sum of Squares – computed in ANOVA statistical analysis
SS	Straight Section sampling region within figure-8 pattern
SST	Straight Section sampling location within figure-8 pattern for track location only
SWEEP	Single-event Wind Erosion Evaluation Program
TR	Tracked vehicle (M1A1 tank or M88-A1 tank retriever used in experiments)
Upper.CL	Upper Confidence Interval value (95%) from statistical analysis package
USDA	United States Department of Agriculture
V	Vehicle – Used in statistical analysis to discern different military vehicles used
VCI	Vehicle Cone Index – A measurement closely associated with ground pressure

WEPS	Wind Erosion Prediction System
WH	Wheeled vehicle
Windgen	Stochastic subdaily wind generator used in the Wind Erosion Prediction System
WS, WSMR	White Sands Missile Range, New Mexico
WS-L	SoilCode symbol for Loam soil at White Sands Missile Range, NM
WS-SL	SoilCode symbol for Sandy Loam soil at White Sands Missile Range, NM
YK, YTC	Yakima Training Center, Washington
YK-SL	SoilCode symbol for Sandy Loam soil at Yakima Training Center, WA
Y-Length	Distance (m) along Y-axis specified for a SWEEP simulation site
X-Length	Distance (m) along X-axis direction for a SWEEP simulation site
(X ₁ ,Y ₁)	First coordinate point (m) describing a wind barrier location in SWEEP
(X ₂ ,Y ₂)	Second coordinate point (m) describing a wind barrier location in SWEEP

Keywords:

air quality, wind erosion, dust emissions, PM10, particulate matter

Acknowledgements

This project was funded by the Strategic Environmental Research and Development Program (SERDP) under project RC-1767. Special thanks go to the former ITAM (Integrated Training Area Management) coordinator, Dr. Woodford (retired) and Christopher Otto at Fort Riley; Shannon (Tannis) Danley at Fort Benning; Peter Nissen at the Yakima Training Center; Joel (Brian) Wilson at White Sands Missile Range; and William Brown at Dugway Proving Ground.

The assistance of the following individuals in field and laboratory studies is gratefully acknowledged: Neil Baker, Max Erdwien, Jincheng Gao, Lawrence Hagen, Michelle (Bush) Hilburn, Michael Jurgensmeier, Laura Kemp, Matthew Kucharski, Hubert Lagae, Joseph Levin, Ben Li Liu, Jeremy Meeks, Kori Moore, Amare Retta, William Rust, Christopher Shultz, Abigail Stedry, Timothy Todd, Quincy Tuttle, Christy Wagner, Youjie Xu, Jonathan Zeller, and Jiaqiong Zhang.

RC-1767 Abstract

Objectives

The United States (U.S.) Department of Defense (DoD) conducts military training and testing activities on approximately 12 million hectares of land. Training exercises in which wheeled and tracked vehicles are used can result in land conditions susceptible to wind erosion. Particulates from subsequent wind erosion events on previously trafficked landscape may drift across the installation boundary, impacting air quality downwind. Accurately assessing effects of traffic activity on the susceptibility to wind erosion as a function of soil, vehicle, and activity-specific characteristics is critical to understanding the total near-field (within 200 m of the source) impacts on downwind areas. This project sought to: 1) address after-trafficking impacts on wind erosion risk by measurement of important soil, surface, and vegetation characteristics that relate to wind erosion susceptibility; and 2) provide an initial assessment of each site's ability to recover from the trafficking events that may decrease risk of wind erosion; and 3) develop a new particulate measuring device, a Compact Eye-safe Lidar System (CELiS) and method, to monitor particulates crossing a fence-line due to military training/testing and other activities.

The goal of the project was to use a combination of soil science, remote sensing, and meteorological and traditional air quality sampling to accurately measure traffic effects on surface erodibility. Objectives of the study were to: 1) improve understanding of fugitive dust emission potential from military activities, and 2) improve DoD's ability to achieve source compliance and ambient fence-line monitoring for fugitive dust emissions at their installations.

Technical Approach

Field experiments were carried out at four DoD facilities for a range of soil, vegetative, and climatic conditions. Tracked and wheeled vehicles were driven on military lands repeatedly in a "figure-8" pattern, providing multiple pass data in both turning and straight line trafficking configurations. Soil and vegetation data were also collected prior to and after each set of trafficking passes to evaluate the susceptibility to wind erosion as well as after a rest period to determine the initial recovery or change in those soil and vegetation properties as they relate to wind erosion susceptibility.

The technical approach for CELiS was to drive strongly toward a commercial-grade instrument which is small, light, and requires very little training to operate. Specifically, thermal engineering and optical engineering best-practices from military/aerospace instrumentation were applied to the design and operational concept of an elastic lidar instrument. The self-imposed requirement was to maintain an athermal design over a range of at least 60°C; implying careful matching of the coefficients of thermal expansion for all of the materials involved (structural, optical and epoxy). Good athermal design principles have the advantage of driving toward the fewest number of optical surfaces and the fewest number of user adjustments (knobs) as possible. Furthermore, ruggedized lidar control and data acquisition software – LidarView – which has over 10,000 hours of use at Dugway Proving Ground was adapted for CELiS. The wavelength of 1.547 μm was chosen because it is eye-safe at the laser aperture and greatly eases operational constraints.

Results

The key findings are listed here by project sub-objective.

- 1a. Characterize and model individual military vehicle (tracked and wheeled) impacts on the changes in temporal surface and soil properties as functions of the intrinsic soil properties and specific physical attributes/parameters of the vehicles involved.
 - i. Heavy tracked vehicles exhibited a more intense impact overall on the soil surface than the lighter wheeled vehicles tested, especially when turning.
 - ii. Tracked vehicle turning sheared the surface soil layer, throwing soil and vegetation outside the tracked region. This eliminated most vegetation present and developed a track rut in the turn in as little as a single trafficking pass.
 - iii. Wheeled vehicles also exerted a side shear force while turning with the intensity dependent upon vehicle weight, tire dimensions (diameter and width), turning radius, and travel speed, but the effect was less severe than the heavy tracked vehicles studied.
 - iv. Straight trafficked regions retained more vegetation cover and mass under repeated trafficking than in the curve trafficked regions for all vehicles, presumably due to less side shear forces.
 - v. Vegetation cover and mass decreased with increasing passes on straight trafficked areas for all vehicles with the effect more pronounced under heavier vehicles.
- 1b. Characterize relevant temporal and intrinsic soil and surface properties, via laboratory wind tunnel tray studies, to measure total dust as well as PM10 emission potential on a range of disturbed and undisturbed military land soils.
 - i. An increase in particulate emission potential occurred in the straight trafficked regions due to the removal of vegetation cover and mass as well as the continual grinding of the surface soil from repeated trafficking passes for all vehicles.
 - ii. Few significant measurable differences were found between the inside and outside tracks in the curves at all trafficking levels for both vehicles.
- 1c. Collect soil and plant data from plot studies conducted on selected military sites before and after training activities and seasonally thereafter to determine both the impact of the activities on erodibility and the recovery times to less degraded states for the disturbed sites.
 - i. Overwintering processes (freeze/thaw, freeze/dry, and wet/dry cycles) caused a reduction in the 0-5 cm depth bulk densities within the tracked regions at Ft. Riley, KS. It is expected that this will occur at any site where there is sufficient moisture in the soil near the surface and the site's climate is conducive to providing freeze/thaw, freeze/dry and wet/dry cycles over the winter. Unfortunately, the Yakima and White Sands Missile Range soils were too dry to verify that expectation during resampling.
 - ii. Vegetation re-growth nearly a year (~10 months) later at White Sands Missile Range was measurably significant. The HMMWV wheeled figure-8 plots were nearly indistinguishable from the surrounding un-trafficked areas when re-sampling occurred. It is speculated that part of the reason was due to above average precipitation (128%) between the two sampling periods. Extrapolating this result, it is expected that vegetation

regrowth could be enhanced by correctly timing and applying sufficient supplemental water, when feasible, to multi-trafficked areas on any military training lands in arid or semi-arid regions.

- iii. At White Sands Missile Range, some of the tracked vehicle straight traffic regions, which originally contained sparse vegetation at the time of trafficking (**Figure 46**), had significant visual gramma grass growth compared to the adjacent, still nearly bare un-trafficked regions, at the time of re-sampling. In this case it is speculated that the repeated trafficking mixed existing gramma seed into the soil and the pulverizing effect on the surface created a more favorable seedbed than the adjacent un-trafficked areas. Based upon these observations, it is speculated that many similar initially bare surface regions could be coerced to generate enhanced vegetation growth by simulating these seed-bed enhancing effects on such surfaces, as witnessed at White Sands with the tracked vehicle.
- 1d. Use data collected in tasks 1a, 1b, and 1c to develop algorithms and incorporate them into the WEPS model to predict changes in susceptibility to wind erosion due to military vehicle disturbances on DoD training lands and their natural recovery to less degraded states.
- i. A trafficking compaction model has been developed from the bulk density measurements taken at the multi-pass trafficking experiments (in section: Development of a Trafficking Compaction Process Model). This compaction model has been incorporated into WEPS to allow the trafficking vehicle soil compaction effect to be simulated.
 - ii. A list of deficiencies in WEPS along with a discussion of the most feasible remedies have been outlined (in section: Potential use of WEPS for Off-Road Military Trafficking Scenarios). These deficiencies don't preclude its use by military land managers, but addressing these issues would significantly enhance WEPS ability to simulate such scenarios as military trafficking under off-road conditions.
 - iii. An example of using the Single-event Wind Erosion Evaluation Program (SWEEP), a stand-alone version of the wind erosion submodel used in WEPS, has been provided to demonstrate how SWEEP could be applied on military training lands where off-road trafficking has occurred (in section: SWEEP use for Off-Road Military Trafficking Scenarios).
2. Develop and test a prototype, eye-safe, aerosol sensing lidar for real time fugitive dust concentration measurement suitable for monitoring installation fence-line PM levels.
- i. A new rugged lidar instrument - the CELiS and its associated method - was developed and successfully tested for future use in monitoring particulates crossing a fence-line boundary due to military training/testing and other activities.
 - ii. The useful operational range of CELiS is from 300 meters to 4,000 meters. Physical and optical engineering constraints prevent data from being collected too close to CELiS (0-300 m) and signal-to-background constraints (not enough photons) limit the maximum useful range.
 - iii. CELiS is sensitive enough to observe Rayleigh scatter from the atmospheric gases at ranges from 300 – 600 m.

- iv. For the accurate calculation of airborne concentrations of dust, *a priori* knowledge of the particle size distribution of the aerosol is required. Both on-site sampling and the use of literature values are acceptable.
- v. The use of an *in situ* particle counter (MetOne E-Sampler) was useful when dust concentrations were above the detection threshold of the E-Sampler. Conversely, the use of the *in situ* E-Sampler was not useful in clean air conditions. SDL recommends against using an E-Sampler and instead using a particle size distribution measuring instrument such as a GRIMM or a MetOne 212 Profiler.
- vi. While instrument sensitivity is not easily measured, in any given range bin CELiS can typically observe a minimum concentration of wind driven soil dust is $20 \mu\text{g}/\text{m}^3$ for PM_{10} and $10 \mu\text{g}/\text{m}^3$ for $\text{PM}_{2.5}$. This lower limit is defined as a signal-to-background (S/B) ratio of 2.

Benefits

Limited field data are currently available on the impact of military activities on surface characteristics affecting wind erosion susceptibility. In addition measurements of fence-line concentrations of particulate matter from such activities are rarely conducted due to the lack of suitable cost effective field deployable instrumentation. This research will provide a critical step in understanding the impact from off-road military trafficking activities during training exercises on the subsequent change in site susceptibility to wind erosion across a wide range of soils and climates. In addition, the data obtained should assist in evaluating best management practices for mitigating wind erosion events on military sites.

The development of CELiS represents a major breakthrough in providing a cost-effective, portable, field deployable measurement device for use in monitoring fence-line boundary particulate matter concentrations. A small pickup truck can transport the entire CELiS system to the measurement location and an experienced crew of two people can set up the entire CELiS instrument in under two hours. A single CELiS operator can make real time (<10 sec) measurements of airborne dust concentrations at ranges out to 4 km with range resolution of 6 m. A conservative lower limit for CELiS detection sensitivity is $20 \mu\text{g m}^{-3}$ for PM_{10} and $10 \mu\text{g m}^{-3}$ for $\text{PM}_{2.5}$. CELiS can be scanned horizontally over 360° to observe large areas of landscape and create images, or heatmaps, of aerosol concentration. CELiS is eye-safe and does not mandate the use of special safety glasses or to alert the Federal Aviation Administration (FAA) when it is in use.

Objectives

This project was designed to specifically address the following two objectives in the Statement of Need (SoN) proposal request.

1. Improve understanding of fugitive dust emission potential from military activities.

This objective was met by accomplishing a series of four tasks:

- a. Characterizing off-road impacts of military vehicle trafficking on the temporal surface and soil properties as functions of the intrinsic soil properties and the vehicle attributes known to influence vehicle dust emissions and wind erosion susceptibility.
 - b. Determining through laboratory wind tunnel experiments the PM10 emission potential from both undisturbed and trafficked sites.
 - c. Characterizing initial off-road post-trafficking “recovery response” by measuring vegetation and bulk density following trafficking experiments.
 - d. Using data collected from the previous tasks to develop algorithms for eventual incorporation into wind erosion and land management simulation models.
2. Improve DoD’s ability to achieve source compliance and ambient fence-line monitoring for fugitive dust emissions at their installations.

This objective was met by developing and testing new instrumentation to measure fence-line concentrations from large area emission sources as may be produced from military activities on DoD installations. A prototype eye-safe lidar (light detection and ranging) instrument was designed and tested to accomplish this goal. The instrument, known as CELiS (Compact Eye safe Lidar System), provides range-resolved concentrations of PM for a range of 4,000 meters with a spatial resolution of six meters and a time resolution of 10 seconds. Calibration of CELiS data into units of mass concentration (g/m^3) can be accomplished with a single *in situ* point sensor or using archival data of soil types, though the former is preferred.

Background

The U.S. Department of Defense (DoD) conducts military training and testing activities on approximately 12 million hectares of land (Department of Defense, 2013). This land is used for a variety of purposes, which may include residential and commercial activities as well as intensive combat training operations. Many combat training activities require navigating large, heavy off-road vehicles across potentially sensitive and undisturbed off-road locations. These activities can create significant disturbance to the soil surface and affect the local ecosystem (Goran, et al., 1983; Braunack, 1986; Ayers, 1994). The most prevalent impacts include loss of vegetation, soil compaction, and soil loss due to erosion by water and wind (Althoff, et al., 2010). In particular the resulting land condition can create surfaces that are susceptible to dust emissions from wind erosion. This may result in significant air quality challenges, including emissions of regulated particulate matter (i.e., PM₁₀ and PM_{2.5}) and have the potential to impact the local and regional air quality. Although some wind-borne dust events can be classified as exceptional events, soil transport by wind movement can contribute to monitored particulate matter (PM) values that exceed the National Ambient Air Quality Standards (NAAQS) (Ashbaugh, et al., 2003). Suspended wind generated particulate matter (PM) emitted from military installations can be carried long distances from the training land and well beyond property boundaries. Unfortunately, many installations are located in or near existing or proposed air quality non-attainment areas. Accurately quantifying and assessing the particulate emission rates and near-field (within 200 m of the source) deposition resulting from soil-specific, vehicle-specific, and activity-specific scenarios is critical to understanding the impacts in both the near-field area and the downrange area, especially at the installation fence-line.

Soil erosion by wind is a dynamic process that has been well studied in agriculture because it often results in the loss of the fertile top layer of soil, which can reduce agricultural production as well as degrade local air quality (Skidmore & van Donk, 2003; Diaz-Nigenda, et al., 2010). Intensive tillage and other agricultural practices on arid and semi-arid land can contribute to an increase in soil loss due to wind erosion. Many other factors such as unpaved roads, confined animal operations may also contribute to dust emissions due to wind erosion, including the military training exercise effects on the land (Gillies, et al., 2005). The condition of the soil and vegetation after trafficking plays a big role on the amount and length of time that dust could be subsequently emitted from these disturbed areas.

In addition to simulation and field soil studies, previous research on wind erosion has also used wind tunnels under field and laboratory conditions. Several studies (van Pelt, et al., 2010; Sweeney, et al., 2008; Marticorena & Bergametti, 1997) have utilized in-situ semi-portable wind tunnels that are set up directly in the field on the surface of interest. Other studies have utilized large laboratory wind tunnels to control both wind speed and soil surface conditions to some degree (Guoliang, et al., 2003; Kohake, et al., 2010). These studies have shown that wind tunnels can be successfully utilized to study the underlying principles of wind erosion while simulating optimal conditions that contribute to initiating large wind erosion events.

Limited information exists regarding the specific impacts of military training activities on the wind erosion potential of a disturbed (trafficked) site. Many off-road military trafficking studies have been conducted (Althoff & Thien, 2005; Althoff, et al., 2010; Ayers, 1994) but none have focused on the impact on the sites' susceptibility to wind erosion. This study attempts to address that deficiency. In addition, the lack of a portable, cost-effective field deployable fence-line

particulate matter monitoring system has limited the ability to monitor and quantify the emissions generated from military training activities on adjacent off-site locations. An additional task of this project was to conceive and develop a suitable field deployable instrument for quantifying such fence-line emissions.

Off Road Trafficking

Materials and Methods

General Approach

Multi-pass trafficking field experiments were carried out on four U.S. DoD military training sites. At each site, a heavy tracked vehicle and a light wheeled vehicle were used (except at the Yakima Training Center where two different wheeled vehicles were used). The vehicles were driven in figure-8 patterns in cumulative sets of passes to represent a low, medium, and high level of disturbance. One or two soil types were trafficked at each site in three replications for each vehicle/soil combination. After each set of passes, measurements were made and samples extracted for later laboratory analysis to characterize the surface susceptibility to wind erosion and potential emissions of fine particulates. Each measurement or sample was generally taken at specific locations along the figure-8 to include both curved and straight trafficked regions both within the track and from adjacent ridges if present and appropriate for the measurement. Additional measurements were also taken following a “season” of weathering processes (at least through the winter) to occur, which were then used to make an initial assessment on how fast and to what degree the trafficked sites recovered and reduced their susceptibility to wind erosion.

A completely randomized split-plot experimental design was chosen to develop an appropriate statistical analysis of variance for dust emissions measured in the laboratory wind tunnel as well as the other measurements taken in the field. The sampling location (straight path vs curved path), multi-pass and soil effects were examined for both wheeled and tracked vehicles independently. The “R” statistical package (R Core Team, 2015) was used for all analysis conducted.

Field Trafficking Experiments

Site and Vehicle Selections

Sites selected for field experiments (Table 1) included Ft. Riley, KS (FR), Rowan Hill area of Ft. Benning, GA (FB), Yakima Training Center, WA (YTC), and White Sands Missile Range, NM (WSMR). Specific experiment sites were selected in consultation with DOD and SERDP staff. These sites were chosen to represent a diversity of climatic conditions, soil types, and off-road training activities. Two soil textures were identified for testing at FR and WSMR, with one texture class each at FB and YTC.

Table 1. Site characteristics and sampling/re-sampling dates for each trafficking experiment site.

Site*	Trafficking Sampling Dates	Site Latitude Longitude	Elevation (m)	Average Annual		Dominant Vegetation
				Precipitation (mm)	Temperature (°C)	
FR	Oct.-Nov. 2010 Aug. 2011	39° 18' 0" N 96° 55' 19" W and 39° 18' 0" N 96° 55' 6" W	410	838	12.5	big bluestem (<i>Andropogon gerardii</i>), little bluestem (<i>Schizachyrium scoparium</i>), switchgrass (<i>Panicum virgatum</i>), tall dropseed (<i>Sporobolus compositus</i>), and Indiangrass (<i>Sorghastrum nutans</i>)
FB	Jul. 2012	32° 24' 14" N 84° 45' 21" W	145	1234	18.3	southern crabgrass (<i>Digitaria ciliaris</i>), thin paspalum (<i>Paspalum setaceum</i>), orangegrass (<i>Hypericum gentianoides</i>), pine barren ticktrefoil (<i>Desmonium strictum</i>), and sparse small longleaf pine (<i>Pinus palustris</i>)
YTC	Aug. 2012 Jul. 2013	46° 41' 36" N 120° 26' 15" W	480	210	9.3	bluebunch wheatgrass (<i>Pseudoroegneria spicata</i>), prickly lettuce (<i>Lactuca serriola</i>), tumble mustard (<i>Thelypodopsis aurea</i>), thurbers needle grass (<i>Achnatherum thurberianum</i>), cheat grass (<i>Bromus tectorum</i>), sandburg's bluegrass (<i>Poa secunda J. Presl</i>), phlox (<i>Phlox Gracilis</i>), gray rabbit brush (<i>Ericameria Nauseosa</i>) and small flowered willow (<i>Epilobium parviflorum</i>)
WSMR	Jan. 2014 Nov. 2014	32° 24' 58" N 106° 25' 14" W and 32° 24' 49" N 106° 26' 18" W	1224	241	15.9	six-weeks grama (<i>Bouteloua barbata</i>), mouse ear (<i>Tidestromia lanuginosa</i>), narrowleaf globemallow (<i>Sphaeralcea angustifolias</i>), mexican witchgrass (<i>Panicum hirticaule</i>), pigweed (<i>Amaranthus blitoides</i>), trailing windmills (<i>Alliona incarnata</i>) and verbena (<i>Glandularia Bipinnatifida</i>)

*FR = Ft. Riley, KS; FB = Ft. Benning, GA; YTC = Yakima Training Center, WA; and WSMR = White Sands Missile Range, NM.

Two off-road training vehicles were used at each site representing a range of relatively lightweight to very heavy, fully armored military off-road vehicles. Two major categories of vehicles were desired in this study based on their traction type; tracked or wheeled. The vehicles actually used at each site depended upon availability, but both a tracked and a wheeled military vehicle were preferred. Table 2 lists the vehicles used at each site with the month and year trafficking was conducted and travel speed used in the figure-8 trafficking experiments.

Table 2. Vehicles used for trafficking at each experimental site on the specified dates.

Vehicle	Vehicle Type	Approx. Speed (km/h)	Sites*			
			FR	FB	YTC	WSMR
M1025A2 HMMWV	Light Wheeled	25-30	Nov. 2010		Aug. 2012	
M1A1 Abrams tank	Heavy Tracked	8	Oct. 2010	Jul. 2012		
M1151A Up-armored HMMWV	Light Wheeled	25-30		Jul. 2012		Jan. 2014
5 Ton M925A1 Fire Truck	Heavy Wheeled	12			Aug. 2012	
M88-A1 Tank Retriever	Heavy Tracked	8				Jan. 2014

*FR = Ft. Riley, KS; FB = Ft. Benning, GA; YTC = Yakima Training Center, WA; WSMR = White Sands Missile Range, NM.

Table 3 itemizes additional vehicle specifications and other relevant information to this study such as the specific model numbers used, their operating weight, traction type, number of tires on the wheeled vehicles, track width, ground pressure and Vehicle Cone Index (VCI) (Priddy & Willoughby, 2006) for 1 pass (VCI₁) and 50 pass (VCI₅₀) values, which are measures of a ground vehicle's mobility on soft soils. The lower the VCI, the better the basic performance of the vehicle in fine grained soils.

Table 3. Relevant specifications of vehicles used at experimental sites.

Vehicle*	Traction Type	Weight (kg)	Number of tires	Tire or Track width [§] (cm)	Ground pressure (kg cm ⁻²)	Weight per unit area (kPa)	VCI**	
							(1 pass)	(50 pass)
M1025A2 HMMWV	Wheeled	3100	4	32	2.18	N/A	20	47
M1A1 Abrams tank	Tracked	61500	N/A	61	0.97	95	25	58
M1151A Up-armored HMMWV	Wheeled	3800	4	32	0.97	N/A	31	70
5 Ton M925A1 Fire Truck	Wheeled	15000	6	N/A	2.46	N/A	18	N/A
M88-A1	Tracked	50800	N/A	61	0.77	75	20	48

*References:

<http://www.amgeneral.com/vehicles/hmmwv/a2-series/details/m1025a2> [Accessed 1 March 2016]

<http://www.amgeneral.com/files/specs-sheet-m1151-domestic-04-10.pdf> [Accessed 1 March 2016]

<http://fas.org/man/dod-101/sys/land/m1.htm> [Accessed 1 March 2016]

http://en.wikipedia.org/wiki/M939_Truck [Accessed 1 March 2016]

<http://fas.org/man/dod-101/sys/land/m88a1e1.htm> [Accessed 1 March 2016]

<http://www.slideshare.net/QuestSystems/a-primer-on-military-vehicle-mobility-vintage-2003-presentation> [Accessed 1 March 2016]

<http://fas.org/man/dod101/sys/land/m1.htm> [Accessed 1 March 2016]

<http://www.globalsecurity.org/military/library/policy/army/fm/5-430-00-1/CH7.htm> [Accessed 1 March 2016]

<http://www.inetres.com/gp/military/cv/eng/M88.html> [Accessed 1 March 2016]

<http://armyengineer.tpub.com/En5341a/En5341a0127.htm> [Accessed 1 March 2016]

**Vehicle Cone Index (Priddy & Willoughby, 2006) for one pass (VCI₁) and 50 passes (VCI₅₀).

§Single tire or track width, not distance between tires on same axle or distance between tracks.

Bearing pressure on soil equals vehicle's tire pressure for wheeled vehicles (<http://aec.army.mil/portals/3/nepa/asv-pea.pdf> [Accessed 1 March 2016]).

The first installation selected for testing was Ft. Riley, KS (FR). This site is located in the Flint Hills region of North Central Kansas in both Geary and Riley counties. The installation covers 407 km², with 287 km² being utilized for maneuver training (U.S. EPA, 2010). FR is a historic military site that has been an active installation since the mid-1800s. Testing at FR was conducted on both a silty clay loam and a silt loam soil at two nearby locations. Both an M1A1 Abrams tank (Federation of American Scientists, 2014) and a Model M1025A2 High Mobility Multipurpose Wheeled Vehicle (HMMWV) (AM General, 2015) were used for trafficking at FR (Figure 1).



Figure 1. M1A1 Abrams tank (left) and HMMWV (right) used at Ft. Riley, KS.

The second installation site, Ft. Benning, GA (FB) is located on 765 km² of land area in West Central Georgia. This site is located in the humid Southeastern U.S., with relatively high precipitation and is affected by tropical maritime events including frequent thunderstorms and inland moving hurricanes. Testing at FB was done on a loamy sand soil. The two vehicles (**Figure 2**) used were a HMMWV heavily up-armored vehicle (Model M1151A1) (AM General, 2011) and an M1A1 Abrams tank (Federation of American Scientists, 2014).



Figure 2. M1A1 tank (left) and up-armored HMMWV (right) used at Ft. Benning, GA.

The third site tested, the Yakima Training Center, WA (YTC), is situated on 1,323 km² of shrub-steppe land in South Central Washington. This site is located in the Yakima Valley region which is mild in temperature and very dry. YTC has relatively low precipitation, receiving an average of 207 mm of precipitation annually with an average annual temperature of 9.8 °C. The local topography is highly varied with a large variety of local ridges and valleys. Trafficking experiments completed at YTC were conducted on a loam soil type using two wheeled vehicles (**Figure 3**) since a tracked vehicle was not available. Therefore, a fully loaded 5-ton 6x6 M925A1 water tanker fire truck (Fire Truck) (Wikipedia, 2015) was used in addition to a light armored M1025A2 HMMWV (AM General, 2015).



Figure 3. HMMWV (left) and 5-ton Fire Truck (right) used at Yakima Training Center, WA.

The fourth and final site was the White Sands Missile Range, NM (WSMR) located in South Central New Mexico which covers 8,300 km². Vegetation at this site is Chihuahuan desert scrub and desert grasslands. Trafficking (**Figure 4**) utilized a heavily up-armored (Model M1151A1) HMMWV (AM General, 2011) and an M88-A1 tank retriever (Federation of American Scientists, 2014). Each vehicle was trafficked on a loamy sand as well as a sandy loam soil location.



Figure 4. Up-armored HMMWV (left) and M88-A1 Tank Retriever (right) used at White Sands Missile Range, NM.

Site Preparation

At each of the installations, relatively undisturbed sites were identified for testing. The sites may have been utilized for training activities at some point in the past, but all sites had been undisturbed for an extended period of time and consisted of plentiful natural vegetation growth, for the climatic conditions at the sites. In the case of Ft. Riley, the prairie grasses were so dense, that we were afraid that it would take the HMMWV an excessive number of passes to sufficiently destroy enough of the initial vegetation to obtain measurable differences between the desired pass levels. Thus, it was deemed necessary to mow and remove most of the vegetation by raking the excess biomass at this site prior to conducting the trafficking experiments (**Figure 5**). This also allowed for more comparable initial soil surface vegetation conditions with the other lower precipitation sites studied.



Figure 5. Mowing (left) and rake used (right) at Ft. Riley, KS site prior to conducting trafficking experiments.

Rectangular plots (40 m × 80 m) were staked out using GPS equipment at each of the installations. Three replications were randomly labeled for each vehicle/soil combination at each site. Three levels of trafficking intensity were conducted on each replication with samples being taken after each trafficking intensity level as well as before testing to determine initial conditions. Samples collected are described later.

Plots were staked out so that vehicles could be driven in a figure-8 pattern similar to Althoff et al. (2010) trafficking scheme within the rectangular field plots that were established at each experimental site (**Figure 6**). This trafficking pattern was chosen to provide two primary methods of vehicular travel: a) straight-line and b) curved for sampling, as well as a third smaller “center cross-over” region where the number of trafficking passes were doubled. The figure-8 plot locations were selected within the chosen sites so that obstructions such as trees, large brush, ravines, etc. could be avoided.



Figure 6. Example of figure-8 traffic patterns on the landscape at Yakima Training Center, WA.

Field Experiments

The number of trafficking passes for each vehicle was initially determined from pre-experiment test trials conducted using the same figure-8 trafficking pattern previously described at Ft. Riley to represent a low, medium, and high level of disturbance upon the soil and surface state. The number of passes for each vehicle's level of disturbance was visually determined based on the differences expecting to be measurable. Thus, the M1A1 tank on the "tracked" plots were trafficked 1, 4, and 5 times during the three sets of passes for a cumulative total of 1, 5 and 10 passes at the conclusion of each set of passes. Because the HMMWV wheeled vehicle caused significantly less disturbance to the soil surface, the HMMWV on the "wheeled" plots was trafficked 10, 15 and 25 times during the three sets of passes for a cumulative total of 10, 25 and 50 trafficking passes at the conclusion of each set of passes. Likewise, the Fire Truck at Yakima, since it was lighter than the tracked vehicles used and heavier than the HMMWV's, it was trafficked 2, 8 and 10 times during the three pass sets for a cumulative total of 2, 10 and 20 trafficking passes at the conclusion of each set of passes. The three sets of passes are referred to as p1, p2, and p3 throughout this document when referring to all the vehicle experiments, while the un-trafficked initial condition is referred to as p0. The numbers of trafficking passes for each vehicle at each site are summarized in Table 4.

Table 4. Number of passes conducted per trafficking set by each vehicle at each site.

Site†: (Vehicle)	1 st set of passes (p1)*	2 nd set of passes (p2)*	3 rd set of passes (p3)*	Cumulative passes after (p1)*	Cumulative passes after (p2)*	Cumulative passes after (p3)*
FR: (M1A1)	1	4	5	1	5	10
FB: (M1A1)	1	4	5	1	5	10
WSMR: (M88-A1)	1	4	5	1	5	10
YTC: (Fire Truck)	2	8	10	2	10	20
FR: (HMMWV)	10	15	25	10	25	50
FB: (up-armored HMMWV)	10	15	25	10	25	50
YTC: (HMMWV)	10	15	25	10	25	50
WSMR: (up-armored HMMWV)	10	15	25	10	25	50

*p1, p2, p3 = first, second and third levels of figure-8 consecutive trafficking passes.

†FR = Ft. Riley, KS; FB = Ft. Benning, GA; YTC = Yakima Training Center, WA; WSMR = White Sands Missile Range, NM.

The experimental treatments and sampling procedure was as follows: a) prior to any trafficking on a plot, initial conditions were measured (e.g., all relevant wind erodibility samples (defined later) were collected); b) the first set of trafficking passes was applied, at the end of which the same wind erodibility samples were taken; c) the next set of passes was applied to the same plot and again all relevant samples were taken; and d) the last set of trafficking passes was applied with all relevant samples taken for a final time. All initial condition data were typically collected on the first day at each site. All post-trafficking pass level measurements for each figure-8 replication were conducted on the same day, if possible. To minimize the time required for driver availability, more than one figure-8 replication was being trafficked on a given day, so the time between the pass level samplings ranged from 2 to 5 hours, depending upon the interleaving of the trafficking of the figure-8 replications. The vehicle driver was instructed to take extra care to ensure that the vehicles stayed within the same tracks as best possible during all trafficking passes. The degree of disturbance to the soil and the vegetation partly depends on how the vehicles are operated. Disturbances on straight sections were expected to be less severe than vehicles making turns (Ayers, 1994). To accommodate both turning and straight runs, the vehicles were operated in a continuous figure-8 pattern with a minimum inside turning radius of 10 m. All samples were obtained away from the vehicle entry and exit location of the figure-8 pattern, which was noted and kept the same from pass set to pass set. All figure-8 plots for each soil site were randomized for replication and trafficking vehicle used.

An initial set of samples prior to trafficking (p0) was obtained for assessing the relative degree of surface changes that occurred under the different trafficking levels relative to the original un-trafficked condition. These data were taken at location(s) adjacent to or inside the figure-8. Care was taken to ensure that the initial destructive measurement sampling locations would not interfere with the after-trafficked sampling. At Ft. Riley, a single location was sampled for initial data, labeled L0, and was obtained from inside the figure-8 curves. At subsequent sites, the protocol was modified and additional initial samples were taken near the tracks for each sampling location to improve the statistical analysis. No additional data from undisturbed locations were obtained after the start of trafficking. In each of the figure-8 plots, samples were taken from four distinct segments within the vehicle tracks after the trafficking. The sampling segments were designated as Straight Section (SS), Center Cross (CC) (where the tracks crossed and double the trafficking passes occurred), Curve Outside track (CO), and Curve Inside track (CI) as shown in **Figure 7**.

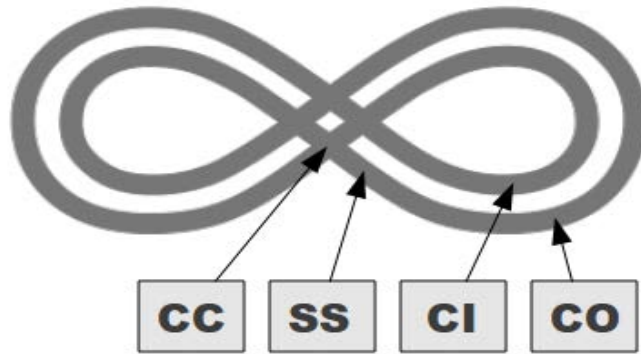


Figure 7. Figure-8 plot with relative sampling locations identified where CC = Center Cross, SS = Straight Section, CI = Curve Inside track, and CO = Curve Outside track, L0 (not shown) = un-trafficked location inside figure-8.

Additional sampling zones are the ridges created due to shearing and soil displacement just outside the curved trafficking sections (i.e., Ridge Inside and Ridge Outside) of the tracks and the deposition regions just outside those ridged areas (i.e., Deposition Inside and Deposition Outside) referred to respectively as the RI, RO, DI and DO sampling zones (**Figure 8**).



Figure 8. Location of additional sampling zones within curved trafficking region, where RI = Ridge Inside, RO = Ridge Outside, DI = Deposition Inside, DO = Deposition Outside from an M1A1 trafficked plot at Ft. Riley after at least 5 trafficking passes (picture of M1A1 tracked vehicle at Ft. Riley).

All of these sampling areas are referred to as “sampling location” in this study. Samples were taken from the center of the tracks in the trafficked regions. Sampling locations from previous trafficking passes were avoided due to the destructive nature of some of the sampling methods. A more complete description of each sampling location and any special consideration for those locations are described in Table 5.

Table 5. Description of all sampling locations on the figure-8 plots.

Symbol	Sampling Location	Sampling Location Definition
LO	Initial sampling location	Un-trafficked area inside the figure-8 (Ft. Riley, KS location only). All other sites contained initial samples taken near the CC, SS, CI and CO locations and thus were identified as such.
SS	Straight Section	The straight trafficked section between the track crossover and the beginning of a curved section.
CI	Curve Inside	The inside curved trafficked sections.
CO	Curve Outside	The outside curved trafficked sections.
CC	Center Cross	One of the four center sections where the tracks crossed over each other and received double the trafficking passes.
RI	Ridge Inside	The ridge outside the inner track on the curved section. This ridge forms from soil displacement due to vehicle tracks or wheels while traversing the turns.
RO	Ridge Outside	The ridge outside the outer track on the curved section. This ridge forms from soil displacement due to vehicle tracks or wheels while traversing the turns.
DI	Deposition Inside	The dust deposition zone just outside the inside track ridge.
DO	Deposition Outside	The dust deposition zone just outside the outer track ridge.

The general locations for each type of sampling conducted or parameter measured are listed in Table 6. Sampling considerations and any deviations from the above stated sampling protocols for each specific sample or parameter are provided later in their respective sampling methods sections. The “Post-trafficking data” column in Table 6 refers to the data sampling that occurred the following year after the initial trafficking. This sampling was conducted after at least one over-wintering season at all sites except Ft. Benning, GA (that site was co-opted by the Army immediately after our initial trafficking experiments for other purposes which did not lend itself to subsequent sampling). The objective of the “post-trafficking” sampling was to obtain an

initial indication of the degree of each site's recovery response to the multi-pass trafficking due to natural weather driven processes such as precipitation, freeze/thawing and freeze/drying on bulk density, moisture content, species diversification, vegetation regrowth, rodent and other animal trafficking/burrowing, etc. compared to the un-trafficked regions.

Table 6. Location sampling zone of each data sample collected from each figure-8 plot (see Table 5 for sampling location definitions).

Sample or parameter measured	Initial condition (p0)[†]	After 1st trafficking set (p1)[†]	After 2nd trafficking set (p2)[†]	After 3rd trafficking set (p3)[†]	Post-trafficking data
Wind Tunnel Trays	L0 (CI,CO,SS)	CI,CO,SS	CI,CO,SS	CI,CO,SS	
BD/MC* (0-5, 5-10, 10-15 cm)	L0 (CC [§] ,CI,CO,SS)	CC,CI,CO,SS	CC,CI,CO,SS	CC,CI,CO,SS	CI,CO,SS
PI-SWERL	L0 (CC,CI,CO,SS)	CC,CI,CO,SS, DI,DO	CC,CI,CO,SS, DI,DO	CC,CI,CO,SS, DI,DO	
ASD [‡]	L0 (CI,CO,SS)	CI,CO,SS,RI, RO	CI,CO,SS,RI, RO	CI,CO,SS,RI, RO	
RR (parallel and perpendicular)	L0 (CI,CO,SS)	CI,CO,SS,RI, RO	CI,CO,SS,RI, RO	CI,CO,SS,RI, RO	
Biomass** (by species)	L0 (CI,CO,SS)	CI,CO,SS,CC	CI,CO,SS,CC	CI,CO,SS,CC	CI,CO,SS
Vegetation Cover	L0 (CI,CO,SS)	CI,COSS	CI,CO,SS	CI,CO,SS	CI,CO,SS

[†]p0, p1, p2, p3 = initial, first, second and third levels of figure-8 consecutive trafficking passes (see Table 4).

*BD/MC = Bulk Density and Moisture Content at three depths (0-5, 5-10, 10-15cm).

**Biomass only split by species for post-trafficking measurements at Fort Riley, KS location due to pre-experiment mowing.

[§]Initial CC location BD/MC data not collected at YTC.

[‡]Ridge samples were not taken for ASD at YTC as no aggregates were formed under trafficking.

PI-SWERL = Portable In-Situ Wind Erosion Research Laboratory device.

ASD = Aggregate Size Distribution; RR = Random Roughness.

L0 = initial conditions sample location (FR only); CI = Curve Inside; CO = Curve Outside; SS = Straight Section.

CC = Center Cross section; DI = Deposition Inside; DO = Deposition Outside; RI = Ridge Inside; RO= Ridge Outside.

Soil Characterization

Particle size distribution data for each site are presented in Figure 9 and Table 7. Across all sites, sand content ranged from 7.9 to 87.7, silt ranged from 9.5 to 70.7, and clay ranged from 2.8 to 28.0. As can be seen in Figure 9, the sites covered a wide range of soil textures, especially so for the sand and silt contents with relatively low clay (<30%) in the surface soils. A range of typical erodible soil textures were obtained from installations where wind erosion is most likely in the U.S. (Figure 10). Figure 10 is simply based on the USDA Soil Conservation Service (now the USDA-NRCS) knowledge of where wind erosion is likely to occur on U.S. croplands based on experience and such factors as soil inherent wind erodibility (e.g., soil texture and resulting aggregates), vegetative cover potential resulting from precipitation patterns, and wind energy across the U.S. The map implies that there is an increased potential for wind erosion in the red areas if military vehicle disturbance is excessive and could continue if vegetative recovery is not promoted.

Soil characterization samples from each figure-8 were taken prior to trafficking as bulk samples from the upper 5 cm of the surface. For dispersed particle-size distribution (%), the clay content was determined by pipette, total sand (2.0 to 0.05 mm) and sand fractions (2 to 1, 1 to 0.5, 0.5 to 0.2, 0.2 to 0.1, and 0.1 to 0.05 mm) by sieving, and silt (0.002 to 0.05 mm) was determined by difference (100-(clay+sand)) according to the method of Gee and Dani (2002).

Soil organic matter (OM), calcium carbonate equivalent (CaCO_3), and cation exchange capacity of the <2.0-mm fraction of each sample was determined by the Kansas State University Soil Testing Laboratory. OM was determined by loss on ignition at 400°C (Schulte and Hopkins, 1996) and CaCO_3 by the method of Leo (1963). CEC was determined by sodium saturation at pH 8.2 (Sumner and Miller, 1996). A summarization of these intrinsic soil property values are provided in Table 8.

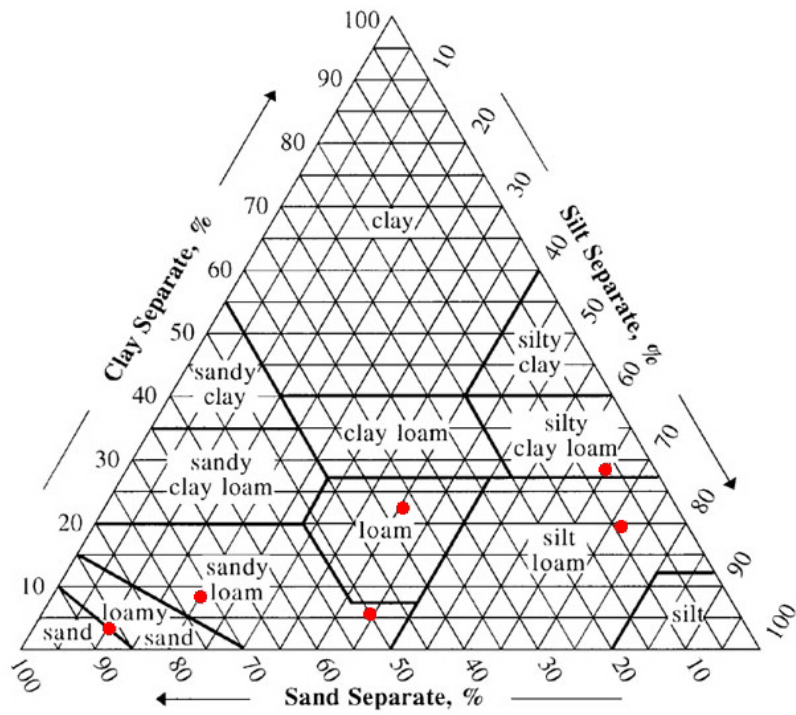


Figure 9. Distribution of soil texture classes among all experiment sites included a loamy sand, two sandy loams, a loam, a silt loam and a silty clay loam (red dots).

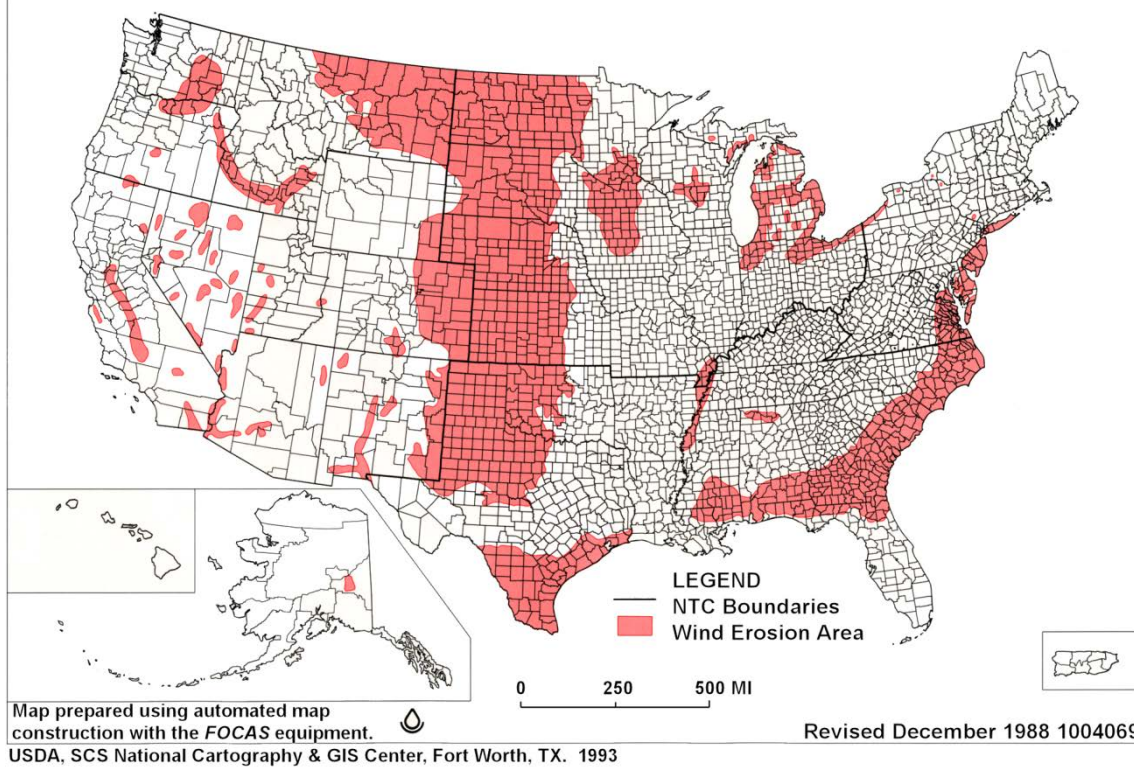
AREAS WHERE WIND EROSION OCCURS ON CROPLAND

Figure 10. Map of areas where wind erosion is likely to occur on cropland in the United States.

Table 7. Soil particle size distribution for the trafficking experiment locations.

Site*	Soil Texture	Clay	Silt	Sand	Very Coarse Sand	Coarse Sand	Medium Sand	Fine Sand	Very Fine Sand
		----- % -----							
FR	silt loam	19.0±4.8	70.8±4.1	10.2±1.1	1.0±0.7	1.5±0.4	1.7±0.5	1.7±0.4	4.5±0.5
FR	silty clay loam	28.0±5.7	64.1±5.6	7.9±1.3	0.8±0.6	1.5±0.3	1.0±0.2	1.1±0.3	3.6±0.7
FB	loamy sand	2.8±1.0	9.5±1.7	87.7±2.4	1.9±0.6	16.3±3.3	37.1±2.5	27.1±3.0	5.4±1.5
YTC	sandy loam	5.0±1.0	43.7±3.4	51.3±3.2	0.9±0.3	1.9±0.3	8.3±0.8	27.5±2.1	12.7±0.5
WSMR	loam	21.9±3.5	39.7±10.0	38.4±9.6	0.8±0.7	1.6±0.9	3.6±1.1	13.6±4.2	18.9±4.7
WSMR	sandy loam	7.7±1.3	19.3±3.7	73.0±4.8	5.5±2.1	7.6±2.1	12.0±1.7	24.1±2.6	23.9±2.7

±Denotes one standard deviation from the mean values of six replicated samples.

* FR = Ft. Riley, KS; FB = Ft. Benning, GA; YTC = Yakima Training Center, WA; WSMR = White Sands Missile Range, NM.

Table 8. Average soil chemical and physical properties for the study sites.

Site	Soil Texture	OM (%)	CaCO ₃ (%)	CEC (meq 100 g ⁻¹)	IWC (%)	IBD (g cm ⁻²)	OWC (%)	PD (g cm ⁻²)
FR	silt loam	4.0±0.6	4.7±1.2	2.3±0.1	15.5±2.4 ^T	1.25±0.02 ^T	20.5±1.1	1.60±0.08
					16.9±1.2 ^W	1.28±0.06 ^W		
	silty clay loam	4.1±0.5	7.6±1.9	2.9±0.3	17.8±1.0 ^T	1.23±0.14 ^T	23.5±1.3	1.51±0.07
					20.7±2.4 ^W	1.21±0.03 ^W		
FB	loamy sand	0.9±0.3	5.2±1.3	0.3±0.02	3.4±0.7 ^T	1.61±0.08 ^T	8.6±0.5	1.82±0.05
					3.2±0.8 ^W	1.62±0.09 ^W		
YTC	sandy loam	2.1±0.5	5.1±1.4	1.2±0.1	3.2±0.5 ^{FT}	1.34±0.09 ^{FT}	17.0±0.8	1.65±0.03
					3.7±0.8 ^W	1.32±0.04 ^W		
WSMR	loam	1.8±0.8	4.0±0.03	20.9±4.0	6.9±1.1 ^T	1.22±0.06 ^T	18.4±1.7	1.67±0.04
					6.3±1.2 ^W	1.25±0.14 ^W		
	sandy loam	0.8±0.1	1.7±0.01	6.3±0.7	2.7±0.2 ^T	1.48±0.05 ^T	8.9±0.5	1.94±0.01
					3.3±0.1 ^W	1.46±0.06 ^W		

OM is soil organic matter; CaCO₃ is calcium carbonate equivalent; CEC is cation exchange capacity

IWC is initial water content; IBD is initial bulk density (0-15 cm depth) prior to trafficking

OWC is the optimum water content; PD is the Proctor Density

T denotes tracked vehicles (M1A1 and M88-A1)

W denotes light wheeled vehicles (HMMWV)

FT denotes the Fire Truck

± denotes one standard deviation of six replicated samples

* FR = Ft. Riley, KS; FB = Ft. Benning, GA; YTC = Yakima Training Center, WA; WSMR = White Sands Missile Range, NM.

Optimum water content and Proctor Density were determined by ASTM Standard D698 (2012). The Proctor Test used a 4-inch-diameter (100 mm) mold which holds 1/30th cubic foot of soil and calls for compaction of three separate lifts of soil using 25 blows by a 5.5 lb (2.5 kg) hammer falling 12 inches (305 mm), for a compaction effort of 12,400 ft-lbf ft⁻³ (593,708 J m⁻³). The equipment for obtaining the Proctor data deviated from the ASTM standard specifications with a 5 inch diameter (127 mm) mold with a depth of 6 5/8" (168 mm). These additional intrinsic soil property values are listed in Table 8 along with the initial temporal soil conditions; initial bulk density (IBD) and initial water contents (IWC) measured prior to the trafficking experiments.

Field Data Collected

Table 6 previously listed the sampling zone locations for all data samples collected prior to and after the trafficking experiments, including the “recovery” data obtained at a later date. The specific data collected included: a) soil extracted and placed in wind tunnel trays for later laboratory wind tunnel analysis; b) bulk density and water content samples by depth (0-5, 5-10 and 10-15cm); c) Portable In-Situ Wind Erosion Laboratory (PI-SWERL) data; d) surface bulk

samples which were rotary sieved in the laboratory to determine their aggregate size distribution (ASD); e) surface roughness measurements to determine the random roughness (RR) of the tracked surfaces and ridges parallel and perpendicular to the track direction; f) vegetation species identification and attached (standing) biomass per unit area for each species; and g) vegetation cover.

Wind Tunnel Trays

Samples for laboratory wind tunnel analysis were collected at each sample location from the top 6 cm of the soil profile. A 122×20 cm area was removed with a flat bottom shovel to an approximate depth of 5 cm (Figure 11). The soil was carefully placed in these specially built wind tunnel trays and transported to the laboratory with care to minimize disturbance. See Appendix A for details on sampling and transportation of wind tunnel trays as well as the wind tunnel specifications and tunnel dust sampling protocols. Appendix A provides a complete description of the procedures followed to remove and transport the wind tunnel trays to the laboratory. Tray samples were taken prior to trafficking at each figure-8 location as well as after each pass level within the tracks at the outside and inside curved sections (CO, CI) and from the straight section (SS) regions as specified previously in Table 6.



Figure 11. Wind tunnel tray sample extracted from the Yakima Training Center, WA site.

In the laboratory, the wind tunnel trays were initially laser scanned to determine their surface random roughness and the vegetation surface cover present on the trays were measured. The trays were then placed within a laboratory wind tunnel to obtain emissions data through two tests. First, a “non-abrader” test was conducted to measure the amount of loose erodible material (LEM) that would be released under a 13 m s^{-1} free-stream wind speed for five minutes duration. Second, an “abrader” test was then conducted where the trays were exposed to a fixed amount of abrader (15 kg) which was introduced upwind to determine the effects of saltation abrasion impacts on emissions from the tray surface. A complete description of the outdoor wind tunnel sampling train, and instrumentation are provided in 0 along with the complete procedures and protocols used for the two laboratory wind tunnel tests.

Portable In-Situ Wind Erosion Laboratory (PI-SWERL)

The PI-SWERL device, shown in Figure 12, is an instrument developed by the Desert Research Institute (DRI) researchers (Etyemezian, et al., 2007) and briefly described here: <http://www.dri.edu/pi-swerl> (accessed Sep. 20, 2016). More detail on the PI-SWERL is provided in Appendix A. The PI-SWERL uses a rotating high-speed annular ring and a digital

portable aerosol monitor to determine emissions as a result of the shear stress caused by the spinning ring. The PI-SWERL is battery powered and is a portable and economical method of testing emissions in a field setting. This instrument was developed to allow ease of transporting and designed to be used in unpaved road and rugged terrain conditions as opposed to utilizing a full-size field wind tunnel setup. This device was utilized to obtain estimates of potential dust emissions in the field at locations specified in Table 6 and to see what, if any, correlations between the standard reference laboratory wind tunnel experiments and PI-SWERL data exist.



Figure 12. Portable In-Situ Wind Erosion Research Laboratory (PI-SWERL).

PI-SWERL measurements were taken in the field at the time of the vehicle trafficking tests to determine the amount of PM10 emissions available on the surface (**Figure 13**) and compare with the standard laboratory wind tunnel tray testing results. At each sampling location where a wind tunnel tray sample was collected, a measurement was also taken with the PI-SWERL instrument. The measurement was taken in close proximity to the tray locations to allow for possible correlation between the two different methods for determining potential loose particulate emissions. As identified in Table 6, in addition to the wind tunnel tray sampling locations (CI,CO,SS), PI-SWERL samples were also taken in the Center Cross (CC) section and within the deposition region zones (DI and DO) outside the ridges created from the vehicles while trafficking in the turns (Figure 8).



Figure 13. PI-SWERL setup in the field at Yakima Training Center, WA for collecting data.

The PI-SWERL allows the user to select the testing scheme to be used with such variables as test duration and rotational speed of the annular ring. For all Ft. Riley tests, a ramp-style test leading to a maximum of 4000 revolutions per minute (rpm) was selected based on previous experiments conducted by DRI researchers (Etyemezian, et al., 2007) and through personal communication with DRI. A ramp-style test was used to simulate three different surface shear stress values that roughly correlate to three increasing wind speeds. After the initial 60 second cleanout period, the spinning ring was first increased from 0 to 2000 rpm over a 60 second interval. It maintained this speed for 60 seconds before being increased to 3000 rpm over the next 60 seconds. This sequence was then continued at 4000 rpm. After 60 seconds at the final rpm speed, the disk rotation was quickly stopped and data collection continued for a final 60-second cleanout period before termination of the test.

After attempting to follow the same protocol at Ft. Benning, the high concentrations measured eventually caused the DustTrak to no longer zero calibrate. Subsequently changes were made to the sampling protocol at Yakima. Because of the very fine texture and minimal aggregation of the surface, a significantly greater quantity of suspended particulate matter was generated by the PI-SWERL at the Ft. Benning, Yakima, and White Sands Missile Range sites at the higher speed settings after trafficking. Therefore, the DustTrak instrument used to measure dust generated by the PI-SWERL would often reach its upper sampling limit of 400 mg m^{-3} of PM₁₀ particles under the higher multi-pass trafficking sets. Because of this, the sampling scheme used on the PI-SWERL at Yakima and White Sands Missile Range was manually adjusted in the field to lower the maximum angular velocity blade speeds when one began reaching the DustTrak

measuring limit. Because of these unplanned but necessary changes in testing parameters, it became more difficult to analyze and compare the PI-SWERL data among the various sites as well as to the wind tunnel tray tests. However, the 2000 rpm setting was used across most of the trafficking and un-trafficked conditions, so only that portion of the data are used for the PI-SWERL data analysis in this study.

Bulk Density and Soil Water Content

Bulk density was taken using the hammer driven core method (Grossman & Reinsch, 2002) with a core diameter of 4.83 cm. The soil cores were split into three layers of 0-5, 5-10, and 10-15 cm and placed in soil moisture cans for both bulk density and water content determination. The soil cores (91.6 cm³) for each depth were weighed before and after drying in an oven at 105°C for at least 48 h. Bulk densities and moisture contents were then calculated using those two weight measurements, the can weights, and volume of the cores samples. The sampling locations are identified as BD/MC in Table 6. Note that there was soil shearing and displacement which occurred within the curved (CI and CO) locations, especially with the heavy tracked vehicles (Figure 8).

This meant that the multi-pass sample depths did not contain the identical soil layers sampled during the initial conditions at these locations. This is again noted when relevant in the analysis and discussion of this data.

Aggregate Size Distribution (ASD)

Aggregate samples were taken for determination of aggregate size distribution (ASD). ASD is important in determining the wind erodible fraction (particles less than 0.84 mm in diameter) within the soil surface. Since aggregates of various sizes contribute to surface roughness, ASD also plays a role in determining the aerodynamic roughness of the soil surface. ASD also defines the quantity of larger non-erodible size aggregates available that can provide sheltered protection to the smaller erodible size aggregates on the surface. As such, it is important to collect all sizes represented in the upper 10 cm of the soil (typically, the sampling depth is adjusted to include the largest size aggregates). Surface aggregates were sampled from the upper 10 cm of the soil using a flat bottom scoop to get a representative sample of all aggregate sizes. Samples were air-dried and ASD determined using a rotary sieve (Lyles et al. 1970) to separate aggregates into size classes (>44.45, 44.45-19.05, 19.05-6.35, 6.35-2.0, 2.0-0.84, 0.84-0.42, <0.42 mm). The erodible fraction (EF - mass % <0.84 mm), and geometric mean diameter (GMD) and geometric standard deviation (GSD) were calculated according to Nimmo and Perkins 2002 from the size distribution. The sampling locations identified in Table 6 were followed at all locations except the HMMWV at Ft. Riley, KS. This was due to an error in ASD sampling where some CI and SS samples were not obtained at Ft. Riley, KS for that vehicle.

Random Roughness (RR)

Surface roughness is an important factor in determining the susceptibility of a soil surface to wind erosion emissions in the absence of vegetative cover. The rougher the surface, in general, the more protection is afforded to erodible size aggregates, due to the increase in the threshold surface friction velocity for a given wind speed. Surface roughness was obtained using a line transect pin meter. The surface random roughness is defined as the standard deviation of the elevation differences at each of the measured points (Allmaras, et al., 1966) after subtracting the average slope of the transect line. The pin meter data is collected with a digital camera and the

photos processed with image analysis software to determine the relative elevation of the pins. The pin meter used contains 101 pins with a pin spacing of 10 mm (**Figure 14**).



Figure 14. Using a pin meter to take transect surface elevation data across tracks at WSMR.

Soil Attached Biomass and Vegetation Cover

Soil attached (standing) biomass within a 0.25 m² square frame was clipped to ground level and divided into grasses and forbs with the species later identified (Figure 15). Clipped plants were dried at 60°C for at least 48 hours and weighed. Surface vegetation cover was measured using a 15 m beaded string containing 100 evenly spaced beads and was laid along a vehicle track (Figure 16). Plant intersections were counted and percent cover calculated according to Sloneker and Moldenhauer (1977). In all locations identified in Table 6, samples were taken both before and after trafficking. Prior to trafficking, samples were taken both pre- and post-mowing at Ft. Riley. Samples were also taken the following summer after sufficient regrowth had occurred at Ft. Riley and similar samplings were conducted at Yakima and White Sands Missile Range. No subsequent vegetation sampling was possible at Ft. Benning due to additional military maneuvers at the site being scheduled shortly after our trafficking experiment was concluded. A more detailed description of the experimental design regarding the vegetation sampling protocols used is given by Retta et al. (2013). In addition, the vegetative cover was also taken on the individual wind tunnel trays to more precisely reflect its effect on the emission measurements from the wind tunnel tests.



Figure 15. Soil attached biomass sampling method used at all sites.



Figure 16. Beaded string method used for measuring surface cover at all sites.

Results and Discussion

Due to the extensive amount of information provided here, it seems appropriate to provide a brief overview of how the data is presented to assist the reader interested in only specific portions of this section. First, key physical processes which were evident and clearly observed during the multi-pass vehicle trafficking experiments are initially presented and discussed, as they ultimately explain many of the results obtained. Second, since vegetation is the principle means available for providing protection against wind erosion at all the study sites and directly influence the resulting measured emissions, the vegetation cover and attached biomass (initial standing vegetation) data are then discussed. Likewise, the aggregate size distribution on the soil surface is then presented, which directly reflects both the availability of material for dust emissions (amount of small erodible size particles and aggregates) and the degree of protection to dust emissions by wind (amount and size of large non-erodible aggregates). Then the non-abrader and abrader wind tunnel data are presented and discussed in relation to both the pre- and post-traffic vegetation present in that test data and the measured aggregate size distribution on the surface.

Since the Desert Research Institute's PI-SWRL was developed as a convenient device for making *in-situ* measurements of PM₁₀ emissions from roadways, these measurements were compared to the standard wind tunnel tray measurements to determine the degree of correlation, if any, between these two measurement test methods. The subsequent compaction that occurred during the multi-pass trafficking experiments is then discussed as it directly affects vegetation re-growth following trafficking and thus impacts the recovery of the primary protection to wind erosion on these sites. The trafficking compaction model developed for WEPS is then presented as well as a discussion of the current WEPS' suitability for use by military land managers followed by an example of using SWEEP (Stand-alone Wind Erosion Evaluation Program) for determining wind erosion susceptibility on trafficked off-road military sites. Finally, the initial natural recovery data obtained from the sites following one over-winter season is presented and discussed.

Field Experiments

Several trends observed in the field while conducting these multi-trafficking experiments ultimately help explain much of the data obtained and were also ultimately supported by the wind tunnel experiments. First, it was observed that the trafficking effects were visually very different between the "curved" and "straight" trafficked regions of the figure-8 plots. This was true not only for all vehicles, but also under all levels of trafficking passes at all sites. Example photos are shown in **Figure 17** from Ft. Riley for both the HMMWV and the M1A1 tank, but similar results occurred at all sites. As anticipated, the heavier vehicles and the tracked vehicles did more "damage" in general to the soil surface and vegetation than the lighter and wheeled vehicles (see **Figure 17**, photos were taken after 50 passes compared to the single pass photo for the M1A1 tank), but the primary visual differences between the curved and straight trafficked regions of the figure-8 plots were still evident across vehicle types. It was hypothesized that change in surface conditions in the curved portions of the figure-8 plots were more extensive since the shearing action due to turning would do more damage to the existing vegetation and soil surface. Obviously, as expected, the shearing action was more intense with the tracked and heavier wheeled vehicles but still very visually evident that the same process was occurring with the lighter wheeled vehicles as well.



Figure 17. Figure-8 plot of curved traffic regions (left) and straight trafficked regions (right) for both the HMMWV (top) after 50 passes and the M1A1 tank (bottom) after one pass at Ft. Riley, KS.

This shearing action not only flattened the existing vegetation, but also removed the surface vegetation, and in some cases the vegetation roots, as the vehicles dug into the soil on the curves. In addition to vegetation removal due to the shearing action, it also displaced the existing surface, especially with the tracked vehicles, in the figure-8 curves, which essentially left previously buried soil on the trafficked surface. The displaced soil created significant (measurable) ridges outside the tracks in these turns. Therefore, existing vegetation disappeared faster in these turns, but the soil surface in the curved region of the trafficked portion of the figure-8 plots did not become as susceptible to wind erosion as expected since less erodible, previously buried soil was now exposed on the surface.

This is in contrast to the straight trafficked region surfaces, which were primarily being impacted with only the weight of the vehicle multiple times from the multi-pass trafficking. This effect presumably caused only a simple crushing and grinding action on the surface as well as compaction, destroying any crust present and pulverizing any surface aggregates. In addition, the vehicles would only flatten the existing standing vegetation since there was little or no side shear in the straight trafficked sections. Thus minimal soil displacement and less vegetation removal/degradation occurred here compared to the curved trafficked regions for all vehicles. This is visually evident in **Figure 17** when comparing the photos from Ft. Riley on the left and right sides for both the HMMWV and M1A1. Similar results were visually observed at all sites.

Tracked Vehicle Trafficking Effects on Vegetative Cover

Vegetation cover is the preferred protection against soil erosion by both water and wind. If the soil surface is not exposed to the wind, it will not erode. The tracked vehicle overall ANOVA results shown in Table 9 indicate that each of the main factors, soil, sampling location and trafficking pass level, along with all the interactions are highly significant with the pass level effect being the greatest. This is not unexpected since the vegetative cover would normally be expected to decrease with any level of trafficking, either wheeled or tracked, and due to the shearing action that occurs in the turns, we would expect to see a greater reduction in vegetative cover in the curved trafficking locations. Likewise, the less aggregated soils containing higher sand content would be expected to be more susceptible to vegetation cover loss than the more aggregated soils containing lower quantities of sand.

Table 9. Overall ANOVA type III table of vegetation cover for tracked vehicles (Sum Sq = sum of squares; Mean Sq = mean of squares; NumDF = numerator degrees of freedom; DenDF = denominator degrees of freedom; F.value = F statistic ratio value; Pr(>F) = Probability p value associated with F statistic).

Factor	Sum Sq	Mean Sq	NumDF	DenDF	F.value	Pr(>F)	Signif.
SoilCode	27759	6940	4	10	83.25	1.2e-07	***
Pass	105498	35166	3	90	421.86	< 2e-16	***
Loc	10542	5271	2	20	63.23	2.3e-09	***
SoilCode:Pass	5157	430	12	90	5.16	1.7e-06	***
SoilCode:Loc	5249	656	8	20	7.87	9.0e-05	***
Pass:Loc	10048	1675	6	90	20.09	9.0e-15	***
SoilCode:Pass:Loc	10950	456	24	90	5.47	1.5e-09	***

SoilCode designates the site and soil, Pass designates the number of consecutive figure-8 trafficking passes conducted with the vehicle and Loc designates the site locations.

Satterthwaite approximation used for degrees of freedom

Signif. codes: '***' 0.001

In Table 10, for the “All Locations” rows, we see that the two soils at Ft. Riley (FR-SiCL and FR-SiL) generated significantly different ($p < 0.05$) results with the tracked vehicle than all the other soils. This is not unexpected as the Ft. Riley soils, besides being more aggregated and containing more clay and less sand in their composition, also had significantly more initial vegetation cover prior to trafficking than the other sites, even after mowing, raking, and removing the majority of the existing vegetation prior to conducting the field experiments. If the Ft. Riley soils are removed from the analysis used in Table 9, the interaction effects including SoilCode are no longer significant.

The difference in the Ft. Riley soil-vegetation effects is also clearly shown by the pre-trafficking mean values in Table 12 and visually obvious in the top two rows of plots in Figure 17. Even when one looks at each of the individual sampling locations (CI, CO, SS) in Table 10, the same significant differences in vegetation cover occurred between the Ft. Riley soils compared to all the other sites' soils.

Table 10. Vegetation cover (%) least square means (lsmean) for tracked vehicles by soil and sampling location. CI is curve inside, CO is curve outside, and SS is straight section. Soil code designates the site and soil where sites are FB = Fort Benning, FR = Fort Riley, and WS = White Sands and soils are LS = loamy sand, SiCL = silty clay loam, SiL = silt loam, SL = sandy loam, and L = loam. SE = standard error of the mean, df = degrees of freedom, lower.CL = lower confidence level (95%), and upper .CL = upper confidence level (95%).

Sampling Location*	SoilCode[†]	lsmean	SE	df	lower.CL	upper.CL	group
All Locations	FB-LS	24.2	2.23	10	19.2	29.2	a
	WS-SL	27.2	2.23	10	22.2	32.2	a
	WS-L	27.2	2.23	10	22.3	32.2	a
	FR-SiCL	63.2	2.23	10	58.2	68.1	b
	FR-SiL	63.5	2.23	10	58.5	68.5	b
CI	FB-LS	19.6	3.81	30	11.8	27.4	a
	WS-L	23.2	3.81	30	15.4	31.0	a
	WS-SL	26.0	3.81	30	18.2	33.7	a
	FR-SiL	43.9	3.81	30	36.1	51.7	b
	FR-SiCL	47.8	3.81	30	40.1	55.6	b
CO	FB-LS	22.4	3.81	30	14.6	30.2	a
	WS-SL	22.8	3.81	30	15.0	30.5	a
	WS-L	22.9	3.81	30	15.1	30.7	a
	FR-SiCL	51.9	3.81	30	44.1	59.7	b
	FR-SiL	52.8	3.81	30	45.1	60.6	b
SS	FB-LS	30.6	3.81	30	22.8	38.4	a
	WS-SL	32.9	3.81	30	25.1	40.6	a
	WS-L	35.6	3.81	30	27.8	43.4	a
	FR-SiCL	89.7	3.81	30	82.0	97.5	b
	FR-SiL	93.7	3.81	30	86.0	101.5	b

*CI is curve inside, CO is curve outside, and SS is straight section of figure-8 tracked sampling locations.

[†]SoilCode designates the site and soil where sites are FB = Fort Benning, GA; FR = Fort Riley, KS; WS = White Sands Missile Range, NM and soils are LS = loamy sand, SiCL = silty clay loam, SiL = silt loam, SL = sandy loam and L = loam.

For a given sampling location, least square mean values (averaged over the levels of Pass and Loc for “All Locations” and by Pass only for the individual sampling locations) with the same group letter (a, b) are not significantly different at 0.05 level by SoilCode (Tukey’s mean separation)

Both the curved traffic sampling locations (CI and CO) showed significant ($p < 0.05$) reductions in vegetation cover after only one trafficking pass and again after an additional four passes (Table 11). Only after five cumulative passes occurred do we not show a significant difference in the level of vegetation cover present. However, Table 11 also reveals the straight trafficked sampling location (SS) did not exhibit a significant ($p < 0.05$) change in vegetation cover across all soils until five passes were conducted. A significant ($p < 0.05$) decrease in vegetation cover then continued though with the additional final five trafficking passes. This is not unexpected since the trafficking in the curves, especially with the tracked vehicles, were much more intense, with the additional side shear forces causing significant soil and vegetation displacement.

Table 11. Vegetation cover (%) least square means (lsmean) for tracked vehicles by trafficking pass across all soils. SE = standard error of the mean, df = degrees of freedom, lower.CL = lower confidence level (95%), and upper .CL = upper confidence level (95%).

Sampling Location*	Pass[†]	lsmean	SE	df	lower.CL	upper.CL	group
CI	p3 (10)	3.66	2.66	106	-1.61	8.93	a
	p2 (5)	7.79	2.66	106	2.52	13.06	a
	p1 (1)	38.14	2.66	106	32.87	43.41	b
	p0 (0)	78.80	2.66	106	73.53	84.07	c
CO	p3 (10)	6.77	2.66	106	1.50	12.04	a
	p2 (5)	11.99	2.66	106	6.72	17.26	a
	p1 (1)	42.71	2.66	106	37.44	47.98	b
	p0 (0)	76.78	2.66	106	71.51	82.06	c
SS	p3 (10)	36.18	2.66	106	30.91	41.45	a
	p2 (5)	47.28	2.66	106	42.01	52.55	b
	p1 (1)	68.07	2.66	106	62.80	73.34	c
	p0 (0)	74.49	2.66	106	69.21	79.76	c

*CI is curve inside, CO is curve outside, and SS is straight section tracked sampling locations.

[†]Pass is the pass level (p0,p1,p2,p3) and the number of cumulative figure-8 trafficking passes conducted with the vehicle are indicated in parentheses.

For a given location, least square mean values (averaged over the level of SoilCode for the individual sampling locations) with the same group letter are not significantly different at 0.05 level by trafficking pass level (Tukey's mean separation).

As expected, the trafficking pass effects, individually by soil and sampling location (Table 12) and from the plots in Figure 17, also indicates that the cumulative loss of vegetative cover in the curved trafficked regions with additional trafficking passes was much more severe than for the straight trafficked regions. However, the soils with lower sand contents and more initial vegetative mass prior to trafficking (Ft. Riley sites) better resisted the trafficking pass effects than at the other sites. These differences between the straight and curved trafficked regions are easily explained due to the heavy tracked vehicles exhibiting significant shear forces on the soil surface in the turns. This removed much of the vegetation, as reflected by the cover values, during the early pass levels, whereas the side shear forces were not present on the straight trafficked regions, thus, the vegetation cover degradation was less severe during the initial trafficking levels.

Table 12. Field vegetation cover comparisons among trafficking pass levels and sampling locations by soil for tracked vehicles.

SoilCode [†]	Sampling Location*	Vegetation Cover (%) - Tracked Vehicles			
		p0 (0) [‡]	p1 (1) [‡]	p2 (5) [‡]	p3 (10) [‡]
FB-LS	CI	97.3a	68.0b	19.7c	6.3c
FB-LS	CO		77.7a	22.3b	10.3b
FB-LS	SS		97.7ax	94.3ax	69.7bx
WS-L	CI	96.7a	63.3bz	11.3c	4.3c
WS-L	CO		79.3by	24.3c	11.0c
WS-L	SS		97.3ax	90.0ax	91.0ax
FB-LS	CI	56.3a	17.7b	1.7b	2.7b
FB-LS	CO	62.3a	18.0b	5.3b	4.0b
FB-LS	SS	46.0ab	54.0ax	17.0bc	5.3c
WS-L	CI	66.4a	19.4b	4.3c	2.7c
WS-L	CO	55.1a	24.3b	5.0b	7.2b
WS-L	SS	62.9a	48.8ax	21.7bx	8.9b
WS-SL	CI	77.2a	22.3b	2.0c	2.3c
WS-SL	CO	72.5a	14.2bx	3.0b	1.3b
WS-SL	SS	69.5a	42.6bx	13.3c	6.0c

[†]SoilCode designates the site and soil where sites are FB = Fort Benning, GA; FR = Fort Riley, KS; WS = White Sands Missile Range, NM and soils are LS = loamy sand, SiCL = silty clay loam, SiL = silt loam, SL = sandy loam and L = loam.

*CI is curve inside, CO is curve outside, and SS is straight section of figure-8 tracked sampling locations.

[‡]Trafficking pass levels, p0, p1, p2, p3 (number of cumulative trafficking passes).

For a given site/soil, mean values by row with same group letter are not significantly different at 0.05 level by trafficking pass level. For a given site/soil, mean values by column are only significantly different at the 0.05 level by sampling location (CI, CO, SS), if identified with the letter x or y.

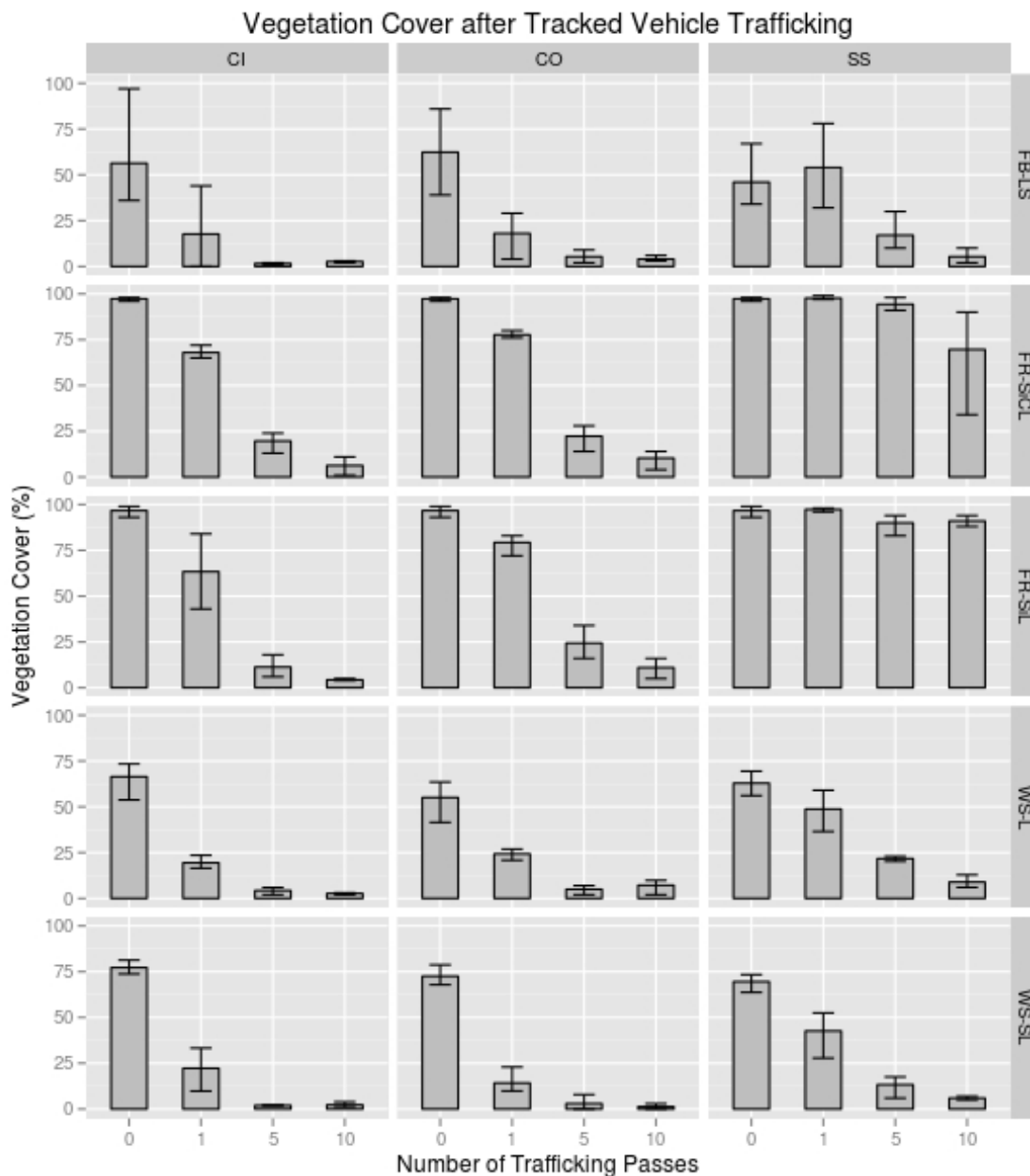


Figure 18. Field vegetation cover after specified trafficking pass levels for tracked vehicles for all specified sites-soils. Bars represent the mean of the measured values and the error bars represent the maximum and minimum measured values. CI is curve inside, CO is curve outside, and SS is the straight section sampling location. Sites are FB = Fort Benning, GA; FR = Fort Riley, KS; WS = White Sands Missile Range, NM; and YK = Yakima Training Center, WA. Soils are LS = loamy sand, SiCL = silty clay loam, SiL = silt loam, SL = sandy loam, and L = loam.

Wheeled Vehicle Trafficking Effects on Vegetative Cover

The wheeled vehicle (HMMWV) overall ANOVA results as shown in Table 13 were similar to the tracked vehicle results. Each of the main factors, soil, sampling location and trafficking pass level were all highly significant, with the interactions also showing varying levels of significance.

Table 13. Overall ANOVA type III table of vegetation cover for wheeled (HMMWV) vehicles (Sum Sq = sum of squares; Mean Sq = mean of squares; NumDF = numerator degrees of freedom; DenDF = denominator degrees of freedom; F.value = F statistic ratio value; PR(>F) = Probability p value associated with F statistic).

Factor	Sum Sq	Mean Sq	NumDF	DenDF	F.value	Pr(>F)	Signif.
SoilCode	19254	3851	5	12.1	23.9	7.3e-06	***
Pass	67363	22454	3	106.1	139.1	< 2e-16	***
Loc	6574	3287	2	23.8	20.4	7.0e-06	***
SoilCode:Pass	6281	419	15	106.1	2.6	0.00237	**
SoilCode:Loc	5091	509	10	23.8	3.2	0.01040	*
Pass:Loc	5002	834	6	106.1	5.2	0.00011	***
SoilCode:Pass:Loc	9840	328	30	106.0	2.0	0.00442	**

Satterthwaite approximation used for degrees of freedom

Signif. codes: 0 '***' 0.001 '**' 0.01 '*' 0.05 '.' 0.1 ' ' 1

In Table 14, for the “All Locations” rows, we see that the two soils at Ft. Riley (FR-SiCL and FR-SiL) and the Yakima Training Center soil (YK-SL) generated significantly different ($p < 0.05$) results with the HMMWV wheeled vehicle than all the other soils. This was likely due to the higher initial vegetation cover existing on these soils. If these soils are removed from the analysis used in Table 13, the interaction effects including SoilCode are no longer significant, verifying that they are the reason for the SoilCode interaction effects listed in Table 13.

These three (FR-SiCL, FR-SiL and YK-SL) soil's vegetation cover effects are also clearly shown to be different by the pre-trafficking mean values in Table 17 and are visually obvious in the 1st, 2nd and 4th rows of plots in Figure 19. Even when one looks at each of the individual sampling locations (CI,CO,SS) in Table 14, the same significant differences in vegetation cover occurred between the Ft. Riley and Yakima soils compared to all the other sites' soils.

Table 14. Vegetation cover (%) least square means (lsmeans) for wheeled vehicles (HMMWV) by soil and sampling location. SE = standard error of the mean, df = degrees of freedom, lower.CL = lower confidence level (95%), and upper.CL = upper confidence level (95%).

Sampling Location*	SoilCode[†]	lsmean	SE	df	lower.CL	upper.CL	group
All Locations	WS-L	35.7	4.15	11.9	26.6	44.7	a
	FB-LS	38.3	4.15	11.9	29.3	47.4	a
	WS-SL	47.7	4.15	11.9	38.6	56.7	a
	FR-SiCL	71.2	4.15	11.9	62.1	80.2	b
	YK-SL	73.9	4.18	12.2	64.8	83.0	b
	FR-SiL	83.5	4.18	12.2	74.4	92.6	b
CI	WS-L	27.4	5.55	29.0	16.1	38.8	a
	FB-LS	36.3	5.55	29.0	24.9	47.6	a
	WS-SL	46.9	5.55	29.0	35.5	58.3	ab
	FR-SiCL	66.4	5.55	29.0	55.1	77.8	bc
	YK-SL	75.2	5.55	29.0	63.9	86.6	c
	FR-SiL	84.5	5.55	29.0	73.1	95.9	c
CO	FB-LS	33.4	5.55	29.0	22.1	44.8	a
	WS-L	34.5	5.55	29.0	23.2	45.9	a
	WS-SL	49.7	5.55	29.0	38.3	61.1	ab
	FR-SiCL	54.0	5.55	29.0	42.6	65.4	ab
	YK-SL	66.9	5.55	29.0	55.6	78.3	b
	FR-SiL	69.3	5.55	29.0	58.0	80.7	b
SS	WS-L	45.0	5.55	29.0	33.7	56.4	a
	FB-LS	45.3	5.55	29.0	34.0	56.7	a
	WS-SL	46.4	5.55	29.0	35.0	57.7	a
	YK-SL	79.6	5.73	32.3	67.9	91.3	b
	FR-SiCL	93.1	5.55	29.0	81.7	104.4	b
	FR-SiL	96.6	5.73	32.3	84.9	108.2	b

*CI is curve inside, CO is curve outside, and SS is straight section of figure-8 tracked sampling locations.

[†]SoilCode designates the site and soil where sites are FB = Fort Benning, GA; FR = Fort Riley, KS; WS = White Sands Missile Range, NM and soils are LS = loamy sand, SiCL = silty clay loam, SiL = silt loam, SL = sandy loam and L = loam. For a given sampling location, least square mean values with the same group letter are not significantly different at 0.05 level by SoilCode (Tukey's mean separation).

The wheeled vehicles also showed an overall accelerated loss of vegetative cover in the curved regions compared to the straight trafficked sections as seen in Table 15 for the HMMWV and Table 16 for the Fire Truck and verified in Table 17, Figure 19 and Figure 20, but not to the extent exhibited by the tracked vehicles. The degree of vegetative cover loss due to wheeled trafficking appears to be related to the original quantity and “resistance” of the vegetation to degradation and the soil’s ability to maintain its original aggregated structure. For example, the denser grass vegetation at Ft. Riley (1-SCL and FR-SiL) and Yakima (YK-SL) did eventually lose cover due to the repeated shearing action of the wheels in the curved sampling locations (CI and CO), but were more resistant to cover loss on the straight trafficked regions (SS) as shown in Figure 19 and Figure 20. However, the cover decay on the other soil/sites, especially WS-L and

WS-SL (Figure 19), exhibited initial resistance to cover loss during the first level of wheeled trafficking passes but quickly deteriorated at the higher pass levels, especially in the curved regions.

Table 15. Vegetation cover (%) least square means (lsmean) for wheeled vehicles (HMMWV) by trafficking pass. SE = standard error of the mean, df = degrees of freedom, lower.CL = lower confidence level (95%), and upper .CL = upper confidence level (95%).

Sampling Location*	Pass[†]	lsmean	SE	df	lower.CL	upper.CL	group
CI	p3 (50)	26.3	3.44	106	19.5	33.1	a
	p2 (25)	51.0	3.44	106	44.2	57.9	b
	p1 (10)	67.4	3.44	106	60.6	74.2	c
	p0 (0)	79.8	3.44	106	72.9	86.6	d
CO	p3 (50)	20.3	3.44	106	13.4	27.1	a
	p2 (25)	41.1	3.44	106	34.3	48.0	b
	p1 (10)	64.7	3.44	106	57.9	71.5	c
	p0 (0)	79.2	3.44	106	72.3	86.0	d
SS	p3 (50)	50.4	3.57	111	43.3	57.4	a
	p2 (25)	65.4	3.44	106	58.5	72.2	b
	p1 (10)	74.6	3.44	106	67.8	81.4	bc
	p0 (0)	80.4	3.57	111	73.3	87.4	c

*CI is curve inside, CO is curve outside, and SS is straight section of figure-8 tracked sampling locations.

[†]Pass is the pass level (p0,p1,p2,p3) and the number of cumulative figure-8 trafficking passes conducted with the vehicle are indicated in parentheses.

For a given location, least square mean values with the same group letter are not significantly different at the 0.05 level by trafficking pass level (Tukey's mean separation).

Table 16. Vegetation cover (%) least square means (lsmean) for wheeled vehicle (Fire Truck) by sampling location. SE = standard error of the mean, df = degrees of freedom, lower.CL = lower confidence level (95%), and upper .CL = upper confidence level (95%).

Sampling Location*	Pass[†]	lsmean	SE	df	lower.CL	upper.CL	group
CI	p3 (20)	16.7	8.29	14.6	-1.058	34.4	a
	p2 (10)	58.3	8.29	14.6	40.609	76.1	b
	p0 (0)	94.7	8.29	14.6	76.942	112.4	c
	p1 (2)	98.7	8.29	14.6	80.942	116.4	c
CO	p3 (20)	17.0	8.29	14.6	-0.725	34.7	a
	p2 (10)	62.0	8.29	14.6	44.275	79.7	b
	p0 (0)	94.0	8.29	14.6	76.275	111.7	c
	p1 (2)	95.3	8.29	14.6	77.609	113.1	c
SS	p3 (20)	32.3	8.29	14.6	14.609	50.1	a
	p2 (10)	71.3	8.29	14.6	53.609	89.1	b
	p0 (0)	94.3	8.29	14.6	76.609	112.1	b
	p1 (2)	95.0	8.29	14.6	77.275	112.7	b

*CI is curve inside, CO is curve outside, and SS is straight section tracked sampling locations.

[†]Pass is the pass level (p0,p1,p2,p3) and the number of cumulative figure-8 trafficking passes conducted with the vehicle are indicated in parentheses.

For a given location, least square mean values (averaged over the level of SoilCode for the individual sampling locations) with the same group letter are not significantly different at 0.05 level by trafficking pass level (Tukey's mean separation).

Table 17. Field vegetation cover comparisons among trafficking pass levels and sampling locations for wheeled vehicles.

SoilCode [†]	Sampling Location*	Vegetation Cover (%)			
		HMMWV			
		p0 (0) [‡]	p1 (10) [‡]	p2 (25) [‡]	p3 (50) [‡]
FR-SiCL	CO	98.7 ^a	63.3 ^{ab}	35.7 ^{bc}	17.3 ^c
FR-SiCL	SS		N/A	N/A	84.0 ^{ax}
FR-SiL	CO	99.3 ^a	92.3 ^{ab}	56.0 ^{bc}	29.7 ^c
FR-SiL	SS		N/A	N/A	92.0 ^{ax}
FB-LS	CI	55.7 ^a	33.7 ^a	29.0 ^a	26.7 ^a
FB-LS	CO	44.3 ^a	35.7 ^a	31.7 ^a	22.0 ^a
FB-LS	SS	52.3 ^{ab}	57.7 ^b	51.7 ^{ab}	19.7 ^a
YK-SL	CI	97.0 ^a	91.0 ^a	88.3 ^a	24.0 ^b
YK-SL	CO	92.0 ^a	88.7 ^{ab}	67.0 ^b	20.0 ^c
YK-SL	SS	97.5 ^a	80.7 ^{ab}	75.7 ^{ab}	67.7 ^{bx}
WS-L	CI	54.6 ^a	41.7 ^a	7.3 ^{by}	6.2 ^b
WS-L	CO	64.9 ^a	51.0 ^a	19.1 ^{bxy}	3.0 ^b
WS-L	SS	65.7 ^a	57.8 ^{ab}	39.7 ^{bcx}	16.9 ^c
WS-SL	CI	71.6 ^a	57.1 ^{ab}	40.9 ^{bc}	17.9 ^c
WS-SL	CO	74.7 ^a	57.2 ^{ab}	37.3 ^{bc}	29.6 ^c
WS-SL	SS	70.8 ^a	56.0 ^{ab}	36.5 ^{bc}	22.2 ^c
		Fire Truck			
		p0 (0) [‡]	p1 (2) [‡]	p2 (10) [‡]	p3 (20) [‡]
YK-SL	CI	94.7 ^a	98.7 ^a	58.3 ^b	16.7 ^c
YK-SL	CO	95.3 ^a	94.0 ^a	62.0 ^b	17.0 ^c
YK-SL	SS	94.3 ^a	95.0 ^a	71.3 ^a	32.3 ^b

[†]SoilCode designates the site and soil where sites are FB = Fort Benning, GA; FR = Fort Riley, KS; WS = White Sands Missile Range, NM and soils are LS = loamy sand, SiCL = silty clay loam, SiL = silt loam, SL = sandy loam and L = loam.

*CI is curve inside, CO is curve outside, and SS is straight section of figure-8 tracked sampling locations.

[‡]Trafficking pass levels (number of cumulative passes)

For a given site/soil, mean values by row with the same group letter are not significantly different at 0.05 level by trafficking pass level. For a given site/soil, mean values by column are only significantly different at the 0.05 level by sampling location (CI, CO, SS), if identified with the letter x. N/A means data was not available.

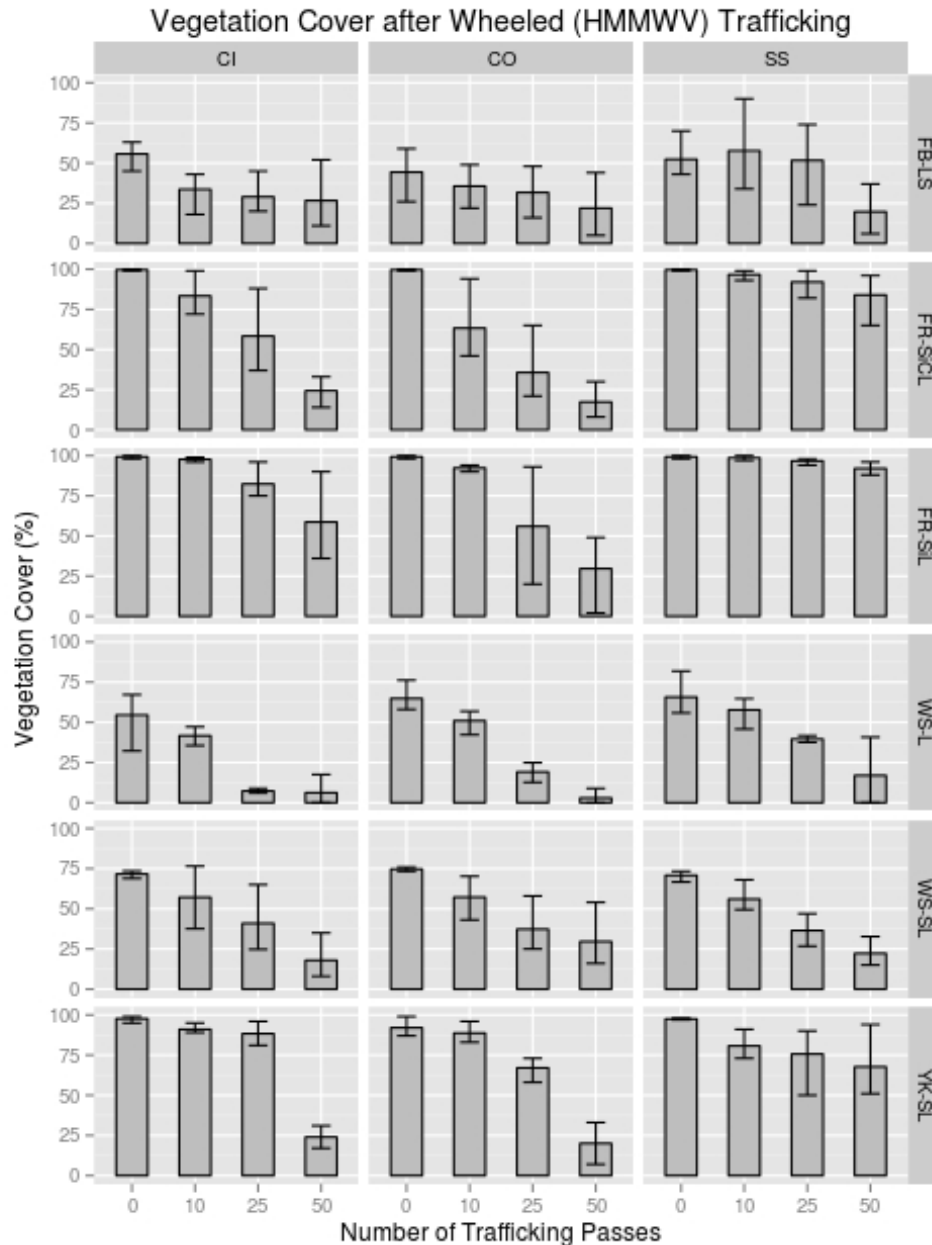


Figure 19. Field vegetation cover after specified trafficking pass levels for wheeled (HMMWV) vehicles for all specified sites-soils. Bars represent the mean of the measured values and the error bars represent the maximum and minimum measured values. CI is curve inside, CO is curve outside, and SS is the straight section sampling location. Sites are FB = Fort Benning, GA; FR = Fort Riley, KS; WS = White Sands Missile Range, NM; and YK = Yakima Training Center, WA. Soils are LS = loamy sand, SiCL = silty clay loam, SiL = silt loam, SL = sandy loam, and L = loam.

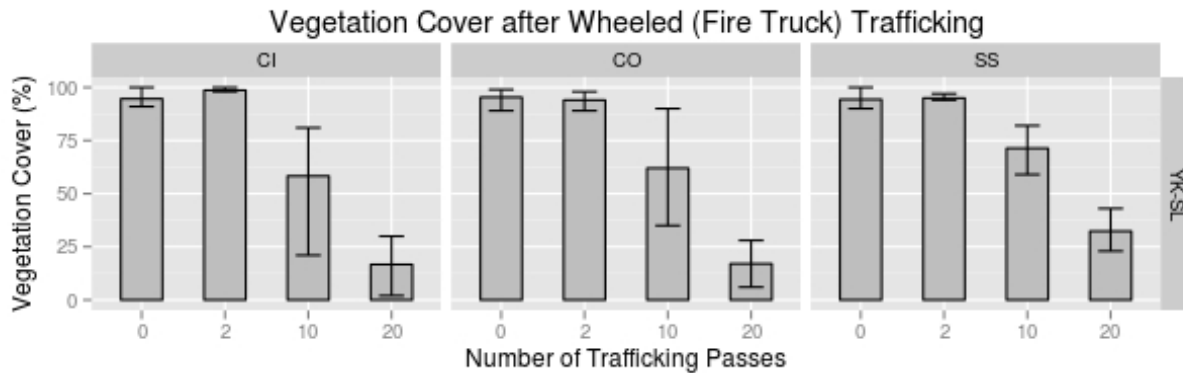


Figure 20. Field vegetation cover after specified trafficking pass levels for wheeled (Fire Truck) vehicle on specified soil/site. Bars represent the mean of the measured values and the error bars represent the maximum and minimum measured values. CI is curve inside, CO is curve outside, and SS is the straight section sampling location. Site designation is YK = Yakima Training Center, WA. Soil is SL = sandy loam.

Vegetation Cover Loss vs. Trafficking Pass Level Relationships

Preliminary relationships between surface cover loss and vehicle pass number were determined for both the curved and straight trafficked regions for all vehicles for each individual soil. The curved trafficked regions (CI and CO) exhibited a strong first order decay relationship, as expected (Table 18). The straight trafficked sections, although statistically appearing to follow a linear decline over the range of vegetation cover measured, the standard first order decay function $y = ae^{-bx}$ (where y is the percent vegetative cover, x is the number of accumulated trafficking passes and a and b are function parameters) fits were still generally very good (Table 18) and were applied to this data as well. The tracked vehicle decay rate constant was significantly less overall at Ft. Riley (Table 18), likely due to the greater initial vegetation cover on this site. The tracked vehicles had higher overall decay rates compared to the wheeled vehicles. There was at least an order of magnitude decrease in the straight trafficked sections' decay rates compared to the curved trafficked regions for the tracked vehicles.

The wheeled vehicles showed the same general trends as the tracked vehicles (Table 18), but the differences between curved and straight trafficked regions were less pronounced, especially on the sandier soils at Ft. Benning and White Sands Missile Range. Those sites also contained less initial vegetative cover as well and were the least aggregated soils evaluated, which likely influenced the computed vegetative cover decay rates. Likewise, the Ft. Riley and Yakima sites' greater initial vegetative cover likely led to their lower decay rate coefficients.

Table 18. Fitted first order vegetation cover decay function parameters for the curved (CI, CO) and straight trafficked (SS) regions for all vehicles at all sites.

SoilCode [†]	Sampling Location*	Vegetation Cover 1 st Order Decay Function Parameters		
		Tracked Vehicles		
		a	b	Adj R ²
FR-SiCL	CI,CO	97.29	0.29	0.98
FR-SiCL	SS	98.25	0.011	0.67 ^{††}
FR-SiL	CI,CO	96.95	0.32	0.93
FR-SiL	SS	97.20	0.0067	0.52 ^{††}
FB-LS	CI,CO	59.30	1.19	0.68
FB-LS	SS	53.11	0.20	0.55
WS-L	CI,CO	60.65	1.00	0.90
WS-L	SS	61.79	0.21	0.92
WS-SL	CI,CO	74.85	1.41	0.96
WS-SL	SS	67.06	0.36	0.91
		Wheeled Vehicles - HMMWV		
		a	b	Adj R ²
FR-SiCL	CO ^{†††}	97.18	0.039	0.74
FR-SiCL	SS	98.67	0.0011	0.30 ^{††}
FR-SiL	CO ^{†††}	104.70	0.023	0.61
FR-SiL	SS	99.33	0.0015	0.50
FB-LS	CI,CO	46.15	0.015	0.22
FB-LS	SS	59.88	0.014	0.12
YK-SL	CI,CO	103.17	0.020	0.74
YK-SL	SS	92.54	0.0071	0.19
WS-L	CI,CO	62.68	0.048	0.80
WS-L	SS	68.63	0.023	0.65
WS-SL	CI,CO	72.62	0.023	0.63
WS-SL	SS	70.70	0.024	0.84
		Wheeled Vehicle - Fire Truck		
		a	b	Adj R ²
YK-SL	CI,CO	102.37	0.067	0.78
YK-SL	SS	100.04	0.046	0.85

[†] SoilCode designates the site and soil where sites are FB = Fort Benning, GA; FR = Fort Riley, KS; WS = White Sands Missile Range, NM and soils are LS = loamy sand, SiCL = silty clay loam, SiL = silt loam, SL = sandy loam and L = loam.

^{††} Extreme outlier data point removed to provide consistent first-order decay function fit.

^{†††} No CI vegetative cover data taken at Ft. Riley on the HMMWV trafficked plots.

*CI is curve inside, CO is curve outside, and SS is straight section of figure-8 tracked sampling locations.

Vegetative Cover Measurements on Wind Tunnel Trays

Vegetative cover was measured, both in the field on the figure-8 plots and on the actual wind tunnel tray samples. The trends in both sets of measurements were similar, but the field samples are better estimates of the average vegetative cover on the actual trafficked figure-8 plots since the bead method outlined by Sloneker and Moldenhauer (1977) covered a much larger region than the smaller wind tunnel trays. However, the vegetative cover measurements on the individual wind tunnel trays allow for a more precise determination of the effect of vegetation cover on the tray emissions measured in the wind tunnel. Therefore the wind tunnel tray sampled data in Table 19 and Table 20 should be referenced rather than the field sampled data when determining the effects on the measured wind tunnel tray emission levels.

Table 19. Wind tunnel tray vegetation cover comparisons among trafficking pass levels and sampling locations for tracked vehicles.

SoilCode [†]	Sampling Location*	Tray Vegetation Cover (%) - Tracked Vehicles			
		p0 (0) [‡]	p1 (1) [‡]	p2 (5) [‡]	p3 (10) [‡]
FR-SiCL	CI	98.3 ^a	41.7 ^b	12.0 ^c	4.3 ^c
FR-SiCL	CO		59.7 ^b	19.7 ^c	8.0 ^c
FR-SiCL	SS		91.7 ^{abx}	87.7 ^{abx}	69.0 ^{bx}
FR-SiL	CI	96.7 ^a	42.0 ^b	5.7 ^c	7.7 ^c
FR-SiL	CO		46.0 ^b	14.3 ^c	9.3 ^c
FR-SiL	SS		95.3 ^{ax}	78.0 ^{ax}	84.6 ^{ax}
FB-LS	CI	40.3 ^{axy}	7.7 ^b	3.7 ^b	2.7 ^b
FB-LS	CO	62.0 ^{ay}	8.3 ^b	3.3 ^b	3.0 ^b
FB-LS	SS	25.0 ^{ax}	21.0 ^a	17.7 ^a	12.0 ^a
WS-L	CI	50.7 ^a	2.3 ^b	4.7 ^b	0.0 ^b
WS-L	CO	67.7 ^a	5.0 ^b	0.0 ^b	0.0 ^b
WS-L	SS	48.0 ^a	13.3 ^{ab}	30.0 ^{ab}	1.7 ^b
WS-SL	CI	39.7 ^a	9.3 ^{by}	0.0 ^b	0.7 ^b
WS-SL	CO	37.7 ^a	16.0 ^{abxy}	0.3 ^b	0.3 ^b
WS-SL	SS	36.0 ^a	29.0 ^{abx}	8.3 ^{bc}	3.3 ^c

[†]SoilCode designates the site and soil where sites are FB = Fort Benning, GA; FR = Fort Riley, KS; WS = White Sands Missile Range, NM and soils are LS = loamy sand, SiCL = silty clay loam, SiL = silt loam, SL = sandy loam and L = loam.

*CI is curve inside, CO is curve outside, and SS is straight section of figure-8 tracked sampling locations.

[‡]Trafficking pass levels, p0,p1,p2,p3 (number of cumulative passes)

For a given site/soil, mean values by row with the same letter (a, b, c) are not significantly different at 0.05 level by trafficking pass level (0, 1, 5, 10). For a given site/soil, mean values by column are only significantly different at the 0.05 level by sampling location (CI, CO, SS), if identified with the letter x or y.

Table 20. Wind tunnel tray vegetation cover comparisons among trafficking pass levels and sampling locations for wheeled vehicles.

SoilCode [†]	Sampling Location*	Tray Vegetation Cover (%)			
		HMMWV			
		p0 (0) [‡]	p1 (1) [‡]	p2 (5) [‡]	p3 (10) [‡]
FR-SiCL	CO	98.0 ^a	32.7 ^b	26.0 ^b	14.7 ^b
FR-SiCL	SS		N/A	N/A	60.3 ^{bx}
FR-SiL	CO	95.7 ^a	63.0 ^{ab}	26.0 ^b	27.0 ^b
FR-SiL	SS		N/A	N/A	93.3 ^{ax}
FB-LS	CI	46.0 ^a	22.7 ^b	21.0 ^b	17.3 ^b
FB-LS	CO	50.0 ^a	35.7 ^{ab}	15.3 ^{bc}	8.7 ^{bc}
FB-LS	SS	44.0 ^a	21.3 ^b	26.3 ^{ab}	20.3 ^b
YK-SL	CI	83.3 ^a	58.7 ^{ab}	40.3 ^b	31.7 ^b
YK-SL	CO	81.0 ^a	57.3 ^{ab}	49.0 ^{bc}	19.0 ^c
YK-SL	SS	90.0 ^a	60.0 ^{ab}	50.3 ^b	37.7 ^b
WS-L	CI	51.0 ^a	14.0 ^b	5.7 ^b	0.0 ^b
WS-L	CO	52.3 ^a	25.7 ^{ab}	6.3 ^b	4.3 ^b
WS-L	SS	68.7 ^a	34.7 ^b	10.7 ^b	16.7 ^b
WS-SL	CI	23.7 ^a	15.3 ^{ab}	9.3 ^{ab}	2.7 ^b
WS-SL	CO	36.0 ^a	20.7 ^{ab}	12.3 ^b	5.3 ^b
WS-SL	SS	38.0 ^a	19.3 ^b	8.7 ^b	4.0 ^b
		Fire Truck			
		p0 (0) [‡]	p1 (2) [‡]	p2 (10) [‡]	p3 (20) [‡]
YK-SL	CI	78.6 ^a	50.0 ^{ab}	38.3 ^b	27.0 ^b
YK-SL	CO	93.7 ^a	60.0 ^b	33.3 ^{bc}	18.0 ^c
YK-SL	SS	80.0 ^a	56.0 ^{ab}	48.0 ^b	30.7 ^b

[†]SoilCode designates the site and soil where sites are FB = Fort Benning, GA; FR = Fort Riley, KS; WS = White Sands Missile Range, NM and soils are LS = loamy sand, SiCL = silty clay loam, SiL = silt loam, SL = sandy loam and L = loam.

*CI is curve inside, CO is curve outside, and SS is straight section of figure-8 tracked sampling locations.

[‡]Trafficking pass levels, p0,p1,p2,p3 (number of cumulative passes)

For a given site/soil, mean values by row with the same letter (a,b,c) are not significantly different at 0.05 level by trafficking pass level (0,10,25,50 or 0.2,10,20). For a given site/soil, mean values by column are only significantly different at the 0.05 level by sampling location (CI,CO,SS), if identified with the letter x.

Plotting both sets of data did reveal similar visual trends but different values for both the tracked (Table 12 and Table 19) and wheeled vehicles (Table 17 and Table 20). To determine if the trends in the two vegetative cover measurements were really similar, we ran statistical tests to verify that assumption. We used a multi-variate analysis in R (R Core Team, 2015) to compare trends as well as plotting the average of the two cover measurements against the difference in the measurements to see if the values were stable around zero, which they generally were.

As anticipated, the vegetation cover values obtained from the trays were generally lower, as shown in Figures 21, 22, and 23. This is likely due to the smaller sample size area (100 points in 1 m transects) for the wind tunnel tray data compared to the field measured transects (100 points in 15.24 m transects) and the fact that the process of removing the wind tunnel tray samples from the field also disturbed (removed some of) the vegetation cover, as well as possible selection bias of the wind tunnel tray soil extraction sites within the trafficking regions.

Since the vegetation cover was lower for the tunnel trays than what was measured in the field on the figure-8 plots, the emission levels from the actual trafficked sites would be expected to be somewhat less than indicated by the wind tunnel tray (abrader and non-abrader) experiments from winds generating the same surface friction velocities.

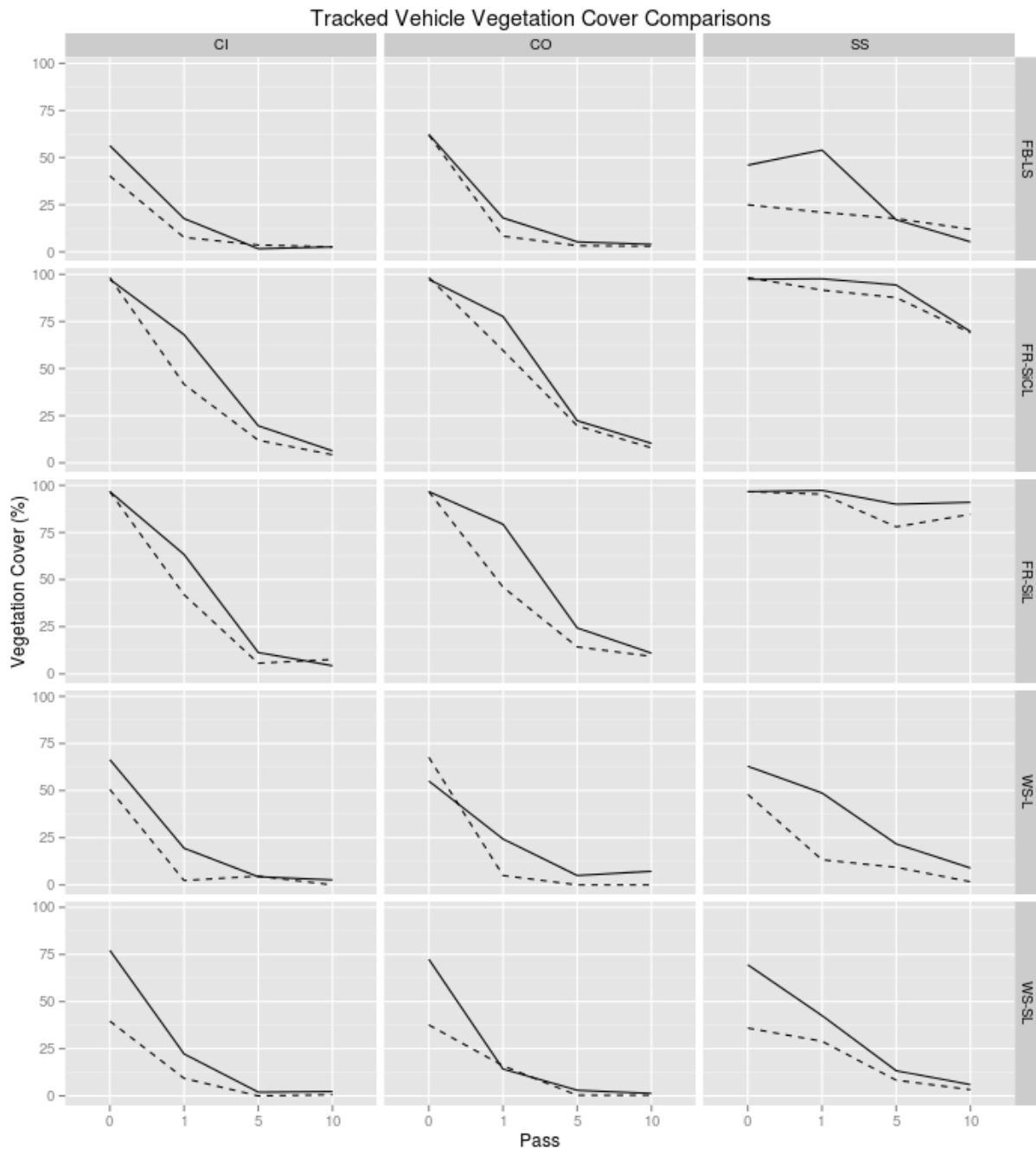


Figure 21. Comparisons between figure-8 plot (solid line) and wind tunnel tray (dashed line) vegetation cover data for tracked vehicles. CI is curve inside, CO is curve outside, and SS is the straight section sampling location. Sites are FB = Fort Benning, GA; FR = Fort Riley, KS; and WS = White Sands Missile Range, NM. Soils are LS = loamy sand, SiCL = silty clay loam, SiL = silt loam, SL = sandy loam, and L = loam.

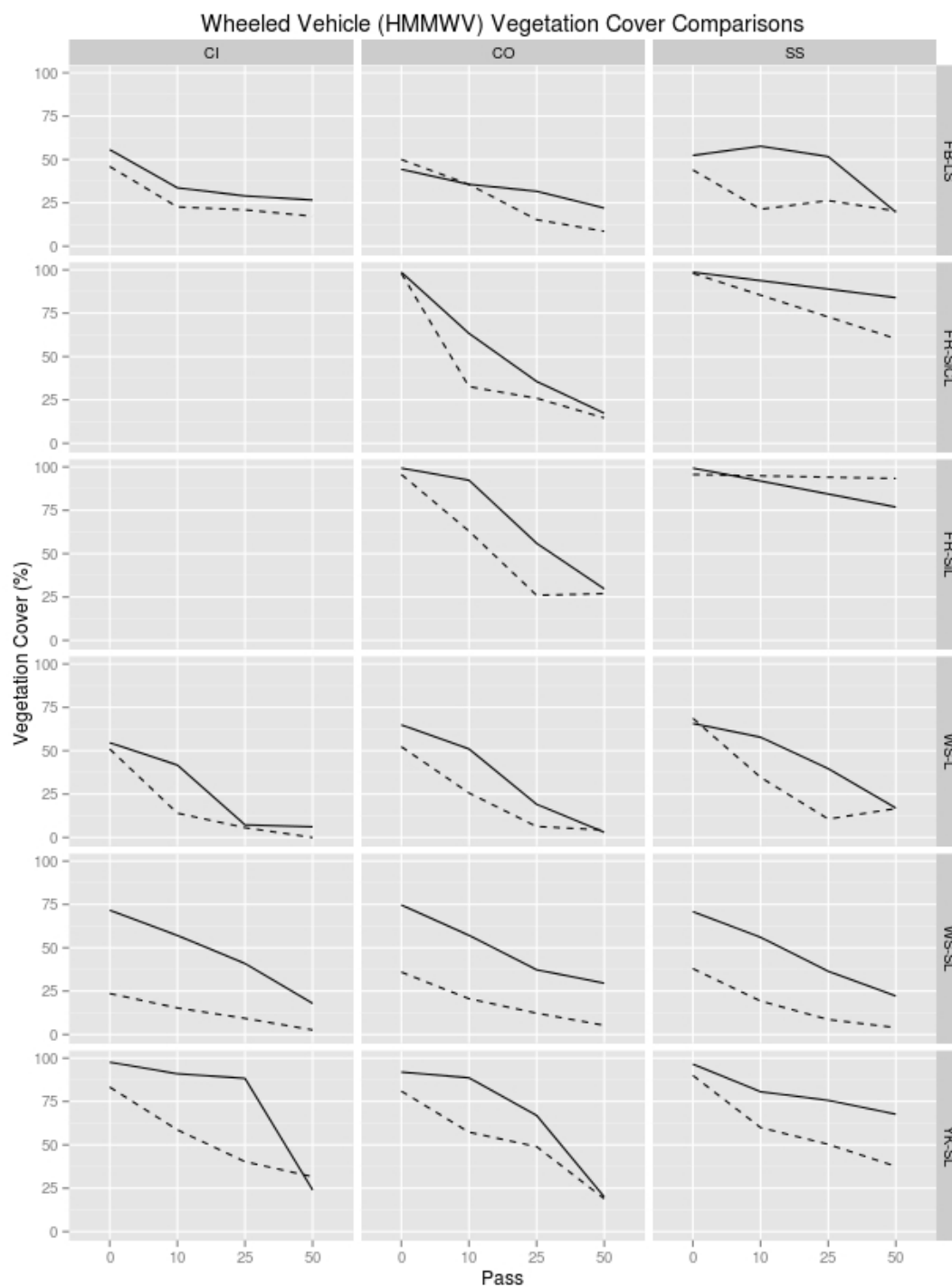


Figure 22. Comparisons between figure-8 plot (solid line) and wind tunnel tray (dashed line) vegetation cover data for wheeled (HMMWV) vehicles. CI is curve inside, CO is curve outside, and SS is the straight section sampling location. Sites are FB = Fort Benning, GA; FR = Fort Riley, KS; and WS = White Sands Missile Range, NM. Soils are LS = loamy sand, SiCL = silty clay loam, SiL = silt loam, SL = sandy loam, and L = loam.

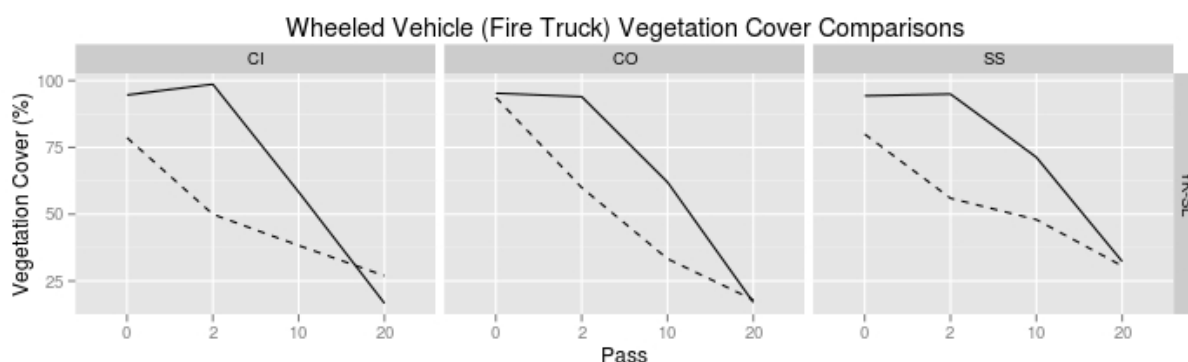


Figure 23. Comparisons between figure-8 plot (solid line) and wind tunnel tray (dashed line) vegetation cover data for wheeled (Fire Truck) vehicle. CI is curve inside, CO is curve outside, and SS is the straight section sampling location. Site is YK = Yakima Training Center, WA. Soil is SL = sandy loam.

Tracked Vehicle Trafficking Effects on Soil Attached (Standing) Vegetation Biomass

Vegetation initially standing prior to trafficking and later flattened but still attached to the soil was clipped and then categorized by vegetation class (grass, herbs and woody plants). The data was originally intended to determine if there was a difference in resistance to trafficking effects on above ground biomass between the different vegetation classes and whether the distribution of the vegetation classes may have an impact on that resistance. However, there were few woody plants on the sites selected at all locations and there was no measurable difference in results that could be directly attributable to the ratio of grass and forb plants at the sites. So, only general qualitative conclusions are made regarding plant species present on the sites and their relative resistance to trafficking.

First, though we will look at the vegetation biomass as a single entity to determine its resiliency to trafficking as a whole. The ANOVA analysis results in Table 21 suggests that trafficking passes (Pass) with the tracked vehicles have the most significant effect followed by the interaction of SoilCode (soil) and Pass effects with other effects and interactions having a lesser significant impact.

Table 21. Overall ANOVA type III table of soil attached vegetation biomass for tracked vehicles. Sum Sq = sum of squares; Mean Sq = mean of squares; NumDF = numerator degrees of freedom; DenDF = denominator degrees of freedom; F.value = F statistic ratio value; PR(>F) = Probability p value associated with F statistic.

Factor	Sum Sq	Mean Sq	NumDF	DenDF	F.value	Pr(>F)	Signif.
SoilCode	19395	4849	4	10	5.4	0.0144	*
Pass	343344	114448	3	150	126.3	< 2e-16	***
Loc	11042	3681	3	150	4.1	0.0083	**
SoilCode:Pass	92599	7717	12	150	8.5	3.4e-12	***
SoilCode:Loc	17733	1478	12	150	1.6	0.0885	.
Pass:Loc	14489	1610	9	150	1.8	0.0770	.
SoilCode:Pass:Loc	16696	464	36	150	0.5	0.9897	*

Satterthwaite approximation used for degrees of freedom
Signif. codes: 0 '***' 0.001 '**' 0.01 '*' 0.05 '.' 0.1 ' ' 1

As shown in the “All Locations” rows in Table 22 for tracked vehicles, the soil effect is not strong, but does exist. Also, there are no significant differences in the samples obtained from the curved regions (CI and CO) of the figure-8 plots for the tracked vehicles across all soil types. However, there are some significant differences ($p < 0.05$) among soils on the straight trafficked regions (SS and CC) with the tracked vehicles as shown in Table 22. The two Ft. Riley sites and the Ft. Benning site show a trend of higher mean concentrations of vegetation biomass than the other sites/soils across all tracked vehicle trafficking pass levels.

Table 22. Soil attached vegetation biomass (g m^{-2}) least square means (lsmeans) for tracked vehicles by soil and sampling location. SE = standard error of the mean, df = degrees of freedom, lower.CL = lower confidence level (95%), and upper .CL = upper confidence level (95%).

Sampling Location*	SoilCode[†]	lsmean	SE	df	lower.CL	upper.CL	group
All Locations	WS-L	9.55	10.1	10	-13.06	32.2	a
	WS-SL	14.83	10.1	10	-7.79	37.4	ab
	FB-LS	24.67	10.1	10	2.06	47.3	ab
	FR-SiL	56.94	10.1	10	34.33	79.6	b
	FR-SiCL	59.12	10.1	10	36.50	81.7	b
CC	WS-SL	9.39	12.6	21.8	-16.827	35.6	a
	WS-L	9.45	12.6	21.8	-16.760	35.7	a
	FB-LS	18.98	12.6	21.8	-7.233	45.2	ab
	FR-SiL	62.87	12.6	21.8	36.653	89.1	bc
	FR-SiCL	74.83	12.6	21.8	48.620	101.0	c
CI	WS-L	8.70	12.6	21.8	-17.517	34.9	a
	WS-SL	17.10	12.6	21.8	-9.113	43.3	a
	FB-LS	26.38	12.6	21.8	0.163	52.6	a
	FR-SiL	41.33	12.6	21.8	15.120	67.5	a
	FR-SiCL	43.07	12.6	21.8	16.853	69.3	a
CO	WS-L	7.57	12.6	21.8	-18.643	33.8	a
	FB-LS	18.63	12.6	21.8	-7.583	44.8	a
	WS-SL	20.80	12.6	21.8	-5.410	47.0	a
	FR-SiL	41.63	12.6	21.8	15.420	67.8	a
	FR-SiCL	43.60	12.6	21.8	17.387	69.8	a
SS	WS-SL	12.02	12.6	21.8	-14.197	38.2	a
	WS-L	12.47	12.6	21.8	-13.740	38.7	a
	FB-LS	34.68	12.6	21.8	8.470	60.9	ab
	FR-SiCL	74.97	12.6	21.8	48.753	101.2	b
	FR-SiL	81.93	12.6	21.8	55.720	108.1	b

*CI is curve inside, CO is curve outside, and SS is straight section of figure-8 tracked sampling locations.

[†]SoilCode designates the site and soil where sites are FB = Fort Benning, GA; FR = Fort Riley, KS; WS = White Sands Missile Range, NM and soils are LS = loamy sand, SiCL = silty clay loam, SiL = silt loam, SL = sandy loam and L = loam.

For a given sampling location, least square mean values (averaged over the levels of Pass and Loc for “All Locations” and by Pass only for the individual sampling locations) with the same group letter (a,b) are not significantly different at 0.05 level by SoilCode (Tukey’s mean separation).

Looking at the effects due to different trafficking levels across all soil types shown in Table 23, reveals that the samples obtained in the curved regions (CI and CO) of the figure-8 plots showed a significant effect (severe loss of attached vegetation biomass) after the first pass with the tracked vehicles across all soils, but no significant differences with subsequent additional trafficking passes. However the straight trafficked regions (SS and CC) with the tracked vehicles showed a significant decline in attached vegetation biomass following each trafficking pass level until the final set of passes where the vegetation loss still occurred but at non-significant ($p < 0.05$) levels. These trends are supported by the same arguments presented with

the related vegetation cover data. The significant side shearing forces acting on the surface in the turns with the tracked vehicles eliminated most of the attached vegetation biomass during the initial trafficking pass. The more gradual loss of attached vegetation biomass measured in the straight trafficked regions with increased number of trafficking passes were primarily due to the repeated crushing and compaction forces being exerted during straight line trafficking on the soil surface and vegetation. Table 24 and Figure 24 show the actual values and the plotted results of the tracked vehicles' trafficking effects on attached vegetation biomass initially (pre-trafficked) and after each trafficking pass level individually for all soils.

Table 23. Soil attached vegetation biomass (g m^{-2}) least square means (lsmeans) for tracked vehicles by trafficking pass across all soils. SE = standard error of the mean, df = degrees of freedom, lower.CL = lower confidence level (95%), and upper.CL = upper confidence level (95%).

Sampling Location*	Pass [†]	lsmean	SE	df	lower.CL	upper.CL	group
CC	p3 (10)	3.32	8.79	93.5	-4.65	30.2	a
	p2 (5)	12.80	8.79	93.5	15.40	50.3	ab
	p1 (1)	32.85	8.79	93.5	74.00	108.9	b
	p0 (0)	91.45	8.79	93.5	17.45	17.4	c
CI	p3 (10)	0.00	8.79	93.5	17.45	17.4	a
	p2 (5)	0.00	8.79	93.5	14.29	20.6	a
	p1 (1)	3.16	8.79	93.5	88.65	123.5	a
	p0 (0)	106.10	8.79	93.5	17.45	17.4	b
CO	p3 (10)	0.00	8.79	93.5	13.14	21.8	a
	p2 (5)	4.31	8.79	93.5	12.76	22.1	a
	p1 (1)	4.69	8.79	93.5	79.35	114.2	a
	p0 (0)	96.79	8.79	93.5	-6.58	28.3	b
SS	p3 (10)	10.87	8.79	93.5	5.37	40.3	a
	p2 (5)	22.82	8.79	93.5	25.49	60.4	ab
	p1 (1)	42.94	8.79	93.5	78.79	113.7	b
	p0 (0)	96.23	8.79	93.5	-4.65	30.2	c

*CI is curve inside, CO is curve outside, and SS is straight section tracked sampling locations.

[†]Pass is the pass level (p0,p1,p2,p3) and the number of cumulative figure-8 trafficking passes conducted with the vehicle are indicated in parentheses.

For a given location, least square mean values (averaged over the level of SoilCode for the individual sampling locations) with the same group letter are not significantly different at 0.05 level by trafficking pass level (Tukey's mean separation).

Table 24. Soil attached vegetation biomass comparisons among trafficking pass levels and sampling locations by soil for tracked vehicles.

SoilCode [†]	Sampling Location*	Soil Attached Vegetation (g m ⁻²) - Tracked Vehicles			
		p0 (0) [‡]	p1 (1) [‡]	p2 (5) [‡]	p3 (10) [‡]
FR-SiCL	CC	166.27 ^a	92.53 ^{bx}	28.80 ^{cx}	11.73 ^c
FR-SiCL	CI		6.00 ^{by}	0.00 ^{by}	0.00 ^b
FR-SiCL	CO		8.13 ^{by}	0.00 ^{by}	0.00 ^b
FR-SiCL	SS		78.00 ^{bx}	39.87 ^{bex}	15.73 ^c
FR-SiL	CC	155.73 ^a	58.13 ^{ab}	33.20 ^{ab}	4.40 ^b
FR-SiL	CI		9.60 ^b	0.00 ^b	0.00 ^b
FR-SiL	CO		10.80 ^b	0.00 ^b	0.00 ^b
FR-SiL	SS		99.47 ^a	47.20 ^a	25.33 ^a
FB-LS	CC	65.49 ^{a††}	7.96 ^b	2.00 ^b	0.47 ^b
FB-LS	CI	105.31 ^a	0.20 ^a	0.00 ^a	0.00 ^a
FB-LS	CO	48.96 ^a	4.01 ^a	21.55 ^a	0.00 ^a
FB-LS	SS	65.49 ^a	34.08 ^{ab}	26.64 ^{ab}	12.52 ^{ab}
WS-L	CC	34.37 ^a	3.44 ^b	0.00 ^b	0.00 ^b
WS-L	CI	34.79 ^a	0.00 ^b	0.00 ^b	0.00 ^b
WS-L	CO	29.80 ^a	0.48 ^b	0.00 ^b	0.00 ^b
WS-L	SS	46.08 ^a	3.07 ^b	0.00 ^b	0.75 ^b
WS-SL	CC	35.37 ^a	2.17 ^b	0.00 ^b	0.00 ^b
WS-SL	CI	68.40 ^a	0.00 ^a	0.00 ^a	0.00 ^a
WS-SL	CO	83.21 ^a	0.00 ^b	0.00 ^b	0.00 ^b
WS-SL	SS	47.60 ^a	0.09 ^b	0.37 ^b	0.00 ^b

[†]SoilCode designates the site and soil where sites are FB = Fort Benning, GA; FR = Fort Riley, KS; WS = White Sands Missile Range, NM and soils are LS = loamy sand, SiCL = silty clay loam, SiL = silt loam, SL = sandy loam and L = loam.

*CI is curve inside, CO is curve outside, and SS is straight section of figure-8 tracked sampling locations.

[‡]Trafficking pass levels, p0, p1, p2, p3 (number of cumulative trafficking passes)

^{††}Initial CC data not recorded. SS initial data substituted.

For a given site/soil, mean values by row with the same letter (a, b, c) are not significantly different at 0.05 level by trafficking pass level (0,1,5,10). For a given site/soil, mean values by column are only significantly different at the 0.05 level by sampling location (CC,CI,CO,SS), if identified with the letter x or y.

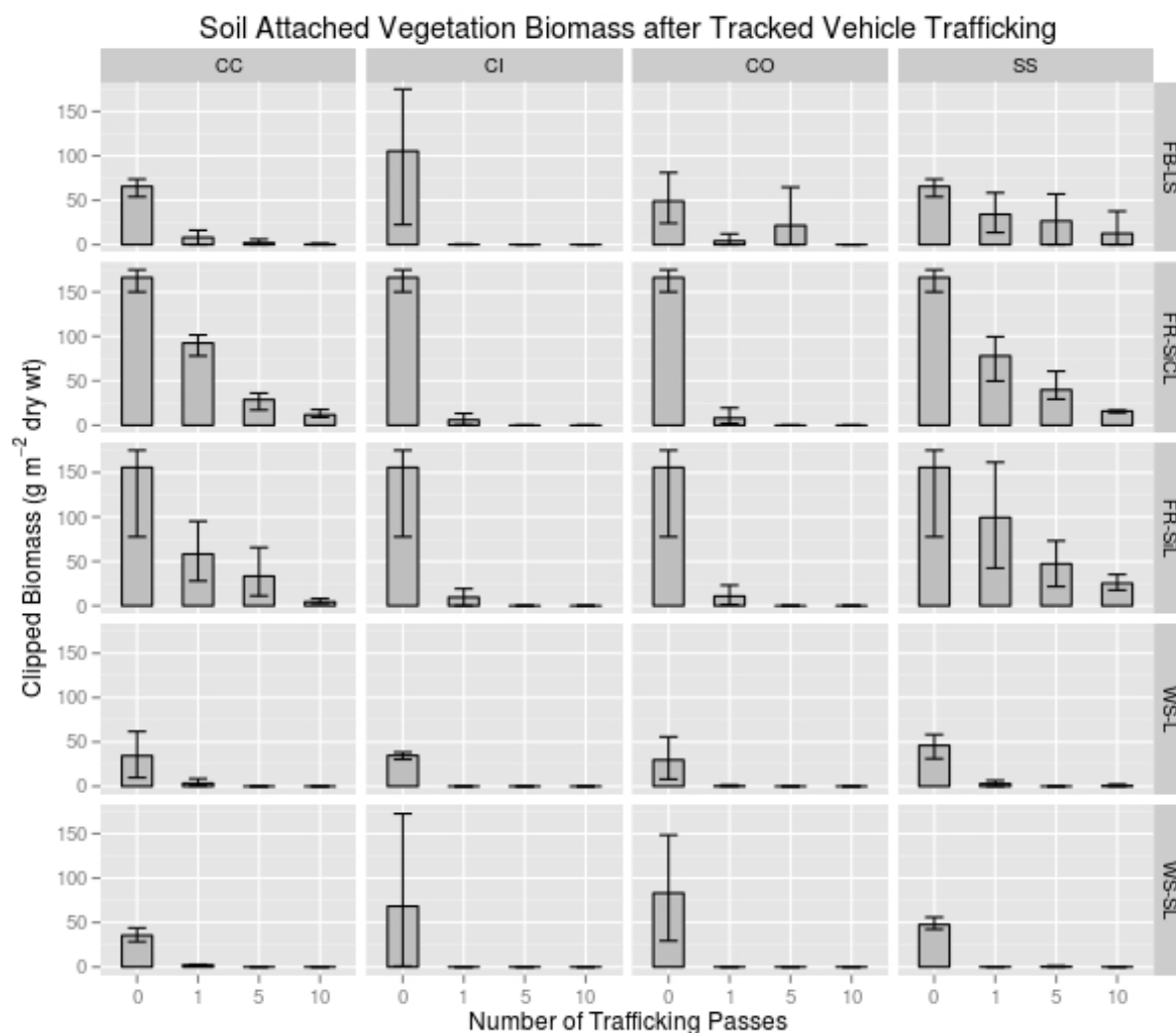


Figure 24. Soil attached vegetation biomass after specified trafficking pass levels for tracked vehicles for all specified soils/sites. Bars represent the mean of the measured values and the error bars represent the maximum and minimum measured values. CI is curve inside, CO is curve outside, and SS is the straight section sampling location. Sites are FB = Fort Benning, GA; FR = Fort Riley, KS; WS = White Sands Missile Range, NM; and YK = Yakima Training Center, WA. Soils are LS = loamy sand, SiCL = silty clay loam, SiL = silt loam, SL = sandy loam, and L = loam.

Wheeled Vehicle Trafficking Effects on Soil Attached (Standing) Vegetation Biomass

The wheeled vehicles showed similar trends overall as the tracked vehicles, but the loss of standing and soil attached vegetation was less severe per pass level, especially in the curved trafficked regions. This is apparent from the limited significance to the location (LOC) factor in Table 25 and the lack of significant differences ($p < 0.05$) among soil types and sampling locations as shown in Table 26.

Table 25. Overall ANOVA type III table of soil attached vegetation biomass for wheeled vehicles (HMMWV). Sum Sq = sum of squares; Mean Sq = mean of squares; NumDF = numerator degrees of freedom; DenDF = denominator degrees of freedom; F.value = F statistic ratio value; PR(>F) = Probability p value associated with F statistic.

Factor	Sum Sq	Mean Sq	NumDF	DenDF	F.value	Pr(>F)	Signif.
SoilCode	18106	3621	5	12	4.5	0.0150	*
Pass	165383	55128	3	180	68.8	<2e-16	***
Loc	6190	2063	3	180	2.6	0.0553	.
SoilCode:Pass	26659	1777	15	180	2.2	0.0072	**
SoilCode:Loc	5640	376	15	180	0.5	0.9532	*
Pass:Loc	5196	577	9	180	0.7	0.6893	***
SoilCode:Pass:Loc	19215	427	45	180	0.5	0.9928	.

Satterthwaite approximation used for degrees of freedom
Signif. codes: 0 '***' 0.001 '**' 0.01 '*' 0.05 '.' 0.1 ' ' 1

Table 26. Soil attached vegetation biomass (g m^{-2}) least square means (lsmeans) for wheeled vehicles (HMMWV) by soil and sampling location. SE = standard error of the mean, df = degrees of freedom, lower.CL = lower confidence level (95%), and upper .CL = upper confidence level (95%).

Sampling Location*	SoilCode [†]	lsmean	SE	df	lower.CL	upper.CL	group
All Locations	WS-SL	11.2	5.53	12	-0.898	23.2	a
	WS-L	21.1	5.53	12	9.095	33.2	ab
	YK-SL	28.9	5.53	12	16.897	41.0	ab
	FR-SiCL	32.3	5.53	12	20.260	44.4	ab
	FB-LS	39.7	5.53	12	27.647	51.7	b
	FR-SiL	42.6	5.53	12	30.596	54.7	b
CC	WS-SL	13.82	8.98	44.1	-4.28	31.9	a
	WS-L	28.27	8.98	44.1	10.18	46.4	a
	YK-SL	28.34	8.98	44.1	10.24	46.4	a
	FR-SiCL	38.60	8.98	44.1	20.50	56.7	a
	FB-LS	47.51	8.98	44.1	29.42	65.6	a
	FR-SiL	49.16	8.98	44.1	31.06	67.3	a
CI	WS-L	9.92	8.98	44.1	-8.17	28.0	a
	WS-SL	10.91	8.98	44.1	-7.18	29.0	a
	FR-SiCL	25.90	8.98	44.1	7.81	44.0	a
	YK-SL	27.96	8.98	44.1	9.86	46.1	a
	FB-LS	32.26	8.98	44.1	14.17	50.4	a
	FR-SiL	34.21	8.98	44.1	16.11	52.3	a
CO	WS-SL	20.80	8.98	44.1	-10.42	25.8	a
	YK-SL	41.63	8.98	44.1	7.78	44.0	a
	FR-SiCL	43.60	8.98	44.1	8.59	44.8	a
	WS-L	12.02	8.98	44.1	8.70	44.9	a
	FR-SiL	12.47	8.98	44.1	12.41	48.6	a
	FB-LS	34.68	8.98	44.1	20.47	56.7	a
SS	WS-SL	74.97	8.98	44.1	-5.90	30.3	a
	WS-L	81.93	8.98	44.1	1.49	37.7	ab
	YK-SL	9.39	8.98	44.1	15.51	51.7	ab
	FR-SiCL	9.45	8.98	44.1	19.95	56.1	ab
	FB-LS	18.98	8.98	44.1	22.34	58.5	ab
	FR-SiL	62.87	8.98	44.1	38.61	74.8	b

*CI is curve inside, CO is curve outside, and SS is straight section of figure-8 tracked sampling locations.

[†]SoilCode designates the site and soil where sites are FB = Fort Benning, GA; FR = Fort Riley, KS; WS = White Sands

Missile Range, NM and soils are LS = loamy sand, SiCL = silty clay loam, SiL = silt loam, SL = sandy loam and L = loam.

For a given sampling location, least square mean values (averaged over the levels of Pass and Loc for “All Locations” and by Pass only for the individual sampling locations) with the same group letter (a,b) are not significantly different at 0.05 level by SoilCode (Tukey’s mean separation).

With the HMMWV wheeled vehicles, the loss of attached vegetation mass was significant ($p < 0.05$) following the first set of 10 trafficking passes for all locations. However, the continued loss of vegetation mass that occurred with additional trafficking passes for all sampling locations

were not significant ($p < 0.05$) as shown in Table 27. The same trends and results were also evident with the heavy wheeled Fire Truck vehicle as well (Table 28 and Table 29), but only the straight trafficked (SS) location was significant (Table 29).

Table 27. Soil attached vegetation biomass (g m^{-2}) least square means (lsmeans) for wheeled vehicles (HMMWV) by trafficking pass across all soils. SE = standard error of the mean, df = degrees of freedom, lower.CL = lower confidence level (95%), and upper .CL = upper confidence level (95%).

Sampling Location*	Pass [†]	lsmean	SE	df	lower.CL	upper.CL	group
CC	p3 (50)	14.72	6.84	185	1.2211	28.2	a
	p2 (25)	18.51	6.84	185	5.0088	32.0	a
	p1 (10)	29.80	6.84	185	16.3044	43.3	a
	p0 (0)	74.10	6.84	185	60.6044	87.6	b
CI	p3 (50)	5.96	6.84	185	-7.5412	19.5	a
	p2 (25)	7.06	6.84	185	-6.4389	20.6	a
	p1 (10)	22.14	6.84	185	8.6411	35.6	a
	p0 (0)	58.96	6.84	185	45.4622	72.5	b
CO	p2 (25)	4.30	6.84	185	-9.2023	17.8	a
	p3 (50)	6.41	6.84	185	-7.0923	19.9	a
	p1 (10)	16.48	6.84	185	2.9822	30.0	a
	p0 (0)	76.89	6.84	185	63.3888	90.4	b
SS	p3 (50)	13.46	6.84	185	-0.0378	27.0	a
	p2 (25)	16.04	6.84	185	2.5400	29.5	a
	p1 (10)	36.82	6.84	185	23.3222	50.3	a
	p0 (0)	67.40	6.84	185	53.9044	80.9	b

*CI is curve inside, CO is curve outside, and SS is straight section of figure-8 tracked sampling locations.

[†]Pass is the pass level (p0,p1,p2,p3) and the number of cumulative figure-8 trafficking passes conducted with the vehicle are indicated in parentheses.

For a given location, least square mean values with the same group letter are not significantly different at 0.05 level by trafficking pass level (Tukey's mean separation).

Table 28. Overall ANOVA type III table of soil attached vegetation biomass for heavy wheeled vehicle (Fire Truck). Sum Sq = sum of squares; Mean Sq = mean of squares; NumDF = numerator degrees of freedom; DenDF = denominator degrees of freedom; F.value = F statistic ratio value; PR(>F) = Probability p value associated with F statistic.

Factor	Sum Sq	Mean Sq	NumDF	DenDF	F.value	Pr(>F)	Signif.
Pass	112512	37504	3	30	6.73	0.0013	**
Loc	18066	6022	3	30	1.08	0.3719	
Pass:Loc	33898	3766	9	30	0.68	0.7237	

Satterthwaite approximation used for degrees of freedom

Signif. codes: 0 '***' 0.001 '**' 0.01 '*' 0.05 '.' 0.1 ' ' 1

Table 29. Soil attached vegetation biomass (g m^{-2}) least square means (lsmeans) for heavy wheeled vehicle (Fire Truck) by sampling location. SE = standard error of the mean, df = degrees of freedom, lower.CL = lower confidence level (95%), and upper .CL = upper confidence level (95%).

Sampling Location*	Pass [†]	lsmean	SE	df	lower.CL	upper.CL	group
CC	p2 (10)	2.733	43.9	31.3	-86.8	92.3	a
	p3 (20)	13.13	43.9	31.3	-76.4	102.7	a
	p2 (2)	16.88	43.9	31.3	-72.7	106.4	a
	p0 (0)	170.71	43.9	31.3	81.1	260.3	a
CI	p3 (20)	0.00	43.9	31.3	-89.6	89.6	a
	p2 (10)	8.10	43.9	31.3	-81.5	97.7	a
	p1 (2)	12.28	43.9	31.3	-77.3	101.8	a
	p0 (0)	132.15	43.9	31.3	42.6	221.7	a
CO	p3 (20)	0.00	43.9	31.3	-89.6	89.6	a
	p1 (2)	12.87	43.9	31.3	-76.7	102.4	a
	p2 (10)	18.41	43.9	31.3	-71.1	108.0	a
	p0 (0)	29.35	43.9	31.3	-60.2	118.9	a
SS	p3 (20)	0.57	43.9	31.3	-89.0	90.1	a
	p1 (2)	23.09	43.9	31.3	-66.5	112.7	ab
	p2 (10)	79.20	43.9	31.3	-10.4	168.8	ab
	p0 (0)	170.71	43.9	31.3	81.1	260.3	b

*CI is curve inside, CO is curve outside, and SS is straight section of figure-8 tracked sampling locations.

[†]Pass is the pass level (p0,p1,p2,p3) and the number of cumulative figure-8 trafficking passes conducted with the vehicle are indicated in parentheses.

For a given location, least square mean values with the same group letter are not significantly different at 0.05 level by trafficking pass level (Tukey's mean separation)

However, the loss of vegetation mass was still greater in the figure-8 turns (CI and CO sampling locations) due to the shearing action of the wheels when turning compared to the straight trafficked locations (SS and CC), even though this trend was not as strong statistically for the wheeled vehicles as the tracked vehicles (Table 30). Figure 25 and Figure 26 show plots that visualize these differences in the degree and rate of loss by trafficking pass level for the wheeled vehicles.

Table 30. Soil attached vegetation biomass (g m^{-2}) comparisons among trafficking pass levels and sampling locations by soil for wheeled vehicles.

SoilCode [†]	Sampling Location*	Soil Attached Vegetation (g m^{-2})			
		HMMWV			
		p0 (0) [‡]	p1 (1) [‡]	p2 (5) [‡]	p3 (10) [‡]
FR-SiCL	CC	66.56 ^{a‡‡}	48.68 ^{ay}	22.76 ^b	16.39 ^b
FR-SiCL	CI		28.41 ^{bx}	6.58 ^{‡‡}	2.07 ^c
FR-SiCL	CO		35.60 ^{axy}	3.60 ^{b‡‡}	0.99 ^b
FR-SiCL	SS		46.67 ^{axy}	19.48 ^{b‡‡}	19.48 ^b
FR-SiL	CC	111.19 ^a	26.68 ^{bxy}	28.61 ^b	30.15 ^b
FR-SiL	CI		18.22 ^{bxy}	3.88 ^b	3.54 ^b
FR-SiL	CO		8.43 ^{bx}	1.96 ^b	0.46 ^{b‡‡}
FR-SiL	SS		50.91 ^{by}	33.57 ^b	31.16 ^{b‡‡}
FB-LS	CC	93.23 ^{††}	68.19	14.65	13.98 ^{††}
FB-LS	CI	65.31	33.59 [‡]	7.39	22.77
FB-LS	CO	93.44	38.27	13.39	9.17
FB-LS	SS	93.23	35.71	21.16	11.67
YK-SL	CC	60.99 ^{††}	29.03	15.87	7.47
YK-SL	CI	38.13	45.55	20.80	7.36
YK-SL	CO	62.17	11.16	2.35	27.81
YK-SL	SS	60.99	54.81	4.37	14.27
WS-L	CC	62.24 ^a	3.31 ^b	27.83 ^b	19.72 ^{ab}
WS-L	CI	32.32 ^a	4.35 ^{ab}	3.03 ^b	0.00 ^b
WS-L	CO	102.95	4.16	0.07	0.00
WS-L	SS	30.19	28.87	15.09	4.19
WS-SL	CC	50.41 ^{ay}	2.93 ^b	1.32 ^b	0.61 ^b
WS-SL	CI	40.25 ^{xy}	2.72	0.68	0.00
WS-SL	CO	25.01 ^{ax}	1.27 ^b	4.41 ^b	0.00 ^b
WS-SL	SS	42.27 ^{axy}	3.96 ^b	2.55 ^b	0.00 ^b
		Fire Truck			
		p0 (0) [‡]	p1 (2) [‡]	p2 (10) [‡]	p3 (20) [‡]
YK-SL	CC	170.71 ^{ay}	16.88 ^{ab}	2.73 ^{ab}	13.13 ^b
YK-SL	CI	132.15 ^{xy}	12.28	8.11	0.00
YK-SL	CO	29.35 ^{ax}	12.87 ^{ab}	18.41 ^{ab}	0.00 ^b
YK-SL	SS	170.71 ^{xy}	23.09	79.2	0.57

[†]SoilCode designates the site and soil where sites are FB = Fort Benning, GA; FR = Fort Riley, KS; WS = White Sands Missile Range, NM and soils are LS = loamy sand, SiCL = silty clay loam, SiL = silt loam, SL = sandy loam and L = loam.

*CI is curve inside, CO is curve outside, and SS is straight section of figure-8 tracked sampling locations.

[‡]Trafficking pass levels, p0,p1,p2,p3 (number of cumulative passes)

^{††}Initial CC data not recorded. SS initial data substituted.

^{‡‡}Missing replication value substituted with average of other two replications.

For a given site/soil, mean values by row with the same letter (a, b, c) are not significantly different at 0.05 level by trafficking pass level (0,1,5,10) or (0,2,10,20). For a given site/soil, mean values by column are only significantly different at the 0.05 level by sampling location (CI,CO,SS), if identified with the letter x or y.

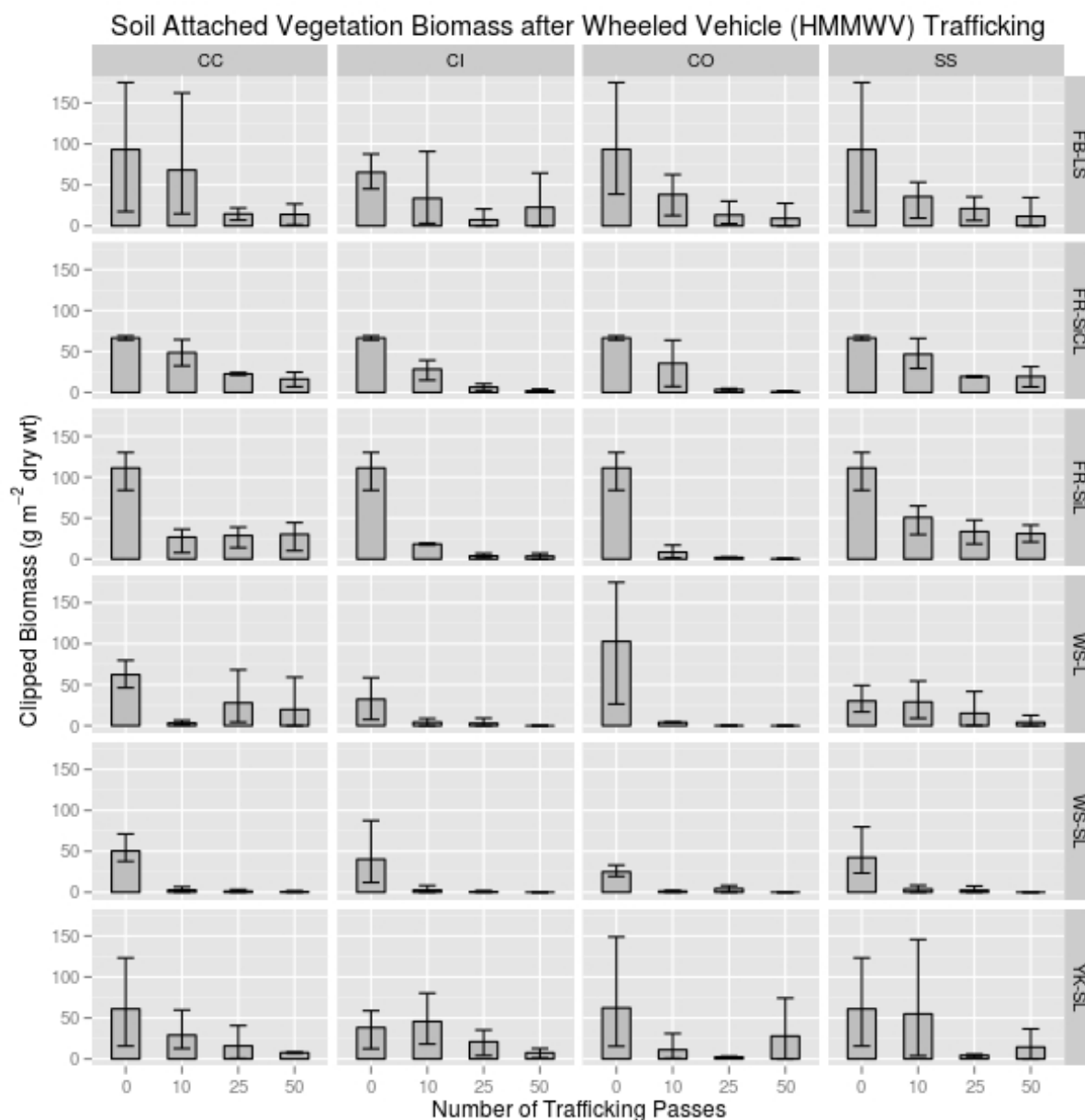


Figure 25. Soil attached vegetation biomass after specified trafficking pass levels for wheeled (HMMWV) vehicles for all specified sites-soils. Bars represent the mean of the measured values and the error bars represent the maximum and minimum measured values. CC is center cross, CI is curve inside, CO is curve outside, and SS is the straight section sampling location. Sites are FB = Fort Benning, GA; FR = Fort Riley, KS; WS = White Sands Missile Range, NM; YK = Yakima Training Center, WA. Soils are LS = loamy sand, SiCL = silty clay loam, SiL = silt loam, SL = sandy loam, and L = loam.

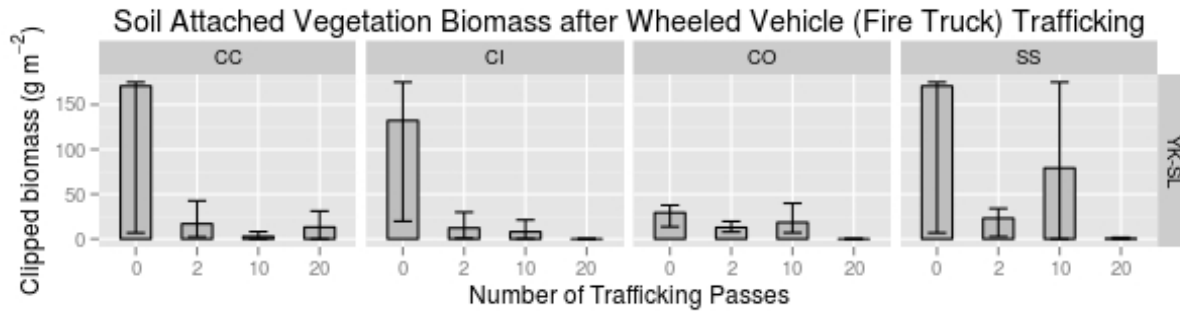


Figure 26. Soil attached vegetation biomass after specified trafficking pass levels for wheeled (Fire Truck) vehicle for the specified site-soil. Bars represent the mean of the measured values and the error bars represent the maximum and minimum measured values. CC is center cross, CI is curve inside, CO is curve outside, and SS is the straight section sampling location. Site is YK = Yakima Training Center, WA. Soil is SL = sandy loam.

Soil Attached Vegetation Biomass Loss vs. Trafficking Pass Level

Preliminary relationships between soil attached vegetation biomass loss and vehicle pass number were determined for both the curved and straight trafficked regions for all vehicles for each individual soil. Again, a simple first order decay model, $y = ae^{-bx}$ (where y is the mass of attached vegetative biomass, x is the number of accumulated trafficking passes, and a and b are function parameters) was used. As expected the curved regions (CI, CO) had higher decay rates (“ b ” values in Table 31) than the straight trafficked regions (SS, CC) for all vehicles and soils. However, the fits were less robust, based upon the adjusted R^2 values, than those obtained for vegetation cover (Table 18). The poor adjusted R square values hint at the excessive sampling variability likely influencing those results.

The data were transformed so that the initial vegetation mass per unit area within each replication and sampling location would equal 100 when fitting the equation. However, the extreme variability of the replicated sample values (an order of magnitude variation in some cases) not only affected the fits but also partially obscures the mean trends. Although less pronounced, the trends were generally similar to the related vegetation cover results (Table 18). The sites with the greatest initial soil attached vegetation biomass (Ft. Riley and Ft. Benning) held up better to the tracked trafficking in the straightaway (SS,CC) sampling locations than on the sites at White Sands Missile Range. Likewise, the wheeled trafficking experiments produced generally similar results. One reason that the White Sands Missile Range sites lost attached vegetation biomass faster is probably because the vegetation was either dormant or had already died when the experiments were conducted (early January). Thus, plants were likely far more susceptible to destruction from the trafficking than at the other sites.

These results imply that resistance to repeat trafficking effects are improved by: 1) more vegetation available prior to trafficking, 2) a denser vegetation root system (grasses tend to have a more extensive fibrous root system than annuals), and 3) more large aggregates in a soil. In the case of Ft. Riley, which consisted of the most aggregated soils tested and was dominated with prairie grasses, the site afforded the most protection by far compared to the other sites (lowest decay rate values as shown in Table 31), even though a significant amount of biomass was

removed prior to the trafficking experiments. So, the Ft. Riley sites would likely have resisted the deterioration of the vegetation due to repeated trafficking even better if the sites had not been mowed and the excess biomass removed prior to conducting the trafficking experiments.

Table 31. Fitted first order soil attached biomass decay function parameters for the curved (CI,CO) and straight trafficked (SS) regions for all vehicles at all sites.

SoilCode [†]	Sampling Location*	Vegetation Biomass 1 st Order Decay Function Parameters		
		<i>a</i>	<i>b</i>	Adj R ²
Tracked Vehicles				
FR-SiCL	CI,CO	100.00	3.16	0.99
FR-SiCL	SS,CC	93.19	0.29	0.87
FR-SiL	CI,CO	100.00	2.73	0.64
FR-SiL	SS,CC	93.99	0.28	0.44
FB-LS	CI,CO	100.00	3.18	0.32
FB-LS	SS,CC	100.06	0.74	0.81
WS-L	CI,CO	100.00	4.82	0.75
WS-L	SS,CC	99.97	2.50	0.73
WS-SL	CI,CO	100.00	12.11	0.44
WS-SL	SS,CC	100.00	6.10	0.96
Wheeled Vehicles - HMMWV				
FR-SiCL	CO,CI	100.92	0.082	0.87
FR-SiCL	SS,CC	95.24	0.022	0.68
FR-SiL	CO,CI	99.98	0.21	0.94
FR-SiL	SS,CC	94.59	0.045	0.66
FB-LS	CI,CO	99.41	0.077	0.27
FB-LS	SS,CC	96.42	0.043	0.26
YK-SL	CI,CO	99.82	0.038	0.17
YK-SL	SS,CC	101.07	0.035	0.17
WS-L	CI,CO	72.43	1.00	0.47
WS-L	SS,CC	93.52	0.019	0.10
WS-SL	CI,CO	77.56	1.00	0.52
WS-SL	SS,CC	74.82	1.00	0.62
Wheeled Vehicle – Fire Truck				
YK-SL	CI,CO	99.86	0.65	0.32
YK-SL	SS,CC	99.90	0.92	0.49

[†]SoilCode designates the site and soil where sites are FB = Fort Benning, GA; FR = Fort Riley, KS; WS = White Sands Missile Range, NM and soils are LS = loamy sand, SiCL = silty clay loam, SiL = silt loam, SL = sandy loam and L = loam.

*CI is curve inside, CO is curve outside, CC is cross-over and SS is straight section of figure-8 tracked sampling locations.

Surface Soil Aggregate Size Distribution (ASD)

Data Analysis

ASD data for erodible fraction (EF), geometric mean diameter (GMD), and Geometric Standard Deviation were analyzed independently for the five vehicle types (M1025A2, M1A1, M1151A, M88A1, and M925A1). For each of these analyses, there were three replications for each vehicle/soil texture combination at each site. Because of the differences in the nature of physical disturbance between tracked (i.e., shearing action) and wheeled (i.e., rolling action) vehicles, each were analyzed separately. All ASD statistical analysis was performed using RStudio (R Core Team, 2015). Preliminary statistical analysis on actual data values indicated normal distribution among data.

ANOVA was used to determine significant difference ($p < 0.05$ level) between sampling location for inside vs. outside curve (CI vs. CO) and ridge vs. track (R vs. T) location. A pairwise analysis for each vehicle type (Tracked vs. Wheeled) by Pass and soil texture was also performed to determine significant difference (0.05 level) for Pass number on each soil texture.

Prediction models for EF, GMD, and GSD were sought from among the following variables: Pass number (Pass), vehicle weight (VehWt), vehicle cone index 1 (VCI1), ground pressure (GP), clay (C), silt (Si), sand (S), very fine sand (VFS), clay+silt (CSi), sand+silt (SSi), sand+very fine sand (SVFS), silt+very fine sand (SiVFS), organic matter (OM), calcium carbonate (CaCO_3), cation exchange capacity (CEC), initial water content IWC, initial bulk density (IBD), optimal water content (OWC), and proctor density (PD) using an iterative selection procedure. GMD and the square root of GMD (GMDSQR) were also included for predicting GSD. The dataset was randomly partitioned into two halves 100 times or 100 iterations. For each of these partitions, a forward selection procedure was applied to determine a regression model using one half of the dataset to select a model using the 'step' function supplied in the 'stats' library of R (R Core Team 2015) and the other half of the dataset to evaluate the selected model with the mean squared error of prediction (mse). Each of the models and their corresponding cross validation statistic, mse, were saved in a list for final evaluation. The frequency of occurrence for each of the models in the list was tallied and the mse was averaged for each model. We chose the most frequently occurring model in the list and then fit it to the full dataset to arrive at a final model. The mse was computed for the case of tie-breakers.

Results

Note that no ridge samples were taken at YTC as no ridges were formed under trafficking of the wheeled vehicles. Also note that the ridge was not sampled on the straight section at all sites for all vehicles (as none was formed) and was therefore not included in the analysis.

Sampling location of CI and CO for tracked vehicles within a pass level had no significant effect ($p < 0.05$) on EF and GMD regardless of vehicle type or soil (see Table 32); therefore curve location was combined as curve only without distinction of inside or outside curve for subsequent analysis. GSD showed an effect ($p < 0.05$) with curve location only for the tracked vehicle within pass level at FTB (GSD has no interaction with EF and little effect on GMD). Ridged vs. tracked location did show significant differences ($p < 0.05$) for all sites and ASD parameters except GSD at FTR and EF and GMD at FTB. Therefore subsequent analysis was conducted separately on ridge and track samples. All curve locations (CI, CO, SS) for all wheeled vehicles within a pass level had no significant effect ($p < 0.05$) on EF, GMD, and GSD

(see Table 32). Similarly, no significant difference for wheeled vehicles was found between ridged and tracked sample locations within a pass level. For the wheeled vehicles, these locations were combined for each sample site (CI, CO, SS, ridge, and track) for subsequent analysis.

Table 32. Significance of difference between location for tracked and wheeled vehicles for measured aggregate parameters at each study site.

Site*	Measured Parameter**	Trafficking Vehicle			
		Ridge vs. Track		Curve Inside vs. Curve Outside	
		Tracked	Wheeled	Tracked	Wheeled
FTR	EF	0.001***	NS	NS	NS
	GMD	0.05	NS	0.1	NS
	GSD	NS	NS	NS	NS
FTB	EF	0.1	NS	NS	NS
	GMD	NS	NS	NS	NS
	GSD	0.01	NS	0.05	NS
YTC	EF	-	-	NS	NS
	GMD	-	-	NS	NS
	GSD	-	-	NS	NS
WSMR	EF	0.01	NS	NS	NS
	GMD	0.001	NS	NS	NS
	GSD	0.01	NS	NS	NS

*FTB = Fort Benning, GA; FTR = Fort Riley, KS; YTC = Yakima Training Center, WA and WSMR = White Sands Missile Range, NM.

**EF = erodible fraction, GMD = geometric mean diameter, GSD = geometric standard deviation.

***Level of significance ($p > F$) where NS indicates no significance.

Note that ridge samples were not taken at YTC.

The ASD response of the measured parameters to the number of passes for wheeled vehicles with all sampling locations combined at each site per pass is presented in Figure 27. The wheeled vehicle effects are consistently described by a 2nd order polynomial equation. EF values show a consistent increase with increasing number of passes with R^2 values ranging from, 0.937 on a sandy loam soil at YTC for the Fire Truck to 0.996 for the Humvee at WSMR on the sandy loam soil. At all sites except FTR, initial EF was significantly lower ($p < 0.05$) than soils subjected to vehicle passes. The lowest initial and subsequent EF with vehicle passes were on the soils with higher clay content at FTR while the sandier soils at FTB, YTC, and the sandy loam soil at WSMR showed the highest initial and subsequent EF. GMD exhibited a similar but opposite trend where the largest aggregates were found for both soils at FTR for the initial condition and the GMD decreased with the number of passes with R^2 values ranging from 0.916 to 0.996. Initial GMD showed significantly higher values ($p < 0.05$) than those under vehicle passes except at FTR on the silty clay loam soil and WSMR on the sandy loam soil where no difference was found between initial and subsequent passes. The higher clay soils at FTR showed higher values of an approximate order of magnitude in GMD compared to the other sites and soils. These trends in EF and GMD in response to soil texture are reasonable since clay soils have been found to form larger aggregates and smaller EF in soils with a clay range of 20 to 35% (Chepil, 1953; Tatarko, 2001) which are similar results to this study. The R^2 for GSD trend

under wheeled traffic ranged from 0.897 on the silt loam at FTR to 0.999 on the loam soil at WSMR. All sites showed a significant difference ($p < 0.05$) in GSD between the initial condition and subsequent passes except for the silty clay loam soil at FTR. GSD showed a mixed response to increasing passes for wheeled vehicles where the GSD at FTR increased with the number of passes, while for the other sites an increase in passes resulted in a decrease in GSD. This could be explained by the finer soils forming larger aggregates as evidenced by the magnitude of GMD values at this site compared to other sites. The lower GMD values at the other sites indicate a low aggregation state as sandier soils tend to be less stable and more subject to break down under traffic. While this is expected for sandier soils, smaller GMD values would tend to indicate a narrower range in aggregate sizes and thus a less effect on GSD.

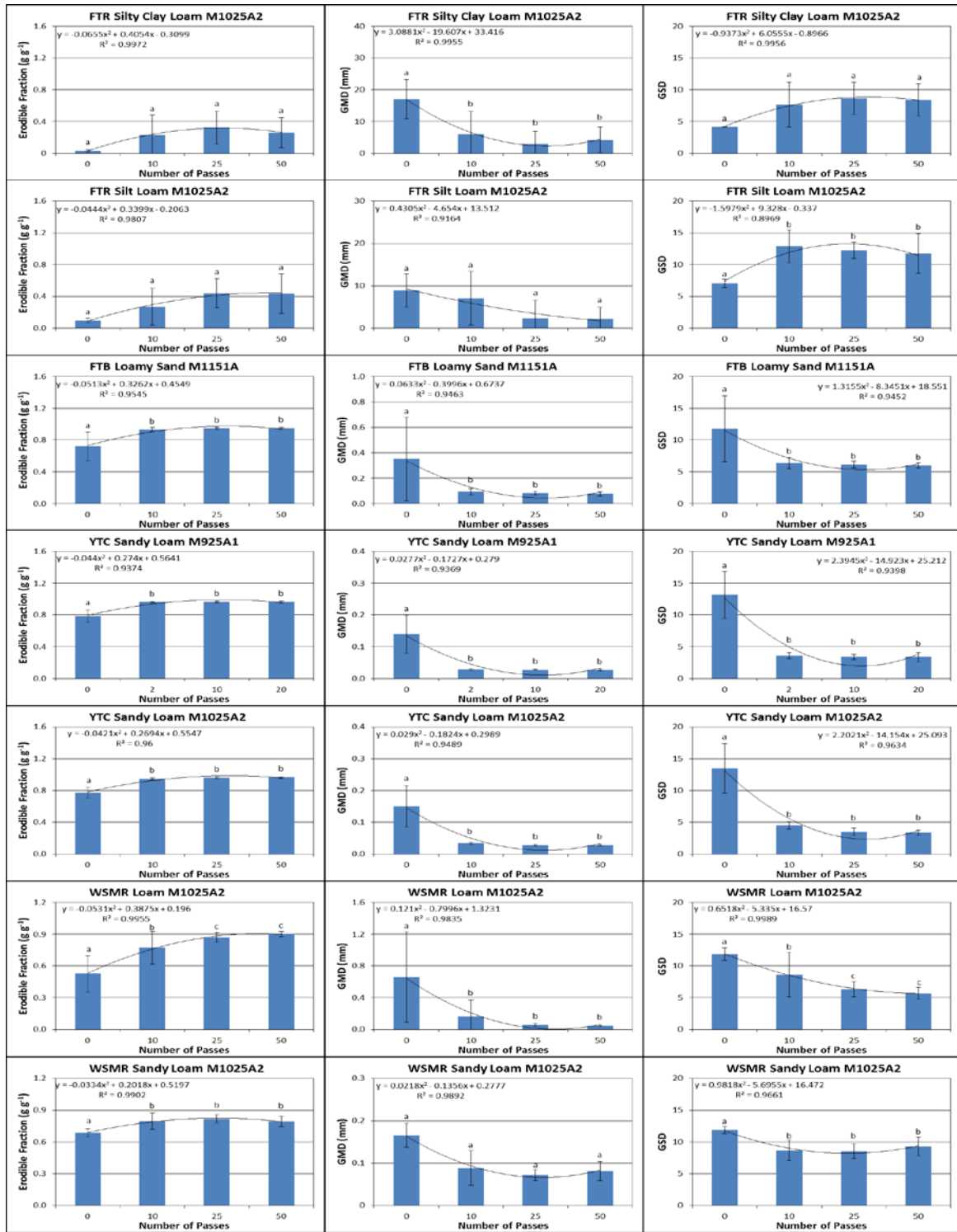


Figure 27. Wheeled vehicles response to pass level on Erodible Fraction, GMD (geometric mean diameter), and GSD (geometric standard deviation). Means with the same letter are not significant ($p < 0.05$) between passes for each soil and vehicle type (see **Table 2**). FTB = Fort Benning, GA; FTR = Fort Riley, KS; YTC = Yakima Training Center, WA and WSMR = White Sands Missile Range, NM.

The ASD response of the measured parameters to number of passes for the tracked vehicles is presented in Figure 27. No tracked vehicles were available at YTC and so data are presented only for FTR, FTB, and WSMR. The ASD response to tracked vehicles was more mixed than for the wheeled vehicles. Preliminary analysis of tracked vehicles showed differences between the tracked and ridge sampling location while inside and outside curve showed no difference for the parameters measured. Therefore, the inside and outside curve data were combined and analyzed as simply either the track or ridge sampling location. The sandier soils studied showed the least differences ($p < 0.5$) with pass number where the WSMR sandy loam showed no response to the number of passes for all parameters and sampling locations. Similarly, the loamy sand at FTB showed no difference with pass number for the curve track and ridge sampling location (CT and CR) for all parameters and the SST location only showed difference in EF between the initial and subsequent passes. The finest textured soil studied at FTR (silty clay loam) showed a more varied response between the initial soil condition and subsequent passes. EF tended to increase and GMD decrease with number of passes for the SST location. However, EF tended to increase and GMD decrease after the first pass at the CT and CR locations and subsequent passes showed a decrease in EF and an increase in GMD. As might be expected, the medium textured soils (silt loam at FTR and loam at WSMR) showed an intermediate response to the number of vehicle passes. The silt loam at FTR only showed a pass effect on EF for the CT position and GSD for the CR location while GMD showed no pass effect. It should be noted that in general for EF and GMD, when there was a difference between initial condition and the first pass, five and ten passes rarely showed difference from the one pass. Similar to the wheeled vehicle response, tracked vehicle GSD for the finer textured soils at FTR showed a slight trend to increase with the number of passes while the more sandy soils at the other sites tended to decrease with increasing passes.

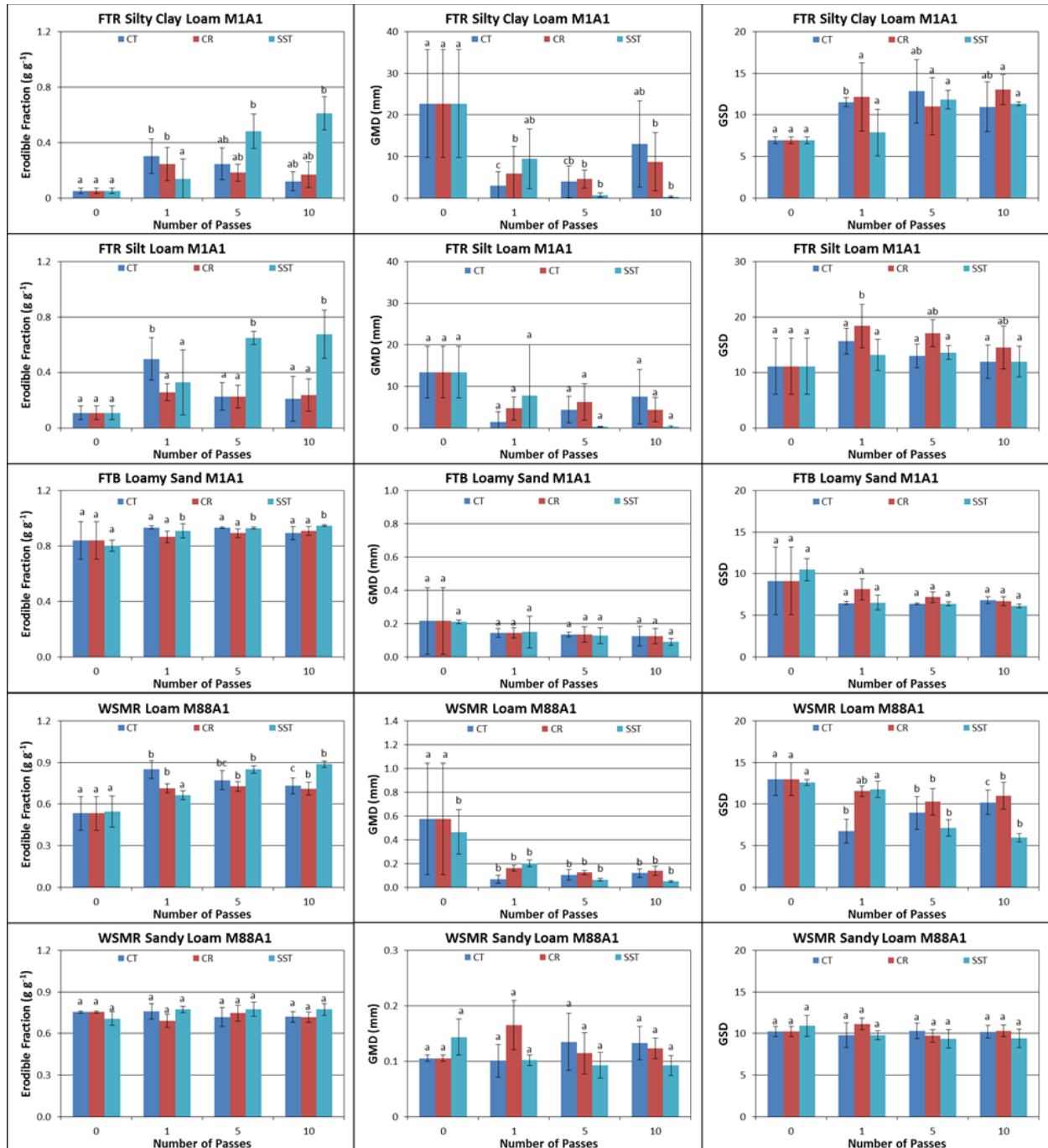


Figure 28. Tracked vehicle response to pass level on Erodible Fraction, GMD (geometric mean diameter), and GSD (geometric standard deviation) within sampling location. Means with the same letter are not significant ($p < 0.05$) between passes for each soil and vehicle type (see Table 2). Note, no tracked vehicles were run at YTC. CT is the curve track sampling location, CR is the curve ridge sampling location, and SST is the straight section track sampling location. FTB = Fort Benning, GA; FTR = Fort Riley, KS and WSMR = White Sands Missile Range, NM.

The result of the prediction models of the various parameters given soil and vehicle properties for the four sampling locations in Table 33 show that the R^2 values for the predicted vs. observed ranged from 0.75 to 0.92 for EF, 0.69 to 0.87 for GMD, and 0.48 to 0.56 for GSD. GMD and GSD were best predicted by the log of the parameters. These prediction equations can be used within the WEPS model to predict the changes in GMD and GSD given the number of vehicle passes, vehicle type, and soil properties at each position on the landscape relative to the vehicle track (i.e., sampling location). As expected and as discussed above, soil texture often appears to have an effect on the measured parameters. In addition, initial water content was also selected which is reasonable since it is a function of soil texture and can affect aggregation. Interestingly, a vehicle characteristic (vehicle weight) was selected only for GSD of wheeled vehicles.

Table 33. Predictive models of aggregate parameters based on soil properties and vehicle passes.

Sampling Location*	ASD Parameter	Model**	R ²
T-C-t	EF	EF = 3.1342 - 0.0428OM - 0.0030Pass - 1.7857PD + 0.0115SVFS	0.8298
	GMD	Log(GMD) = -2.8595 - 0.0417CEC + 0.2473IWC + 0.0202Pass	0.7513
	GSD	Log(GSD) = -0.7325 - 0.0147GMD + 1.4712IBD - 0.0007Pass + 0.0205SVFS	0.4861
T-C-r	EF	EF = 2.7660 - 0.0298OM + 0.0044Pass - 1.6380PD + 0.0118SVFS	0.9199
	GMD	Log(GMD) = -9.1814 + 2.5406OM - 0.0396Pass + 0.0541SVFS	0.8794
	GSD	Log(GSD) = 1.80502 - 0.01412C - 0.0142GMD - 0.00571Pass + 0.0167SIVFS	0.5448
T-SS-t	EF	EF = 0.8118 - 0.0332IWC + 0.0314Pass	0.7467
	GMD	Log(GMD) = -2.0206 + 0.1952IWC - 0.2262Pass	0.6930
	GSD	Log(GSD) = -1.0465 - 0.1337GMDSQR + 1.7590IDB - 0.0331Pass + 0.0222SIVFS	0.5568
W	EF	EF = 1.9296 - 0.0476IWC - 0.5419PD + 0.0034Pass	0.7646
	GMD	Log(GMD) = -1.8336 + 0.3130IWC - 0.1182OWC - 0.0225Pass	0.7461
	GSD	Log(GSD) = 1.8871 - 0.1422CaCO ₃ - 0.2661GMD + 0.9754GMDSQR + 0.0334IWC - 0.0073Pass + 0.0001VehWt	0.5505

*Sampling locations where T-C-t = Tracked vehicles, curve location within the track; T-C-r = Tracked vehicles, curve location within the ridge; T-SS-t = Tracked vehicles, straight section location within the track; W = Wheeled vehicles, all sampling locations.

**Variables selected: C = clay (kg kg⁻¹); CaCO₃ = calcium carbonate (kg kg⁻¹); CEC = cation exchange capacity (meq 100g⁻¹); GMD = geometric mean diameter (mm); GMDSQR = square root of the GMD (mm); IBD = initial bulk density (Mg m⁻³); IWC = initial water content (cm³ cm⁻³); OM = organic matter (kg kg⁻¹); OWC = optimum water content (cm³ cm⁻³); Pass = number of passes; PD = proctor density; SIVFS = silt plus very fine sand (kg kg⁻¹); SVFS = sand plus very fine sand (kg kg⁻¹), and VehWt = vehicle weight (kg).

Random Roughness

If the vegetative cover is limited or non-existent, random roughness can affect a soil surface's ability to resist the erosive force of the wind at the surface by increasing the threshold friction velocity at the surface. The greater the random roughness, the greater the required surface friction velocity required by the wind to initiate saltation (movement of erodible size particles, between 0.5 and 1 mm in diameter, by a series of short bounces along the surface where they dislodge additional particles on each impact with the surface), which usually accounts for most

of the total movement of soil by wind. The greater the quantity of larger non-erodible size particles/aggregates (>2 mm in diameter) that make up the surface random roughness, the more resistant the surface will be at controlling wind erosion. However, at most of the experimental sites studied, the multi-pass trafficking ground down the surface soil aggregates, leaving the surface random roughness consisting of small highly erodible sized aggregates (<0.84 mm) and single grain particles (Figure 27 and Figure 28). Thus, the available random roughness would be expected to be limited in its ability to control or reduce wind erosion emissions on these sites. However, this is not necessarily true for the roughness on the ridges, assuming sufficient amounts of non-erodible size aggregates (>0.84 mm) are remaining on the ridges, when formed from the surface shearing action of the turning vehicles.

For tracked vehicles, Table 34 suggests that the interaction of soil type and traffic pass level (SoilCode:Pass) was significant in determining the resulting random roughness ($p < 0.001$), with traffic pass level (Pass) next ($p < 0.01$), followed by the soil type (SoilCode). Table 35 shows inconsistent random roughness results between soil type and sampling locations for the tracked vehicles. Likewise, Table 36 shows no significant differences between the tracked vehicle trafficking passes and the resulting random roughness levels. Thus, the surface random roughness differences between soil type and trafficking pass level are not expected to significantly impact wind erosion among the sites.

Table 34. Overall ANOVA type III table of random roughness values for tracked vehicles (Sum Sq = sum of squares; Mean Sq = mean of squares; NumDF = numerator degrees of freedom; DenDF = denominator degrees of freedom; F.value = F statistic ratio value; PR(>F) = Probability p value associated with F statistic).

Factor	Sum Sq	Mean Sq	NumDF	DenDF	F.value	Pr(>F)	Signif.
SoilCode	111.5	27.86	4	10	4.94	0.01856	*
Pass	77.7	25.91	3	110	4.59	0.00457	**
Loc	19.9	9.97	2	110	1.77	0.17598	
SoilCode:Pass	234.6	19.55	12	110	3.46	0.00024	***
SoilCode:Loc	66.3	8.28	8	110	1.47	0.17751	
Pass:Loc	28.9	4.82	6	110	0.85	0.53141	
SoilCode:Pass:Loc	162.3	6.76	24	110	1.20	0.26016	

Satterthwaite approximation used for degrees of freedom

Signif. codes: 0 '***' 0.001 '**' 0.01 '*' 0.05 '.' 0.1 ' ' 1

Table 35. Random roughness (mm) least square means (lsmean) for tracked vehicles by soil and sampling location. CI is curve inside, CO is curve outside, and SS is straight section. Soil code designates the site and soil where sites are FB = Fort Benning, FR = Fort Riley, and WS = White Sands and soils are LS = loamy sand, SiCL = silty clay loam, SiL = silt loam, SL = sandy loam, and L = loam. SE = standard error of the mean, df = degrees of freedom, lower.CL = lower confidence level (95%), and upper .CL = upper confidence level (95%).

Sampling Location*	SoilCode[†]	lsmean	SE	df	lower.CL	upper.CL	group
All Locations	FB-LS	4.18	0.549	10	2.96	5.40	a
	FR-SiCL	4.99	0.549	10	3.77	6.22	ab
	WS-L	5.03	0.549	10	3.80	6.25	ab
	FR-SiL	6.78	0.549	10	5.55	8.00	b
	WS-SL	6.96	0.549	10	5.74	8.18	b
CI	WS-L	3.56	0.784	27	1.95	5.17	a
	FB-LS	3.92	0.784	27	2.31	5.53	a
	FR-SiCL	5.15	0.784	27	3.54	6.76	ab
	WS-SL	6.31	0.784	27	4.70	7.91	ab
	FR-SiL	7.39	0.784	27	5.79	9.00	b
CO	FB-LS	4.40	0.784	27	2.79	6.01	a
	WS-L	5.38	0.784	27	3.77	6.99	ab
	FR-SiCL	5.42	0.784	27	3.81	7.03	ab
	FR-SiL	6.90	0.784	27	5.29	8.51	ab
	WS-SL	8.13	0.784	27	6.52	9.74	b
SS	FB-LS	4.22	0.784	27	2.61	5.83	a
	FR-SiCL	4.41	0.784	27	2.80	6.02	a
	FR-SiL	6.04	0.784	27	4.43	7.65	a
	WS-L	6.14	0.784	27	4.53	7.75	a
	WS-SL	6.44	0.784	27	4.83	8.05	a

*CI is curve inside, CO is curve outside, and SS is straight section of figure-8 tracked sampling locations.

[†]SoilCode designates the site and soil where sites are FB = Fort Benning, GA; FR = Fort Riley, KS; WS = White Sands Missile Range, NM and soils are LS = loamy sand, SiCL = silty clay loam, SiL = silt loam, SL = sandy loam and L = loam.

For a given sampling location, least square mean values (averaged over the levels of Pass and Loc for “All Locations” and by Pass only for the individual sampling locations) with the same group letter (a, b) are not significantly different at 0.05 level by SoilCode (Tukey’s mean separation)

Table 36. Random roughness (mm) least square means (lsmean) for tracked vehicles by trafficking pass across all soils. SE = standard error of the mean, df = degrees of freedom, lower.CL = lower confidence level (95%), and upper .CL = upper confidence level (95%).

Sampling Location*	Pass [†]	lsmean	SE	df	lower.CL	upper.CL	group
CI	p0 (0)	4.18	0.637	114	2.92	5.45	a
	p2 (5)	5.15	0.637	114	3.89	6.41	a
	p1 (1)	5.66	0.637	114	4.39	6.92	a
	p3 (10)	6.08	0.637	114	4.82	7.34	a
CO	p0 (0)	5.02	0.637	114	3.76	6.28	a
	p3 (10)	5.48	0.637	114	4.21	6.74	a
	p1 (1)	6.61	0.637	114	5.35	7.87	a
	p2 (5)	7.08	0.637	114	5.82	8.34	a
SS	p0 (0)	4.40	0.637	114	3.13	5.66	a
	p3 (10)	5.07	0.637	114	3.80	6.33	a
	p2 (5)	6.02	0.637	114	4.75	7.28	a
	p1 (1)	6.32	0.637	114	5.06	7.58	a

*CI is curve inside, CO is curve outside, and SS is straight section tracked sampling locations.

[†]Pass is the pass level (p0,p1,p2,p3) and the number of cumulative figure-8 trafficking passes conducted with the vehicle are indicated in parentheses.

For a given location, least square mean values (averaged over the level of SoilCode for the individual sampling locations) with the same group letter are not significantly different at 0.05 level by trafficking pass level (Tukey's mean separation).

Table 37 and Table 40 show that for wheeled vehicles the traffic pass level (Pass) was most significant for the resulting random roughness ($p < 0.001$ and $p < 0.05$) and the interaction of soil type and traffic pass level (SoilCode:Pass) next ($p < 0.01$), followed by the sampling location (Loc) for the HMMWV vehicles. Table 38 indicates that traffic on the Ft. Riley and Yakima soils resulted in the higher random roughness values for "All Locations" and individual sampling locations, with the Ft. Benning and White Sands Missile Range soils providing lower random roughness values for the wheeled HMMWV vehicles. Table 39 showed mostly non-significant differences between the wheeled HMMWV vehicle trafficking passes and the resulting random roughness levels, while Table 41 shows no significant differences between the wheeled Fire Truck vehicle passes and the and resulting random roughness.

When vegetation is limited or non-existent, soil random roughness is one of the few options left that can limit wind erosion emissions, but only if sufficient non-erodible size (> 0.84 mm) aggregates compose that roughness. Unfortunately, both the low random roughness and the high percentage of erodible size (< 0.84 mm) aggregates present created by trafficking means that these trafficked site conditions become highly susceptible to wind erosion. Thus, land managers with limited or non-existent vegetative cover following trafficking events may consider restoring vegetation cover as quickly as possible to reduce that immediate risk following trafficking until sufficient vegetation growth is achieved.

Table 37. Overall ANOVA type III table of random roughness values for wheeled (HMMWV) vehicles (Sum Sq = sum of squares; Mean Sq = mean of squares; NumDF = numerator degrees

of freedom; DenDF = denominator degrees of freedom; F.value = F statistic ratio value; PR(>F) = Probability p value associated with F statistic).

Factor	Sum Sq	Mean Sq	NumDF	DenDF	F.value	Pr(>F)	Signif.
SoilCode	758	151.7	5	12.8	23.83	4.6e-06	***
Pass	29	9.7	3	114.1	1.52	0.212	
Loc	37	18.7	2	112.5	2.94	0.057	.
SoilCode:Pass	185	12.4	15	113.7	1.94	0.026	*
SoilCode:Loc	48	4.8	10	112.5	0.75	0.678	
Pass:Loc	38	6.4	6	112.7	1.01	0.424	
SoilCode:Pass:Loc	124	5.2	24	112.7	0.81	0.713	

Satterthwaite approximation used for degrees of freedom
Signif. codes: 0 '***' 0.001 '**' 0.01 '*' 0.05 '.' 0.1 ' ' 1

Table 38. Random roughness (mm) least square means (lsmean) for wheeled (HMMWV) vehicles by soil and sampling location. CI is curve inside, CO is curve outside, and SS is straight section. Soil code designates the site and soil where sites are FB = Fort Benning, FR = Fort Riley, and WS = White Sands and soils are LS = loamy sand, SiCL = silty clay loam, SiL = silt loam, SL = sandy loam, and L = loam. SE = standard error of the mean, df = degrees of freedom, lower.CL = lower confidence level (95%), and upper .CL = upper confidence level (95%).

Sampling Location*	SoilCode[†]	lsmean	SE	df	lower.CL	upper.CL	group
All Locations ^{††}	WS-L	2.37	0.530	10.8	1.20	3.54	a
	WS-SL	3.24	0.530	10.8	2.07	4.41	ab
	FB-LS	3.97	0.530	10.8	2.80	5.14	ab
	FR-SiCL	5.02	0.593	14.9	3.76	6.29	bc
	YK-SL	7.52	0.530	10.8	6.35	8.69	cd
	FR-SiL	9.35	0.563	12.8	8.13	10.57	d
CI	WS-L	3.48	0.754	23.5	1.93	5.04	a
	FB-LS	3.65	0.754	23.5	2.09	5.21	a
	WS-SL	4.40	0.754	23.5	2.84	5.95	a
	YK-SL	9.78	0.754	23.5	8.22	11.34	b
	FR-SiCL	NA	NA	NA	NA	NA	
	FR-SiL	NA	NA	NA	NA	NA	
CO	WS-L	2.22	0.735	21.6	0.695	3.75	a
	WS-SL	2.92	0.735	21.6	1.398	4.45	ab
	FB-LS	4.50	0.735	21.6	2.971	6.02	ab
	FR-SiCL	5.72	0.867	33.4	3.956	7.48	bc
	YK-SL	8.13	0.735	21.6	6.603	9.65	cd
	FR-SiL	9.55	0.782	25.6	7.942	11.16	d
SS	WS-L	2.51	0.735	21.6	0.989	4.04	a
	FB-LS	3.45	0.735	21.6	1.921	4.97	a
	WS-SL	3.56	0.735	21.6	2.033	5.09	a
	FR-SiCL	4.33	0.781	25.6	2.721	5.93	ab
	YK-SL	6.90	0.735	21.6	5.377	8.43	bc
	FR-SiL	9.15	0.782	25.6	7.540	10.76	c

*CI is curve inside, CO is curve outside, and SS is straight section of figure-8 tracked sampling locations.

[†]SoilCode designates the site and soil where sites are FB = Fort Benning, GA; FR = Fort Riley, KS; WS = White Sands Missile Range, NM and soils are LS = loamy sand, SiCL = silty clay loam, SiL = silt loam, SL = sandy loam and L = loam. For a given sampling location, least square mean values with the same group letter are not significantly different at 0.05 level by SoilCode (Tukey's mean separation).

^{††}No CI data used in the "All Locations" analysis, due to lack of CI data from Fort Riley.

NA – Not Available

Table 39. Random roughness (mm) least square means (lsmean) for wheeled (HMMWV) vehicles by trafficking pass across all soils. SE = standard error of the mean, df = degrees of freedom, lower.CL = lower confidence level (95%), and upper .CL = upper confidence level (95%).

Sampling Location*	Pass[†]	lsmean	SE	df	lower.CL	upper.CL	group
CI ^{††}	p0 (0)	4.56	0.724	95.1	3.12	5.99	a
	p2 (25)	5.12	0.724	95.1	3.69	6.56	a
	p1 (10)	5.64	0.724	95.1	4.20	7.08	a
	p3 (50)	5.99	0.724	95.1	4.55	7.42	a
CO	p1 (10)	4.69	0.591	89.9	3.52	5.87	a
	p2 (25)	5.53	0.617	90.0	4.30	6.76	a
	p3 (50)	5.67	0.616	90.0	4.44	6.89	a
	p0 (0)	6.14	0.641	90.0	4.86	7.41	a
SS	p3 (50)	4.26	0.591	89.9	3.09	5.43	a
	p2 (25)	4.35	0.591	89.9	3.18	5.53	a
	p1 (10)	4.62	0.591	89.9	3.45	5.79	ab
	p0 (0)	6.70	0.642	90.0	5.43	7.97	b

*CI is curve inside, CO is curve outside, and SS is straight section tracked sampling locations.

[†]Pass is the pass level (p0,p1,p2,p3) and the number of cumulative figure-8 trafficking passes conducted with the vehicle are indicated in parentheses.

^{††}No CI data from Fort Riley soils (FR-SiL and FR-SiCL) used in the “CI” analysis, due to lack of CI data from those soils.

For a given location, least square mean values (averaged over the level of SoilCode for the individual sampling locations) with the same group letter are not significantly different at 0.05 level by trafficking pass level (Tukey’s mean separation).

Table 40. Overall ANOVA type III table of random roughness values for heavy wheeled (Fire Truck) vehicle (Sum Sq = sum of squares; Mean Sq = mean of squares; NumDF = numerator degrees of freedom; DenDF = denominator degrees of freedom; F.value = F statistic ratio value; PR(>F) = Probability p value associated with F statistic).

Factor	Sum Sq	Mean Sq	NumDF	DenDF	F.value	Pr(>F)	Signif.
Pass	156.0	52.0	3	23	1.52	4.09	*
Loc	27.9	13.9	2	23	2.94	1.10	
Pass:Loc	40.1	6.7	6	23	1.01	0.53	

Satterthwaite approximation used for degrees of freedom

Signif. codes: 0 ‘***’ 0.001 ‘**’ 0.01 ‘*’ 0.05 ‘.’ 0.1 ‘ ’ 1

Table 41. Random roughness (mm) least square means (lsmean) for heavy wheeled (Fire Truck) vehicle by trafficking pass across all soils. SE = standard error of the mean, df = degrees of freedom, lower.CL = lower confidence level (95%), and upper .CL = upper confidence level (95%).

Sampling Location*	Pass [†]	lsmean	SE	df	lower.CL	upper.CL	group
CI	p2 (10)	4.41	2.06	23	0.152	8.67	a
	p3 (20)	5.12	2.06	23	0.860	9.38	a
	p1 (2)	5.28	2.06	23	1.018	9.54	a
	p0 (0)	8.97	2.06	23	4.716	13.23	a
CO	p2 (10)	5.37	0.591	23	1.109	9.63	a
	p3 (20)	5.39	0.617	23	1.127	9.64	a
	p1 (2)	8.64	0.616	23	4.386	12.90	a
	p0 (0)	12.97	0.641	23	8.712	17.23	a
SS	p1 (2)	4.62	0.591	23	0.362	8.88	a
	p2 (10)	6.75	0.591	23	1.229	12.27	a
	p3 (20)	7.23	0.591	23	2.971	11.49	a
	p0 (0)	10.13	0.642	23	5.874	14.39	a

*CI is curve inside, CO is curve outside, and SS is straight section tracked sampling locations.

[†]Pass is the pass level (p0,p1,p2,p3) and the number of cumulative figure-8 trafficking passes conducted with the vehicle are indicated in parentheses.

For a given location, least square mean values (averaged over the level of SoilCode for the individual sampling locations) with the same group letter are not significantly different at 0.05 level by trafficking pass level (Tukey's mean separation).

Soil Bulk Density

Changes in bulk density due to trafficking by vehicles impact not only the short-term surface conditions with respect to the surface soil aggregate size distribution, but also possible long-term effects on vegetative response and recovery if compaction becomes great enough to impede root growth, water infiltration and available water holding capacity. Although not statistically significant on all soil/site locations, as indicated in Table 45 and Table 50, there are several trends that can be reasonably explained. For the tracked vehicle 0-15cm depth bulk densities, Table 42 shows that trafficking pass level and soil (SoilCode) were significant with some interactions including SoilCode as a participant.

Table 42. Overall ANOVA type III table of soil bulk density (0-15cm depth) for tracked vehicles. Sum Sq = sum of squares; Mean Sq = mean of squares; NumDF = numerator degrees of freedom; DenDF = denominator degrees of freedom; F.value = F statistic ratio value; PR(>F) = Probability p value associated with F statistic.

Factor	Sum Sq	Mean Sq	NumDF	DenDF	F.value	Pr(>F)	Signif.
SoilCode	2.883	0.721	4	10	164.7	4.4e-09	***
Pass	0.621	0.207	3	150	47.3	< 2e-16	***
Loc	0.005	0.002	3	150	0.4	0.74123	
SoilCode:Pass	0.172	0.014	12	150	3.3	0.00033	***
SoilCode:Loc	0.107	0.009	12	150	2.0	0.02493	*
Pass:Loc	0.015	0.002	9	150	0.4	0.94052	
SoilCode:Pass:Loc	0.184	0.005	36	150	1.2	0.25647	

Satterthwaite approximation used for degrees of freedom
Signif. codes: 0 '***' 0.001 '**' 0.01 '*' 0.05 '.' 0.1 ' ' 1

As expected, the “All Locations” rows as well as the individual sampling locations provided in Table 43 highlight the major soil effect differences in the 0-15cm depth bulk density values on the study sites. However, the tracked vehicle trafficking pass effects are generally significant by location across all soils as shown in Table 44.

Table 43. Soil bulk density (0-15 cm depth) (mg m⁻³) least square (lsmean) for tracked vehicles by soil and sampling location. SE = standard error of the mean, df = degrees of freedom, lower.CL = lower confidence level (95%), and upper .CL = upper confidence level (95%).

Sampling Location*	SoilCode[†]	lsmean	SE	df	lower.CL	upper.CL	group
All Locations	WS-L	1.27	0.0126	10	1.24	1.30	a
	FR-SiCL	1.32	0.0126	10	1.29	1.35	ab
	FR-SiL	1.35	0.0126	10	1.32	1.38	b
	WS-SL	1.55	0.0126	10	1.52	1.58	c
	FB-LS	1.64	0.0126	10	1.62	1.67	d
CC	WS-L	1.28	0.0208	37.3	1.24	1.32	a
	FR-SiCL	1.29	0.0208	37.3	1.25	1.33	a
	FR-SiL	1.33	0.0208	37.3	1.29	1.38	a
	WS-SL	1.59	0.0208	37.3	1.55	1.63	b
	FB-LS	1.67	0.0208	37.3	1.63	1.71	b
CI	WS-L	1.26	0.0208	37.3	1.22	1.30	a
	FR-SiCL	1.32	0.0208	37.3	1.28	1.36	ab
	FR-SiL	1.38	0.0208	37.3	1.33	1.42	b
	WS-SL	1.53	0.0208	37.3	1.49	1.57	c
	FB-LS	1.66	0.0208	37.3	1.62	1.70	d
CO	WS-L	1.28	0.0208	37.3	1.24	1.32	a
	FR-SiCL	1.35	0.0208	37.3	1.31	1.39	ab
	FR-SiL	1.38	0.0208	37.3	1.33	1.42	b
	WS-SL	1.52	0.0208	37.3	1.48	1.56	c
	FB-LS	1.63	0.0208	37.3	1.58	1.67	d
SS	WS-L	1.27	0.0208	37.3	1.23	1.31	a
	FR-SiCL	1.31	0.0208	37.3	1.27	1.36	a
	FR-SiL	1.32	0.0208	37.3	1.28	1.37	a
	WS-SL	1.57	0.0208	37.3	1.53	1.61	b
	FB-LS	1.62	0.0208	37.3	1.58	1.66	b

[†]SoilCode designates the site and soil where sites are FB = Fort Benning, GA; FR = Fort Riley, KS; WS = White Sands Missile Range, NM and soils are LS = loamy sand, SiCL = silty clay loam, SiL = silt loam, SL = sandy loam and L = loam. For a given sampling location, least square mean values (averaged over the levels of Pass and Loc for “All Locations” and by Pass only for the individual sampling locations) with the same group letter (a,b) are not significantly different at 0.05 level by SoilCode (Tukey’s mean separation).

*CI is curve inside, CO is curve outside, CC is cross-over and SS is straight section of figure-8 tracked sampling locations.

Table 44. Soil bulk density (0-15 cm depth) (mg m^{-3}) least square means (lsmean) for tracked vehicles by trafficking pass across all soils. SE = standard error of the mean, df = degrees of freedom, lower.CL = lower confidence level (95%), and upper .CL = upper confidence level (95%).

Sampling Location*	Pass [†]	lsmean	SE	df	lower.CL	upper.CL	group
CC	p0 (0)	1.35	0.0175	156	1.32	1.38	a
	p1 (1)	1.42	0.0175	156	1.39	1.45	b
	p2 (5)	1.45	0.0175	156	1.42	1.49	bc
	p3 (10)	1.50	0.0175	156	1.47	1.54	c
CI	p0 (0)	1.37	0.0175	156	1.33	1.40	a
	p1 (1)	1.41	0.0175	156	1.37	1.44	ab
	p2 (5)	1.45	0.0175	156	1.41	1.48	bc
	p3 (10)	1.49	0.0175	156	1.46	1.52	c
CO	p0 (0)	1.36	0.0175	156	1.33	1.40	a
	p1 (1)	1.39	0.0175	156	1.36	1.43	ab
	p2 (5)	1.45	0.0175	156	1.41	1.48	b
	p3 (10)	1.51	0.0175	156	1.48	1.55	c
SS	p0 (0)	1.35	0.0175	156	1.32	1.39	a
	p1 (1)	1.40	0.0175	156	1.37	1.44	ab
	p2 (5)	1.44	0.0175	156	1.41	1.48	bc
	p3 (10)	1.48	0.0175	156	1.44	1.51	c

*CI is curve inside, CO is curve outside, CC is cross-over and SS is straight section of figure-8 tracked sampling locations.

[†]Pass is the pass level (p0,p1,p2,p3) and the number of cumulative figure-8 trafficking passes conducted with the vehicle are indicated in parentheses.

For a given location, least square mean values (averaged over the level of SoilCode for the individual sampling locations) with the same group letter are not significantly different at 0.05 level by trafficking pass level (Tukey's mean separation).

For the tracked vehicles, the entire 0-15 cm measurement depth, bulk density generally increased with increased levels of trafficking under all sampling locations on all soils, but only the Ft. Riley and White Sands Missile Range sites showed any statistically significant differences between trafficking pass levels (Table 44). The Ft. Riley locations showed an increased amount of total compaction in the CI and CO locations over the SS and CC locations. This was primarily due to the significant surface shearing that occurred in the turns with the tracked vehicles. Thus, the original drier surface was removed and the wetter soil deeper in the profile was exposed. This wetter soil reflected higher compaction levels in those locations since those moisture levels were closer to the Optimum Water Content for these soils (Table 8) allowing for greater soil compaction.

Table 45. Bulk density comparisons at 0-15 cm depth among trafficking pass levels and sampling locations for tracked vehicles.

SoilCode [†]	Sampling Location [*]	Bulk density (mg m ⁻³) - Tracked Vehicles			
		p0 (0) [‡]	p1 (1) [‡]	p2 (5) [‡]	p3 (10) [‡]
FR-SiCL	CC	1.23 ^a	1.29	1.30	1.33
FR-SiCL	CI		1.20 ^a	1.36 ^b	1.49 ^b
FR-SiCL	CO		1.27 ^a	1.41 ^b	1.48 ^b
FR-SiCL	SS		1.25	1.36	1.40
FR-SiCL	CC	1.25 ^a	1.29 ^a	1.37 ^{ab}	1.44 ^{by}
FR-SiCL	CI		1.35 ^b	1.45 ^b	1.46 ^{by}
FR-SiL	CO		1.30 ^a	1.45 ^b	1.51 ^{by}
FR-SiL	SS		1.34 ^b	1.38 ^b	1.33 ^{bx}
FB-LS	CC	1.61	1.62	1.70	1.71
FB-LS	CI	1.61	1.62	1.70	1.71
FB-LS	CO	1.59	1.61	1.57	1.72
FB-LS	SS	1.61	1.60	1.60	1.67
WS-L	CC	1.16 ^a	1.30 ^b	1.32 ^b	1.34 ^b
WS-L	CI	1.26	1.28	1.27	1.23
WS-L	CO	1.27	1.27	1.27	1.30
WS-L	SS	1.20 ^a	1.28 ^{ab}	1.29 ^{ab}	1.32 ^b
WS-SL	CC	1.50 ^a	1.59 ^b	1.62 ^{bc}	1.65 ^{cx}
WS-SL	CI	1.50	1.51	1.55	1.56 ^y
WS-SL	CO	1.48	1.51	1.54	1.55 ^y
WS-SL	SS	1.47 ^a	1.56 ^{ab}	1.59 ^{bc}	1.67 ^{cx}

[†]SoilCode designates the site and soil where sites are FB = Fort Benning, GA; FR = Fort Riley, KS; WS = White Sands Missile Range, NM and soils are LS = loamy sand, SiCL = silty clay loam, SiL = silt loam, SL = sandy loam and L = loam.

^{*}CI is curve inside, CO is curve outside, CC is cross-over and SS is straight section of figure-8 tracked sampling locations.

[‡]Trafficking pass levels, p0,p1,p2,p3 (number of cumulative passes)

For a given site/soil, mean values by row with the same letter (a, b, c) are not significantly different at 0.05 level by trafficking pass level (0,1,5,10). For a given site/soil, mean values by column are only significantly different at the 0.05 level by sampling location (CI,CO,SS), if identified with the letter x or y (Tukey's mean separation).

Table 46 reveals that both SoilCode and trafficking pass level are significant as well as sampling location (Loc) along with some interaction between SoilCode and trafficking pass level for the HMMWV wheeled vehicles. Soil differences for the HMMWV wheeled vehicles are highlighted in Table 47 for all locations and individual sampling locations. Across soil types, only trafficking pass levels showed any significant differences for the CO sampling locations, even though there was a general increase in bulk density (0-15cm) with an increasing number of passes for both sets of wheeled vehicles (Table 48 for the HMMWV and Table 49 for the Fire Truck).

Table 46. Overall ANOVA type III table of soil bulk density (0-15cm depth) for wheeled vehicles (HMMWV). Sum Sq = sum of squares; Mean Sq = mean of squares; NumDF = numerator degrees of freedom; DenDF = denominator degrees of freedom; F.value = F statistic ratio value; PR(>F) = Probability p value associated with F statistic.

Factor	Sum Sq	Mean Sq	NumDF	DenDF	F.value	Pr(>F)	Signif.
SoilCode	0.621	0.1242	5	12	28.20	3.1e-06	***
Pass	0.081	0.0271	3	144	6.16	0.00057	***
Loc	0.045	0.0149	3	36	3.38	0.02870	*
SoilCode:Pass	0.118	0.0079	15	144	1.78	0.04210	*
SoilCode:Loc	0.050	0.0033	15	36	0.76	0.71378	
Pass:Loc	0.030	0.0033	9	144	0.75	0.66641	
SoilCode:Pass:Loc	0.204	0.0045	45	144	1.03	0.43851	

Satterthwaite approximation used for degrees of freedom
Signif. codes: 0 '***' 0.001 '**' 0.01 '*' 0.05 '.' 0.1 ' ' 1

Table 47. Soil bulk density (0-15 cm depth) (mg m^{-3}) least square means (lsmean) for wheeled vehicles (HMMWV) by soil and sampling location. SE = standard error of the mean, df = degrees of freedom, lower.CL = lower confidence level (95%), and upper .CL = upper confidence level (95%).

Sampling Location*	SoilCode [†]	lsmean	SE	df	lower.CL	upper.CL	group
All Locations	FR-SiCL	1.23	0.0315	12	1.16	1.30	a
	FR-SiL	1.29	0.0315	12	1.22	1.36	a
	WS-L	1.30	0.0315	12	1.23	1.37	a
	YK-SL	1.31	0.0315	12	1.24	1.38	a
	WS-SL	1.52	0.0315	12	1.45	1.59	b
	FB-LS	1.66	0.0315	12	1.59	1.73	b
CC	FR-SiCL	1.21	0.0362	20.4	1.14	1.29	a
	WS-L	1.28	0.0362	20.4	1.21	1.36	a
	FR-SiL	1.29	0.0362	20.4	1.21	1.36	a
	YK-SL	1.30	0.0362	20.4	1.22	1.37	a
	WS-SL	1.53	0.0362	20.4	1.46	1.61	b
	FB-LS	1.64	0.0362	20.4	1.56	1.71	b
CI	FR-SiCL	1.25	0.0362	20.4	1.17	1.32	a
	WS-L	1.29	0.0362	20.4	1.22	1.37	a
	YK-SL	1.30	0.0362	20.4	1.22	1.37	a
	FR-SiL	1.32	0.0362	20.4	1.25	1.40	a
	WS-SL	1.51	0.0362	20.4	1.44	1.59	b
	FB-LS	1.67	0.0362	20.4	1.59	1.74	b
CO	FR-SiCL	1.26	0.0362	20.4	1.18	1.33	a
	FR-SiL	1.29	0.0362	20.4	1.22	1.37	a
	YK-SL	1.31	0.0362	20.4	1.24	1.39	a
	WS-L	1.33	0.0362	20.4	1.26	1.41	a
	WS-SL	1.52	0.0362	20.4	1.45	1.60	b
	FB-LS	1.70	0.0362	20.4	1.62	1.77	c
SS	FR-SiCL	1.20	0.0362	20.4	1.12	1.27	a
	FR-SiL	1.27	0.0362	20.4	1.19	1.34	a
	WS-L	1.29	0.0362	20.4	1.21	1.36	a
	YK-SL	1.32	0.0362	20.4	1.24	1.39	a
	WS-SL	1.50	0.0362	20.4	1.43	1.58	b
	FB-LS	1.64	0.0362	20.4	1.56	1.71	b

*CI is curve inside, CO is curve outside, CC is cross-over and SS is straight section of figure-8 tracked sampling locations.

[†]SoilCode designates the site and soil where sites are FB = Fort Benning, GA; FR = Fort Riley, KS; WS = White Sands Missile Range, NM; YK = Yakima Training Center, WA and soils are LS = loamy sand, SiCL = silty clay loam, SiL = silt loam, SL = sandy loam and L = loam.

For a given sampling location, least square mean values with the same group letter are not significantly different at 0.05 level by SoilCode (Tukey's mean separation).

Table 48. Soil bulk density (0-15 cm depth) (mg m^{-3}) least square means (lsmean) for wheeled vehicles (HMMWV) by trafficking pass across all soils. SE = standard error of the mean, df = degrees of freedom, lower.CL = lower confidence level (95%), and upper .CL = upper confidence level (95%).

Sampling Location*	Pass[†]	lsmean	SE	df	lower.CL	upper.CL	group
CC	p0 (0)	1.35	0.0201	62.7	1.31	1.39	a
	p1 (10)	1.36	0.0201	62.7	1.32	1.40	a
	p3 (50)	1.39	0.0201	62.7	1.35	1.43	a
	p2 (25)	1.40	0.0201	62.7	1.36	1.44	a
CI	p0 (0)	1.36	0.0201	62.7	1.32	1.40	a
	p3 (50)	1.40	0.0201	62.7	1.36	1.44	a
	p1 (10)	1.40	0.0201	62.7	1.36	1.44	a
	p2 (25)	1.40	0.0201	62.7	1.36	1.44	a
CO	p0 (0)	1.37	0.0201	62.7	1.33	1.41	a
	p1 (10)	1.40	0.0201	62.7	1.36	1.44	ab
	p2 (25)	1.40	0.0201	62.7	1.36	1.44	ab
	p3 (50)	1.44	0.0201	62.7	1.40	1.48	b
SS	p0 (0)	1.35	0.0201	62.7	1.31	1.39	a
	p1 (10)	1.37	0.0201	62.7	1.33	1.41	a
	p3 (50)	1.37	0.0201	62.7	1.33	1.41	a
	p2 (25)	1.39	0.0201	62.7	1.35	1.43	a

*CI is curve inside, CO is curve outside, CC is cross-over and SS is straight section of figure-8 tracked sampling locations.

[†]Pass is the pass level (p0,p1,p2,p3) and the number of cumulative figure-8 trafficking passes conducted with the vehicle are indicated in parentheses.

For a given location, least square mean values with the same group letter are not significantly different at 0.05 level by trafficking pass level (Tukey's mean separation).

Table 49. Soil bulk density (0-15 cm depth) (mg m^{-3}) least square means (lsmean) for wheeled vehicle (Fire Truck) by sampling location. SE = standard error of the mean, df = degrees of freedom, lower.CL = lower confidence level (95%), and upper .CL = upper confidence level (95%).

Sampling Location*	Pass[†]	lsmean	SE	df	lower.CL	upper.CL	group
CC	p1 (2)	1.31	0.0556	6.27	1.17	1.44	a
	p0 (0)	1.34	0.0556	6.27	1.21	1.48	a
	p2 (10)	1.36	0.0556	6.27	1.23	1.49	a
	p3 (20)	1.40	0.0556	6.27	1.27	1.53	a
CI	p1 (2)	1.28	0.0556	6.27	1.15	1.42	a
	p0 (0)	1.33	0.0556	6.27	1.19	1.46	a
	p2 (10)	1.36	0.0556	6.27	1.23	1.49	a
	p3 (20)	1.36	0.0556	6.27	1.23	1.49	a
CO	p1 (2)	1.31	0.0556	6.27	1.18	1.45	a
	p2 (10)	1.34	0.0556	6.27	1.20	1.47	a
	p0 (0)	1.34	0.0556	6.27	1.21	1.47	a
	p3 (20)	1.36	0.0556	6.27	1.22	1.49	a
SS	p1 (2)	1.31	0.0556	6.27	1.17	1.44	a
	p2 (10)	1.31	0.0556	6.27	1.18	1.45	a
	p0 (0)	1.34	0.0556	6.27	1.21	1.48	a
	p3 (20)	1.37	0.0556	6.27	1.24	1.51	a

*CI is curve inside, CO is curve outside, CC is cross-over and SS is straight section of figure-8 tracked sampling locations.

[†]Pass is the pass level (p0,p1,p2,p3) and the number of cumulative figure-8 trafficking passes conducted with the vehicle are indicated in parentheses.

For a given site/soil, mean values by row with the same letter (a, b, c) are not significantly different at 0.05 level by trafficking pass level (Tukey's mean separation).

Table 50. Bulk density comparisons at 0-15 cm depth among trafficking pass levels and sampling locations for wheeled vehicles.

SoilCode [†]	Sampling Location*	Soil bulk density (mg m ⁻³)			
		HMMWV			
		p0 (0) [‡]	p1 (10) [‡]	p2 (25) [‡]	p3 (50) [‡]
FR-SiCL	CC	1.21 ^a	1.26	1.19	1.18 ^x
FR-SiCL	CI		1.27	1.22	1.28 ^{xy}
FR-SiCL	CO		1.25 ^{ab}	1.27 ^{ab}	1.31 ^{by}
FR-SiCL	SS		1.16	1.23	1.19 ^x
FR-SiL	CC	1.28	1.26	1.27	1.35
FR-SiL	CI		1.35	1.32	1.35
FR-SiL	CO		1.27	1.24	1.38
FR-SiL	SS		1.28	1.27	1.24
FB-LS	CC	1.57	1.54	1.71	1.72
FB-LS	CI	1.64	1.66	1.73	1.65
FB-LS	CO	1.65	1.74	1.71	1.70
FB-LS	SS	1.57	1.69	1.64	1.64
YK-SL	CC	1.35	1.25	1.36	1.24
YK-SL	CI	1.28	1.27	1.31	1.32
YK-SL	CO	1.33	1.29	1.30	1.34
YK-SL	SS	1.35	1.29	1.34	1.30
WS-L	CC	1.20	1.32	1.30	1.31
WS-L	CI	1.26	1.34	1.31	1.25
WS-L	CO	1.31	1.33	1.37	1.33
WS-L	SS	1.25	1.29	1.29	1.33
WS-SL	CC	1.48	1.56	1.56	1.53
WS-SL	CI	1.50	1.51	1.52	1.53
WS-SL	CO	1.44 ^a	1.52 ^{ab}	1.53 ^b	1.60 ^b
WS-SL	SS	1.44 ^a	1.49 ^{ab}	1.54 ^{ab}	1.55 ^b
		Fire Truck			
		p0 (0) [‡]	p1 (2) [‡]	p2 (10) [‡]	p3 (20) [‡]
YK-SL	CC	1.34	1.31	1.36	1.40
YK-SL	CI	1.33	1.28	1.36	1.36
YK-SL	CO	1.34	1.31	1.34	1.36
YK-SL	SS	1.34	1.31	1.31	1.37

[†]SoilCode designates the site and soil where sites are FB = Fort Benning, GA; FR = Fort Riley, KS; WS = White Sands Missile Range, NM and soils are LS = loamy sand, SiCL = silty clay loam, SiL = silt loam, SL = sandy loam and L = loam.

*CI is curve inside, CO is curve outside, and SS is straight section of figure-8 tracked sampling locations.

[‡]Trafficking pass levels, p0,p1,p2,p3 (number of cumulative passes)

For a given site/soil, mean values by row with the same letter (a, b, c) are not significantly different at 0.05 level by trafficking pass level (0,10,25,50 or 0,2,10,20). For a given site/soil, mean values by column are only significantly different at the 0.05 level by sampling location (CI,CO,SS), if identified with the letter x or y.

Bulk density is an indicator of soil compaction. It affects infiltration, rooting depth, available water capacity, soil porosity and aeration, availability of nutrients for plant use, and activity of soil micro-organisms, all of which influence key soil processes and productivity (USDA-NRCS, 2014). Although, soil bulk density did increase with trafficking in this study (Table 45 and Table 50), we did not reach the densities that restrict root growth (Table 51), likely due to the low water contents at most of these sites. As such, trafficking should be done at low soil water contents when feasible, to reduce compaction levels. In addition, when re-establishing vegetation, a variety of plants is recommended that include diverse rooting depths and pattern to aid in beraking up compacted soils.

Table 51. General relationship of soil bulk density to root growth based on soil texture (source: USDA-NRCS, 2014).*

Soil Texture	Ideal bulk density for plant growth	Bulk density that affects root growth	Bulk density that restricts root growth
	-----(mg m^{-3}) -----		
sand, loamy sand	<1.60	1.69	>1.80
sandy loam, loam	<1.40	1.63	>1.80
sandy clay loam, clay loam	<1.40	1.60	>1.75
silt, silt loam	<1.40	1.60	>1.75
silt loam, silty clay loam	<1.40	1.55	>1.65
sandy clay, silty clay, clay loam	<1.10	1.49	>1.58
clay (>45% clay)	<1.10	1.39	>1.47

*Does not apply to red clayey soils and volcanic ash soils.

Wind Tunnel Testing of PM10 Emissions

Potential PM10 emissions from wind erosion are initially dependent upon the amount of loose erodible PM10 material present on the soil surface that is not protected from the wind. This loose material is the source of the initial PM10 dust that can be emitted into the atmosphere. The “non-abrader” laboratory wind tunnel test is designed to measure loose PM10 emissions from the soil surface. In addition, many erodible surfaces with limited particulate emission also have saltating particles which continue the erosion process. The breakdown of larger aggregates and crusts caused by saltation impacts on the soil surface and the breakage of the saltating particles themselves create additional erodible size material, including PM10, to be emitted into the atmosphere (Mirzamostafa, et al., 1998). A surface’s resistance to saltation can also be evaluated with a laboratory wind tunnel where a known quantity of “abrader” sand (0.29 to 0.42 mm size) is provided upstream to simulate the saltation effects on the surface and the subsequent dust emissions generated from that surface. Both non-abrader (loose emissions) and abrader (saltation induced emissions) wind tunnel tests were conducted for each soil/site on samples extracted from both the curved and straight sections of the trafficked figure-8 plots to assess the PM10 emission levels. Of course, the surface conditions such as cloddiness, presence of a crust, roughness, vegetation cover, and standing vegetation all impact the potential PM10 emissions. These mitigating factors are also discussed as appropriate.

Non-abrader Wind Tunnel Tests

The non-abrader wind tunnel tests provide information on the level of PM10 dust that is available for direct emission from the soil surface. All PM10 emission data was log-transformed before analysis, due to emissions between soil types and trafficking levels spanning several orders of magnitude. Results presented in Table 52 show that pass level is the most significant individual factor affecting PM10 emissions for the tracked vehicles with SoilCode and several interactions also being significant.

Table 52. Overall ANOVA type III table of wind tunnel non-abrader PM10 (mg m⁻²) dust emissions (log transformed) for tracked vehicles. Sum Sq = sum of squares; Mean Sq = mean of squares; NumDF = numerator degrees of freedom; DenDF = denominator degrees of freedom; F.value = F statistic ratio value; PR(>F) = Probability p value associated with F statistic.

Factor	Sum Sq	Mean Sq	NumDF	DenDF	F.value	Pr(>F)	Signif.
SoilCode	45.5	11.4	4	10	24.3	3.9e-05	***
Pass	186.4	62.1	3	90	132.5	< 2e-16	***
Loc	0.6	0.3	2	20	0.6	0.55	
SoilCode:Pass	36.3	3.0	12	90	6.4	3.9e-08	***
SoilCode:Loc	3.4	0.4	8	20	0.9	0.53	
Pass:Loc	21.4	3.6	6	90	7.6	1.3e-06	***
SoilCode:Pass:Loc	13.3	0.6	24	90	1.2	0.28	

Satterthwaite approximation used for degrees of freedom

Signif. codes: 0 ‘***’ 0.001 ‘**’ 0.01 ‘*’ 0.05 ‘.’ 0.1 ‘ ’ 1

Wind tunnel results in Table 53 show that there are significant differences in measured PM10 emission values for the two Ft. Riley soils (FR-SiCL and FR-SiL) compared to the other soils. This trend shows for both the “All Locations” tracked data, as well as the individual sampling location data (CI,CO, SS).

Table 53. Wind tunnel (log transformed) non-abrader PM10 (mg m⁻²) least square means (lsmeans log transformed) for tracked vehicles by soil and sampling location. SE = standard error of the mean, df = degrees of freedom, lower.CL = lower confidence level (95%), and upper .CL = upper confidence level (95%).

Sampling Location*	SoilCode[†]	lsmean	SE	df	lower.CL	upper.CL	group
All Locations	FR-SiCL	4.87	0.225	10	4.37	5.37	a
	FR-SiL	4.89	0.225	10	4.38	5.39	a
	WS-SL	6.67	0.225	10	6.16	7.17	b
	FB-LS	6.87	0.225	10	6.37	7.37	b
	WS-L	7.11	0.225	10	6.61	7.61	b
CI	FR-SiL	4.72	0.283	21.4	4.13	5.31	a
	FR-SiCL	4.94	0.283	21.4	4.35	5.53	a
	FB-LS	6.65	0.283	21.4	6.06	7.23	b
	WS-SL	6.69	0.283	21.4	6.11	7.28	b
	WS-L	7.12	0.283	21.4	6.53	7.71	b
CO	FR-SiCL	5.01	0.283	21.4	4.43	5.60	a
	FR-SiL	5.11	0.283	21.4	4.52	5.70	a
	FB-LS	6.53	0.283	21.4	5.94	7.12	b
	WS-SL	6.83	0.283	21.4	6.25	7.42	b
	WS-L	7.33	0.283	21.4	6.75	7.92	b
SS	FR-SiCL	4.65	0.283	21.4	4.07	5.24	a
	FR-SiL	4.83	0.283	21.4	4.24	5.42	a
	FB-LS	6.82	0.283	21.4	6.23	7.41	b
	WS-L	6.87	0.283	21.4	6.29	7.46	b
	WS-SL	7.08	0.283	21.4	6.49	7.66	b

*CI is curve inside, CO is curve outside, and SS is straight section of figure-8 tracked sampling locations.

[†]SoilCode designates the site and soil where sites are FB = Fort Benning, GA; FR = Fort Riley, KS; WS = White Sands Missile Range, NM and soils are LS = loamy sand, SiCL = silty clay loam, SiL = silt loam, SL = sandy loam and L = loam. For a given sampling location, least square mean values (averaged over the levels of Pass and Loc for “All Locations” and by Pass only for the individual sampling locations) with the same group letter (a,b) are not significantly different at 0.05 level by SoilCode (Tukey’s mean separation).

The tracked wind tunnel tray non-abrader test PM10 emissions were found to be significantly different ($p < 0.05$) between the initial condition (p0) and first pass (p1) trafficked conditions for all locations across all soils (Table 54). As expected, the SS location generally showed a significant increase ($p < 0.05$) in emissions with additional trafficking until the final set of 5 passes (p3). The CI and CO curved locations on the other hand, showed a general reduction in PM10 emissions across all soils after the first trafficking pass for the tracked vehicles.

These differences between the curved and straight trafficked regions can generally be explained by the following: a) subsurface soil (soil not previously affected by crushing and grinding forces on the surface due to trafficking) being continuously exposed in the curves; and b) the repeated trafficking effects (crushing and grinding forces) on the same soil surface in the straight trafficked regions. Thus, the surface soil in the straight trafficked regions continued to degrade

with increased trafficking, whereas the curve trafficked regions plateaued after the first pass due to subsurface soil continually being exposed to the surface.

Table 54. Wind tunnel (log transformed) non-abrader PM10 (mg m⁻²) least square means (log transformed) for tracked vehicles by trafficking pass across all soils. SE = standard error of the mean, df = degrees of freedom, lower.CL = lower confidence level (95%), and upper .CL = upper confidence level (95%).

Sampling Location*	Pass[†]	lsmean	SE	df	lower.CL	upper.CL	group
CI	p0 (0)	4.31	0.199	86	3.91	4.70	a
	p2 (5)	6.32	0.199	86	5.93	6.72	b
	p3 (10)	6.36	0.199	86	5.96	6.75	b
	p1 (1)	7.11	0.199	86	6.71	7.50	c
CO	p0 (0)	4.31	0.199	86	3.92	4.71	a
	p2 (5)	6.62	0.199	86	6.23	7.02	b
	p3 (10)	6.71	0.199	86	6.32	7.11	b
	p1 (1)	7.01	0.199	86	6.61	7.40	b
SS	p0 (0)	4.35	0.199	86	3.95	4.74	a
	p1 (1)	5.86	0.199	86	5.46	6.25	b
	p2 (5)	6.74	0.199	86	6.35	7.14	c
	p3 (10)	7.26	0.199	86	6.86	7.65	c

*CI is curve inside, CO is curve outside, and SS is straight section tracked sampling locations.

[†]Pass is the pass level (p0,p1,p2,p3) and the number of cumulative figure-8 trafficking passes conducted with the vehicle are indicated in parentheses.

For a given location, least square mean values (averaged over the level of SoilCode for the individual sampling locations) with the same group letter are not significantly different at 0.05 level by trafficking pass level (Tukey's mean separation).

The previously stated trends generally occurred on all soils with the variability at least partially due to the different levels of vegetation cover present at the different sites as shown in Table 55. For example, looking at the straight trafficked region (SS) sampled data from the sandy loam soil on the WSMR site (WS-SL in Table 55) for the tracked vehicles, the trend in the non-abrader PM10 emissions steadily increased from the low initial, crusted condition of 190 mg m⁻² to a high of over 5600 mg m⁻², with the increase being statistically significant between all pass levels except the final two. One can contrast that with curved trafficked data (CI, CO) where the PM10 emissions at first increased at a statistically significant level (p<0.05) with the first pass due to the destruction of the initial crust and removal of vegetation cover on the surface and then decreased due to less erodible fresh soil being exposed on the surface and the original surface soil being displaced out of the track in the curved trafficked sections (WS-SL in Table 55). Note that the straight trafficked section (SS) for the sandy loam soil at WSMR (WS-L in Table 55) for the tracked vehicles showed a significant increase in PM10 emissions as the number of trafficking passes increased. The values after the first pass were significantly less statistically than the two curved trafficked regions. However, the straight trafficked PM10 were statistically higher in the two subsequent higher pass levels while the curved trafficked regions essentially plateaued in their PM10 emission levels. The WSMR loam soil (WS-L in Table 55) showed the identical trend as the WSMR sandy loam soil (WS-SL in Table 55). All other sites/soils generally follow these same trends for the tracked vehicles, even though the measurement differences obtained do not necessarily show statistical significance at the p <0.05 level.

Table 55. Non-abrader PM10 emission (mg m⁻²) comparisons among trafficking pass levels and sampling locations (tracked vehicles).

SoilCode [†]	Sampling Location*	Non-abrader PM10 emission (mg m ⁻²) - Tracked Vehicles			
		p0 (0) [‡]	p1 (1) [‡]	p2 (5) [‡]	p3 (10) [‡]
FR-SiCL	CI	47.87 ^a	231.96 ^{ab}	154.40 ^b	266.94 ^b
FR-SiCL	CO		180.01 ^{ab}	247.70 ^{ab}	323.22 ^b
FR-SiCL	SS		151.07 ^{ab}	146.88 ^{ab}	258.61 ^b
FR-SiL	CI	52.57 ^a	364.46 ^a	114.79 ^a	125.07 ^a
FR-SiL	CO		212.97 ^{ab}	259.03 ^{ab}	421.97 ^b
FR-SiL	SS		115.81 ^a	292.90 ^a	311.09 ^a
FB-LS	CI	151.99 ^a	2485.02 ^b	1129.73 ^b	3560.48 ^b
FB-LS	CO	69.76 ^a	2431.13 ^b	1106.96 ^b	3153.35 ^b
FB-LS	SS	227.10 ^a	2133.37 ^{ab}	2079.24 ^{ab}	5548.49 ^b
WS-L	CI	83.69 ^a	5659.92 ^b	3303.18 ^b	2188.12 ^b
WS-L	CO	117.00 ^a	6864.60 ^b	4888.11 ^b	2639.83 ^b
WS-L	SS	61.86 ^a	739.29 ^{bx}	4523.46 ^c	7320.68 ^c
WS-SL	CI	162.52 ^a	4913.17 ^b	1037.41 ^b	625.28 ^c
WS-SL	CO	225.06 ^a	3409.10 ^b	1275.11 ^b	1059.41 ^c
WS-SL	SS	190.90 ^a	826.27 ^{bx}	3416.09 ^{cx}	5653.09 ^{cx}

[†] SoilCode designates the site and soil where sites are FB = Fort Benning, GA; FR = Fort Riley, KS; WS = White Sands Missile Range, NM and soils are LS = loamy sand, SiCL = silty clay loam, SiL = silt loam, SL = sandy loam and L = loam.

*CI is curve inside, CO is curve outside, and SS is straight section of figure-8 tracked sampling locations.

[‡]Trafficking pass levels, p0,p1,p2,p3 (number of cumulative passes).

For a given site/soil, mean values by row with the same letter (a, b, c) are not significantly different at 0.05 level by trafficking pass level (0,1,5,10). For a given site/soil, mean values by column are only significantly different at the 0.05 level by sampling location (CI,CO,SS), if identified with the letter x (Tukey's mean separation).

The wheeled vehicles also exhibited significant ($p < 0.05$) differences for trafficking pass level (Table 56 and Table 57), followed by the interaction between soil and pass level and by soil alone (Table 56). Again, the soil differences show up with the wheeled vehicles like they did with the tracked vehicles (Table 58).

Table 56. Overall ANOVA type III table of wind tunnel non-abrader PM10 (mg m^{-2}) dust emissions (log transformed) for wheeled vehicles (HMMWV). Sum Sq = sum of squares; Mean Sq = mean of squares; NumDF = numerator degrees of freedom; DenDF = denominator degrees of freedom; F.value = F statistic ratio value; PR(>F) = Probability p value associated with F statistic.

Factor	Sum Sq	Mean Sq	NumDF	DenDF	F.value	Pr(>F)	Signif.
SoilCode	68.6	13.7	5	12.4	52.6	6.6e-08	***
Pass	235.5	78.5	3	90.3	301.0	< 2e-16	***
Loc	0.4	0.2	2	30.7	0.8	0.44	
SoilCode:Pass	39.6	2.6	15	90.3	10.1	1.2e-13	***
SoilCode:Loc	1.0	0.1	10	28.6	0.4	0.94	
Pass:Loc	1.2	0.2	6	90.3	0.8	0.58	
SoilCode:Pass:Loc	6.6	0.3	20	90.3	1.3	0.23	

Satterthwaite approximation used for degrees of freedom

Signif. codes: 0 '***' 0.001 '**' 0.01 '*' 0.05 '.' 0.1 ' ' 1

Table 57. Overall ANOVA type III table of wind tunnel non-abrader PM10 (mg m^{-2}) dust emissions (log transformed) for heavy wheeled vehicle (Fire Truck). Sum Sq = sum of squares; Mean Sq = mean of squares; NumDF = numerator degrees of freedom; DenDF = denominator degrees of freedom; F.value = F statistic ratio value; PR(>F) = Probability p value associated with F statistic.

Factor	Sum Sq	Mean Sq	NumDF	DenDF	F.value	Pr(>F)	Signif.
Pass	76636855	25545618	3	18.2	27.03	6.4e-07	***
Loc	719324	359662	2	6.0	0.38	0.70	
Pass:Loc	1902655	317109	6	18.2	0.34	0.91	

Satterthwaite approximation used for degrees of freedom

Signif. codes: 0 '***' 0.001 '**' 0.01 '*' 0.05 '.' 0.1 ' ' 1

Table 58. Wind tunnel (log transformed) non-abrader PM10 (mg m⁻²) least square means (log transformed) for wheeled vehicles (HMMWV) by soil and sampling location. SE = standard error of the mean, df = degrees of freedom, lower.CL = lower confidence level (95%), and upper.CL = upper confidence level (95%).

Sampling Location*	SoilCode [†]	lsmean	SE	df	lower.CL	upper.CL	group
All Locations	YK-SL	6.17	0.17	10.7	5.80	6.55	a
	FB-LS	6.87	0.17	10.7	6.50	7.24	ab
	WS-SL	7.33	0.17	10.7	6.96	7.71	bc
	WS-L	7.86	0.17	10.7	7.49	8.24	c
	FR-SiCL [‡]	NA	NA	NA	NA	NA	
	FR-SiL [‡]	NA	NA	NA	NA	NA	
CI	YK-SL	6.16	0.229	26.2	5.69	6.63	a
	FB-LS	6.91	0.229	26.2	6.44	7.38	ab
	WS-SL	7.37	0.229	26.2	6.90	7.84	bc
	WS-L	8.10	0.229	26.2	7.62	8.57	c
	FR-SiCL [‡]	NA	NA	NA	NA	NA	
	FR-SiL [‡]	NA	NA	NA	NA	NA	
CO	FR-SiCL	4.07	0.229	26.2	3.60	4.54	a
	FR-SiL	4.67	0.229	26.2	4.20	5.14	a
	YK-SL	6.26	0.229	26.2	5.79	6.73	b
	FB-LS	6.82	0.229	26.2	6.35	7.29	bc
	WS-SL	7.48	0.229	26.2	7.01	7.95	cd
	WS-L	7.84	0.229	26.2	7.37	8.31	d
SS	YK-SL	6.09	0.229	26.2	5.62	6.56	a
	FB-LS	6.88	0.229	26.2	6.40	7.35	ab
	WS-SL	7.15	0.229	26.2	6.68	7.62	b
	WS-L	7.66	0.229	26.2	7.19	8.13	b
	FR-SiCL [‡]	NA	NA	NA	NA	NA	
	FR-SiL [‡]	NA	NA	NA	NA	NA	

*CI is curve inside, CO is curve outside, and SS is straight section of figure-8 tracked sampling locations.

[†]SoilCode designates the site and soil where sites are FB = Fort Benning, GA; FR = Fort Riley, KS; WS = White Sands Missile Range, NM and soils are LS = loamy sand, SiCL = silty clay loam, SiL = silt loam, SL = sandy loam and L = loam.

[‡]Since sampling location data were incomplete across pass levels, this statistical analysis procedure could not be applied. For a given sampling location, least square mean values with the same group letter are not significantly different at 0.05 level by SoilCode (Tukey's mean separation).

NA – Not Available.

Wind tunnel results shown in Table 59 indicate that the effects of trafficking pass level on non-abrader emissions across all soils for the wheeled vehicles (HMMWV). For all sampling locations, there was a significant ($p < 0.05$) increase in PM10 emissions due to any level of trafficking from the un-trafficked condition across all soils. There were also generally measurable differences (increases) in PM10 emission levels as the trafficking levels increased, but were not significant ($p < 0.05$) between 25 and 50 trafficking passes. A similar pattern occurred across all sampling locations on the single soil for the Fire Truck as well (Table 60).

Table 59. Wind tunnel (log transformed) non-abrader PM10 (mg m⁻²) least square means (log transformed) for wheeled vehicles (HMMWV) by trafficking pass across all soils. SE = standard error of the mean, df = degrees of freedom, lower.CL = lower confidence level (95%), and upper.CL = upper confidence level (95%).

Sampling Location*	Pass[†]	lsmean	SE	df	lower.CL	upper.CL	group
CI [‡]	p0 (0)	4.57	0.163	69.5	4.24	4.89	a
	p1 (10)	7.55	0.163	69.5	7.23	7.88	b
	p2 (25)	8.09	0.163	69.5	7.77	8.42	c
	p3 (50)	8.32	0.163	69.5	7.99	8.65	c
CO	p0 (0)	4.69	0.14	93.3	4.07	4.63	a
	p1 (10)	7.27	0.14	93.3	6.12	6.67	b
	p2 (25)	7.96	0.14	93.3	6.56	7.11	bc
	p3 (50)	8.49	0.14	93.3	6.90	7.46	c
SS [‡]	p0 (0)	4.64	0.163	69.5	4.32	4.97	a
	p1 (10)	7.07	0.163	69.5	6.75	7.40	b
	p2 (25)	7.80	0.163	69.5	7.48	8.13	c
	p3 (50)	8.25	0.163	69.5	7.93	8.58	c

*CI is curve inside, CO is curve outside, and SS is straight section of figure-8 tracked sampling locations.

[†]Pass is the pass level (p0,p1,p2,p3) and the number of cumulative figure-8 trafficking passes conducted with the vehicle are indicated in parentheses.

[‡]Does not include Ft. Riley soils (FR-SiCL, 2-SCL) due to insufficient data collected for analysis.

For a given location, least square mean values (averaged over the level of SoilCode for the individual sampling locations) with the same group letter are not significantly different at 0.05 level by trafficking pass level (Tukey's mean separation).

Table 60. Wind tunnel (log transformed) non-abrader PM10 (mg m⁻²) least square means (lsmeans) (log transformed) for heavy wheeled vehicle (Fire Truck) by trafficking pass across all soils. SE = standard error of the mean, df = degrees of freedom, lower.CL = lower confidence level (95%), and upper.CL = upper confidence level (95%).

Sampling Location*	Pass[†]	lsmean	SE	df	lower.CL	upper.CL	group
CI	p0 (0)	4.42	0.302	23.1	3.80	5.04	a
	p1 (2)	6.74	0.302	23.1	6.11	7.36	b
	p2 (10)	7.39	0.302	23.1	6.77	8.01	bc
	p3 (20)	8.34	0.302	23.1	7.72	8.97	c
CO	p0 (0)	4.10	0.302	23.1	3.48	4.73	a
	p1 (2)	5.79	0.302	23.1	5.17	6.41	b
	p2 (10)	7.43	0.302	23.1	6.81	8.06	c
	p3 (20)	8.13	0.302	23.1	7.50	8.75	c
SS	p0 (0)	3.97	0.302	23.1	3.35	4.60	a
	p1 (2)	6.66	0.302	23.1	6.04	7.28	b
	p2 (10)	7.15	0.302	23.1	6.53	7.77	bc
	p3 (20)	8.14	0.302	23.1	7.52	8.77	c

*CI is curve inside, CO is curve outside, and SS is straight section of figure-8 tracked sampling locations.

[†]Pass is the pass level (p0,p1,p2,p3) and the number of cumulative figure-8 trafficking passes conducted with the vehicle are indicated in parentheses.

For a given location, least square mean values (averaged over the level of SoilCode for the individual sampling locations) with the same group letter are not significantly different at 0.05 level by trafficking pass level (Tukey's mean separation).

Wind tunnel results (Table 61) show the individual average measured non-abrader PM10 emission levels for each soil at each pass level for the wheeled vehicles by location. Note the significant ($p < 0.05$) difference between the initial values and the first pass level for all soils at all sites (except Ft. Riley, but the same trends were evident). Subsequent levels of additional wheeled vehicle trafficking did generally produce increased PM10 emissions, but not always at a statistically significant ($p < 0.05$) level.

Table 61. Non-abrader PM10 emission (mg m^{-2}) comparisons among trafficking pass levels and sampling locations (wheeled vehicles).

SoilCode [†]	Sampling Location*	Non-abrader PM10 emission (mg m^{-2})			
		HMMWV			
		p0 (0) [‡]	p1 (10) [‡]	p2 (25) [‡]	p3 (50) [‡]
FR-SiCL	CO	53.55 ^a	66.98 ^a	70.55 ^a	69.96 ^a
FR-SiCL	SS		N/A	N/A	141.53 ^a
FR-SiL	CO	37.13 ^a	203.63 ^a	170.57 ^a	235.61 ^a
FR-SiL	SS		N/A	N/A	183.72 ^a
FB-LS	CI	83.68 ^a	1727.18 ^b	2648.17 ^b	3322.80 ^b
FB-LS	CO	108.47 ^a	662.05 ^b	3721.68 ^c	4093.79 ^c
FB-LS	SS	213.27 ^a	1147.76 ^b	2084.51 ^b	3628.78 ^b
YK-SL	CI	58.37 ^a	277.85 ^b	2687.76 ^c	1403.66 ^c
YK-SL	CO	56.09 ^a	572.42 ^b	1410.04 ^{bc}	2396.55 ^c
YK-SL	SS	46.42 ^a	470.53 ^b	1432.14 ^c	1597.30 ^c
WS-L	CI	169.46 ^a	9444.95 ^b	6083.78 ^b	16396.37 ^b
WS-L	CO	161.77 ^a	4848.15 ^b	8084.66 ^b	9597.67 ^b
WS-L	SS	173.28 ^a	4973.21 ^b	8405.43 ^b	7217.70 ^b
WS-SL	CI	145.84 ^a	3474.49 ^b	3275.57 ^b	5267.13 ^b
WS-SL	CO	193.49 ^a	3198.58 ^b	2561.13 ^{bc}	9663.32 ^c
WS-SL	SS	117.14 ^a	1630.04 ^b	2548.66 ^{bc}	6949.08 ^c
		Fire Truck			
		p0 (0) [‡]	p1 (2) [‡]	p2 (10) [‡]	p3 (20) [‡]
YK-SL	CI	94.86 ^a	971.81 ^b	1689.02 ^{bc}	4594.31 ^c
YK-SL	CO	63.76 ^a	373.02 ^b	1799.8 ^{1c}	3665.02 ^c
YK-SL	SS	58.09 ^a	933.57 ^b	1348.81 ^{bc}	3560.00 ^c

[†] SoilCode designates the site and soil where sites are FB = Fort Benning, GA; FR = Fort Riley, KS; WS = White Sands Missile Range, NM and soils are LS = loamy sand, SiCL = silty clay loam, SiL = silt loam, SL = sandy loam and L = loam.

*CI is curve inside, CO is curve outside, and SS is straight section of figure-8 tracked sampling locations.

[‡]Trafficking pass levels, p0,p1,p2,p3 (number of cumulative passes)

For a given soil, mean values by row with the same letter (a,b,c) are not significantly different at 0.05 level by trafficking pass level (0,10,25,50 or 0,2,10,20) (Tukey's mean separation).

N/A – Not Available (data not collected at the specified pass levels)

The most important finding from the non-abrader wind tunnel tests is that there was generally a significant increase in PM10 emissions across all soil types and sampling locations, for both tracked and wheeled vehicles and between the un-trafficked (p0) and first level of passes (p1).

Depending upon the soil type and the degree of shearing action caused by the vehicles, subsequent pass levels (p2 and p3) emissions of PM10 could increase, decrease or plateau. Thus, there is a tradeoff between exposing fresh soil to the surface due to side shear forces that may or may not generate higher PM10 emissions versus degrading the current surface soil with increased trafficking. For example, the tracked vehicles (Table 55) still exhibited a general but not significant increase in PM10 emissions with increased trafficking after pass level p1 in the all trafficked areas. However, the increase in emissions was generally much less than in the straight

trafficked sections where the shearing action was less, especially for the high sand/silt content soils at Ft. Benning, Yakima and White Sands Missile Range. This implies that subsurface soil exposed to the surface in the curved trafficking areas was limiting the potential emissions due to the increased trafficking effects on the soil surface for all sites/soils. The wheeled vehicles (Table 61) however, showed increased PM10 emissions following the initial set of passes (p1) for all soils/sites, and in many cases exceeded the straight trafficked emission rates. This is likely due to the wheeled vehicle providing some shearing forces that did not displace as much soil as the tracked vehicles in the curved trafficked areas that allowed additional grinding and crushing of the surface soil due to the side shear increasing the amount of erodible size particles compared to the straight trafficked areas.

The straight trafficked regions (SS), however, always increased PM10 emissions (Table 55 and Table 61) with increased trafficking for both tracked and wheeled vehicles, due to the continual degrading of the surface with both the removal of vegetation and the repeated grinding of the soil on the surface in the absence of the side shear forces.

Regardless, the surface degradation due to trafficking is significant and manifests itself in higher PM10 emissions across all soil types and pass levels, vehicle type (tracked vs wheeled) and trafficking patterns (turns vs. straight-sections) compared to un-trafficked conditions.

The non-abrader tests essentially represent erodible size particles available on the surface that are mobile and susceptible to emission.

Abrader Wind Tunnel Tests

Most soil movement by wind is entrained and transported by particle saltation, a bouncing motion of windblown grains (Bagnold, 1941; Shao, et al., 1993; Eames & Dalziel, 2000). Saltating soil particles are lifted up into the air and then drop back to the surface as they are too heavy to remain suspended, which can cause additional saltating particles. These particles may impact and cause smaller particles to become suspended into the atmosphere (Gillette, 1981; Shao, et al., 1993; Rice, et al., 1996). Saltation impact is well recognized as the principal mechanism by which dust sized particles are ejected into the air in many arid environments (Gillette, 1977; Shao, et al., 1993). Therefore, abrader wind tunnel tests were conducted to determine the level of wind erosion susceptibility each site's soils have under active abrasion for both the un-trafficked and trafficked conditions.

The ANOVA test results in Table 62 shows that trafficking pass level (Pass) is significant ($p < 0.05$) as is the soil (SoilCode), along with pass level (Pass) interactions for the tracked vehicles.

Table 62. Overall ANOVA type III table of wind tunnel abrader PM10 (mg m⁻²) dust emissions (log transformed) for tracked vehicles. Sum Sq = sum of squares; Mean Sq = mean of squares; NumDF = numerator degrees of freedom; DenDF = denominator degrees of freedom; F.value = F statistic ratio value; PR(>F) = Probability p value associated with F statistic.

Factor	Sum Sq	Mean Sq	NumDF	DenDF	F.value	Pr(>F)	Signif.
SoilCode	116.6	29.14	4	30	249.7	< 2e-16	***
Pass	64.3	21.45	3	90	183.8	< 2e-16	***
Loc	0.0	0.01	2	30	0.0	0.95	
SoilCode:Pass	41.5	3.45	12	90	29.6	< 2e-16	***
SoilCode:Loc	0.3	0.04	8	30	0.3	0.94	
Pass:Loc	13.5	2.26	6	90	19.3	2.3e-14	***
SoilCode:Pass:Loc	8.5	0.35	24	90	3.0	8.1e-05	***

Satterthwaite approximation used for degrees of freedom
Signif. codes: 0 '***' 0.001

The “All Locations” rows in Table 63 shows the significant differences among the soils based upon the abraded PM10 emission measurements. The same differences still hold when the sampling locations are delineated.

Table 63. Wind tunnel (log transformed) abrader PM10 (mg m⁻²) least square means (lsmean) (log transformed) for tracked vehicles by soil and sampling location. SE = standard error of the mean, df = degrees of freedom, lower.CL = lower confidence level (95%), and upper .CL = upper confidence level (95%).

Sampling Location*	SoilCode[†]	lsmean	SE	df	lower.CL	upper.CL	group
All Locations	FR-SiCL	4.68	0.0894	10	4.48	4.88	a
	FR-SiL	4.74	0.0894	10	4.54	4.94	a
	WS-SL	6.93	0.0894	10	6.73	7.13	b
	FB-LS	7.09	0.0894	10	6.89	7.29	b
	WS-L	7.69	0.0894	10	7.49	7.89	c
CI	FR-SiL	4.63	0.155	30	4.32	4.95	a
	FR-SiCL	4.73	0.155	30	4.41	5.04	a
	WS-SL	6.99	0.155	30	6.68	7.31	b
	FB-LS	7.15	0.155	30	6.84	7.47	b
	WS-L	7.63	0.155	30	7.31	7.95	b
CO	FR-SiCL	4.74	0.155	30	4.42	5.06	a
	FR-SiL	4.87	0.155	30	4.55	5.18	a
	WS-SL	6.86	0.155	30	6.54	7.18	b
	FB-LS	7.02	0.155	30	6.70	7.33	b
	WS-L	7.71	0.155	30	7.39	8.02	c
SS	FR-SiCL	4.58	0.155	30	4.26	4.89	a
	FR-SiL	4.71	0.155	30	4.39	5.02	a
	WS-SL	6.94	0.155	30	6.63	7.26	b
	FB-LS	7.09	0.155	30	6.77	7.40	b
	WS-L	7.73	0.155	30	7.41	8.05	c

*CI is curve inside, CO is curve outside, and SS is straight section of figure-8 tracked sampling locations.

[†]SoilCode designates the site and soil where sites are FB = Fort Benning, GA; FR = Fort Riley, KS; WS = White Sands

Missile Range, NM and soils are LS = loamy sand, SiCL = silty clay loam, SiL = silt loam, SL = sandy loam and L = loam. For a given sampling location, least square mean values (averaged over the levels of Pass and Loc for “All Locations” and by Pass only for the individual sampling locations) with the same group letter (a,b) are not significantly different at 0.05 level by SoilCode (Tukey’s mean separation).

There were significant differences ($p < 0.05$) between the un-trafficked condition (p_0) and almost all the trafficked conditions (p_1 , p_2 , & p_3) across all soil types (Table 64). The straight tracked region also showed an increase in PM10 emissions after the first trafficking pass, but was not statistically significant. Likewise, the PM10 emission level peaked after the first trafficking pass in both curved regions and then decreased for additional passes. This is likely due to the extensive surface shearing and soil displacement in the curve trafficked regions. The initial pass removed any protective crust and vegetative cover, increasing abrader generated PM10 emission levels. Subsequent trafficking though, continued to expose fresh subsurface soil.

If that newly exposed soil was less susceptible to erosion due to higher water content, different soil primary particle distribution, or was less degraded due to the lack of grinding and crushing from repeated trafficking compared to the original soil surface, then the PM10 emissions declined. The Ft. Riley soils for example, contained higher water contents at the time of trafficking (IWC closer to the soil’s OWC as shown in Table 8) than the other sites. This,

combined with the higher clay and low sand in those soil textures (Table 7) created a more compacted and consolidated surface which tended to reduce or limit the measured PM10 emissions in the curve trafficked regions after the first pass (Table 65).

However, if that exposed subsurface soil was more susceptible to erosion compared to the original surface soil, the PM10 emissions could increase.

In most of the sites studied (FB, Yakima and WSMR), the soils were very dry at time of trafficking (Table 8) and consisted of textures containing relatively high sand and/or silt content (Table 7). These soil textures do not tend to create stable, non-erodible size aggregates, even under ideal moisture conditions, due to their low clay contents. Therefore, the lack of stable, non-erodible size aggregates available for surface armoring and the availability of loose, erodible size particles on the surface, make these soils highly susceptible to increased emissions. So, for these soils, the PM10 emissions continued to increase with increased trafficking in the curved trafficked regions (Table 65).

The straight trafficked section (SS) did not exhibit this behavior, but instead continued to show a significant increase ($p < 0.05$) in abrader generated PM10 emissions with increased trafficking passes for all soils. This is likely due to the repeated grinding effect from the tracks on the same surface soil, crushing larger, non-erodible aggregates, creating a continually more erodible condition with additional trafficking. The trafficking level effects by soil type for all soils for the tracked vehicles are provided in Table 65.

Table 64. Wind tunnel (log transformed) abrader PM10 (mg m^{-2}) least square means (lsmean) (log transformed) for tracked vehicles by trafficking pass across all soils. SE = standard error of the mean, df = degrees of freedom, lower.CL = lower confidence level (95%), and upper .CL = upper confidence level (95%).

Sampling Location*	Pass [†]	lsmean	SE	df	lower.CL	upper.CL	group
CI	p0 (0)	5.24	0.103	98.7	5.03	5.44	a
	p2 (5)	6.32	0.103	98.7	6.12	6.53	b
	p3 (10)	6.39	0.103	98.7	6.19	6.60	b
	p1 (1)	6.96	0.103	98.7	6.75	7.16	c
CO	p0 (0)	5.06	0.103	98.7	4.85	5.26	a
	p2 (5)	6.55	0.103	98.7	6.34	6.75	b
	p3 (10)	6.64	0.103	98.7	6.44	6.85	b
	p1 (1)	6.71	0.103	98.7	6.50	6.91	b
SS	p0 (0)	5.30	0.103	98.7	5.10	5.51	a
	p1 (1)	5.90	0.103	98.7	5.70	6.11	b
	p2 (5)	6.58	0.103	98.7	6.37	6.78	c
	p3 (10)	7.06	0.103	98.7	6.85	7.26	d

*CI is curve inside, CO is curve outside, and SS is straight section tracked sampling locations.

[†]Pass is the pass level (p0,p1,p2,p3) and the number of cumulative figure-8 trafficking passes conducted with the vehicle are indicated in parentheses.

For a given location, least square mean values (averaged over the level of SoilCode for the individual sampling locations) with the same group letter are not significantly different at 0.05 level by trafficking pass level (Tukey's mean separation).

Table 65. Abrader PM10 emission (mg m^{-2}) comparisons among trafficking pass levels and sampling locations (tracked vehicles).

SoilCode [†]	Sampling Location*	Abrader PM10 emission (mg m^{-2}) - Tracked Vehicles			
		p0 (0) [‡]	p1 (1) [‡]	p2 (5) [‡]	p3 (10) [‡]
FB-LS	CI	72.18 ^a	163.11 ^{bcx}	85.59 ^{ab}	181.75 ^c
FB-LS	CO		125.41 ^{abxy}	133.11 ^{ab}	184.30 ^b
FB-LS	SS		83.23 ^{aby}	98.92 ^{ab}	155.96 ^b
WS-L	CI	62.89 ^a	190.40 ^b	105.97 ^{ab}	102.39 ^{ab}
WS-L	CO		148.13 ^{ab}	167.63 ^{ab}	277.60 ^b
WS-L	SS		89.71 ^{ab}	169.55 ^{ab}	188.55 ^b
FB-LS	CI	349.42 ^a	3421.35 ^{by}	1479.20 ^b	1977.61 ^b
FB-LS	CO	195.77 ^a	2121.20 ^{bxy}	1928.58 ^b	2522.92 ^b
FB-LS	SS	676.36 ^a	1093.64 ^{ax}	1451.50 ^{ab}	3476.19 ^b
WS-L	CI	173.29 ^a	12423.68 ^b	3314.21 ^{cy}	2616.03 ^c
WS-L	CO	186.94 ^a	8550.96 ^b	4802.53 ^{cxy}	3706.42 ^{cx}
WS-L	SS	180.93 ^a	1619.49 ^{bx}	6955.64 ^{cx}	14354.10 ^d
WS-SL	CI	1077.15 ^a	1225.87 ^a	1297.01 ^a	976.28 ^a
WS-SL	CO	618.20 ^a	1196.15 ^a	1138.85 ^a	1242.80 ^a
WS-SL	SS	718.29 ^{ab}	646.08 ^a	1475.53 ^{bc}	1798.66 ^c

[†] SoilCode designates the site and soil where sites are FB = Fort Benning, GA; FR = Fort Riley, KS; WS = White Sands Missile Range, NM and soils are LS = loamy sand, SiCL = silty clay loam, SiL = silt loam, SL = sandy loam and L = loam.

*CI is curve inside, CO is curve outside, and SS is straight section of figure-8 tracked sampling locations.

[‡]Trafficking pass levels, p0,p1,p2,p3 (number of cumulative passes)

For a given site/soil, mean values by row with the same letter (a, b, c) are not significantly different at 0.05 level by trafficking pass level (0,1,5,10). For a given site/soil, mean values by column are only significantly different at the 0.05 level by sampling location (CI,CO,SS), if identified with the letter x or y (Tukey's mean separation).

The ANOVA test results (Table 66 and Table 67) for the wheeled vehicles' abrader wind tunnel tests show that the trafficking passes (Pass) were significant ($p < 0.05$). In addition, the soil (SoilCode) with interactions (Table 66) were also significant ($p < 0.05$) and similar to the tracked vehicles' results.

Table 66. Overall ANOVA type III table of wind tunnel abrader PM10 (mg m⁻²) dust emissions (log transformed) for wheeled vehicles (HMMWV). Sum Sq = sum of squares; Mean Sq = mean of squares; NumDF = numerator degrees of freedom; DenDF = denominator degrees of freedom; F.value = F statistic ratio value; PR(>F) = Probability p value associated with F statistic.

Factor	Sum Sq	Mean Sq	NumDF	DenDF	F.value	Pr(>F)	Signif.
SoilCode	94.8	19.0	5	13.7	122.8	7e-11	***
Pass	103.0	34.3	3	92.3	222.3	<2e-16	***
Loc	1.1	0.5	2	30.3	3.6	0.041	*
SoilCode:Pass	39.8	2.7	15	92.3	17.2	<2e-16	***
SoilCode:Loc	0.6	0.1	10	30.0	0.4	0.929	
Pass:Loc	1.4	0.2	6	92.3	1.5	0.184	
SoilCode:Pass:Loc	3.4	0.2	20	92.3	1.1	0.355	

Satterthwaite approximation used for degrees of freedom

Signif. codes: 0 '***' 0.001 '**' 0.01 '*' 0.05 '.' 0.1 ' ' 1

Table 67. Overall ANOVA type III table of wind tunnel abrader PM10 (mg m⁻²) dust emissions (log transformed) for heavy wheeled vehicle (Fire Truck). Sum Sq = sum of squares; Mean Sq = mean of squares; NumDF = numerator degrees of freedom; DenDF = denominator degrees of freedom; F.value = F statistic ratio value; PR(>F) = Probability p value associated with F statistic.

Factor	Sum Sq	Mean Sq	NumDF	DenDF	F.value	Pr(>F)	Signif.
Pass	73.7	24.57	3	24	69.6	6.5e-12	***
Loc	0.2	0.10	2	24	0.3	0.76	
Pass:Loc	1.9	0.31	6	24	0.9	0.52	

Satterthwaite approximation used for degrees of freedom

Signif. codes: 0 '***' 0.001 '**' 0.01 '*' 0.05 '.' 0.1 ' ' 1

Again, like the tracked vehicle results, the “All Locations” rows show the soil differences in Table 68 and similarly by each sampling location.

Table 68. Wind tunnel (log transformed) abrader PM10 (mg m⁻²) least square means (lsmean) (log transformed) for wheeled vehicles (HMMWV) by soil and sampling location. SE = standard error of the mean, df = degrees of freedom, lower.CL = lower confidence level (95%), and upper .CL = upper confidence level (95%).

Sampling Location*	SoilCode[†]	lsmean	SE	df	lower.CL	upper.CL	group
All Locations	WS-SL	6.82	0.111	10.3	6.58	7.07	a
	FB-LS	6.99	0.111	10.3	6.75	7.24	a
	YK-SL	7.27	0.111	10.3	7.02	7.51	a
	WS-L	8.19	0.111	10.3	7.94	8.43	b
	FR-SiCL	NA	NA	NA	NA	NA	
	FR-SiL	NA	NA	NA	NA	NA	
CI	WS-SL	6.77	0.178	30.4	6.40	7.13	a
	FB-LS	7.10	0.178	30.4	6.74	7.47	a
	YK-SL	7.37	0.178	30.4	7.01	7.73	a
	WS-L	8.27	0.178	30.4	7.90	8.63	b
	FR-SiCL	NA	NA	NA	NA	NA	
	FR-SiL	NA	NA	NA	NA	NA	
CO	FR-SiCL	4.50	0.178	30.4	4.14	4.87	a
	FR-SiL	4.81	0.178	30.4	4.45	5.17	a
	WS-SL	6.91	0.178	30.4	6.55	7.28	b
	FB-LS	7.04	0.178	30.4	6.67	7.40	b
	YK-SL	7.43	0.178	30.4	7.06	7.79	b
	WS-L	8.37	0.178	30.4	8.00	8.73	c
SS	WS-SL	6.79	0.178	30.4	6.43	7.16	a
	FB-LS	6.84	0.178	30.4	6.47	7.20	a
	YK-SL	7.01	0.178	30.4	6.64	7.37	a
	WS-L	7.93	0.178	30.4	7.56	8.29	b
	FR-SiCL	NA	NA	NA	NA	NA	
	FR-SiL	NA	NA	NA	NA	NA	

*CI is curve inside, CO is curve outside, and SS is straight section of figure-8 tracked sampling locations.

[†]SoilCode designates the site and soil where sites are FB = Fort Benning, GA; FR = Fort Riley, KS; WS = White Sands Missile Range, NM and soils are LS = loamy sand, SiCL = silty clay loam, SiL = silt loam, SL = sandy loam and L = loam. For a given sampling location, least square mean values with the same group letter are not significantly different at 0.05 level by SoilCode (Tukey's mean separation).

NA – Not Available.

Table 69 reveals significant differences ($p < 0.05$) between the un-trafficked condition (p_0) and all the trafficked conditions (p_{10} , p_{25} , p_{50}) for wheeled vehicles across all soil types. Unlike the tracked vehicles, the curved sampling locations behaved more similarly to the straight trafficked region. They generally tended to show a significant increase ($p < 0.05$) in abrader generated PM10 emissions with additional trafficking passes. The similarity in results between the curved and straight trafficked regions is likely due to the limited side shear forces exhibited by the wheeled vehicles compared to the tracked vehicles. The heavier wheeled vehicle (Fire Truck) yielded similar results to the HMMWV. The trafficking level effects by soil type of all soils for all the wheeled vehicles are provided in Table 71.

Table 69. Wind tunnel (log transformed) abrader PM10 (mg m⁻²) least square means (lsmean) (log transformed) for wheeled vehicles (HMMWV) by trafficking pass. SE = standard error of the mean, df = degrees of freedom, lower.CL = lower confidence level (95%), and upper .CL = upper confidence level (95%).

Sampling Location*	Pass[†]	lsmean	SE	df	lower.CL	upper.CL	group
CI [‡]	p0 (0)	5.72	0.138	74.3	5.45	6.00	a
	p1 (10)	7.49	0.138	74.3	7.22	7.77	b
	p2 (25)	7.80	0.138	74.3	7.53	8.08	b
	p3 (50)	8.47	0.138	74.3	8.20	8.75	c
CO	p0 (0)	5.23	0.108	103	5.02	5.45	a
	p1 (10)	6.52	0.108	103	6.31	6.74	b
	p2 (25)	7.01	0.108	103	6.79	7.22	c
	p3 (50)	7.27	0.108	103	7.05	7.48	c
SS [‡]	p0 (0)	5.68	0.138	74.3	5.40	5.95	a
	p3 (50)	6.95	0.138	74.3	6.68	7.23	b
	p1 (10)	7.58	0.138	74.3	7.30	7.86	c
	p2 (25)	8.35	0.138	74.3	8.07	8.62	d

*CI is curve inside, CO is curve outside, and SS is straight section of figure-8 tracked sampling locations.

[†]Pass is the pass level (p0,p1,p2,p3) and the number of cumulative figure-8 trafficking passes conducted with the vehicle are indicated in parentheses.

[‡]Does not include Ft. Riley soils (FR-SiCL, FR-SCL) due to insufficient data collected for analysis.

For a given location, least square mean values with the same group letter are not significantly different at 0.05 level by trafficking pass level (Tukey's mean separation).

Table 70. Wind tunnel (log transformed) abrader PM10 (mg m⁻²) least square means (lsmean) (log transformed) for heavy wheeled vehicle (Fire Truck) by sampling location. SE = standard error of the mean, df = degrees of freedom, lower.CL = lower confidence level (95%), and upper .CL = upper confidence level (95%).

Sampling Location*	Pass[†]	lsmean	SE	df	lower.CL	upper.CL	group
CI	p0 (0)	5.22	0.343	24	4.51	5.93	a
	p1 (2)	7.30	0.343	24	6.60	8.01	b
	p2 (10)	8.19	0.343	24	7.48	8.90	bc
	p3 (20)	9.01	0.343	24	8.30	9.72	c
CO	p0 (0)	5.01	0.343	24	4.30	5.72	a
	p1 (2)	6.58	0.343	24	5.88	7.29	b
	p2 (10)	8.30	0.343	24	7.59	9.01	c
	p3 (20)	9.17	0.343	24	8.46	9.88	c
SS	p0 (0)	5.13	0.343	24	4.42	5.83	a
	p1 (2)	7.47	0.343	24	6.76	8.18	b
	p2 (10)	7.86	0.343	24	7.15	8.57	b
	p3 (20)	8.68	0.343	24	7.98	9.39	b

*CI is curve inside, CO is curve outside, and SS is straight section of figure-8 tracked sampling locations.

[†]Pass is the pass level (p0,p1,p2,p3) and the number of cumulative figure-8 trafficking passes conducted with the vehicle are indicated in parentheses.

For a given location, least square mean values with the same group letter are not significantly different at 0.05 level by trafficking pass level (Tukey's mean separation).

Table 71. Abrader PM10 emission (mg m⁻²) comparisons among trafficking pass levels and sampling locations (wheeled vehicles).

SoilCode [†]	Sampling Location*	Abrader PM10 emission (mg m ⁻²)			
		HMMWV			
		p0 (0) [‡]	p1 (10) [‡]	p2 (25) [‡]	p3 (50) [‡]
FR-SiCL	CO	81.98 ^{ab}	110.01 ^b	114.40 ^b	70.75 ^a
FR-SiCL	SS		N/A	N/A	101.63 ^a
FR-SiL	CO	67.87 ^a	129.40 ^a	182.79 ^a	250.81 ^a
FR-SiL	SS		N/A	N/A	81.79 ^a
FB-LS	CI	310.63 ^a	1774.56 ^b	1889.98 ^b	3005.51 ^b
FB-LS	CO	319.10 ^a	744.71 ^a	4072.96 ^b	2603.27 ^b
FB-LS	SS	302.09 ^a	714.02 ^{ab}	1430.36 ^{bc}	2828.34 ^c
YK-SL	CI	206.23 ^a	1121.71 ^b	3533.51 ^c	9499.75 ^c
YK-SL	CO	194.89 ^a	1973.60 ^b	2759.88 ^b	10623.59 ^b
YK-SL	SS	174.10 ^a	873.58 ^b	2520.14 ^{bc}	5610.43 ^c
WS-L	CI	495.30 ^a	6533.43 ^b	7581.07 ^b	13010.99 ^b
WS-L	CO	517.88 ^a	4940.61 ^b	11223.71 ^{bc}	15957.92 ^c
WS-L	SS	497.14 ^a	3378.70 ^b	6287.50 ^{bc}	9190.04 ^c
WS-SL	CI	330.92 ^a	1210.24 ^b	853.74 ^b	1869.69 ^b
WS-SL	CO	332.29 ^a	1439.11 ^b	1219.09 ^b	2294.31 ^b
WS-SL	SS	338.82 ^a	887.18 ^b	946.43 ^b	2707.45 ^c
		Fire Truck			
		p0 (0) [‡]	p1 (2) [‡]	p2 (10) [‡]	p3 (20) [‡]
YK-SL	CI	225.19 ^a	1750.21 ^b	4002.06 ^{bc}	8552.22 ^c
YK-SL	CO	165.31 ^a	851.93 ^b	4229.39 ^c	10034.81 ^c
YK-SL	SS	218.63 ^a	1959.60 ^b	2963.58 ^b	5953.00 ^b

[†] SoilCode designates the site and soil where sites are FB = Fort Benning, GA; FR = Fort Riley, KS; WS = White Sands Missile Range, NM and soils are LS = loamy sand, SiCL = silty clay loam, SiL = silt loam, SL = sandy loam and L = loam.

*CI is curve inside, CO is curve outside, and SS is straight section of figure-8 tracked sampling locations.

[‡]Trafficking pass levels, p0,p1,p2,p3 (number of cumulative passes)

For a given soil, mean values by row with the same letter (a,b,c) are not significantly different at 0.05 level by trafficking pass level (0,10,25,50 or 0,2,10,20) (Tukey's mean separation)

N/A – Not Available (data not collected at the specified pass levels)

To summarize, the effects of the abrader wind tunnel tray tests generally mirror the non-abrader wind tunnel tray tests with respect to increased emissions with increased trafficking, etc. The non-abrader tests, however, only give an estimate of total PM10 particulates available for emission from the surface whereas the abrader tests give an indication of potential sustained PM10 emissions due to the saltation abrader effects on generating additional surface emission particulates. The PM10 emission differences across soil types in the abrader wind tunnel tray tests are primarily due to the amount of PM10 size particulates available and the soil's ability to resist saltation abrasion. The sites with higher water contents at sampling (i.e., FR soils), had lower PM10 emissions. Likewise, the soils that were high in sand content (i.e., FB loamy sand and WSMR sandy loam soils) had less PM10 material content available and generated lower

relative PM10 emissions, even at maximum trafficking levels compared to the soils with high silt content (i.e., WSMR loam and YTC sandy loam soils) as shown in Table 65 and Table 71.

PI-SWERL Measurements and Comparison with Wind Tunnel Data

The PI-SWERL was originally conceived and developed by the Desert Research Institute (DRI) to have a portable instrument to quickly obtain repeatable measurements of dust emission on paved roads (Etyemezian, et al., 2007). It was desired to see if the standard laboratory wind tunnel measurements in this study could be correlated to the PI-SWERL measurements. The summarized PI-SWERL results are shown in **Figure 29**, **Figure 30** and **Figure 31** for both the tracked and wheeled vehicles (HMMWV and Fire Truck) respectively. Notice that the trends were in general similar to the wind tunnel tray data.

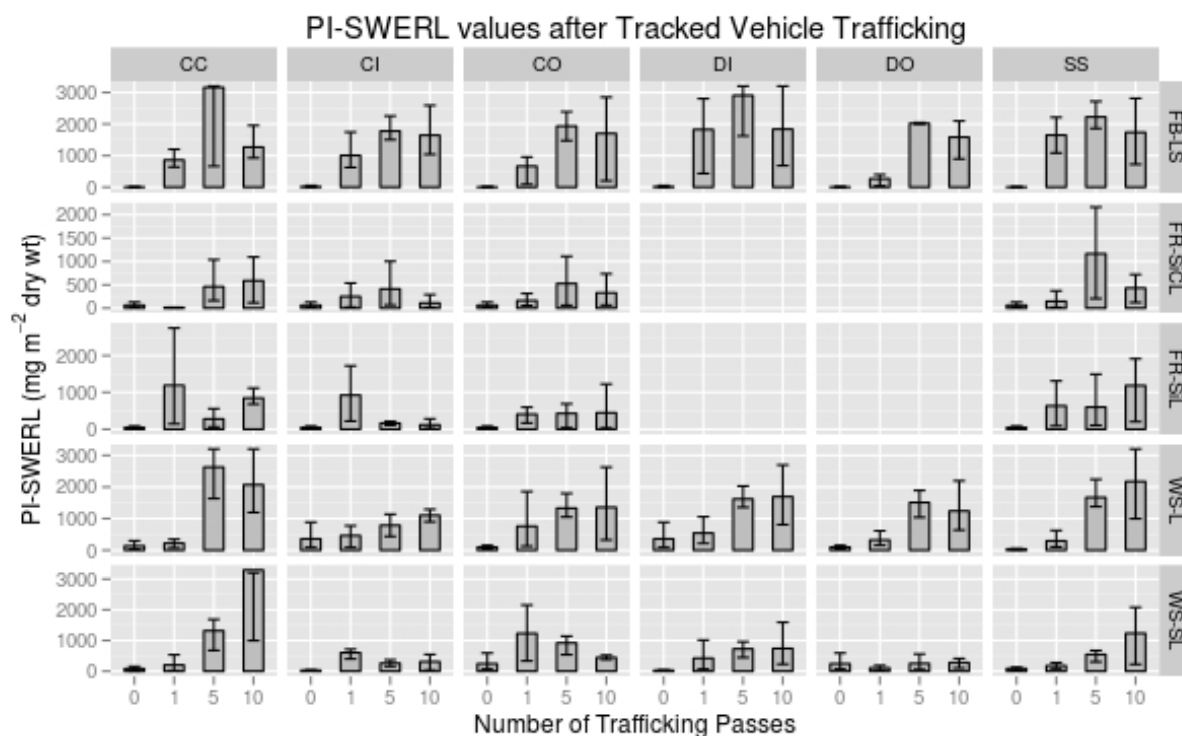


Figure 29. PM10 emission values obtained from PI-SWERL at 2000 rpm setting for all sampling locations on all soils for the tracked vehicles. Bars represent the mean of the measured values and the error bars represent the maximum and minimum measured values. CC is center cross, CI is curve inside, CO is curve outside, DI is deposition inside, DO is deposition outside, and SS is the straight section sampling location. Sites are FB = Fort Benning, GA; FR = Fort Riley, KS and WS = White Sands Missile Range, NM. Soils are LS = loamy sand, SiCL = silty clay loam, SiL = silt loam, SL = sandy loam, and L = loam.

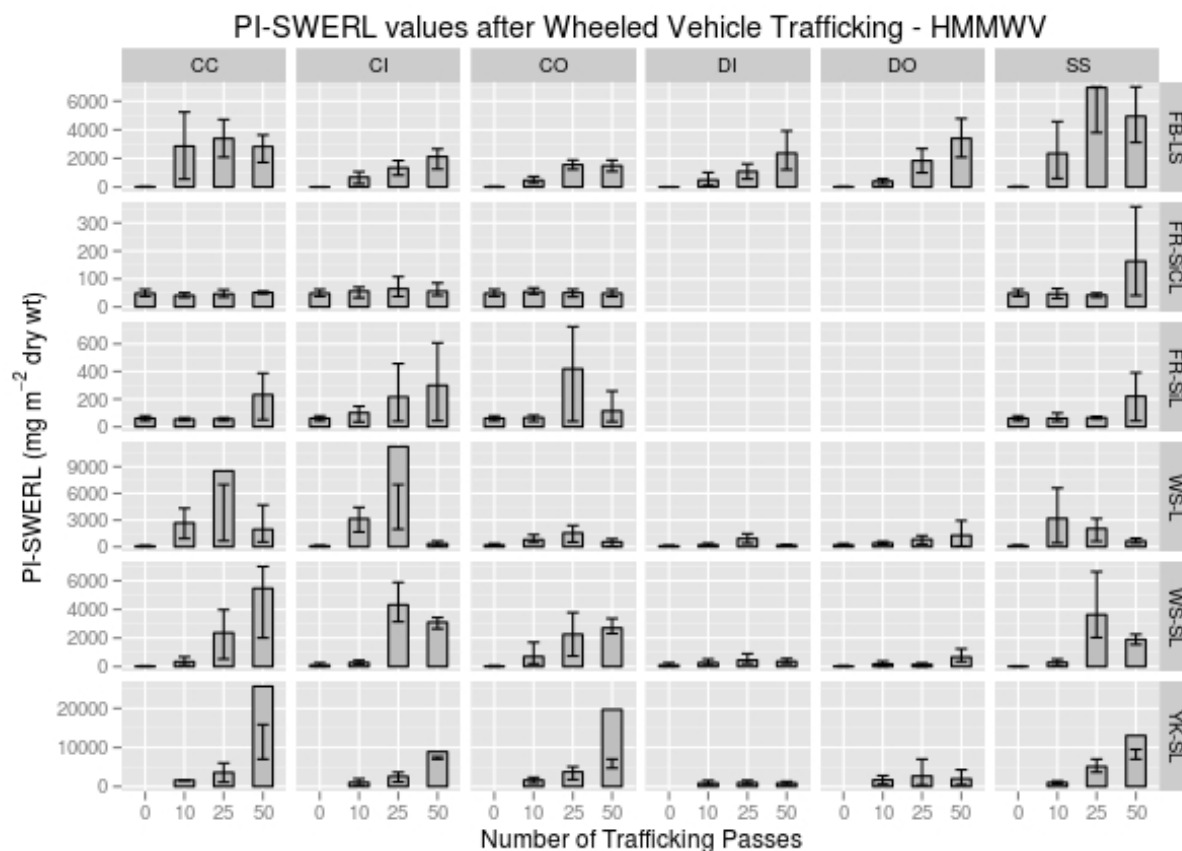


Figure 30. PM₁₀ emission values obtained from PI-SWERL at 2000 rpm setting for all sampling locations on all soils for the wheeled vehicles (HMMWV). Bars represent the mean of the measured values and the error bars represent the maximum and minimum measured values. CC is center cross, CI is curve inside, CO is curve outside, DI is deposition inside, DO is deposition outside, and SS is the straight section sampling location. Sites are FB = Fort Benning, GA; FR = Fort Riley, KS and WS = White Sands Missile Range, NM. Soils are LS = loamy sand, SiCL = silty clay loam, SiL = silt loam, SL = sandy loam, and L = loam.

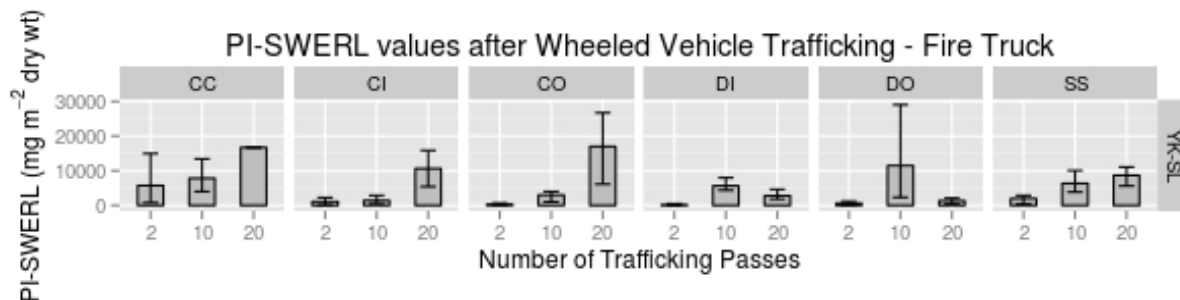


Figure 31. PM10 emission values obtained from PI-SWERL at 2000 rpm setting for all sampling locations on the Yakima soil for the heavy wheeled vehicle (Fire Truck). Bars represent the mean of the measured values and the error bars represent the maximum and minimum measured values. CC is center cross, CI is curve inside, CO is curve outside, DI is deposition inside, DO is deposition outside, and SS is the straight section sampling location. Site is YK = Yakima Training Center, WA. Soil is SL = sandy loam.

Several issues arose when first using the PI-SWERL. We originally consulted with DRI prior to our first set of field experiments at Ft. Riley on how best to use the instrument for the conditions we expected to experience. They had not attempted to use it in a similar environment (e.g., off-road conditions). Their recommendation was to use one of the standard step functions that would: a) initially clean out the chamber without the rotor turning (60 s); b) ramp up to first rpm setting (45 s); c) hold rpm setting for specified time (60 s); d) ramp to second rpm setting (45 s); e) hold rpm setting (60 s); f) ramp to third rpm setting (45 s); g) hold rpm setting (60 s); and h) shut down the rotor and clean out the chamber (60 s). They felt that type of measurement method would yield the most useful data from the PI-SWERL. The initial settings we used at Ft. Riley had rpm settings of 2000, 3000 and 4000 rpm.

The single biggest issue recognized at Ft. Riley was that this particular PI-SWERL (on loan from DRI) used the older model TSI DustTrack (model 8520), which had a documented maximum dust concentration measurement level of 100 mg m^{-3} . We exceeded that value several times following some trafficked conditions. However, we were fortunate that the unit actually computed values exceeding 100 mg m^{-3} (up to 150 mg m^{-3}), so we still obtained usable data at Ft. Riley. This DustTrack limitation was also mentioned as an issue in (Kunhs, et al., 2010) research when evaluating wheeled and tracked vehicle emission levels on unpaved roads with a PI-SWERL.

When data was collected at the second site (Ft. Benning, GA), we expected that our PI-SWERL would not exceed its measurement range, because the newer model TSI DustTrack 8531 that came with the unit had a documented maximum dust concentration level measurement limit of 400 mg m^{-3} , four times the limit of the older DustTrack model 8520 with the PI-SWERL used at Ft. Riley. However, the Ft. Benning soil generated much higher levels of PM10 than we saw at Ft. Riley (**Figure 29** and **Figure 30**). PM10 emission values obtained from PI-SWERL at 2000 rpm setting for all sampling locations on all soils for the wheeled vehicles (HMMWV). Bars represent the mean of the measured values and the error bars represent the maximum and minimum measured values. CC is center cross, CI is curve inside, CO is curve outside, DI is deposition inside, DO is deposition outside, and SS is the straight section sampling location. Sites are FB = Fort Benning, GA; FR = Fort Riley, KS and WS = White Sands Missile Range,

NM. Soils are LS = loamy sand, SiCL = silty clay loam, SiL = silt loam, SL = sandy loam, and L = loam.

We used the same settings as were used at Ft. Riley, but frequently exceeded the DustTrack's maximum measurement level at the higher rpm settings. We decided to continue using the same settings after discovering this issue. We expected that the lower (2000) rpm data would still be useable, which it was, even if the higher (4000 and some 3000) rpm data weren't. This was later determined to not be a wise decision because we eventually could not zero the original DustTrack 8531 and had to replace it with a second unit. We ultimately had to return that unit to the company to get cleaned and recalibrated.

After the experiences at Ft. Benning, we decided to change our measurement protocol for the remaining sites. We now knew that we should not allow the PI-SWERL to generate dust concentrations greater than what the DustTrack could read to keep the instrument operational and to obtain useable data. The approach we used was to manually monitor the DustTrack levels during the measurement interval. If we witnessed the DustTrack nearing its measurement limits, we dropped the higher rpm setting from the test for the remaining trafficking pass levels for that vehicle on that figure-8. At Yakima, we started out running with the original 2000, 3000 and 4000 rpm step settings. As we conducted the trafficking, we found that we not only had to eliminate the 4000 rpm setting, but also the 3000 rpm setting in some scenarios. So, we ended up with only 2000 rpm setting measurements for some sampling locations following the higher trafficking pass levels. We used that same protocol at White Sands Missile Range as well.

When we first began to analyze the PI-SWERL data, we ran into additional issues. First, we didn't know what the actual friction velocity the PI-SWERL rotating annular blade was generating at different rpm settings. DRI initially provided us with a reference paper (Etyemezian, et al., 2007), which contained an equation relating PI-SWERL rotation speed to friction velocity but it did not correlate well with our wind tunnel non-abrader tray emission levels. This was not unexpected since that relationship was obtained under a very smooth surface condition that was not indicative of the surface roughness conditions we experienced in the field and on the wind tunnel trays. Also, that study was conducted with an early, larger dimensioned version of the PI-SWERL, which would also affect the friction velocity relationship. They have since released another publication (Etyemezian, et al., 2014) that looked at various surface roughness levels and rotor speeds and developed another equation to estimate friction velocity which is dependent upon surface roughness. In addition, they used the miniature PI-SWERL, the same version we used, for determining this relationship.

Now that we could relate the PI-SWERL emission readings to the rpm of the rotor with different roughness values, we needed to convert from the roughness units Etyemezian et al. (2014) used to the standard Allmaras roughness units (Allmaras, et al., 1966) used in WEPS and other wind erosion studies. Larry Hagen did the analysis and produced the following equation:

$$\alpha = 0.806 + 0.1185 * \exp\left(-\frac{RR}{1.523}\right) \quad (7)$$

Where:

α = roughness parameter used in friction velocity estimate from PI-SWERL rotor rpm
 RR = Allmaras std. dev. random roughness (mm) obtained from pin meter measurements

With these two relationships, one could estimate the friction velocities generated by the PI-SWERL at various rpm settings. However, actual surface friction velocities are also dependent upon the amount of standing (vertical) vegetation present, which is usually represented as unitless ($\text{m}^2 \text{ m}^{-2}$) stem area index (SAI) and leaf area index (LAI) values, where the leaf area is discounted by about a factor of ten due to their tendency to streamline with the wind. Unfortunately, that data, mostly in the untrafficked samples, were not recorded. Since the PI-SWERL data we presented is limited to only the 2000 rpm range, only a fraction of the particulate emissions actually measured by the PI-SWERL are presented due to this limited rpm range of data collected across all sites and conditions.

After several attempts at trying to interpret the PI-SWERL data for possible use in determining its correlation with the non-abrader wind tunnel tray data, it was decided that the effort would provide little benefit compared to the effort to do so within the timeframe available. Previous research determined a strong correlation between PI-SWERL data and wind tunnel data (Sweeney, et al., 2008). However, there were several concerns with this study, none of which necessarily negate the conclusions made (e.g., that the PI-SWERL measurements correlate well with the wind tunnel measurements). First, the older PI-SWERL used in that experiment is not the same as the miniature PI-SWERL that we used in our study. Second, the friction velocity values computed for their PI-SWERL used the original previously published equation that applied only to a very smooth surface and did not take into account the actual soil surface roughness. Since the surface roughness was usually much greater, they were under estimating the friction velocity generated with the PI-SWERL, which was confirmed with their adjacent wind tunnel measurements. Also, both the wind tunnel and PI-SWERL tests were apparently consistent across the whole study with regards to the wind speed steps and the time intervals held for each of them. As mentioned in that publication, there were only brief periods of dust emissions, suggesting that the surfaces were usually source limited. This brings into question their comparisons with flux measurements rather than just total emissions per unit area. However, since their time intervals were consistent among sites and between the wind tunnel and PI-SWERL, the relative values should be comparable even if the absolute flux values are questionable due to large periods of test time with no emissions occurring.

In short, the question of whether the PI-SWERL “correlates” with wind tunnel data is probably not the question to ask. They will be correlated (e.g., higher emissions will be measured with both devices on soils that contain higher concentrations of erodible material). However differences still exist due to the different approaches used to generate shear stress at the soil surface. The PI-SWERL advantages is that it is very portable, which lends itself to obtaining replicated measurements more easily and quickly than with a portable wind tunnel. Our only negative experiences with the PI-SWERL were due to the limited range of particulate concentrations the DustTrack could measure. We believe that this could be at least partially overcome with a more dynamic sampling protocol than the fixed rpm settings we used. Providing an active feedback control on the rotor speed to limit the concentration levels within the PI-SWERL canister should alleviate the excessive levels being measured with the DustTrack. In addition, the ability to dynamically adjust the time the PI-SWERL stays at a set rpm would allow all the emitted particles at that rpm setting to be measured by the DustTrack and thus attributed to that specific rpm setting (i.e. surface friction velocity). Also, such an approach, used in conjunction with a finer rpm step interval could allow the PI-SWERL to potentially be used

for determining the initial threshold friction velocity. We believe that such a dynamic protocol for using the PI-SWERL would make the obtained data much more useful than the current methods available and also easier to compare to traditional wind tunnel experimental data.

Development of a Trafficking Compaction Process Model

To simulate the trafficking compaction process within the Wind Erosion Prediction System (WEPS) model, we normalized the bulk density data across soil types and bound the upper and lower ranges for use in developing a universal trafficking compaction process based upon a soil's intrinsic properties. WEPS uses the “settled” bulk density as defined by (Rawls, 1983) which is defined as the natural bulk density a soil will trend towards over time due to natural climatic effects such as freeze/thawing, freeze/drying, precipitation, etc. It is defined as a function of the primary soil particles (fractions of the sand, silt and clay content) and the fraction of organic matter content. This is used as the lower bulk density limit for compaction, which equals a normalized bulk density of 0. The upper bulk density limit is defined here as the Proctor Density (PD) value for the soil, which occurs at the Optimum Water Content (OWC), under prescribed test conditions as specified by ASTM Standard D698 (2012). The soil PD and OWC values are presented in **Table 8**. The Proctor density data from (Wagner, et al., 1994) along with the data from this study were used to develop an updated relationship for Optimum Water content. This is then used with the Proctor bulk density relationship from (Wagner, et al., 1994) to compute the upper bulk density limit, which equals a normalized bulk density of 1. The final normalization relationship is shown in Eqn 7.

$$BD_{normalized} = (BD_{Settled} - BDP)/(BD_{Settled} - BD_{Proc@wc}) \quad (7)$$

Where:

$BD_{normalized}$ is the normalized bulk density (unitless)

$BD_{Settled}$ is the “settled” bulk density (mg m^{-3})

$BD_{Proc@wc}$ is the Proctor bulk density at the specified water content (mg m^{-3})

The normalized bulk density data for the tracked vehicles are presented in **Figure 32**. Note that the trends mentioned previously for the 0-15 cm bulk density due to trafficking passes still exist, where the normalized bulk density zero value represents the “settled” bulk density value. However, the negative numbers that appear in the loam White Sands Missile Range soil (WS-L) suggests that the primary particle size distribution may not have been uniform by depth.

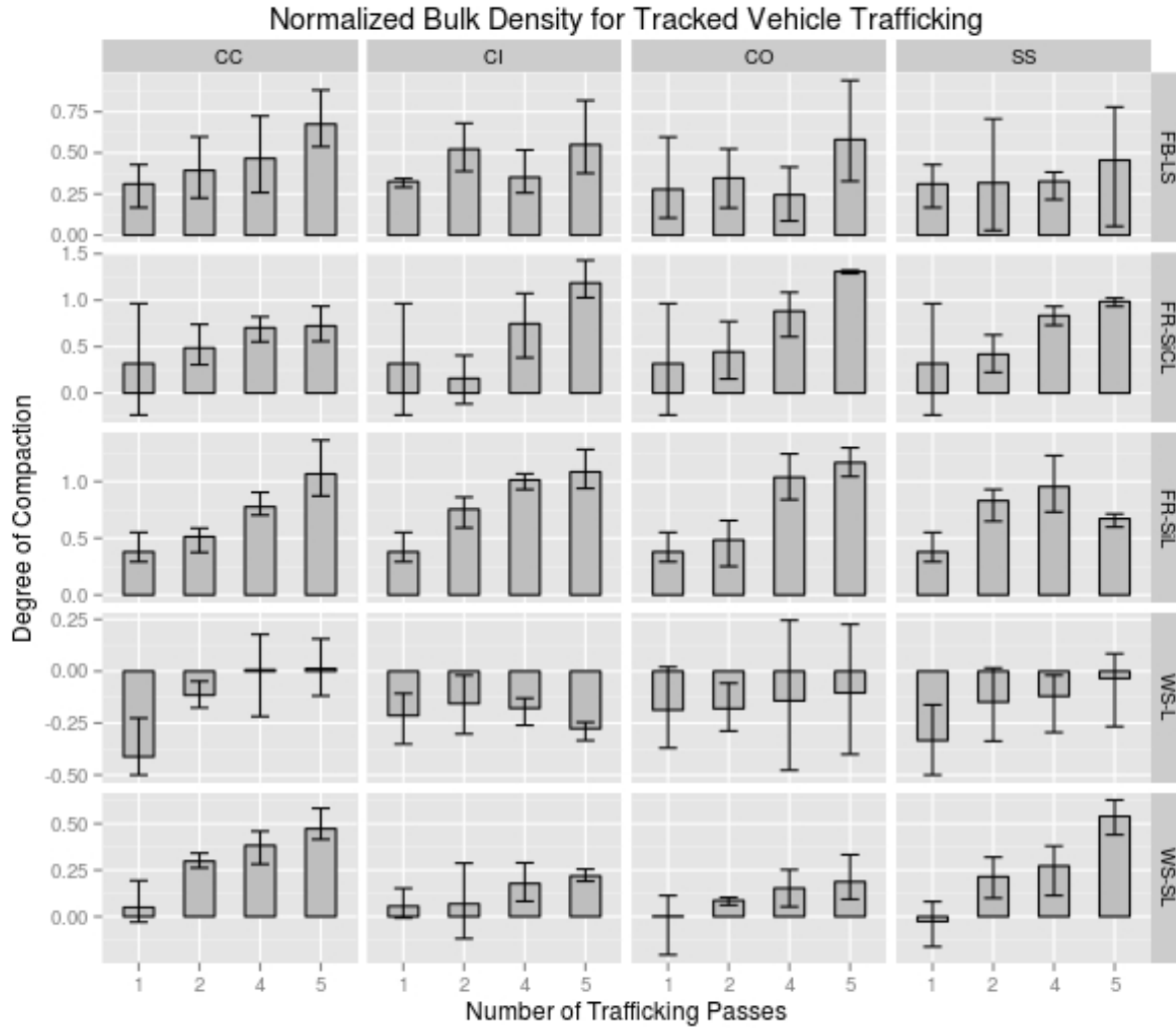


Figure 32. Normalized bulk density due to tracked vehicle trafficking passes. CC is center cross, CI is curve inside, CO is curve outside, and SS is the straight section sampling location. Sites are FB = Fort Benning, GA; FR = Fort Riley, KS and WS = White Sands Missile Range, NM. Soils are LS = loamy sand, SiCL = silty clay loam, SiL = silt loam, SL = sandy loam, and L = loam.

Likewise, the normalized bulk density data are also presented for the wheeled vehicles (HMMWV in **Figure 33**) and (Fire Truck in **Figure 34**).

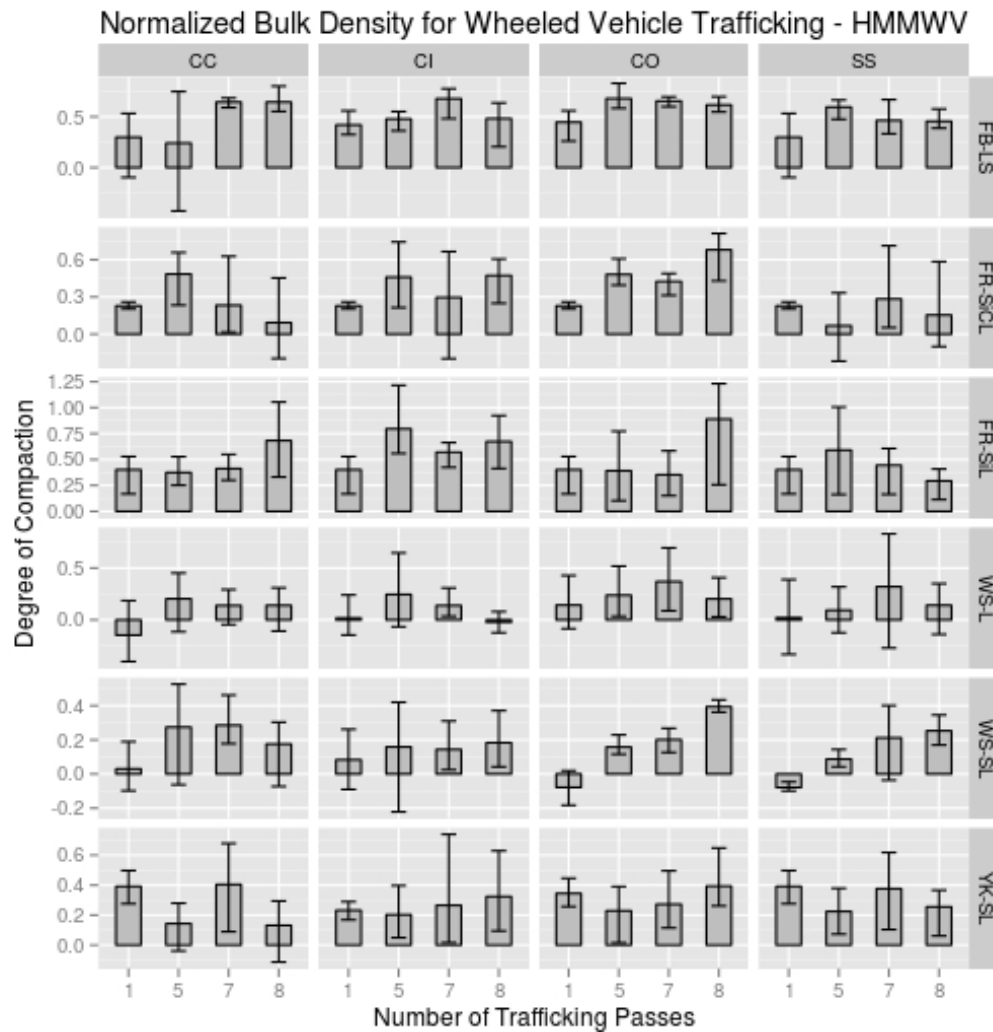


Figure 33. Normalized bulk density due to HMMWV wheeled vehicle trafficking passes. CC is center cross, CI is curve inside, CO is curve outside, and SS is the straight section sampling location. Sites are FB = Fort Benning, GA; FR = Fort Riley, KS and WS = White Sands Missile Range, NM. Soils are LS = loamy sand, SiCL = silty clay loam, SiL = silt loam, SL = sandy loam, and L = loam.

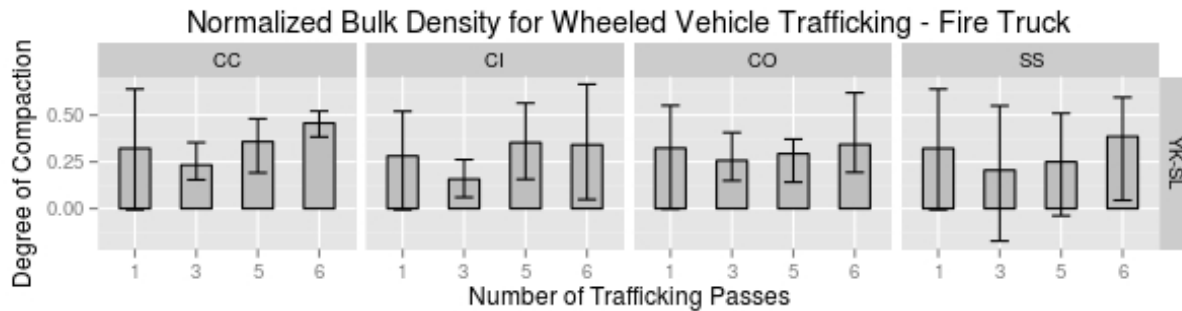


Figure 34. Normalized bulk density due to Fire Truck wheeled vehicle trafficking passes. CC is center cross, CI is curve inside, CO is curve outside, and SS is the straight section sampling location. Site is YK = Yakima Training Center, WA. Soil is SL = sandy loam.

Potential use of WEPS for Off-Road Military Trafficking Scenarios

Wind Erosion Prediction System (WEPS) is a process based, continuous daily time-step model that simulates weather, site conditions and wind erosion. WEPS was initially targeted for managed agricultural lands with expectations of eventually being extended to natively handle rangelands and be applied in non-agriculture uses, such as construction sites, mining reclamation, etc. It simulates wind erosion based upon the surface friction velocity produced by the wind at the surface exceeding the threshold friction velocity of the surface itself. WEPS simulates the principle physical processes that affect the surface (soil/vegetation) state on a daily basis, including both the effects caused by weather and through actions initiated by people. Natural processes such as vegetation growth and residue decay are simulated in response to available soil water and climatic conditions. Surface wetting and drying, changes in soil aggregate status, surface roughness and crusting due to weather as well as human induced effects are also simulated. Many typical agricultural operations (management processes) are represented in WEPS and are simulated as a series of specific physical processes that modify the surface, soil and vegetation state of a site. A more complete description of WEPS is available in Wagner (2013).

After discussing range management issues with the military liaisons on this project and becoming more educated in their specific simulation needs, it became apparent that the WEPS model's current limitations make it unsuitable for their typical use cases at this time.

Issues that are especially problematic are: 1) simulating vegetation growth of heterogeneous plant species simultaneously on military controlled rangeland and unmanaged natural areas is not easily represented within WEPS at this time; 2) the multi-subregion version of WEPS is required to correctly represent trafficking effects on wind erosion susceptibility. A multi-subregion version of WEPS has been developed, however it has had limited testing and there is no interface currently available to easily describe the variability of surface conditions spatially, such as those caused by military trafficking (an interface is under development though); 3) the "daily" surface conditions typically change slowly in response to many weathering effects compared to agricultural cropping conditions, especially in arid military training land regions, so computing and updating those surface properties on a daily basis is probably not the best simulation approach to use in this situation. Many long periodic intervals, weeks to months in length, could be considered to have the same or very similar surface conditions. When precipitation occurs, rapid vegetation growth and ground cover can occur in arid regions like several of the sites

studied here. These surface and vegetation conditions might be more easily modeled and represented as unchanging for long periods of time with specific weather (precipitation, freeze/thaw cycles, etc.) and trafficking events creating a changed surface state that persists, again for another long stretch of time, e.g. more than a single day; 4) WEPS does not simulate dust emissions during military vehicle trafficking, only the dust generated from the surface by subsequent winds (wind erosion), when the wind speed generated surface friction velocity exceeds the surface threshold friction velocity of the surface for the direction specified, and; 5) WEPS does not contain a “dispersion” model, so it cannot simulate the distance airborne particles may travel from the emission site, nor any localized deposition that may occur. Such a dispersion/deposition model component is required for assessing total dust emission levels directly due to military trafficking and indirectly due to increased surface susceptibility to wind erosion events as well as the particulate concentration levels downwind, e.g. at the fence-line and their contribution to monitored offsite particulate levels downstream.

Although WEPS itself is not a complete solution at this time for military training land managers, the erosion submodel component of WEPS does provide the ability to simulate wind erosion if the surface conditions are provided and the wind speed generates a surface friction velocity that exceeds the threshold friction velocity of the surface(s). The erosion submodel within WEPS simulates whether erosion or deposition occurs on a spatial basis, since it grids the simulation site into uniformly sized rectangular cells. Thus, the WEPS erosion submodel could be used to predict the susceptibility of a military trafficked site to wind erosion events if historical hourly wind speed and direction data were available and statistically summarized by at least monthly wind speed/direction frequency distributions (van Donk, et al., 2005).

SWEEP use for Off-Road Military Trafficking Scenarios

The Single-event Wind Erosion Evaluation Program (SWEEP) consists of the WEPS erosion submodel component with a user interface to allow users to easily input required surface and sub-daily wind conditions. SWEEP simulates wind erosion for a single day (or period) storm event. The erosion submodel is coupled with a graphical user interface to allow users to provide the surface conditions and the wind data necessary to run the model. SWEEP is usually used to determine amounts of wind erosion under the stated conditions for the subdaily wind speed and direction data provided. Erosion output is provided on a spatial grid basis for the site and presents gross and net total erosion from the site as well as erosion by particle size diameter: a) creep+saltation size ($\geq 100\mu\text{m}$); b) suspension size ($< 100\mu\text{m}$); and c) PM10 ($< 10\mu\text{m}$). Three dimensional plots are also available for viewing the output (see **Figure 36**). A complete description of SWEEP is available in the SWEEP User Guide, which is accessible from within the SWEEP program. It is distributed as a component of the public WEPS release package: <http://www.ars.usda.gov/services/software/download.htm?softwareid=415> (Accessed 26 October, 2016).

The required inputs for SWEEP are divided into five input sections within its interface: a) Field (Simulation Site) and Wind Barriers; b) Biomass (live and dead vegetation); c) Surface (upper) Soil Layer Properties; d) Surface Properties; and e) Weather. The required inputs for military trafficking under off-road conditions are briefly described here.

Field Description and Wind Barriers: SWEEP requires the site (e.g., field) to be represented as a rectangular area that can be rotated, if necessary, to match the physical site description. Thus, the required inputs are the X-length (m) and Y-length (m) dimensions and orientation angle (\pm

degrees) with respect to north. Wind barriers can be placed anywhere on the simulation site and are represented simply as line segments with the bounding (X_1, Y_1) , (X_2, Y_2) transect coordinates specified in meters. A list of typical wind barriers used in agricultural settings is provided in a barrier database. However, custom barriers can easily be described by providing the required barrier properties: average barrier height (m), width (m) and porosity (fraction).

For military vehicle trafficking under off-road conditions, the user would be expected to provide SWEEP with the total area of the two tracks for either a straight line trafficked condition or a curved tracked condition. The straight line trafficked simulation would be the width of the two tracks (computing from values provided in Error! Reference source not found., it would be ~2.4m for HMMWV and ~3.7m for the M88-A1), and the length of the straight section (m) in the direction specified (degrees from north). The curved section would also be represented as the width of the two tracks (m) plus the ridge width outside the outside track (again computing from the values provided in **Table 72**, it would be ~2.7m for HMMWV and ~4.7m for the M88-A1), the ridge height (m), ridge width (m) and spacing between the ridges (m), for a curved region, and the perimeter length of the curved region (outside perimeter length of figure-8 tracks were ~80m for the HMMWV and ~100m for the M88-A1, assuming a 180 degree turn). The direction from north would be specified as the direction tangential to the radius at the center of the curved region perimeter. Undisturbed vegetation existing next to a trafficked region can optionally be represented in SWEEP as a wind barrier on one or both sides of the tracked region, if desired.

Note that when the multi-subregion version of WEPS and SWEEP become available with a suitable user interface, the user would be expected to simply provide a map of the trafficked regions, both straight and curved. The different trafficked areas (straight and curved) would be treated as separate subregions for analysis purposes and would also include the surrounding terrain outside the trafficked area as additional subregion(s) that could impact the trafficked region's susceptibility to wind erosion.

Table 72. Military vehicles' trafficking average ridge dimensions and impact widths for individual tracks measured at White Sands Missile Range, NM.

Vehicle	Track/Tire Width [§] (cm)	Track Width ^{§§} (cm)	Sampling Locations	Ridge Width [†] (cm)	Ridge Height [†] (cm)	Impact Width* (cm)
M88-A1 Tank Retriever	61	343	CI,CO	40±4	6±3	189±54
			SS	0	0	84±35
M1151A Up-armored HMMWV	32	214	CI,CO	18±9	3±1	88±29
			SS	0	0	57±9

[§]Single tire or track width, not distance between tires on same axle or distance between tracks.

^{§§}Outside distance between tires on same axle or outside distance between tracks.

Track Width References:

<http://www.amgeneral.com/files/specs-sheet-m1165-domestic-09-15.pdf> [Accessed 30 March 2016]

<http://fas.org/man/dod-101/sys/land/m88a1e1.htm> [Accessed 30 March 2016]

[†] Average values measured among different pass levels at CO location only. All height measurements from original surface (not from within track rut) to ridge peak.

*The values represent the average impact (rut + ridge) width per vehicle track in the curved trafficked sampling regions (CI and CO) and the straight trafficked sampling region (SS).

±denotes the standard deviation of the measured values.

Biomass: The Biomass section consists of both live vegetation (growing crop) and dead vegetation (residue) parameters. The pertinent vegetation properties important in wind erosion assessments are required: a) average vegetation height (m); b) stem area index (SAI) and leaf area index (LAI), both in ($\text{m}^2 \text{m}^{-2}$) units; and c) flat surface cover for the dead vegetation ($\text{m}^2 \text{m}^{-2}$). Some of these measurements may not be available, so the SWEEP interface provides a quick calculation method for SAI from the average stem diameter (mm), stem height (cm) and stem population per unit area ($\# \text{m}^{-2}$). Likewise pictures of different levels of flat residue cover are provided if measured cover values are not known.

For military vehicle trafficking, the pertinent live and dead vegetation properties can be combined and the average values provided for the “dead” vegetation (residue) inputs only, leaving the “crop” fields set to zero. The after trafficking vegetation measurements would be taken within the tracks for both straight and curved traffic regions separately.

Soil Layer Properties: Only the surface (top) soil layer properties are required for estimating wind erosion. They consist of: a) layer thickness (mm); b) sand fraction (Mg Mg^{-1}); c) very fine sand fraction (Mg Mg^{-1}); d) silt fraction (Mg Mg^{-1}); d) clay fraction (Mg Mg^{-1}); e) rock volume fraction ($\text{m}^3 \text{m}^{-3}$); f) dry bulk density (Mg m^{-3}); g) average aggregate density (Mg m^{-3}); h) average dry aggregate stability ($\ln(\text{J kg}^{-1})$); i) geometric mean diameter (GMD) of aggregate sizes (mm); j) geometric standard deviation (GSD) of aggregate sizes (mm mm^{-1}); k) minimum aggregate size (mm); l) maximum aggregate size (mm); and m) surface soil layer wilting point water content (Mg Mg^{-1}). Most of these properties can be obtained by SWEEP automatically from the NRCS soil survey data records (layer thickness, silt fraction, clay fraction, sand fraction, very fine sand fraction, soil wilting point, rock volume fraction). SWEEP provides estimating equations for the following properties (average aggregate density, average dry

aggregate stability, GMD, GSD, minimum and maximum aggregate size diameters). Estimation of bulk density values based upon texture are described in (Rawls, 1983) and (Saxton, et al., 1986). Soil bulk density and the aggregate size distribution represented by the GMD and GSD properties are the primary surface layer properties that change with military trafficking which are reported in this document and required for wind erosion estimates.

For military vehicle trafficking, it is expected that the NRCS SSURGO soil data would be utilized, if available. There is an option under the “File” menu labeled “Load SSURGO File”. The user would normally first select the State, then the County that the site resided in. The user would then select the appropriate SSURGO soil map unit that defines the general soil texture and pick the desired soil component from the list that makes up the soil map unit number. Normally, the soil component selected will be the one representing the greatest area percent. However if a significant portion of the simulation area contains a more erodible soil (e.g., greater sand vs. the other soil), or has sparser vegetation, one would consider using this soil in place of the soil with the greatest areal extent. The SSURGO data will populate all the soil layer properties and estimate the temporal properties using the methods described above. For trafficked effects to be properly reflected in the SWEEP results, the GMD and GSD values should be computed using the equations provided in **Table 33** and bulk density values from **Table 45** and **Table 50** entered into the SWEEP Soil Layers tab.

Surface Properties: The soil surface properties required are: a) crust properties; b) random roughness in (mm); c) the oriented roughness properties, if it exists, e.g. ridge height (mm), ridge spacing (mm) and ridge width (mm); and d) hourly surface soil water contents (Mg Mg^{-1}), if not dry.

For military vehicle trafficking, it is expected that no crust will be present following trafficking, therefore no crust properties will be input except when simulating the un-trafficked areas (i.e., for comparisons). The Allmaras random roughness (Allmaras, et al., 1966) values for various vehicle types and number of passes can be obtained from **Table 36**, **Table 39** and **Table 41**. The ridge height, spacing and width values for curved trafficked regions can be obtained from **Table 72**. Normally all hourly surface soil water content values would be set to zero to match typical conditions.

Weather: The required weather properties are: a) wind direction for the day (degrees from north); b) air density (can be estimated from site elevation (m) and average daily temperature (deg. C) from within SWEEP); c) anemometer height (m) of recorded wind data, aerodynamic roughness at anemometer site (mm); d) subdaily (usually hourly) wind speeds (m s^{-1}) and daily wind direction.

For military vehicle trafficking, the user may provide the subdaily (hourly) wind speeds and daily direction information relevant to the desired SWEEP simulation along with the corresponding anemometer related wind station meta data (anemometer height, aerodynamic roughness, etc.). One can alternatively use the SWEEP capabilities for determining probabilities of an erosion event occurring given the simulated site surface parameters (see discussion below).

This completes the data input requirements for a standard SWEEP simulation run which will estimate total soil loss for the day (24 hour period), under the specified conditions, by particle size (creep+saltation, suspension and PM10 components) from the simulation site (trafficked

region). Additional, more detailed output and 3-dimensional plots of the output are available (Figure 35). See the SWEEP User Manual for complete details for running SWEEP.

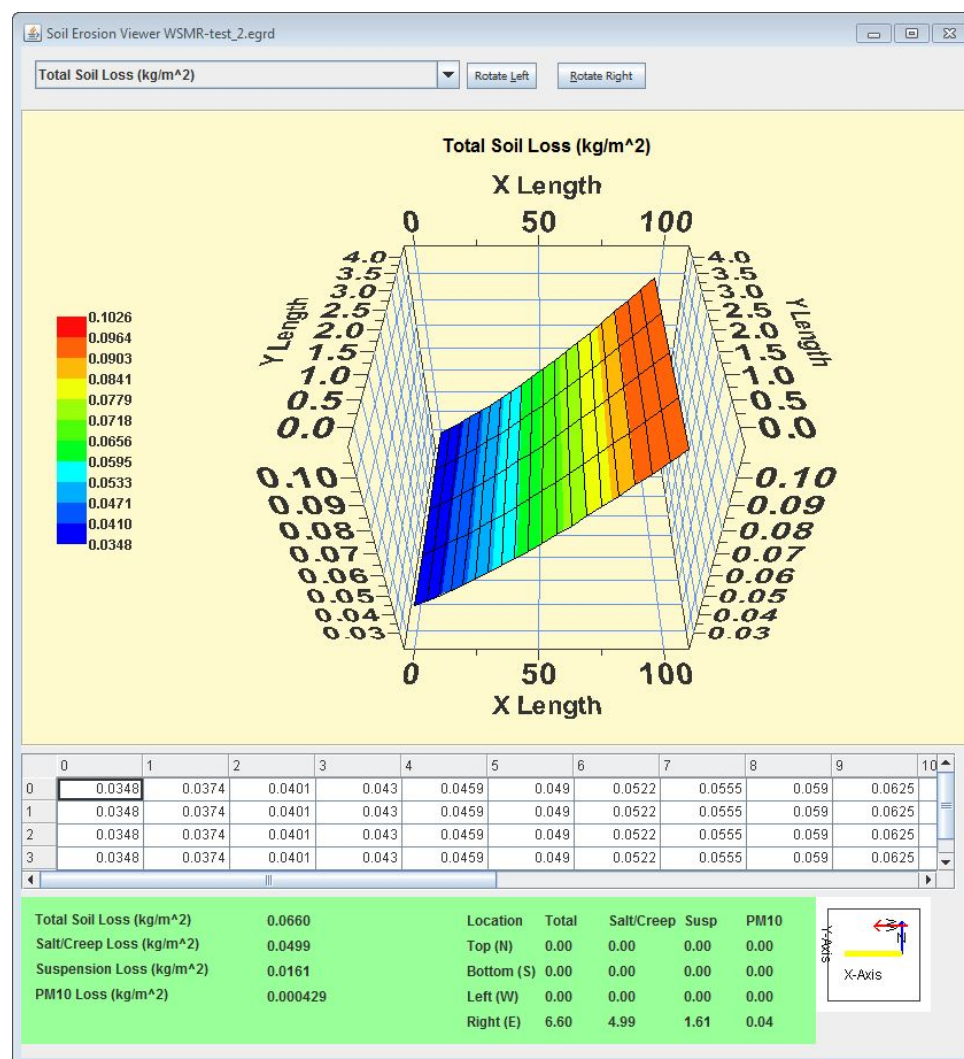


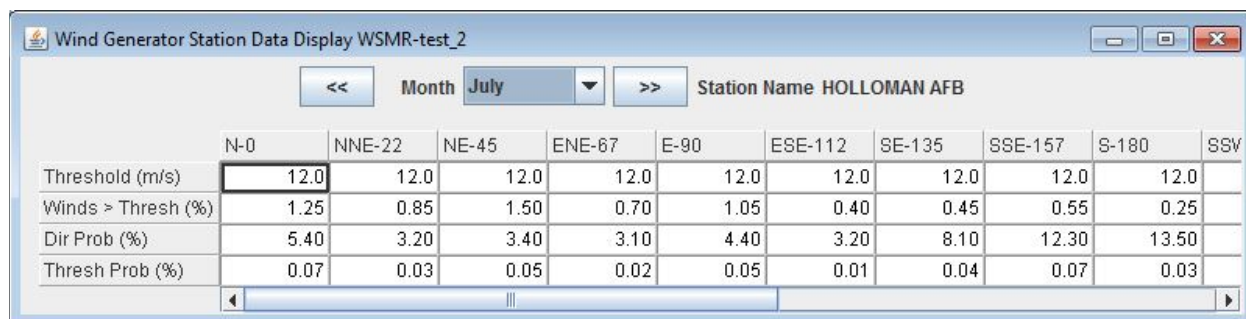
Figure 35. Single-event Wind Erosion Evaluation Program (SWEEP) Run example results.

If the user is interested in determining the risk or probability of wind erosion occurring under the specified conditions, SWEEP can be run in an alternate “Threshold Run” mode available under the “Run” menu. When this option is selected, the user is not required to complete the “Weather” related inputs and is presented with a secondary input screen where the user selects the representative Windgen wind station. The Windgen records provide the statistical information by month for the wind speed distribution frequency for each of the 16 cardinal directions (van Donk, et al., 2005).

SWEEP can be used to determine the probability of an erosion event under the specified surface conditions by determining the threshold wind velocity at which erosion will be initiated for each of the 16 cardinal directions. These results are then compared with the historical monthly

statistical distribution of wind speeds by direction for the location, which is obtained from the selected Windgen station. This will determine the probability or likelihood that wind erosion will occur on the site and at what wind speed for each of the 16 cardinal directions under the specified surface conditions for any month of the year.

When SWEEP is run in “Threshold” mode, it will generate a monthly table that displays all 16 cardinal directions and “total” (all directions) in seventeen columns and four rows (**Figure 36**) where: “Threshold (m s^{-1})” is the wind speed at which erosion will occur (m s^{-1}); “Winds > Thresh (%)” is the probability of winds exceeding that threshold when it comes from the direction specified (%); “Dir Prob (%)” is the probability the wind will come from the specified direction (%); and “Thresh Prob (%)” is the probability that the wind will exceed the threshold for the direction specified (%). The desired month’s data can be selected for display via the “Month” dropdown list at the top of the window. Again, see the SWEEP User Manual for complete details for running SWEEP in the “Threshold” mode for wind erosion risk analysis.



	N-0	NNE-22	NE-45	ENE-67	E-90	ESE-112	SE-135	SSE-157	S-180	SSW
Threshold (m/s)	12.0	12.0	12.0	12.0	12.0	12.0	12.0	12.0	12.0	12.0
Winds > Thresh (%)	1.25	0.85	1.50	0.70	1.05	0.40	0.45	0.55	0.25	
Dir Prob (%)	5.40	3.20	3.40	3.10	4.40	3.20	8.10	12.30	13.50	
Thresh Prob (%)	0.07	0.03	0.05	0.02	0.05	0.01	0.04	0.07	0.03	

Figure 36. Single-event Wind Erosion Evaluation Program (SWEEP) Threshold Run example results screen.

Recovery from Trafficking

Additional vegetation and soil sampling were also conducted on each site (excluding Ft. Benning, due to that site being co-opted by the Army immediately after our initial trafficking experiments for other purposes which did not lend it to subsequent re-sampling). The additional sampling was planned and executed to evaluate the initial multi-pass trafficking recovery response the following year (one over-winter weathering cycle) and its impact on the sites’ susceptibility to wind erosion. Since only a single subsequent set of measurements were taken, we cannot make definitive statements on the degree multi-pass trafficking had on soil surface conditions and vegetation species over time since growing periods vary by time of year (cool season vs. warm season grasses, etc.). However, there are some observations and conclusions that can be made from the second vegetation sampling process.

The additional vegetation sampling after trafficking highlights the native resiliency of the original site vegetation and environment’s ability to “recover” or “compensate” for the initial multi-trafficking effects on the soil, surface and vegetative cover, especially if adequate precipitation is available following the multi-trafficking exercises. The protection afforded by the vegetation, in most cases for these experimental sites, was much better than originally anticipated. Ft. Riley and Ft. Benning were expected to respond favorably, from strictly a wind

erosion risk viewpoint, due to adequate precipitation levels (838 and 1234 mm average annual precipitation respectively, **Table 73** and **Table 74**), and in the case of Ft. Riley, the existence of prairie grasses enhancing the multi-trafficking “recovery response”. However, the response was not expected to be as rapid or as pronounced for the arid Yakima and WSMR locations due to their lack of yearly precipitation (210 and 241 mm average annual precipitation respectively, **Table 75** and **Table 76**). Note that WSMR experiences monsoonal rains in the late summer-early fall which was immediately prior to re-sampling at this site. These rains, in conjunction with a disturbed soil surface likely contributed to good seed germination conditions at this site.

The re-sampled vegetation cover differences between the multi-trafficked and un-trafficked regions presented here are just a single snapshot in time, but they still reflected the resiliency provided by each respective site’s vegetation and environment. In some cases, the visual differences that occurred between the two sampling periods in the multi-trafficked regions were profound and the re-sampled measured vegetation cover differences between the un-trafficked and trafficked regions were surprisingly quite similar, especially for the arid WSMR site.

As expected, the visual changes to the landscape were quite different at Ft. Riley due to the amount of precipitation received annually (838 mm) and the dominant grassland vegetation. The changes were accelerated due to above average precipitation (+169%) being received between the two sampling periods (**Table 73**).

Table 73. Fort Riley monthly precipitation and freeze/thaw cycles between sampling dates in October and November, 2010 and August of 2011 (~310 days).

Month	Historical Monthly Precip[†] (mm)	2010-2011 Monthly Precip^{††} (mm)	2010-2011 Monthly Freeze/Thaw Cycles
Oct	68.3	81.3	0
Nov	37.3	164.8	21
Dec	25.7	21.1	28
Jan	16.3	12.7	18
Feb	29.0	12.4	18
Mar	60.5	61.2	22
Apr	74.4	289.6	2
May	121.2	190.0	0
Jun	123.2	152.9	0
Jul	103.6	93.5	0
Aug	99.8	201.7	0
Total	759.3	1281.2	109

[†]<http://www.intellicast.com/Local/History.aspx?location=USKS0197>
[Accessed 1 September 2016]

^{††}<https://gis.ncdc.noaa.gov/maps/ncei/cdo/hourly> (Marshall Army Airfield
station ID:72455013947) [Accessed 1 September 2016]

The vegetation cover of the prairie grasses and initial above average precipitation at Ft. Riley are evident in the two Google Earth images shown in **Figure 37** taken about 2 years (upper photo) and 4 years (lower photo) after conducting the trafficking experiments. The figure-8 plots are still visible, especially if one zooms in closer in the 2012 image, but are much more difficult to discern in the 2014 image, even when zoomed in with Google Earth.



Figure 37. Google Earth images of the Ft. Riley trafficking sites taken on Sep. 21, 2012 (upper photo) and on Aug. 11, 2014 (lower photo).

Ft. Riley also experiences cyclic freezing temperatures throughout the winter, as shown in **Table 73**, which causes freeze/thaw and freeze/dry cycles to occur, typically resulting in the unconsolidation of soil. However, the combination of melting snow precipitation (left photo in **Figure 38**) and wet/drying cycles both have an ameliorating effects on the surface of the trafficked plots, causing a re-consolidation (crusting) of the original loose erodible material on the trafficked surfaces. A figure-8 plot (right photo in **Figure 38**) shows a puddled and crusted previously trafficked surface the following spring of 2012 at Ft. Riley, KS. Thus, the wind

erodibility of the initial bare trafficked surfaces was significantly reduced, in this situation, even before new vegetation appeared later in the spring.



Figure 38. Snow covered figure-8 plot at Ft. Riley in early 2011(left photo) and later in April 2011 (right photo).

As mentioned previously, there were no photos from Ft. Benning because the Army co-opted our experimental site literally days after we completed our trafficking experiments and began construction at the site (**Figure 39**). Note that the figure-8 patterns that were not destroyed by the construction activity are still clearly visible in this Google Earth image taken about 6 months after the trafficking experiment was conducted. A later Google Earth image (**Figure 40**) taken about 2 ½ years later still shows some remnants of the figure-8 patterns, but they are mostly covered with vegetation now. The vegetation cover increase would be expected due to the relatively high precipitation received at Ft. Benning (**Table 74**), even though the soil was very sandy (**Table 7**).



Figure 39. Google Earth image of the Ft. Benning, GA experimental site that was taken on Dec. 18, 2012, about 6 months after the trafficking experiments were conducted.



Figure 40. Google Earth image of the Ft. Benning, GA experimental site that was taken on Dec. 10, 2014, about 2 ½ years after the trafficking experiments were conducted.

Table 74. Fort Benning, GA monthly precipitation and freeze/thaw cycles after the sampling date in July 2012 through June of 2013 (365 days).

Month	Historical Monthly Precip[†] (mm)	2012-2013 Monthly Precip^{††} (mm)	2012-2013 Monthly Freeze/Thaw Cycles
Jul	128.0	261.6	0
Aug	96.0	142.5	0
Sep	78.0	72.4	0
Oct	59.2	40.9	0
Nov	100.8	34.5	16
Dec	111.8	214.6	15
Jan	121.4	103.4	5
Feb	113.8	414.8	8
Mar	146.1	127.0	7
Apr	97.5	159.5	0
May	91.9	78.2	0
Jun	89.2	168.4	0
Total	1233.7	1817.9	51

[†] <http://www.intellicast.com/Local/History.aspx?location=USGA0220>
[Accessed 1 September 2016]

^{††} <https://gis.ncdc.noaa.gov/maps/ncei/cdo/hourly> (Lawson Army Airfield
station ID:72225013829) [Accessed 1 September 2016]

We can see limited canopy cover in the trafficked regions from a Google Earth image of the Yakima, WA site, taken near the time the re-sampling occurred (see left photo in **Figure 41**), even though the precipitation (**Table 75**) received between the two sampling periods was above average (+138%). The right photo in **Figure 41** shows the continued recovery of the canopy growth though, nearly 3 years later following the multi-trafficking experiments. Like Ft. Riley, Yakima receives many freeze/thaw cycles over the winter, which tends to loosen the soil near the surface and reducing the compaction effects due to the multiple trafficking passes. However, the limited precipitation received during this period likely did not re-consolidate the sandy loam soil surface like it did at Ft. Riley (right photo in **Figure 38**) on its higher clay content soils (**Table 7**). Unfortunately, no re-sampling photos or plot surface samples were obtained at Yakima to verify this.



Figure 41. Google Earth images of the Yakima Training Center, WA experimental site taken on July 9, 2013 (left photo) and May 6, 2015 (right photo), about one year and nearly 3 years respectively, after the trafficking experiments were conducted.

Table 75. Yakima Training Center, WA monthly precipitation and freeze/thaw cycles between sampling dates in Aug 2012 and July of 2013 (~360 days).

Month	Historical Monthly Precip[†] (mm)	2012-2013 Monthly Precip^{††} (mm)	2012-2013 Monthly Freeze/Thaw Cycles
Aug	9.1	0.0	0
Sep	9.9	1.5	0
Oct	13.5	37.6	9
Nov	26.7	23.6	15
Dec	35.1	101.9	30
Jan	29.7	4.8	14
Feb	20.3	1.0	34
Mar	17.8	25.4	16
Apr	13.5	11.4	14
May	13.0	72.1	1
Jun	15.7	10.2	0
Jul	5.6	0.0	0
Total	209.8	289.6	133

[†] <http://www.intellicast.com/Local/History.aspx?location=USWA0502>
[Accessed 1 September 2016]

^{††} <https://gis.ncdc.noaa.gov/maps/ncei/cdo/hourly> (Yakima Air
Terminal/Mcalsr Field AP station ID:72781024243) [Accessed 1
September 2016]

We were not expecting significant differences on the White Sands Missile Range sites' multi-trafficked regions, due to the limited vegetation cover, even in the un-trafficked areas, combined with a limited annual average rainfall (241 mm) for the region. However, the changes noticed at WSMR were quite illuminating. Like the other sites, above average precipitation occurred at WSMR following our multi-trafficking experiments. WSMR experienced 128% of its annual precipitation for the 10 months between the two sampling periods (**Table 76**).

Table 76. WSMR monthly precipitation and freeze/thaw cycles between sampling dates in January and November of 2014 (~310 days).

Month	Historical Monthly Precip[†] (mm)	2014 Monthly Precip^{††} (mm)	2014 Monthly Freeze/Thaw Cycles
Jan	12.7	0.0	16
Feb	10.2	0.0	5
Mar	5.1	11.7	0
Apr	5.1	1.5	0
May	7.6	0.8	0
Jun	17.8	0.0	0
Jul	35.6	31.2	0
Aug	58.4	79.5	0
Sep	35.5	134.4	0
Oct	22.9	10.4	0
Nov	12.7	22.9	8
Total	210.8	269.5	29

[†]<http://www.intellicast.com/Local/History.aspx?location=USNM0351>
[Accessed 1 September 2016]

^{††}WSMR museum weather station at 32.3843N, 106.4788W [Accessed
1 September 2016]

Observing the Google Earth satellite images shown in **Figure 42** taken on May 27, 2016, about 1½ years after the initial sampling, we see that the original figure-8 plots created by the tracked M88-A1 tank retriever are still visible, but those created by the HMMWV vehicle are no longer easily identifiable.

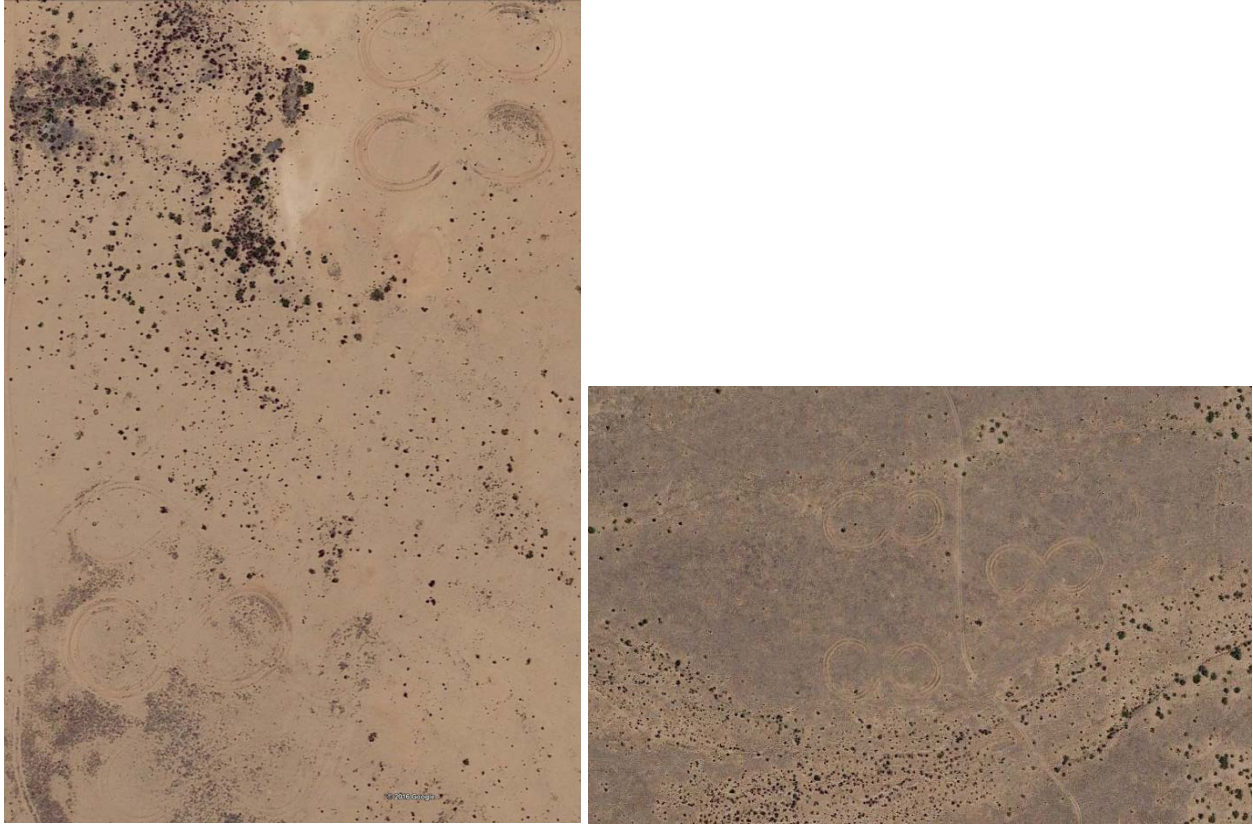


Figure 42. Google Earth images (left photo is sandy loam soil site and right photo is loam soil site) of the two locations at the White Sands Missile Range site taken on May 27, 2016, about 1 ½ years after the multi-trafficking experiments were conducted.

We have ground level photos depicting the changes that occurred at WSMR on re-sampling in November 2014, about 10 months after the trafficking experiments were conducted. See **Figure 43** for visual evidence of the significant vegetation regrowth that occurred. This is attributed to the wetter than normal year that brought above average (128%) precipitation (**Table 76**) during those 10 months, to the WSMR site following the trafficking experiments.



Figure 43. WSMR track vehicle tracks in curved section of figure-8 plot after trafficking in Jan. 2014 (upper photo) and ~10 months later (lower photo).

Note the significant animal activity that also occurred at the WSMR site with the rodent burrows and small animal trafficking lanes shown in **Figure 44** (upper photo). Also, numerous flags were placed to outline the figure-8 plots originally created by an HMMWV wheeled vehicle in (lower photo). It took careful scrutiny by two individuals familiar with the location of the original wheeled vehicle figure-8 plots to identify and flag the trafficked regions. The lower photo in **Figure 45** also illustrates this, where the two flags pictured locate the outside edge of

the trafficked region. The upper photo in **Figure 45** shows the original after trafficked condition of a typical figure-8 plot at WSMR created by an HMMWV wheeled vehicle.

We did not expect the WSMR wheel trafficked figure-8 plots to have changed so dramatically in such a short amount of time that we would actually have great difficulty in determining where the original tracks were located. Obviously, the above normal precipitation received after trafficking probably had a significant influence on the rapid recovery of the wheel trafficked figure-8 surfaces. But, the tremendous small animal activity, as noted in the figure-8 plots shown in **Figure 44** (upper photo) and **Figure 45** (lower photo) also significantly influenced both the tracked and wheeled vehicle figure-8 plots as well.



Figure 44. A figure-8 plot created by the tracked vehicle contains numerous small burrows and animal trails (upper photo) and a flagged HMMWV wheeled vehicle figure-8 location (lower photo), both ~10 months after conducting the multi-trafficking experiments at WSMR.



Figure 45. A HMMWV wheeled vehicle created figure-8 on the loam soil site immediately following the conclusion of the multi-trafficking experiments in Jan. 2014 (upper photo) and another HMMWV wheeled vehicle figure-8 plot ~10 months later that was being flagged (lower photo).

In addition, another surprising observation was the significant increase in vegetation cover in the straight region and cross-over sections of several of the M88-A1 tank retriever track trafficked plots at WSMR. As shown in the upper photo of **Figure 46**, there was no remaining vegetation and the continual grinding of the surface due to the repeated trafficking on the straight sections of the figure-8 plots created a significant amount of loose, erodible material on the surface. However, the straight trafficked regions of the tracked vehicle traffic figure-8 plots on the loam soil at WSMR contained significant vegetation within the straight regions 10 months later. The gramma grass effectively looked as if it had been seeded into the tracks because of the pronounced visual difference between the track trafficked and the adjacent un-trafficked areas (lower photo **Figure 46**). It is assumed that the grinding and stirring action of the vehicle tracks mixed the gramma seed into the soil surface, providing a better seed bed for germination later when the monsoonal rains came.



Figure 46. Straight trafficked section on loam soil of figure-8 plot after tracked vehicle trafficking at WSMR (upper photo) and the resulting heavily vegetated straight away and cross-over sections 10 months later (lower photo).

The conclusion drawn from the visual observations at WSMR is that the trafficking disturbance at these sites created positive as well as negative effects. The physical displacement of the soil in the curved regions caused by the tracked vehicle created micro-topographic changes that, at least in the short-term, changed the vegetation type and amount of biomass produced from the additional locally ponded runoff water that was retained in the track furrows. However, as can be seen in **Figure 47**, **Figure 48** and **Figure 49**, trafficking did not result in more vegetative mass recovery than the control areas and often tracked areas had lower vegetative mass than the control. This may have also stimulated the increased small animal activity. This was evident from the increased burrowing and animal traffic creating the numerous trails as shown in the upper photo in **Figure 44**.

Although generally less vegetative mass, but not always significantly less, was obtained during re-sampling in most measurement sampling locations. Thus, the level of vegetation recovery at all sites improved their resistance to wind erosion during the period since trafficking occurred and is supported by the measured levels of standing vegetation mass at the time of re-sampling. This was observed at all the sites in both curved (CO) and straight trafficked (SS) regions compared to the un-trafficked regions (Control) for the tracked (M1-A1 tank and M88-A1 tank retriever) and wheeled (both HMMWV and Fire Truck) vehicles (see **Table 77**, **Figure 47**, **Table 78**, **Figure 48**, **Table 79** and **Figure 49**).

Table 77. Vegetation mass (mg m^{-2}) least square means (lsmean) for tracked vehicles by sampling location. CO is curve outside, and SS is straight section. Pass = the number of trafficking passes conducted, SE = standard error of the mean, df = degrees of freedom, lower.CL = lower confidence level (95%), and upper .CL = upper confidence level (95%).

Sampling Location*	Pass[†]	lsmean	SE	df	lower.CL	upper.CL	group
CO	0	149.0	21.3	30	105.5	192.6	a
	10	92.5	21.3	30	49.0	136.1	b
SS	0	156.3	21.3	30	112.8	199.9	a
	10	138.7	21.3	30	95.2	182.2	b

*CO is curve outside, and SS is straight section of figure-8 tracked sampling locations.

[†]Pass is the number of trafficking passes conducted previously during the trafficking experiments.

For a given sampling location, least square mean values averaged over all SoilCodes, (WS-L, WS-SL, FR-SiL, FR-SiCL) trafficked with a tracked vehicle for each Pass level with the same group letter (a, b) are not significantly different at 0.05 level by Pass (Tukey's mean separation).

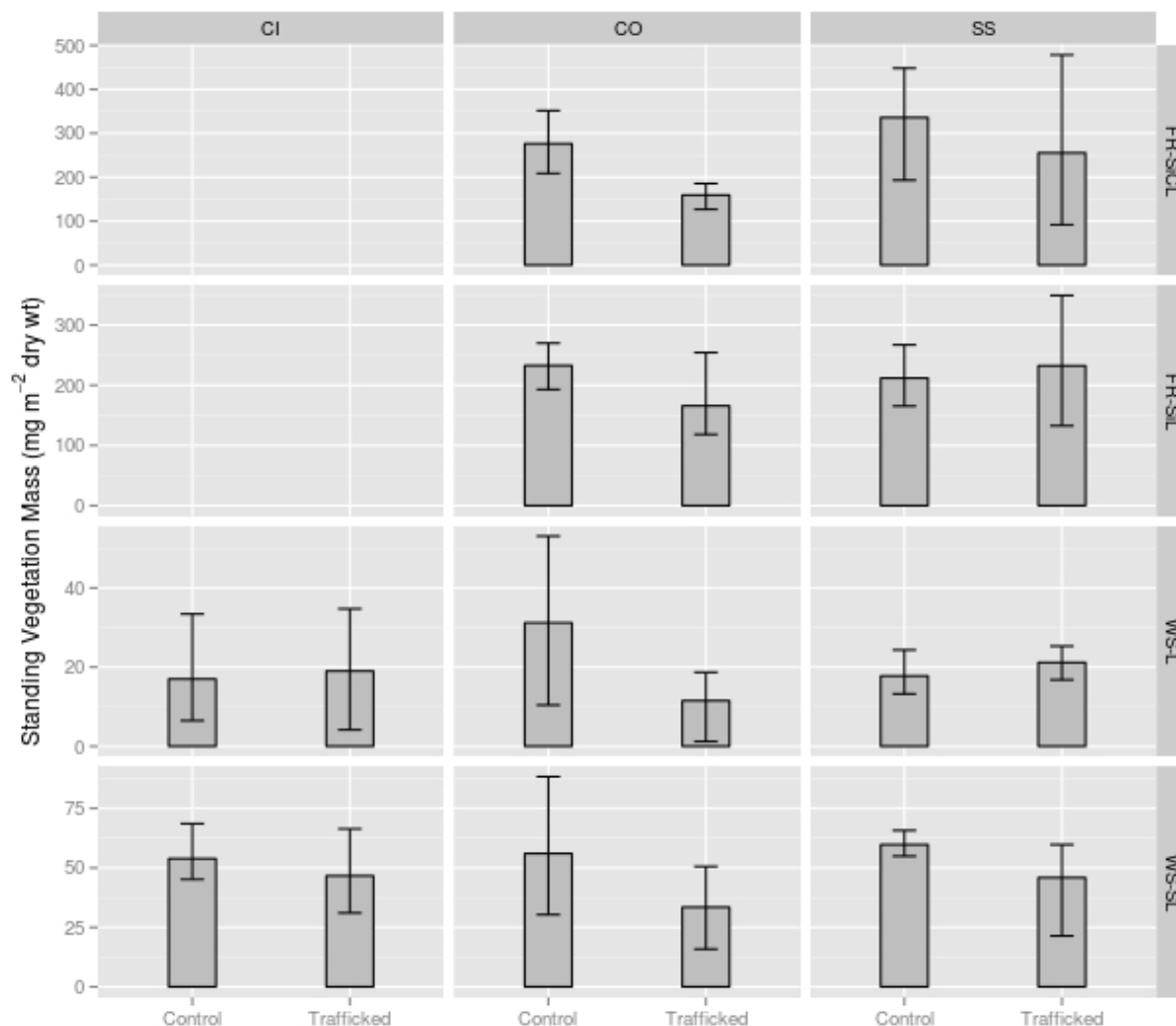


Figure 47. Comparison of vegetation mass levels for tracked vehicle trafficked conditions under curved and straight regions and un-trafficked regions (Control) for all sites. Sampling dates were in Aug. 2011 at Ft. Riley, KS and Nov. 2014 at White Sands Missile Range, NM. CI is curve inside, CO is curve outside, and SS is the straight section sampling location. Sites are FR = Fort Riley and WS = White Sands. Soils are SiCL = silty clay loam, SiL = silt loam, and SL = sandy loam.

Table 78. Vegetation mass (mg m^{-2}) least square means (lsmean) for wheeled (HMMWV) vehicles by sampling location. CO is curve outside, and SS is straight section. Pass = the number of trafficking passes conducted, SE = standard error of the mean, df = degrees of freedom, lower.CL = lower confidence level (95%), and upper .CL = upper confidence level (95%).

Sampling Location*	Pass[†]	lsmean	SE	df	lower.CL	upper.CL	group
CO	0	120.5	12.3	36	95.5	145.5	a
	50	83.2	12.3	36	58.2	108.2	b
SS	0	139.5	12.3	36	114.5	164.5	a
	50	123.2	12.3	36	98.2	148.1	b

*CO is curve outside, and SS is straight section of figure-8 tracked sampling locations.

[†]Pass is the number of trafficking passes conducted previously during the trafficking experiments.

For a given sampling location, least square mean values averaged over all SoilCodes, (WS-L, YK-SL, WS-SL, FR-SiL, FR-SiCL) trafficked with a wheeled (HMMWV) vehicle for each Pass level with the same group letter (a, b) are not significantly different at 0.05 level by Pass (Tukey's mean separation).

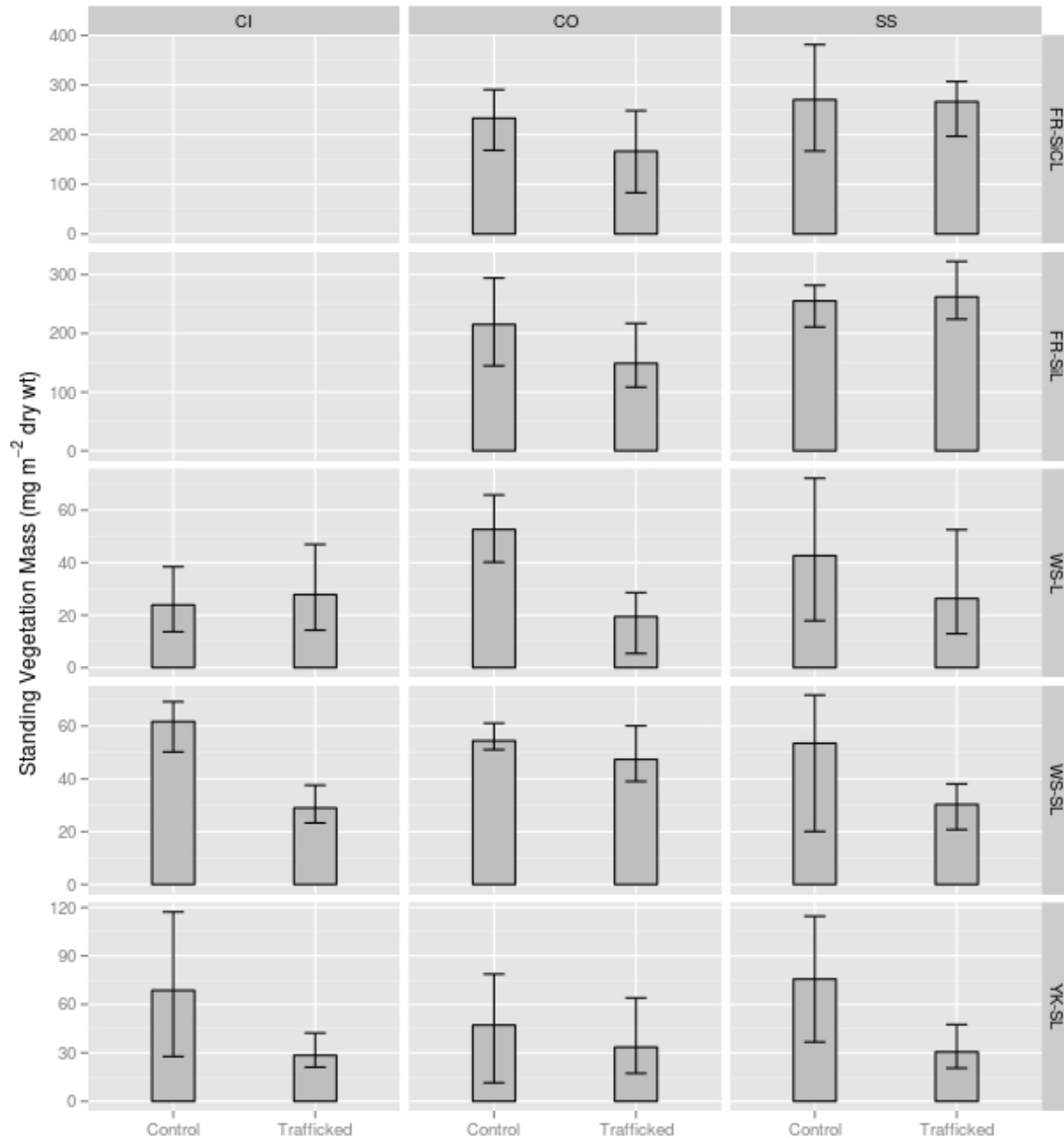


Figure 48. Comparison of vegetation mass levels for wheeled (HMMWV) vehicle trafficked conditions under curved and straight regions and un-trafficked regions (Control) for all sites. Sampling dates were in Aug. 2011 at Ft. Riley KS in Jul. 2013 at Yakima Training Center, WA and in Nov. 2014 at White Sands Missile Range, NM. Sites are FB = Fort Benning, GA; FR = Fort Riley, KS; WS = White Sands Missile Range, NM, and YK = Yakima Training Center, WA. CC is center cross, CI is curve inside, CO is curve outside, and SS is the straight section sampling location. Sites are FB = Fort Benning, FR = Fort Riley, WS = White Sands, and YK = Yakima. Soils are SiCL = silty clay loam, SiL = silt loam, SL = sandy loam, and L = loam.

Table 79. Vegetation mass (mg m^{-2}) least square means (lsmean) for a wheeled (Fire Truck) vehicle by sampling location. CO is curve outside, and SS is straight section. Pass = the number of trafficking passes conducted, SE = standard error of the mean, df = degrees of freedom, lower.CL = lower confidence level (95%), and upper .CL = upper confidence level (95%).

Sampling Location*	Pass [†]	lsmean	SE	df	lower.CL	upper.CL	group
CI	0	48.5	28.3	12	-13.0	110.2	a
	20	25.4	28.3	12	-36.2	87.0	a
CO	0	49.8	28.3	12	-11.8	111.4	a
	20	40.7	28.3	12	-20.9	102.3	a
SS	0	135.3**	28.3	12	73.7	197.0	a
	20	35.7	28.3	12	-26.0	97.3	b

*CO is curve outside, and SS is straight section of figure-8 tracked sampling locations.

[†]Pass is the number of trafficking passes conducted previously during the trafficking experiments.

**One of the three replication values was an order of magnitude higher than the other values as well as any of the other p0 measurements. Thus, the likely reason for the inconsistent results for the SS data. However, we could not determine definitively if an error was made in the measurement or the transferring of the value to the original data sheet, so the data was merely retained and noted here.

For a given sampling location, least square mean values for the SoilCode, YK-SL) trafficked with a wheeled (Fire Truck) vehicle for each Pass level with the same group letter (a, b) are not significantly different at 0.05 level by Pass (Tukey's mean separation).

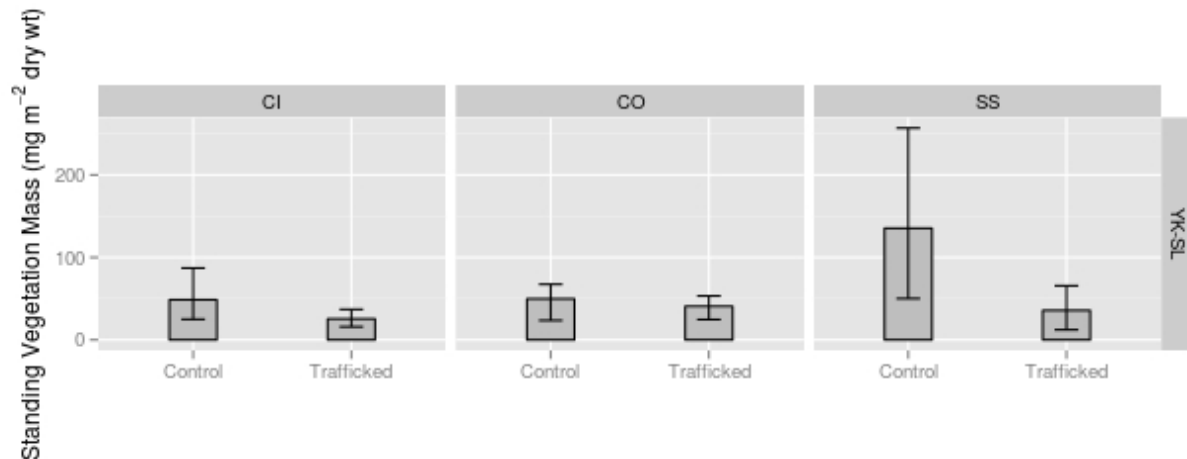


Figure 49. Comparison of vegetation mass levels for wheeled (Fire Truck) vehicle trafficked conditions under curved (CI,CO) and straight (SS) regions and un-trafficked regions (Control) for all sites. Sampling date was in Jul. 2013 at Yakima Training Center, WA. YK = Yakima Training Center, WA and SL = sandy loam.

Summary

Wind erosion is a result of the physical interaction of the erodibility of the surface with the erosivity of the wind. In total, wind erosion is a combination of many physically based processes and this study was designed to account for those processes. As such, the results of this study are applicable to any location where vehicle trafficking would leave the surface in an erodible state (vegetation removed and poor surface aggregation) under winds of sufficient energy to initiate particle movement and dust emissions. Installation sites (e.g., soils and vegetation) and activities (e.g., wheeled vs. tracked vehicles) that result in greater disturbance of the surface will have higher dust emissions than those with less fragile soils and vegetation. Likewise, locations (e.g. Western U.S or large open areas) and seasons (e.g., February through May in most of the U.S.) that have inherently stronger winds will also have higher erosion potential compared to areas with inherently calmer winds even if the soil is disturbed. Also note that the larger the exposed area, the more likely strong winds can initiate the erosion process.

The sites studied represented a range in soil textures typically found in the wind erosion prone areas of the U.S. (see Fig. 10). Soil intrinsic properties measured included texture, ranging in clay (2.8 to 28.0%), silt (9.5 to 70.8%), sand (7.9 to 87.7%) as well as organic matter (0.8 to 4.1%), and calcium carbonate (1.7 to 7.6%). These soil properties are quite common throughout the arid and semi-arid western U.S. where wind erosion is more frequent due to the combination of the increased erodibility of these soils as well as the higher frequency of erosive winds. However, it should be noted that wind erosion can occur anywhere that soils are poorly aggregated or single grained (e.g., Ft. Benning), are lacking in vegetation potential (e.g., White Sands Missile Range and Yakima Training Center), or occur in areas with a high frequency of erosive winds (e.g., Ft. Riley).

The soils at Ft. Riley had the lowest components of sand (7.9 and 10.1%) and greatest organic matter (4.0 and 4.1%) of the sites studied, which typically result in improved aggregation and less erosion. However, if vehicle trafficking is performed on any soils when the soil is relatively dry, aggregation is quickly destroyed and coupled with vegetation removal, they are subject to significant dust emissions by wind.

Ft. Benning had the sandiest soils (87.7%) and near the lowest organic matter content (0.9%) of the sites studied. Such soils with little clay to bind particles into aggregates tend to have very poor aggregation and high erodibility after trafficking, regardless of moisture content level. Although not known as a wind erosion prone area because of the lower probability of erosive winds, the Ft. Benning site, if a large area is left bare and with little inherent structure, can experience dust emissions if winds are great enough.

The Yakima Training Center had relatively high sand (51.3%) and silt (43.7%) contents. Trafficking on these sites was performed under dry soil conditions, leaving a poorly aggregated surface within the wheel tracks. If trafficking would be performed during wetter conditions, the surface erodibility would be expected to decrease as a result of better aggregation with additional moisture in the soil and at the surface.

Experiments at White Sands Missile Range were also conducted under dry conditions. The sandy loam soil at this location also had a high sand content (73%) resulting in very poor aggregation

after trafficking. Likewise the loam soil at this site with 22% clay and 38% sand, exhibited similarly reduced aggregation after trafficking due to the dry conditions.

Wind erosion is controlled by three main factors: 1) surface conditions (e.g., aggregation and roughness), 2) vegetation (e.g., flat cover and standing material), and 3) winds sufficient to initiate particle movement. Typical military training lands are by nature, too vast for the wind to be practically reduced using such methods as wind fencing or established tree windbreaks. Therefore the inherent erosivity of the winds at a given site cannot normally be mitigated, essentially leaving the process to be the result of soil and vegetation conditions. That leaves only factors 1) and 2) typically being modifiable via land management practices. Of these two factors, vegetation management is almost always preferable over bare soil (surface aggregation, random and oriented roughness, surface moisture, etc.) management to control or mitigate wind erosion.

From this study, it is obvious that trafficking is destructive to vegetation and generally increases with the number of vehicle passes. In addition, compared to wheeled vehicles, tracked vehicle turning is much more destructive of vegetation than straight trafficking, removing on average across all soils between 44 to 52% within the first pass alone. The degree of vegetation destruction is also dependent upon the density (amount of above ground biomass) and to a lesser extent the root density near the surface (not measured in this study) and the amount of aggregation (cohesiveness) of the soil at the time of trafficking. However, these vegetation/soil traits are insufficient when pitted against the shearing forces imposed during turning maneuvers with these military vehicles.

Thus, limiting unnecessary turning during military training scenarios will always be desirable under all climate, site, vegetation, and soil surface conditions. Likewise, eliminating unnecessary repeated trafficking on the same locations within a site is also desirable as it will reduce the loss of vegetation and the degree of dis-aggregation (pulverization) of the soil surface, regardless of a site's original condition and pre-existing susceptibility to wind erosion.

To the extent possible, activities that can expose less of the soil to the surface, e.g. loss of vegetation cover and pulverization of a bare surface, will reduce wind erosion potential. For example, directing general traffic into a single file during transport from one location to another, while minimizing the number and degree of turns, will reduce the amount of disturbed area to erosive winds. In addition, if as much travel as possible is done perpendicular to prevailing winds or on more stable roads (e.g., paved or caliche or otherwise treated roads) when available, will also disturb and expose less of the total land surface to degraded soil and vegetation conditions and help mitigate the risk to the site as a whole to wind erosion.

Soil properties were generally degraded with increased vehicle traffic. Although some roughness was created on the curved trafficked portions, only on the higher clay soils were ridges comprised of large and relatively stable (non-erodible size) aggregates. Such ridges, although occupying higher landscape positions, are exposed to stronger surface winds, but when composed of stable aggregates afford some wind erosion control. Ridges on the sandy soils however, are single grained, e.g. non-aggregated, and therefore create an increased wind erosion potential.

Vehicle trafficking generally degraded not only the soil aggregation but also disturbed protective crusts and desert pavement (an erosion resistant thin layer of rocks and stable clods often present

in arid areas) in the regions devoid of vegetation. In the sites studied, areas that were dry in the soil layers affected (i.e., all but Ft. Riley), the soil aggregation was reduced to a highly erodible state because of a lack of moisture and clay to bind the soils together into erosion resistant aggregates.

However, in areas or seasons of higher precipitation coupled with warmer temperatures, the rate of vegetative recovery is faster. Therefore training land managers that schedule activities prior to such seasons and delaying activities during such recovery periods will allow for improved vegetation recovery and better erosion control.

Random roughness increases the threshold friction velocity for a given wind speed, meaning that rougher surfaces lower the erosive winds at the surface. When vegetation is limited or non-existent, soil random roughness is one of the few options left that can limit wind erosion emissions, but only if sufficient non-erodible size (>0.84 mm) aggregates compose that roughness. However, both the low random roughness and the high percentage of erodible size (<0.84 mm) aggregates present created by trafficking means that these trafficked site conditions become highly susceptible to wind erosion.

Thus, land managers with limited or non-existent vegetative cover following trafficking events should consider restoring vegetation cover as quickly as possible. In the interim, they can armor the bare surface to reduce risk to wind erosion until sufficient vegetation cover is again available. Some potential surface armoring options are: a) applying water or a chemical dust suppressant to re-consolidate the soil mobile particles and aggregates (create a surface crust), which may also trigger seed germination where water is used; b) apply artificial roughness in the form of gravel or rock aggregates to the bare surfaces to increase the fraction of non-erodible size materials on the surface and immediately reduce the risk to wind erosion; and c) mechanically apply and insert a vegetative mulch into the soil on the bare trafficked regions to provide temporary protection from wind erosion and also keep the applied residue from being blown away.

Using straw mulch requires anchoring by matting, crimping, or other methods to prevent blowing or the washing away of the mulch and any applied seed. A crimper is a tractor attachment that has serrated disk blades about 10-20 cm apart which forces straw mulch into the soil and leaves much of the straw in a vertical position. Since standing vegetation is much more effective than flat residue in reducing the force of the wind on soils (Hagen, 1996) and because anchoring prevents blowing, crimping is a preferred method of control as opposed to blowing straw into a flat, loose position on the surface (Chepil, et al., 1960).

Also, as demonstrated at the WSMR locations, when sufficient water is available for the re-growth of vegetation, a multi-pass trafficked site can recover quickly and become similarly protected from wind erosion events as it was prior to the trafficking events (**Figure 47**, **Figure 48** and **Figure 49**). The precipitation at White Sands Missile Range following the multi-pass trafficking experiments was above normal (128%) through the re-sampling period (**Table 76**). However, the favorable weather conditions did reveal how quickly the trafficked sites can recover, even in arid regions, if adequate water is available for vegetation regrowth. As mentioned previously, the vegetation recovery was so complete at the WSMR sites, especially on the HMMWV traffic locations, that the outline of the figure-8 plots could barely be discerned on the sites.

Even though this was only one location (WSMR), it does lead to the possibility that if one has access to water, can deliver it to the trafficked sites, and apply sufficient quantities to the surface appropriately, it could very likely jumpstart the vegetation regrowth process in arid and semi-arid regions. This of course will only work if there is also an adequate seed bank and/or viable root mass available in the soil to regrow vegetation. Although, if necessary, seeding operations, e.g. arial broadcasting and/or physical sub-surface planting of seeds, can alleviate issues of inadequate seed bank conditions where they occur. Such seeding operations can also be combined with the application of residue mulches, mentioned previously, to mitigate the site's susceptibility to wind erosion until the new vegetation gets established.

Conclusions

Off-Road Trafficking

Off-road military vehicle trafficking presents some unique conditions with respect to wind driven dust emissions following trafficking. Off-road sites will usually have some vegetation and likely will not be overly compacted. Even though soil bulk density does not directly influence a soil's susceptibility to wind erosion, it can impact vegetation growth if the soil gets compacted, restricting root growth. In addition, highly compacted soils tend to have lower water infiltration rates, causing greater water runoff and less soil water being available for plants. Thus the negative, indirect effect of excessive soil compaction directly influences vegetation growth, which is considered to be one of the best methods for controlling wind erosion. It was found that military vehicle trafficking can affect the density of the soil near the surface, especially if the soil is near the optimum water content, as determined by the Proctor test (ASTM Standard D698, 2012) as shown in **Table 45** and **Table 50**.

Based on the soil density data collected, a bulk density normalization procedure was derived for use in developing surface compaction routines that can be applied for a variety of different military vehicles (tracked vs. wheeled) and their weight (pressure on the soil surface) and has been implemented in WEPS. If a soil is traffic compacted in a climate that has frequent freeze/thaw cycles and contains sufficient moisture at that time, the freeze/thaw cycles can ameliorate the compacted soil (Retta, et al., 2013).

Vegetation cover and standing biomass loss were shown to be susceptible to military vehicle trafficking and generally decreased with multiple passes (**Figures 18-20** and **Figures 24-26**). There was less effect on the vegetation in the straight trafficked regions compared to the curved regions. Tracked vehicles tended to destroy the vegetation much more quickly than the wheeled vehicles, especially in the curves. The quantity of vegetation (mass density per area) generally appeared to mitigate the influence of repeated trafficking passes, where greater amounts of vegetation mass provided more material for cover, thus shielding more of the soil surface from the direct crushing and pulverizing effects from the vehicles passing over. This was especially so in the straight traffic regions. Vegetation cover and mass loss relationships to trafficking pass level under both turning and straight trafficked regions were determined and presented as first order decay functions. These functions can be used to estimate the relative vehicle trafficking damage to the existing vegetation.

In addition to the effects of vehicle traffic on loss of vegetation, the change in soil surface wind erodibility relative to the amount of erodible size particles available on the surface for emission under trafficked conditions were also measured. The size distribution of surface aggregates represented by the GMD and GSD values and the erodible size aggregates were related to the significant vehicle and soil properties.

Sampling was also conducted following at least one over-winter season to examine initial recovery of a multi-trafficked site (i.e., return to a level where susceptibility to wind erosion is back to within the range of the original un-trafficked conditions). The initial recovery response to multi-pass trafficking is likely dependent upon the precipitation amount and timing following vehicle trafficking, which the WSMR site measurements appeared to confirm.

Due to many military training sites being located in very dry regions of the country, the time allowed to let the disturbed regions “recover” sufficiently before additional activity is scheduled could be quite variable and very dependent upon the amount of vegetation recovery. Below normal precipitation would likely extend this time period while above average precipitation could significantly shorten that time.

This study suggests that even though multi-pass trafficking will significantly increase the risk of wind erosion initially, when sufficient precipitation is received, wind erosion risk diminishes as plant cover increases. The key is to manage the trafficking appropriately to obtain the recovery benefits seen in this study and to minimize the exposure risk to increased wind erosion susceptibility until sufficient vegetation regrowth occurs. Possible mitigation practices, such as applying additional water to the trafficked regions during or just prior to germination season to enhance vegetation re-growth, adding mulch or dust suppressants, roughening the surface, or installing wind fencing, should be evaluated to determine the best management practice(s) for each site.

The research for this project has resulted in numerous scientific meeting proceedings, Master’s Theses, and peer-reviewed publications which are listed in Appendix E.

Future Research

Experience with the PI-SWERL during this study revealed several areas that would improve the usefulness of that data obtained under similar field conditions and make it easier to compare directly with traditional wind tunnel studies. Even though a previous study (Sweeney, et al., 2008) made side by side comparisons with a portable wind tunnel on similar surfaces, the PI-SWERL could not determine the surface threshold friction velocity.

It is believed that software changes could be made to keep from exceeding the limited measurable concentration level of emitted particulates by the DustTrak, (i.e., by providing a feedback loop to control the step size and rate of increase in rotor speed based upon the measured concentration in real-time). In addition, using a smaller step size would allow the possibility of determining the threshold friction velocity for emissions. This could theoretically be made more efficient by determining the surface aerodynamic roughness at low rpms, possibly by determining the degree of turbulence with another sensor. If this could be done, the PI-SWERL would be able to estimate surface friction velocity and thus the rpm speed to attain it. Therefore, it could more quickly determine the rpm range of interest and then drop the rpm step size to minimize the rpm range once the initial threshold friction velocity was determined. PI-SWERL control software that was suitably improved would greatly enhance the ability to obtain repeatable emission data from sites too small or inaccessible for portable wind tunnels and negate the need to extract samples for laboratory wind tunnel analysis.

The ability to remotely (e.g., via satellite or drones) determine vegetation growth and cover following multi-trafficked events on military lands could significantly improve the ability of military land managers, such as ITAM coordinators, to monitor such sites frequently. This would allow them to respond if necessary to imminent or existing unfavorable weather conditions with possible emergency control practices. In addition, remote sensing of vegetation would allow land managers to determine when a site could again be exposed to military vehicle trafficking activity in response to the weather conditions existing following the trafficking activity.

The possibility of applying adequate water to off-road tracks should be studied as a possible emergency control option, possibly via water trucks, on military rangelands to consolidate fine particulates on the surface into non-erodible aggregates or crusts to mitigate the risk of wind erosion. In addition, this practice should also be considered prior to or during seed germination as a possible means for land managers to support vegetation recovery on traffic disturbed sites. Some parameters to evaluate in such a study should include: a) availability of water; b) methods to apply water; c) amount and frequency of water application required; d) determination of seed quantity and viability in the soil; e) supplementing the natural seed bank by planting seeds or transplanting additional native plants; and f) natural precipitation patterns. In addition, evaluation of the effect of soil type, soil nutrients, application of mulch, lower the bulk density by tillage, etc. on germination and vegetation growth as well as conditions such as temperature, rainfall, etc. would have on the timing of such watering and the vegetation regrowth is needed.

Although outside the scope of this project, the contacts made with other researchers during this study has identified the possibility of incorporating the WEPS model into DUSTRAN, which could significantly increase DUSTRAN's ability to assess wind erosion risk and estimate emission levels when it occurs. DUSTRAN's spatial capabilities would greatly enhance WEPS ability to accurately represent the effects of small highly erosive regions, such as those created by off-road multi-pass trafficking activities, as well as permanent unpaved roadways, and provide the off-site spatial suspension deposition component not available in WEPS.

Emission factors are often used to describe the kinetic emissions of stationary sources (e.g., unpaved roads) by vehicle traffic. The EPA AP-42: "Compilation of Air Emission Factors" defines an emissions factor as "a representative value that attempts to relate the quantity of a pollutant released to the atmosphere with an activity associated with the release of that pollutant" (U.S. EPA, 2013), usually expressed as the weight of pollutant divided by a unit weight, volume, distance, or duration of the activity emitting the pollutant. When a vehicle travels across the landscape, the wheels or tracks pulverize aggregates and lift particulates into the air by turbulent shear caused by the vehicle motion. Thus emissions factors are appropriate to the trafficking activity itself not subsequent erosion resulting from trafficking effects on the surface. As an emission factor is a "representative value" it is not accurate for a specific set of conditions unless it accounts for variables of each surface condition and vehicle.

Determining dust emission factors were not within the scope of this work. The determination of these factors was included in the first proposed version of this study but was subsequently removed after review and before approval of the final version of the proposal. Since measurement of dust in the air during vehicle trafficking activity was not planned nor completed for this study, emissions factors were not measured or otherwise determined. Objective 1 was designed, in part to measure in the field and with laboratory wind tunnel studies, the change in surface erodibility and therefore subsequent erosion potential as a result of trafficking.

Dust emission factors have been determined for unpaved roads and the U.S. EPA (2006) and others (e.g., Etyemezian et al., 2003) have outlined methods for their determination. However, emission factors have not been derived for vehicle traffic across an undisturbed landscape. To determine dust emission factors for military off-road vehicle traffic, it is recommended that further studies be conducted for these conditions following the U.S. EPA (2006) methodology.

Compact Eye safe Lidar System (CELiS)

Fugitive dust emitted from military training grounds has the potential to impact local and regional air quality, leading to work to identify and quantify potential impacts since the late 1990's. Previous SERDP projects have investigated emission rates of active vehicles under various scenarios (CP-1191, SI-1399, and RC-1729). Two important findings were that 1) most emitted particles were $< 20 \mu\text{m}$ in diameter and dispersed downwind rather than deposited near the point of emission; and 2) soils were more susceptible to wind erosion after vehicular traffic. The current project further investigated wind erosion susceptibility, finding emissions potential increases of 500% or greater for particles $< 20 \mu\text{m}$ after tracked or wheeled military vehicles were driven over various soils, as reported in Meeks et al. (2015).

In addition to emissions quantification, the previous SERDP projects developed and refined air dispersion models to estimate local and regional impacts from fugitive dust emissions. However, the ability to provide measurements of the spatial distribution of emitted plumes and quantify wide area impacts was lacking. The current project met this need by developing a simple, robust, laser-based light detection and ranging (lidar) system. This lidar system, called CELiS (Compact Eye-safe Lidar System), is small, tactical, easy to operate, and has low power requirements relative to other lidar systems of similar capabilities. It can scan 270 degrees in azimuth and 100 degrees in elevation with an operable sensing range between 600 m and 2,000 m away from the lidar system. It can detect variations in background aerosols and particle plumes not visible to the human eye with a laser beam that is eye-safe for humans upon exiting the lidar box. It is relatively small, with a footprint of about 100 ft², and operationally simple relative to other lidar systems, allowing for routine operation by non-scientific personnel. In addition, a relatively simple data analysis algorithm was herein demonstrated; however, data analysis and interpretation requires more technical skill than data collection and additional algorithm development is needed for broad application. CELiS provides robust, tactical fugitive dust plume tracking capabilities over large areas in an easy-to-operate system.

The SON for this work addressed active monitoring technologies for airborne particulates stemming from off-road vehicle traffic; the eye-safe lidar system CELiS was designed to address this need. The fundamental utility of CELiS is to provide site operation managers a tool to assess the impact of training operations that is nearly real-time and has a coverage area of tens of square kilometers with an intuitive data product. The main design goals of CELiS were to create a system ruggedized to the point where a military (or contractor) end user can operate the system in a nearly turn-key manner. Though beyond the scope of this effort, the ultimate goal would be for CELiS to operate virtually unattended and provide alerts to a site manager when airborne particulate matter concentrations exceed a threshold.

Materials and Methods

CELiS Development

The initial work focused on the procurement and fabrication of the CELiS (Compact Eye-safe Lidar System) demonstration unit. The first few months were spent on finalizing the mechanical, optical, and electrical design. Appropriate engineering drawings were completed. Fabrication of the lidar system followed. Specific activities involved procurement and inspection of COTS (commercial off the shelf) parts and also machining of custom parts. Specific attention was paid

to the design of the detector optics. A custom aspheric meniscus lens had to be designed and fabricated in order to ensure adequate performance of the system. The remaining time has been focused on two major tasks: 1) refining the algorithm used to determine particulate matter mass concentrations (PM) from CELiS backscatter measurements and 2) to develop a user manual for CELiS to aid in its adoption as a management tool by end users. The first of these, the calibration algorithm, represents a major advance in the field of lidar.

Description of CELiS

This section describes the concept of operations (CONOPS) for the CELiS lidar operation. In order to quantify the dust emissions from off-road vehicle operations the lidar, meteorology station and the optical particle counter (OPC) are setup downwind from vehicle operations at a range of 0.5 km to 1 km from the fence line. An OPC is setup at a distance from 1 km to 2 km distant from the lidar, within its field of view and at a height of <10 m. Via a radio frequency (RF) link, the OPC transmits particle data back to the data collection system. Raw lidar, meteorological conditions, and particle data are collected for each laser shot and stored for later analysis. **Figure 50** and **Figure 51** indicate different views of a typical planned site layout.

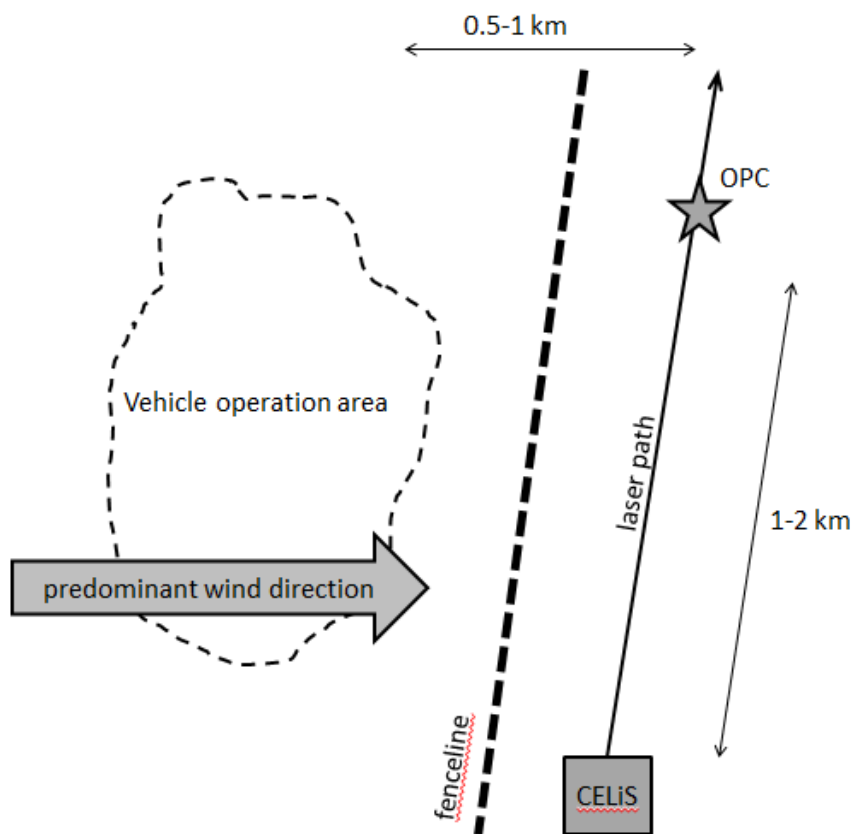


Figure 50. Plan view of CELiS located adjacent to fence line.

CELiS Retrieval Code

The method for using *in situ* point sensors for the calibration of lidar imagery for accurate PM concentrations is an open research question. SDL has successfully used an OPC/gravimetric pair

of sensors and a three-wavelength lidar to generate size-speciated PM_{2.5}/PM₁₀/TSP lidar imagery (Marchant, et al., 2010; Marchant, et al., 2012). This data processing algorithm used by SDL's Aglite system takes raw lidar data from three wavelengths (1064 nm, 532 nm, and 355 nm) and converts it to PM_{2.5}, PM₁₀, and TSP concentrations with units of $\mu\text{g m}^{-3}$; the algorithm is sophisticated enough that the data turnaround time – including QA/QC – is several days. The Aglite method represents the most sophisticated method for providing mass calibrated lidar imagery. On the other end of the spectrum, Hiscox, et al. (2006), have presented an extremely simple method for providing lidar imagery calibrated only for volume concentration.

Neither of these methods is completely appropriate for the CELiS application. The Aglite method is experimentally complex, requiring too many wavelengths and taking too long to generate the final data product. The fundamental assumption of (Hiscox, et al., 2006) is that the magnitude of photon backscatter is linear in PM concentration, making the data analysis computationally much easier as it can be executed in nearly real time, but it suffers from an important drawback. The particular shortcoming of the Hiscox method is that the calibration of the data is only valid for lidar ranges between the lidar itself and the calibration point. For fence line monitoring of some operations, notably stationary emission sources, this is not a severe limitation. However, for the monitoring of moving sources such as off-road vehicle traffic this has some clear drawbacks. For the purposes of CELiS, a hybrid approach that includes the computational simplicity of the Hiscox method without the inherent limitations of the fixed calibration distance was selected.

The flowchart for the CELiS algorithm is shown in **Figure 51** and **Figure 52**; these two charts highlight the different aspects of the algorithm. Conceptually, the algorithm is a non-linear, least squares approach which determines the total pollutant amplitude as a function of range. The total pollutant amplitudes are then combined with specific PM volume concentrations and densities that are measured by OPC to get a final mass concentration. OPC data is used together with scattering theory and Klett inversion to indirectly determine a number density for the PM of interest (Klett, 1981; Klett, 1983; Dias, et al., 2004).

The steps involved in our data processing algorithm requires lidar data to be converted into backscatter coefficients as a function of range using a standard Klett inversion with reverse integration (starting from far ranges and moving to near ranges). The Klett results are further processed by removing the background atmosphere component from the backscattering coefficients. As a result, the post-processed Klett inversion accounts only for the pollutant component in the backscattering coefficients as a function of range. Using OPC data for the pollutant we calculate both the Mie theory backscatter coefficients and the volume concentrations for the PMs of interest. The Mie calculated coefficients are then divided by the volume concentrations. This gives backscatter per volume concentration for PM of interest at the OPC location. The Klett inversion backscatter as a function of range is divided by the backscatter per volume concentration to give volume concentration $\mu\text{g m}^{-3}$ for PM 'x' as a function of range (Eqn 1).

$$\frac{\beta_{Lidar(z)}}{\frac{\beta_{OPC(z_m)}}{N_{PM}}} \rightarrow \frac{\beta_{Lidar(z)}}{\beta_{OPC(z_m)}} N_{PM} \quad (1)$$

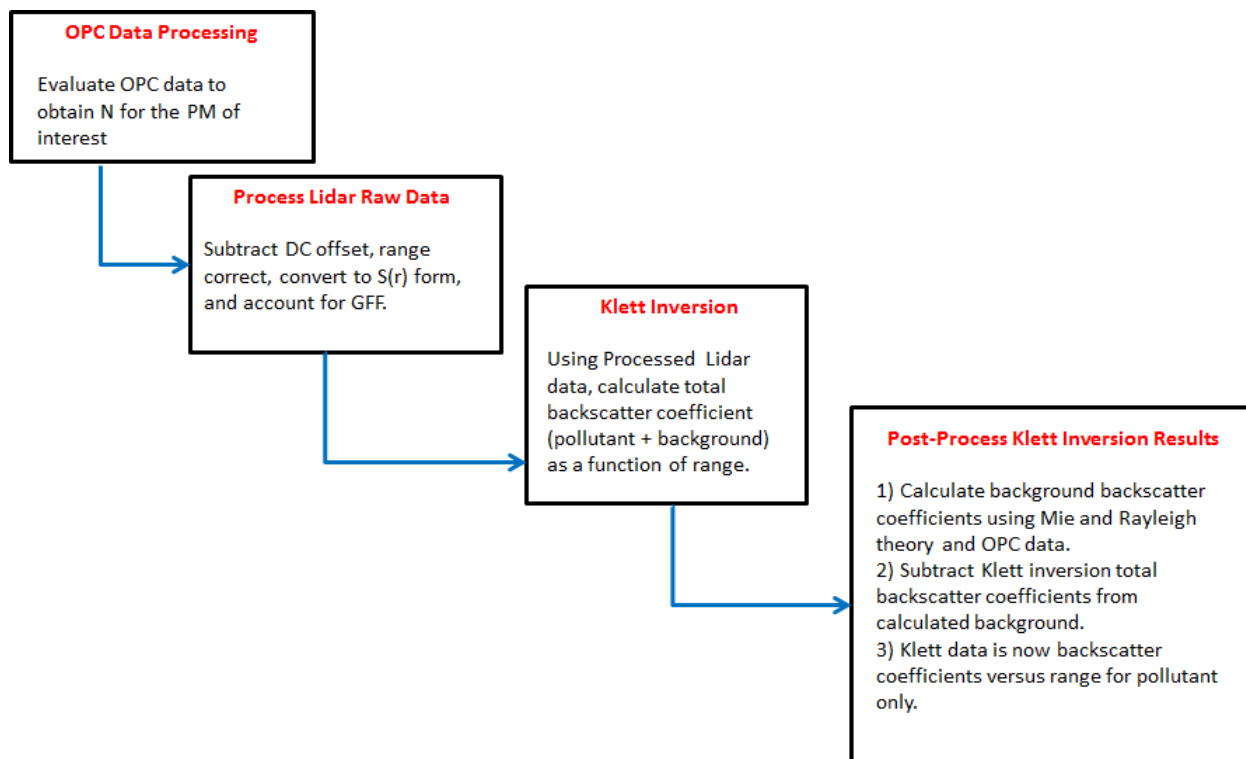


Figure 51. Approach for CELiS Retrieval of PM Concentrations. OPC: optical particle counter. DC: direct current. GFF: geometric form factor.

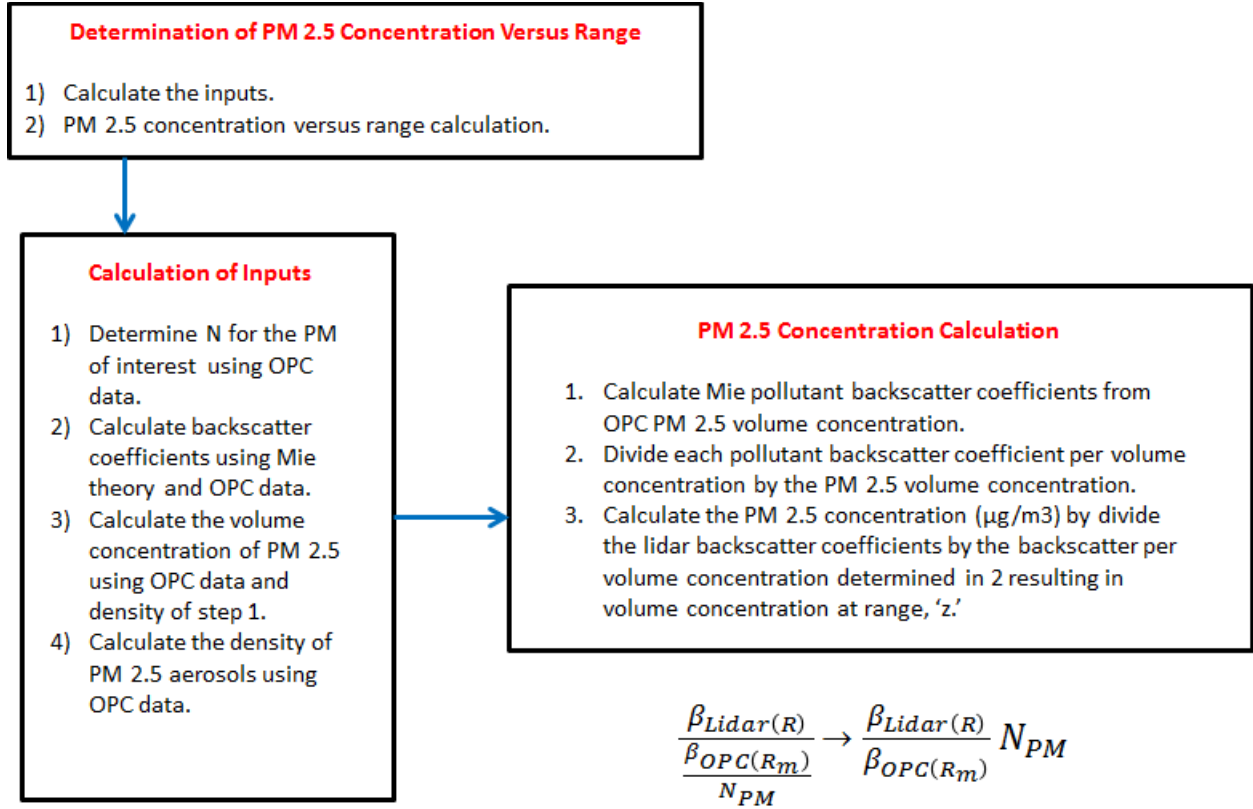


Figure 52. Approach for CELiS Retrieval of PM Concentrations.

CELiS Calibration and Testing

Calibration of CELiS required determining the optimum set of guiding microphysical assumptions that best apply to measuring airborne PM using a single wavelength lidar system. Meteorological and in situ particle measurements were used to estimate the total extinction (σ) and backscatter (β) at a calibration point located within the field of view of CELiS. Furthermore it is best to make the in situ particle measurement at a range beyond the operational range of interest, for example if one wanted to measure a dust cloud at a range 600-900 m distant from the lidar, the particle sampler should be placed at a distance of 1500 m from the lidar. These σ and β values are then used in conjunction with the Klett inversion technique to estimate range resolved σ and β over the entire beam path. A relationship between β , σ and PM mass concentrations at the calibration point is then derived, which then allows the β and σ values at each range bin to be converted to PM using the previously derived “calibration plot” for each β , σ and PM.

Results are presented from a CELiS calibration exercise where CELiS and the new PM measurement algorithm was benchmarked against several other lidar systems at Dugway Proving Ground in the Joint Ambient Breeze Tunnel (JABT).

An elastic backscatter lidar system emits a laser pulse and measures the return signal from molecules and particles in the atmosphere. The lidar equation for a single wavelength is given by Eqn 2:

$$P(R) = P_0 \frac{c\eta A(R)}{2} T_{sys} [\beta_a(R) + \beta_m(R)] \exp \left[-2 \int_0^R (\alpha_a(R') + \alpha_m(R')) dR' \right] \quad (2)$$

where, P_0 is the transmitted laser power, c is the speed of light, η is the time between digitizer measurements, $A(R)$ is the overlap function corrected area, T_{sys} is the system (transmitted and received) efficiency, $\beta_a(R) + \beta_m(R)$ are the aerosol and molecular backscatter coefficient and $\alpha_a(R) + \alpha_m(R)$ are the aerosol and molecular extinction coefficient. The backscatter and extinction coefficient are estimated using Mie and Rayleigh scatter models.

Hiscox, (Hiscox, et al., 2006) demonstrated that β is linearly related to scattering volume. This algorithm develops a process for range resolved PM_k from a single wavelength lidar (CELiS), meteorological measurements and a particulate measurement at a calibration point. This algorithm exploits the linear relationship of scattering volume (PM_k) to backscatter. A procedure has been developed for extracting needed data from PM (E-Sampler) or practical counter (APS) particulate measurements.

The process can be broken down into several steps:

- 1) Collection lidar return signal, apply signal conditioning and range correct the data.
- 2) Generation of particle distributions for atmospheric aerosols chemical constituents at a calibration point using literature values or direct measurements of aerosol properties.
- 3) Generation of backscatter and extinction for molecular and aerosol chemical constituents at a calibration point.
- 4) Perform a linear fit of PM to backscatter at the calibration point.
- 5) Calculate the range resolved backscatter from the lidar signal using the backscatter and extinction at the calibration point in conjunction with a Klett-Fernal-Sasano inversion.
- 6) Calculate range resolved PM using the relationships derived in steps 4) and 5)

Figure 53 shows the process flow diagram.

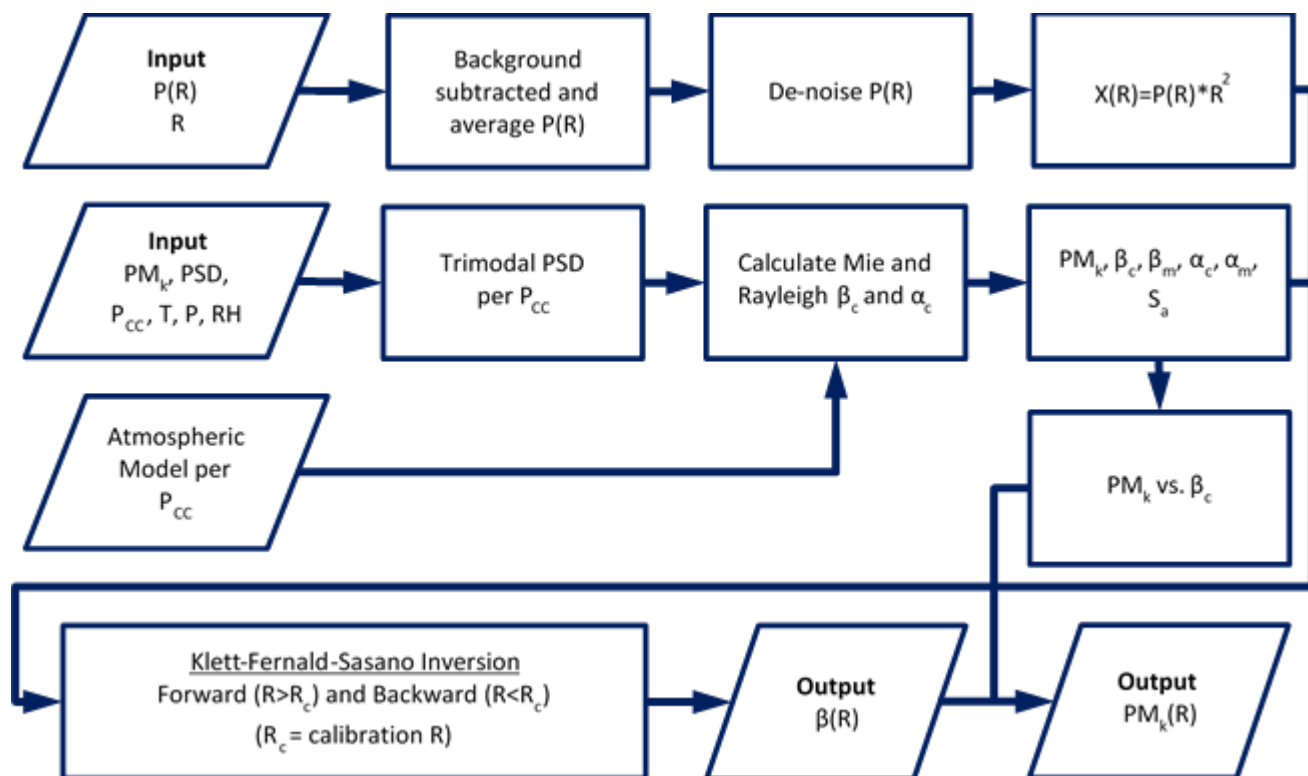


Figure 53. Process flow diagram of CELiS range resolved PM algorithm.

Algorithm validation data was collected at Dugway Proving Ground using the JABT. The setup for this test is shown in **Figure 54** and **Figure 55**. All lidar instrumentation were located approximately 1.2 km from entrance of JABT. The JABT is approximately 170 m long with particulates being release from back at approximately 1.37 km from lidar staging area. Data shown are for CELiS and SAMPLE. SAMPLE is a photon counting lidar owned and operated by Dugway. APS particle counters are located at 1.25 km from the lidar inside chamber.

Testing samples included Arizona Road Dust, diesel smoke, kaolinite, and three bio-weapon simulants such as BG (anthrax simulant). For the purposes of this report we use the Arizona Road Dust results as they are most relevant for the off-road vehicle emissions. A typical sample trial began with 2 minutes of clean background, followed by 10 minutes of aerosol generation, followed by 2 minutes of clean background. Each trial was repeated three times.

For the purposes of this side-by-side comparison experiment, CELiS data was directly compared to another small eye-safe lidar system called SAMPLE. SAMPLE is a fiber laser based micropulse lidar constructed by Exelis (formerly ITT). There is no open source description of SAMPLE. However, private communication with the Dugway staff indicates it operates at 1.47 μm wavelength, 25 kHz repetition rate and 2 μJ /pulse of laser energy. In terms of wavelength, SAMPLE is a very close match to CELiS so we have good reason to believe the scattering physics are the same between each lidar system. In terms of overall emitted laser power, CELiS has a factor of 10x more power per second (500 mW total vs. 50 mW total). However, the sensitivity of a lidar system is also driven by optical collection efficiency and by detector sensitivity. Overall, we expect that SAMPLE will be somewhat more sensitive because photon

counting is a very efficient and high-gain process and also because it was very difficult to align the CELiS detector and said difficulty indicates that it is probably not optimally positioned.

For visualizing lidar data, especially data collected when the lidar beam is not being scanned in angle, it is common to use something called a “waterfall plot”. Waterfall plots are one method to display three-dimensional data on a two-dimensional plot. One can think of a waterfall plot as a “heatmap” of lidar signal intensity (color scale) plotted against a set of range (vertical) vs. time (horizontal) axes. Another way to think about a waterfall plot is a stripchart of stripcharts. Imagine that each laser pulse creates an oscilloscope trace (an oscilloscope trace is itself a stripchart of voltage vs. range) of signal vs. range (vertical axis). As the laser emits more and more pulses during an experiment, each new oscilloscope trace gets stacked next to the previous oscilloscope trace. The end result looks much like a loaf of bread composed of many, many individual slices of bread, where each slice of bread is one laser shot. The color scale is used to indicate voltage (or number of photons, or concentration), the y-axis is the distance range from the laser, and the x-axis represents the timescale of the experiment.

For Dugway JABT trials herein described we shall make use of waterfall plots.



Figure 54. Dugway Proving Ground particulate chambers.

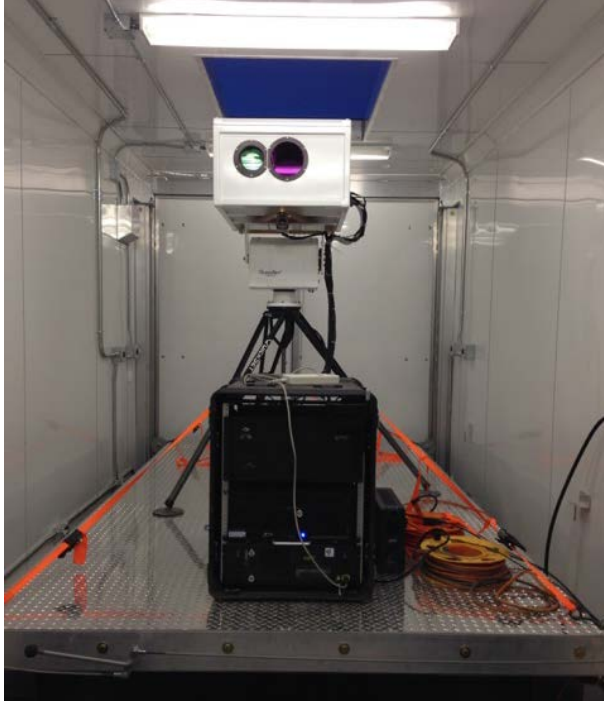


Figure 55. CELiS installed inside a Dugway Proving Ground test trailer and in position for use at the JABT. The left picture is the complete CELiS system placed on a hydraulic lift inside the trailer. The right picture is CELiS hoisted into position.

Step 1. Lidar data pre-processing

Generating range corrected lidar signal from background subtracted lidar signal. Lidar backscatter data is collected at the repetition rate of the laser, in this case it is 20 Hz. For the purposes of this test the native 20 Hz signals were averaged for 1 second, though more or less averaging can be done depending your application. The time-averaged data is then de-noised by removing spikes or artifacts such as hard-target returns. The de-noised data is then range corrected by multiplying each range bin by the square of its range as indicated by the Eqn 3 below.

$$X(R) = (P(R) - P_{Bkg})R^2 \quad (3)$$

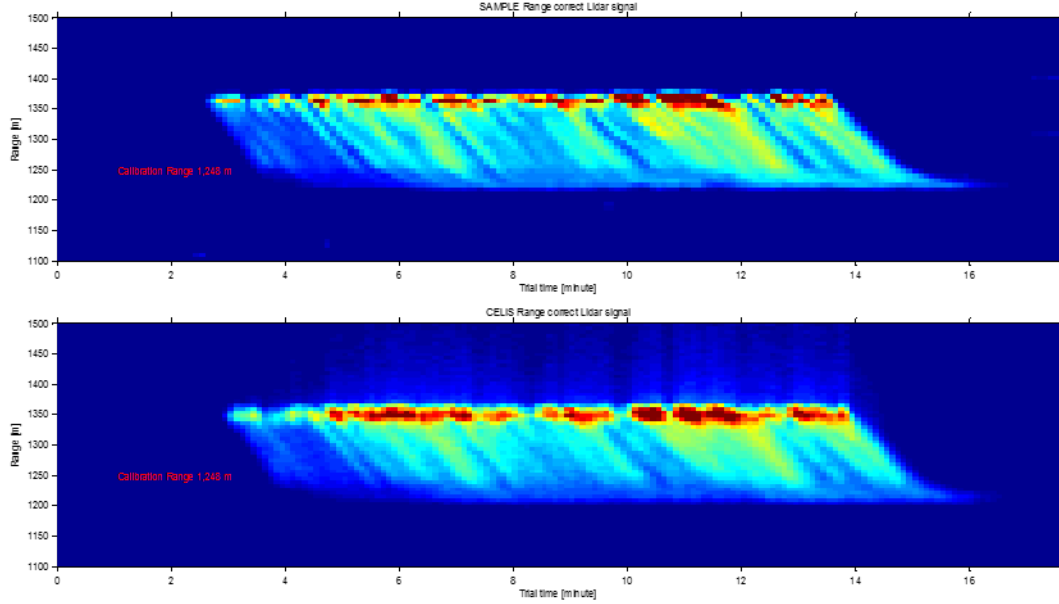


Figure 56. Range corrected data for SAMPLE (top) and CELiS (bottom) with relative amplitude on a common scale. These data are shown as waterfall plots with range on the vertical axis and time on the horizontal axis.

The next two steps relate the observed σ and β values to either observed PM or observed PSDs. The final step of this process calculates the optical scattering of these PSDs depending on the chemical composition of the aerosol. If empirical knowledge of the aerosol composition is known the fidelity of the calculation improves.

Step 2. Calculate a net trimodal PSD for each P_{CC}.

Particle size distributions (PSDs) were calculated for each lidar averaging period. Background aerosol PSDs were assumed to be trimodal, composed of Aitken (nucleation), accumulation, and coarse modes as described by Seinfeld and Pandis (2006). Plumes were assumed to be bi-modal or mono-modal. Each mode j ($1 = \text{Aitken} < 100 \text{ nm}$, $2 = \text{accumulation } 200 \text{ nm} - 800 \text{ nm}$, and $3 = \text{course} > 1 \mu\text{m}$) was assumed to be lognormal. Below is the functional form of a single mode lognormal distribution used in this analysis (Eqn 4). The overall PSD is the sum of up to three log-normal distributions.

$$\frac{dN_j}{d \ln(D_p)} = \frac{N_j}{(2\pi)^{1/2} D_p \ln(\sigma_g)} \exp\left(-\frac{(\ln(D_p) - \ln(\overline{D_{pg}}))^2}{2 \ln(\sigma_g)^2}\right) \quad (4)$$

N_j is the total aerosol number concentration in a single mode, D_p is particle diameter in μm , $\overline{D_{pg}}$ is mean mode diameter and σ_g standard deviation of the lognormal distribution.

There are two different methods to calculate PSDs, depending on what sort of *in situ* calibration instrument is used. Direct PSD measurements may be provided by an optical particle counter (OPC) or Aerodynamic Particle Sizer (APS) and this is the preferred *in situ* sensor. It is also possible to calculate a PSD using a PM_k measurement as may be provided by E-Sampler. The majority of systems measuring PSDs provide sizing coverage of approximately two particle size decades but are not individually capable of sizing over the three to four decades of particle sizes

that influence backscatter measurements. Since subsequent analysis steps require that PSDs be continuous over all particle sizes, additional assumptions are needed to extend the experimental PSDs.

If a true PSD measurement cannot be taken it is possible to estimate the PSD from a direct PM_k measurement. The k is the mean aerodynamic diameter cutpoint of the PM measurement (e.g., 1.0, 2.5, or 10.0 μm). In this case the initial values for $\overline{D_{pg}}$ and σ_g were necessarily assumed to be representative and fixed, as were the initial ratios of number concentrations (N) for each size mode (for a multimodal distribution). The PSD must be related to the PM_k measurement which is done by estimating the effective mass associated with different slices of an assumed PSD – essentially numerically integrating the mass size distribution. Briefly, this is done using the following steps:

- a) Calculate the volume concentration (V) of a single particle at all D_p values
- b) Calculate the volume distribution by multiplying the result of step a) by the assumed PSD
- c) Sum the result of step b) up to the D_p of interest to get the total volume concentration of the mass fraction
- d) Multiply the result of step c) by an assumed particle density (ρ) to get $PM_{k,PSD}$, which is the mass concentration of the assumed PSD.

The ratio of PM_k to $PM_{k,PSD}$ was then used as a scalar adjustment to all N_j values in order to estimate the PSD associated with the given value of PM_k .

Step 3. Chemical speciation of optical scattering and determination of α and β at the calibration point

The total scattering of laser light has both aerosol (a) and molecular (m) contributions. Here, we calculate molecular scattering using standard Rayleigh scattering models, pressure, temperature and humidity. We then build a look-up table of Mie coefficients for each laser wavelength for each chemical constituent and atmospheric condition. The aerosol backscatter (β_a) and extinction (α_a) are calculated using this lookup table and PSD (Step 2) at calibration point (R_c).

The equations (Eqn 5) below describe this relationship.

$$\begin{aligned}\alpha(R_c) &= \alpha_a(R_c) + \alpha_m(R_c) \\ \beta(R_c) &= \beta_a(R_c) + \beta_m(R_c)\end{aligned}\tag{5}$$

The α and β values must be calculated separately for each aerosol chemical group, each chemical group having its own PSD (step 2, above). In this analysis, five chemical groups were used; these are organic, soot, mineral, water soluble, and insoluble. Each of these five chemical groups was used to determine the respective backscatter values and thus require individual optical parameterization. The atmospheric aerosol chemical composition (P_{cc}) is determined (or estimated) for the measurement location and atmospheric conditions.

After the initial chemical group PSD has been calculated the chemical speciation for each mode j is applied and the modes are summed to yield effective full PSDs per specified chemical group. Actual chemical speciation preferably comes from *in situ* measurements, though these may also be estimated from literature values.

Step 4: Perform a linear fit of PM to backscatter at the calibration point

In order to link backscatter (CELiS raw data) to PM concentration, the relationship between β and PM needs to be explicit (Hiscox et al.). Using a time series of *in situ* point sampler data and the backscatter modeling results from step 3 it is possible to make a simple correlation plot for the two quantities. A linear relationship is derived using the following expression (Eqn 6),

$$PM_k(R) = \beta_a(R) * slope + intercept \quad (6)$$

Results are shown below. Note the linear trend across all PSDs. This linearity of the relationship is an extremely gratifying result as it reaffirms that photon backscatter is indeed linear in PM concentration for all PM size fractions. The use of “all straight lines” makes the application of the linear transform from backscatter to concentration (step 6) a straightforward exercise and also indicates that the underlying assumptions we used for calculation of the Mie and Rayleigh scattering components.

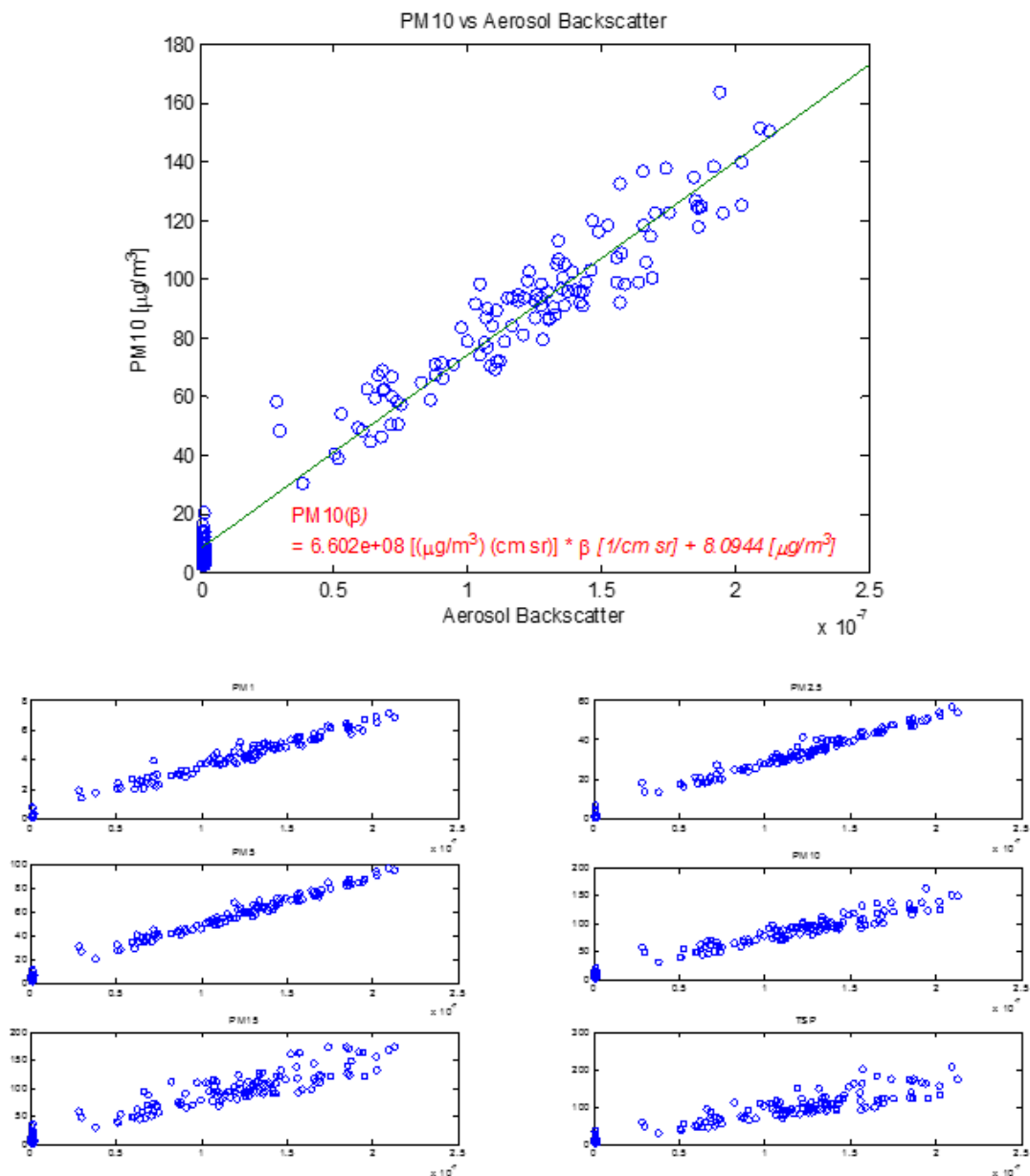


Figure 57. Top plot, linear fit of PM₁₀ vs Aerosol Backscatter. Bottom cluster of plots, PM₁, PM_{2.5}, PM₅, PM₁₀, PM₁₅ and TSP vs total aerosol backscatter. Note the linear trend across all PSDs.

Step 5: Klett inversion

It is worth noting that the location of the calibration point R_C is important to the overall quality of the lidar data. This is due to a numerical feature of the Klett-Fernald-Sasano inversion algorithm whereby it works best (converges reliably) if the location of the *in situ* point sensor (calibration point) is taken as the furthest range point (in meters) of the numerical integration range, and then one integrates “backwards” from the calibration point towards the lidar. The location of R_C is also subject to signal-to-background and signal-to-noise limitations.

Range corrected lidar signal, α_c and β_c , are used in a Klett-Fernald-Sasano inversion in both the forward and backwards direction to determine a range resolved backscatter and extinction. Forward inversion has been shown to be occasionally unstable and generate higher uncertainties so we use forward integration as a check for consistency. **Figure 58** shows total backscatter (molecular and aerosol) for SAMPLE and CELiS. The streaks are an unfortunate artifact of how the non-linear response of the CELiS detector behaves when exposed to fast changes in concentration. A subsequent redesign of the detector electronics has diminished this effect drastically.

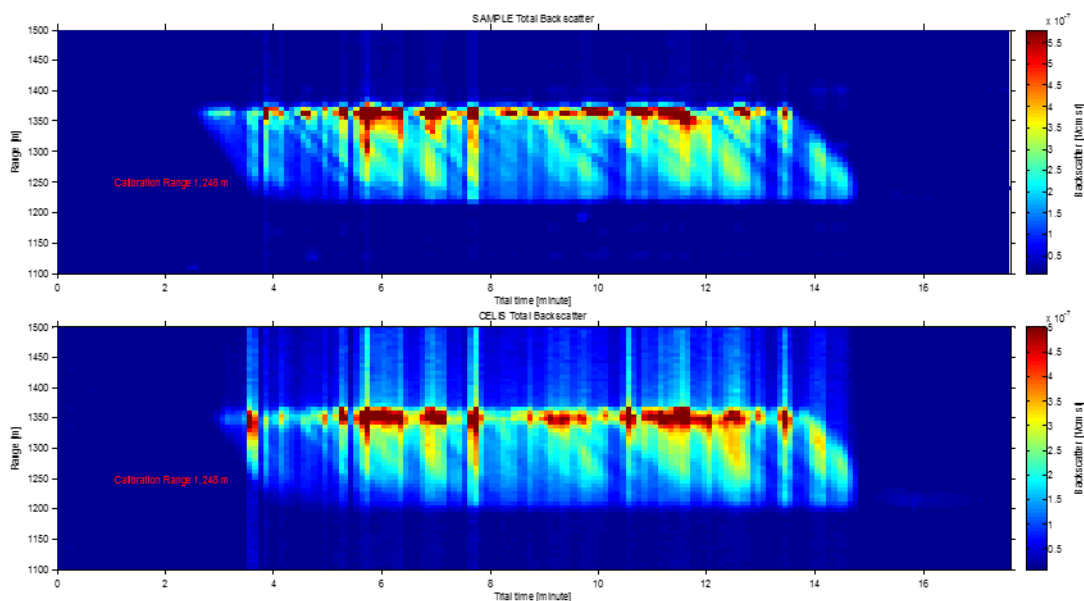


Figure 58. Total backscatter ($\beta_a(R) + \beta_m$) for SAMPLE and CELiS.

Conversion from the range-resolved backscatter (**Figure 58**) to range resolved PM_k is accomplished by applying the linear transform derived in Step 4. **Figure 59** shows PM₁₀ concentrations based on Step 4 linear fit of backscatter to PM_k.

As a reality check we compared a time series of the lidar derived PM₁₀ concentration data (a horizontal stripe) from **Figure 58** to the *in situ* APS referee instrument. The agreement is excellent, and to a certain extent it's an expected result insomuch as the **Figure 60** data is derived from the original APS data. A more useful check of the algorithm would be to compare the lidar-derived concentrations with several other APS instruments at ranges both greater and shorter than the calibration APS. This exact experiment is scheduled to occur at a cattle feedlot in collaboration with the Texas AgriLife research station near Amarillo, TX in early June 2015.

As of the writing of this report, the algorithm exists as a MatLab script and not a turnkey software product. In part this is due to its developmental nature and due to the fact that the robustness of this algorithm has not yet been fully tested. As this algorithm is subjected to additional validation data it may need some adjustment. We expect to continue to test this algorithm throughout calendar year 2015 though an ongoing collaboration with Dugway Proving Ground. After this testing season is complete an effort to implement the algorithm in C++ and to semi-automate the data acquisition will be made (subject to guidance from Dugway Proving Ground).

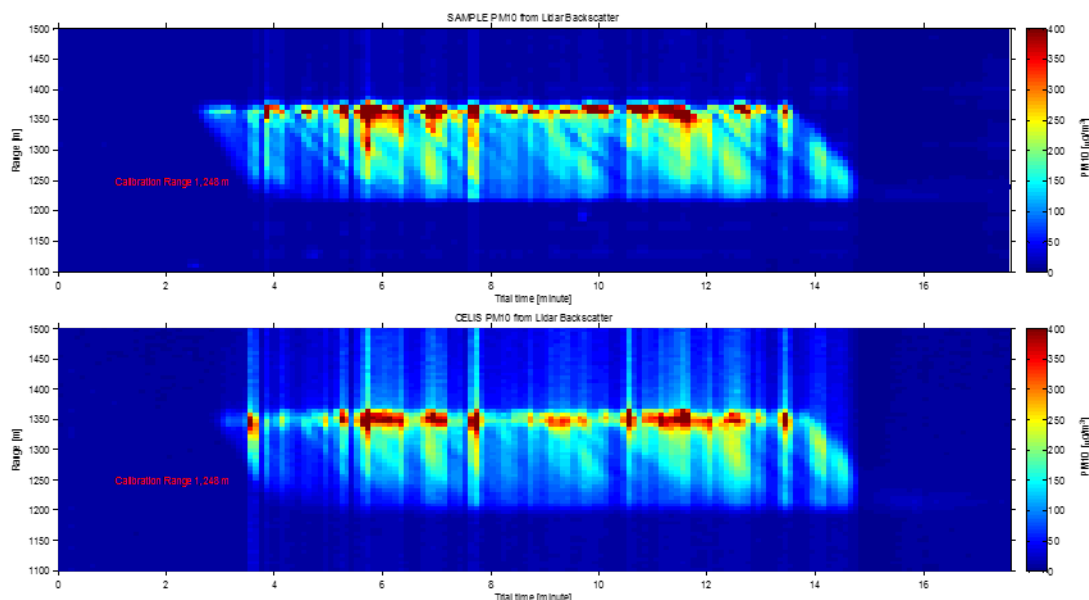


Figure 59. Range resolved PM10 for SAMPLE and CELiS.

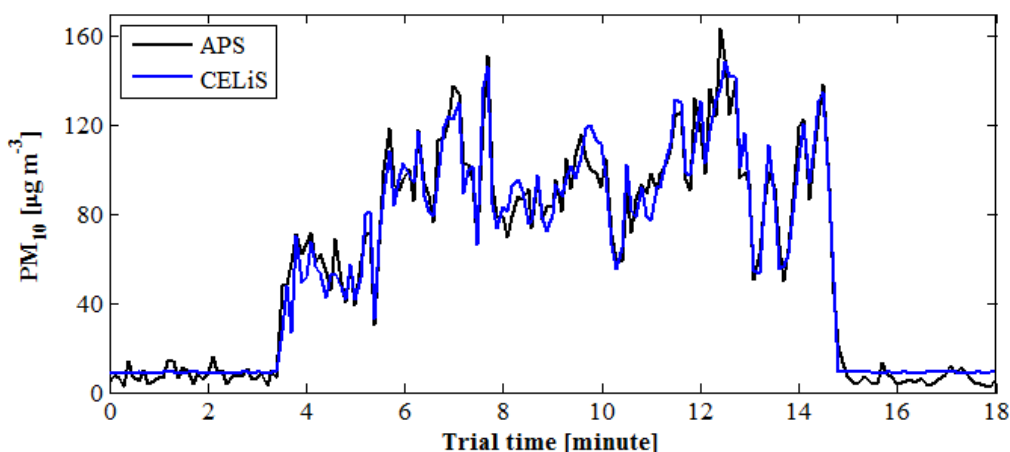


Figure 60. A comparison of the lidar-derived PM10 data (blue) and the original calibration data (black).

CELiS: Accomplishments Under SERDP Funding

We have built a rugged and turnkey 1.57 μm wavelength lidar system that can be used to measure the fence line PM concentration of dust generated from off-road vehicle activity. CELiS has been designed to be operated by relatively unskilled operators. The optomechanical and electrical design of CELiS was specific to the fenceline monitoring application and is unlike any other compact lidar on the market. It is an “eye-safe” system and therefore requires no special safety glasses for users or observers. CELiS may be operated over the temperature range of 0-80° C without any additional optical alignment tasks, this is critical for outdoor operation. The physical footprint of CELiS and its associated control electronics is 1 m³. CELiS requires 2

kW of 120 V AC power. An additional particle sampler accessory can be used to increase the accuracy of the system. An existing software package for operating CELiS, called LidarView, was adapted for use with CELiS and both collects/stores CELiS data and also controls the CELiS instrument. An operator's manual was written for CELiS with a target audience of a high school graduate.

What did it lead to?

First, CELiS is now the best tactical eyesafe lidar on the “market”. SDL has presented CELiS five different conferences in both oral presentation and poster formats. These conference presentations have stimulated interest from several lidar companies regarding possible paths to a technology licensing agreement and commercialization. A provisional patent application was submitted for the optical receiver lens assembly.

Second, a critical science accomplishment was to derive a physically motivated method to determine mass concentration of PM from lidar backscatter data. This algorithm development took a substantial amount of time; this is because the physics of the lidar process is either a 7 or a 13 dimensional problem depending on how many assumptions one makes about the meteorology, soil composition, and particle shape. To the extent these are empirically known the dimensionality of the problem is reduced.

Our PM retrieval method described herein is a novel combination of several well-established techniques for transforming lidar backscatter data. Our algorithm marries a Mie/Rayleigh modeling exercise to a calculation of particle size distributions which have specific chemical compositions to generate estimated aerosol scattering efficiency. We then scale the actual aerosol scatter magnitude (lidar data) to the estimated scattering efficiency to achieve a CELiS data output in units of mass concentration (g m^{-3}). This algorithm is not specific to CELiS and can be used for any single-wavelength lidar system. SDL is currently preparing a manuscript for a refereed journal article detailing this method. It is expected that the manuscript will be split into a pair of manuscripts that will be jointly submitted.

Conference presentations also led to a contract with Texas AgriLife of Amarillo, TX to use CELiS to measure wind-blown dust concentrations from a feedlot. This was a contract for a one week field measurement exercise in Amarillo, TX and a written deliverable report of the data. SDL used the CELiS hardware and the single-wavelength algorithm developed under SERDP. The value of the contract was \$130,000.

Another very positive result of having tested CELiS at Dugway Proving Ground against the SAMPLE lidar led to a \$1,000,000 contract to design, build and deliver two improved CELiS instruments – essentially to implement any lesson learned during the SERDP-CELiS project. The Dugway calibration testing showed that CELiS was approximately 50% as sensitive as SAMPLE, though still sensitive enough to be useful. In addition, CELiS was found to be substantially easier to operate, substantially more reliable, and has a far lower unit cost than SAMPLE. Therefore Dugway Proving Ground contracted with SDL to develop a second generation of CELiS – called CELiS NextGen – to exceed the performance of SAMPLE. In January 2016 SDL delivered to Dugway two CELiS-NextGen instruments with more powerful laser, a larger telescope, and a quieter detector. Initial testing indicates it is at least 2.5x more sensitive than SAMPLE.

CELiS Future Related Research Needs

There are three outstanding engineering tasks which would make CELiS truly a turnkey instrument

- a. Subjecting the single-wavelength retrieval algorithm to a formal software hardening treatment. Currently the real time data from CELiS is displayed in units of “backscatter” which is *proportional* to concentration (g/m^3) and the operator has to run a MatLab script to convert the backscatter data into absolute mass concentration. An additional software development cycle would formally bundle the retrieval into LidarView for true-real time mass concentration data.
- b. The electronics rack for CELiS is still a collection of commercial off the shelf (COTS) components. A top-to-bottom redesign of the power conditioning and the instrument communication protocols is needed. Specifically, implementation of a dedicated FPGA computer is highly desired. We estimate that such a design cycle would reduce the complexity of the cabling/electronics by 60% and reduce power consumption by 30%

Literature Cited

- Allmaras, R. R., Burwell, R. E., Larson, W. E. & Holt, R. F., 1966. Total Porosity and Random Roughness of the Interrow Zone as Influenced by Tillage. *USDA Conser. Res. Rep.* 7., pp. 1-22.
- Althoff, P. S. & Thien, J., 2005. Impact of M1A1 Main Battle Tank Disturbance on Soil Quality, Invertebrates and Vegetation Characteristics. *Journal of Teramechanics*, Volume 42, pp. 159-176.
- Althoff, P. S., Thien, S. J. & Todd, T. C., 2010. Primary and Residual Effects of Abreams Tank Traffic on Prairie Soil Properties. *SSSAJ*, 74(6), p. 2151.
- AM General, 2011. *specs-sheet-m1151-domestic-04-10.pdf*. [Online]
Available at: <http://www.amgeneral.com/files/specs-sheet-m1151-domestic-04-10.pdf>
[Accessed 24 Feb. 2015].
- AM General, 2015. *M1025A2 / A2 Series / HMMWV (Humvee) / AM General LLC - Mobility solutions for the 21st Century*. [Online]
Available at: <http://www.amgeneral.com/vehicles/hmmwv/a2-series/details/m1025a2>
[Accessed 24 Feb. 2015].
- Anderson, A. B., Ayers, P. D., Howard, H. & Newlin, K. D., 2007. Vehicle Impacts on Vegetation Cover at Camp Atterbury, Indiana: Part 1. Initial Impacts and Vegetation Recovery. *Proceedings of the Indiana Academy of Science*, Volume 116, pp. 126-138.
- Anon., 2000. *American National Standard for the Safe Use of Lasers*, New York: Laser Institute of America, ANSI.
- Ashbaugh, L. L. et al., 2003. Soil Sample Collection and Analysis for the Fugitive Dust Characterization Study. *Atmos. Environ.*, 30(9-10), pp. 1163-1173.
- ASTM Standard D698, 2012. Standard Test Methods for Laboratory Compaction Characteristics of Soil Using Standard Effort. *ASTM International*.
- Ayers, P. D., 1994. Environmental Damage from Tracked Vehicle Operation. *J. Terrramechanics*, Volume 31, pp. 173-183.
- Bagnold, R. A., 1941. *The Physics of Blown Sand and Desert Dunes*. London: Methuen.
- Baylot, A. E. et al., 2005. *Standard for Ground Vehicle Mobility*, Vicksburg, Miss.: US Army Corps of Engineers, Engineer Research and Development Center, Geotechnical and Structures Laboratory.
- Boyd, D. W., Skidmore, E. L. & Thompson, J. G., 1983. A Soil-Aggregate Crushing-Energy Meter. *Soil Sci. Soc. Am. J.*, 47(2), pp. 313-316.

Braunack, M. V., 1986. The residual effects of tracked vehicles on soil surface properties. *Journal of Terramechanics*, 23(1), pp. 141-151.

Chepil, W. S., 1953. Factors that influence clod structure and erodibility of soil by wind. *Soil Sci.*, Volume 75, pp. 473-483.

Chepil, W. S., Woodruff, N. P., Soddoway, F. H. & Lyles, L., 1960. Anchoring vegetative mulches. *Agric. Eng.*, 41(11), pp. 754-755,759.

CP-1191. Final Report for SERDP Project CP-1191: Characterizing and quantifying local and regional particulate matter emissions from Department of Defense installations. March 2005. Available: <https://www.serdp-estcp.org/Program-Areas/Resource-Conservation-and-Resiliency/Air-Quality/RC-1191/RC-1191>.

Department of Defense, 2013. *Base structure report: FY13 Baseline*. [Online] Available at: http://www.acq.osd.mil/ie/download/bsr/Base%20Structure%20Report%202013_Baseline%2030%20Sept%202012%20submission.pdf [Accessed 20 Nov. 2013].

Dias, J. M., Leitao, J. M. & Fonseca, E. S., 2004. Reconstruction of backscatter and extinction coefficients in lidar: a stochastic filtering approach. *IEEE TRans. Geosci. Remote Sensing*, Volume 42, pp. 443-456.

Diaz-Nigenda, E. et al., 2010. A Modeling Study of Aeolian Erosion Enhanced by Surface Wind Confluences over Mexico City. *Aeolian Research*, Volume 2, pp. 143-157.

Eames, I. & Dalziel, S. B., 2000. Dust resuspension by the flow around an impacting sphere. *Journal of Fluid Mechanics*, Volume 403, pp. 305-328.

Etyemezian, V. et al., 2014. Accounting for surface roughness on measurements conducted with PI-SWERL: Evaluation of a subjective visual approach and photogrammetric technique. *Aeolian Research*, Volume 13, pp. 35-50.

Etyemezian, V. et al., 2007. The Portable In Situ Wind Erosion Laboratory (PI-SWERL): A New Method to Measure PM10 Windblown Dust Properties and Potential for Emissions. *Atmospheric Environment*, 41(18), pp. 3789-3796.

Federation of American Scientists, 2014. *M1 Abrams Main Battle Tank*. [Online] Available at: <http://fas.org/man/dod-101/sys/land/m1.htm> [Accessed 24 Feb. 2015].

Federation of American Scientists, 2014. *M88 Hercules Recovery Vehicle*:. [Online]
Available at: <http://fas.org/man/dod-101/sys/land/m88a1e1.htm>
[Accessed 24 Feb. 2015].

Fernald, F. G., 1984. Analysis of atmospheric lidar observations: some comments. *Applied Optics*, 23(5), pp. 652-653.

Gee, G. W. & Dani, O., 2002. Particle-size Analysis. In: J. Dane & G. C. Topp, eds. *Methods of Soil Analysis: Part 4, Physical Methods*. Madison(WI): SSSA book Ser. No. 5. SSSA and ASA, pp. 255-293.

Gillette, D. A., 1977. Fine particulate emissions due to wind erosion. *Transactions of ASAE*, 20(5), pp. 890-897.

Gillette, J. A., 1981. Production of dust that may be carried great distances. *Geological Society of America Special Papers*, Volume 186, pp. 11-26.

Gillies, J. A. et al., 2005. Effect of vehicle characteristics on unpaved road dust emissions. *Atmospheric Environment*, 39(13), pp. 2341-2347.

Goran, W. D., Radke, L. L. & Severinghaus, W. D., 1983. *An overview of the ecological effects of tracked vehicles on major U.S. Army installations*, s.l.: United States Army Corps of Engineers, Construction Engineering Research Laboratory, Technical Report N-142..

Grossman, R. B. & Reinsch, T. G., 2002. Bulk Density and Linear Extensibility: Part 4. Physical Methods. In: W. A. Dick, ed. *Methods of Soil Analysis*. Madison(WI): SSSA book Ser. No. 5. SSSA and ASA, pp. 201-228.

Guoliang, L., Xuan, J. & Park, S., 2003. A New Method to Calculate Wind Profile Parameters of the Wind Tunnel Boundary Layer. *J. Wind Engineering and Industrial Aerodynamics*, Volume 91, pp. 1155-1162.

Hagen, L. J., 1996. Crop Residue Effect on Aerodynamic Processes and Wind Erosion. *Theor. Appl. Climatol.*, Volume 54, pp. 39-46.

Hagen, L. J., 1999. Assessment of Wind Erosion Parameters using Wind Tunnels. *Sustaining the Global Farm*, pp. 742-746.

Hiscox, A. L., Miller, D. R., Nappo, C. J. & Ross, J., 2006. Dispersion of fine spray from aerial applicatons in stable atmospheric conditions. *Trans. of the ASABE*, 49(5), pp. 1513-1520.

Kavouras, I. G. et al., 2009. A New Technique for Characterizing the Efficacy of Fugitive Dsut Suppressants. *Journal of the Air and Waste Management Association*, 59(5), pp. 603-612.

- Klett, J. D., 1981. Stable analytical inversion solution for processing lidar returns. *Appl. Opt.*, Volume 20, pp. 211-220.
- Klett, J. D., 1983. Extinction boundary value algorithms for lidar inversion. *Appl. Opt.*, Volume 22, pp. 514-515.
- Klett, J. D., 1985. Lidar inversion with variable backscatter/extinction ratios. *Applied Optics* , 24(11), pp. 1638-1643.
- Kohake, D. J., Hagen, L. J. & Skidmore, E. L., 2010. Wind Erodibility of Organic Soils. *Soil Science Society of America Journal*, 74(1), p. 250.
- Kovalev, V. A. & Eichinger, W. E., 2004. *ElasticLidar: Theory, Practice, and Analysis Methods*. Hoboken, NJ: Wiley-Interscience.
- Kunhs, H. et al., 2010. Effect of Soil Type and Momentum on Unpaved Road Particulate Matter Emissions from Wheeled and Tracked Vehilces. *Aerosol Science and Technology*, Volume 44, pp. 187-196.
- Lyles, L., Dickerson, J. D. & Disrud, L. A., 1970. Modified Rotary Sieve for Improved Accuracy. *Soil Sci.*, 109(3), pp. 207-210.
- Marchant, C. C., Moon, T. K. & Gunther, J. H., 2010. An Iterative Least Square Approach to Elastic-Lidar Retrievals for Well-Characterized Aerosols. *IEEE Trans. on Geoscience and Remote Sensing*, 48(5), pp. 2430-2440.
- Marchant, C. C. et al., 2009. Aglite lidar: a portable elastic lidar system for investigating aerosol and wind motions at or around agricultural production facilities. *J. Appl. Remote Sens.*, 20 February.3(033511).
- Marchant, C. C., Wojcik, M. D. & Bradford, W. J., 2012. Estimation of Aerosol Effective Radius by Multiwavelength Elastic Lidar. *IEEE Trans. on Geoscience and Remote Sensing*, 50(2), pp. 645-660.
- Marticorena, B. & Bergametti, G., 1997. Factors Controlling Threshold Friction Velocity in Semiarid and Arid Areas of the United States. *J. Geophys. Res.*, 102(D19), pp. 23277-23287.
- Mayor, S. & et. al., 2009. *BioWatch and Public Health Surveillance: Evaluating Systems for the Early Detection of Biological Threats*, Washington, D.C.: National Academy of Sciences.
- Measures, R., 1984. *Laser Remote Sensing*. New York : John Wiely & Sons.
- Meeks, J.C., L.E. Wagner, R.G. Maghirang, J. Tatarko, and N. Bloedow. 2015. Fugitive dust emissions from off-road vehicle maneuvers on military training lands. *Transactions of ASABE*, 58:49-60.

- Mirzamostafa, N., Hagen, L. J., Stone, L. L. & Skidmore, E. L., 1998. Soil aggregate and texture affects on suspension components from wind erosion. *Soil Sci. Soc. Am. J.*, Volume 62, pp. 1351-1361.
- Nimmo, J. R. & Perkins, K. S., 2002. Aggregate Stability and Size Distribution. In: J. H. Dane & G. C. Topp, eds. *Methods of Soil Analysis, Part 4*. Madison(WI): SSA Book Ser. 5. SSSA, pp. 317-327.
- Owensby, C. E., 1973. Modified Step-Point System for Botanical Composition and Basal Cover Estimates. *J. Range Management*, Volume 26, pp. 302-303.
- Priddy, J. D. & Willoughby, W. E., 2006. Clarification of vehicle cone index with reference to mean maximum pressure. *Journal of Terramechanics*, 43(2), pp. 85-96.
- R Core Team, 2015. *R: A language and environment for statistical computing.*, Vienna, Austria: R Foundation for Statistical Computing.
- RC-1729. Characterizing and quantifying emissions and transport of fugitive dust emissions due to Department of Defense activities. September 2015. Available: <https://www.serdp-estcp.org/Program-Areas/Resource-Conservation-and-Resiliency/Air-Quality/RC-1729/RC-1729>.
- Rae, W. H. J. & Pope, A., 1984. *Low-Speed Wind Tunnel Testing*. New York(New York): John Wiley & Sons.
- Rawls, W. J., 1983. Estimating soil bulk density from particle size analysis and organic matter content. *Soil Science*, 135(2), pp. 123-125.
- Retta, A., Wagner, L. E., Tatarko, J. & Todd, T. C., 2013. Evaluation of bulk density and vegetation as affected by military vehicle traffic at Ft. Riley, Kansas. *Trans. of ASABE*, 56(2), pp. 653-665.
- Rice, M. A., Willetts, B. B. & McEwan, I. K., 1996. Wind erosion of crusted soil sediments. *Earth Surface Processes and Landforms*, 21(3), pp. 279-293.
- Sasano, Yasuhiro, Browell, E. V. & Ismail, S., 1985. Error caused by using a constant extinction/backscattering ratio in the lidar solution. *Applied Optics*, 24(22), pp. 3929-3932.
- Saxton, K. E., Rawls, W. J., Romberger, J. S. & Papendick, R. I., 1986. Estimating generalized soil-water characteristics from texture. *Soil Sci. Soc. Am. J.*, 50(4), pp. 1031-1036.
- Shao, Y., Raupach, M. R. & Findlater, P. A., 1993. Effect of saltation bombardment on the entrainment of dust by wind. *Journal of Geophysical Research*, 98(D7), pp. 12719-12726.

Shaw, R. B. & Diersing, V. E., 1990. Tracked vehicle impacts on vegetation at the Pinyon Canyon Maneuver Site, Colorado. *J. Environ. Qual.*, 19(2), pp. 234-243.

SI-1399. Final Report: Particulate matter emissions factors for dust from unique military activities. June 2010. Available:

<https://www.serdp-estcp.org/content/download/8513/104423/file/SI-1399-FR.pdf>.

Skidmore, E. L. & van Donk, S. J., 2003. Soil Erosion and Conservation. In: D. B. a. R. Neider, ed. *Handbook of Processes in the Soil-Plant Systems: Modeling Concepts and Applications*. Binghamton, NY: The Haworth Press.

Sloneker, L. L. M. W. C., 1977. Measuring the Amounts of Crop Residue Remaining after Tillage. *J. Soil Water Conserv.*, Volume 32, pp. 231-236.

Stetler, L. D., 1997. An Isokinetic Sampler for Wind Tunnel Use. *ASAE Annual International Meeting*, Volume 972031.

Sweeney, M. et al., 2008. Comparison of PI-SWERL with Dust Emission Measurements from a Straight-line Field Wind Tunnel. *Journal of Geophysical Research*, 113(F01012), pp. 1-12.

Tatarko, J., 2001. Soil Aggregation and Wind Erosion - Processes and Measurements. *Annals of Arid Zone*, 40(3), pp. 251-263.

Tyree, C. & Allen, J., 2004. Diffusional Particle Loss Upstream of Isokinetic Sampling Inlets. *Aerosol Science and Technology*, 38(10), pp. 1019-1026.

U.S. EPA, 2010. [Online]

Available at: http://www.epa.gov/region07/cleanup/npl_files/ks6214020756.pdf

[Accessed 27 March 2013].

USDA-NRCS, 2014. *Soil Bulk Density/Moisture/Aeration*. [Online]

Available at: http://www.nrcs.usda.gov/Internet/FSE_DOCUMENTS/nrcs142p2_050936.pdf

[Accessed 30 September 2016].

van Donk, S. J., Wagner, L. E., Skidmore, E. L. & Tatarko, J., 2005. Comparison of the Weibull model with measured wind speed distributions for stochastic wind generation.. *Transactions of the ASABE*, 48(2), pp. 503-510.

van Pelt, R. S., Zobeck, T. M., Baddock, M. C. & Cox, J. J., 2010. Design, Construction and Calibration of a Portable Boundary Layer Wind Tunnel for Field Use. *Trans. ASABE*, 53(5), pp. 1413-1422.

Wagner, L. E., 2013. A history of wind erosion prediction models in the United States Department of Agriculture: The Wind Erosion Prediction System (WEPS). *Aeolian Research*, Volume 10, pp. 9-24.

Wagner, L. E., Ambe, N. & Ding, D., 1994. Estimating a Proctor Density Curve from Intrinsic Soil Properties. *Transactions of ASAE*, 37(4), pp. 1121-1125.

Wikipedia, 2015. *M939 Truck - Wikipedia, the free encyclopedia*:. [Online]
Available at: http://en.wikipedia.org/wiki/M939_Truck
[Accessed 24 Feb. 2015].

Zavyalov, V. V. et al., 2010. *Integration of remote lidar and in-situ measured data to estimate particulate flux and emission from tillage operations*. s.l., Proc. SPIE 7832, 78320H (2010);
<http://dx.doi.org/10.1117/12.865140>.

Zavyalov, V. V. et al., 2009. Aglite lidar: calibration and retrievals of well characterized aerosols from agricultural operations using a three-wavelength elastic lidar. *J. Appl. Remote Sens.*, 31 March.3(033522).

Zobeck, T., 1989. Fast-Vac - A Vacuum System to Rapidly Sample Loose Granular Material. *Trans. ASAE*, 32(4), pp. 1316-1318.

Appendices

Appendix A: Field Sampling/Transportation/Laboratory Protocols

Wind Tunnel Tray Field Sampling/Transportation Protocol

The top 5 cm of the soil profile was carefully removed from a 122 x 20 cm area for each sample location. In the case of the Ft. Riley samples, the soil was so compacted that a battery powered portable circular saw was used to cut the rectangular border of each sample into the soil profile (**Figure A-1**).



Figure A-1. Wind tunnel tray sample being extracted from the surface at Ft. Riley, KS.

Since the goal was to retain as much of the surface condition as possible, samples were carefully removed with a flat-bottom shovel and placed into specially made wind tunnel trays. After the Ft. Riley samples, a special made shovel (**Figure A-2**) was modified to assist in this process.



Figure A-2. Specially modified shovel for extracting wind tunnel tray samples.

Premade wooden and metal trays allowed consistent samples to be collected and also aided in ease of transportation, storage and testing. The trays were retrieved from the field and stored on closely spaced shelving (**Figure A-3**) placed in the transport trailers. For the Ft. Benning, Yakima, and White Sands samples, the trays were wrapped first in aluminum foil and then plastic wrap (Saran Wrap) to reduce disturbance of the samples during the long transport back to the laboratory.



Figure A-3. Wind tunnel tray storage rack.

Wind Tunnel Experimental Setup

In the upwind portion of the tunnel (**Figure A-4**), directly after the fan, is a screen followed by a honeycomb structure. This setup has been shown to decrease both lateral and longitudinal turbulence (Rae and Pope, 1984). Directly after the honeycomb structure are spires extending upward from the floor surface. The spires are used to generate turbulence near the floor which serves to slightly increase the initial boundary layer. Pea-sized gravel was sieved to a size range of 5 to 7 mm and applied to the entire length of the tunnel floor. The gravel was used to simulate roughness conditions more similar to soil tray conditions than the smooth plywood tunnel floor. The roughness provided boundary layer conditions within the air stream that better replicate those found in actual field conditions (Kohake, et al., 2010; Hagen, 1999).

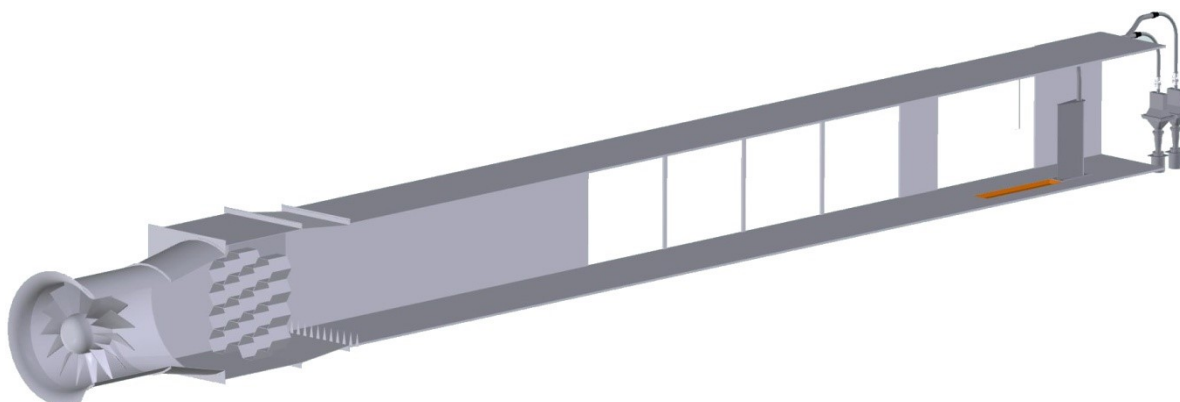


Figure A-4. Diagram of outdoor laboratory wind tunnel used in the study.

Soil trays collected at the test sites were placed evenly with the wind tunnel floor directly upwind of a vertically integrated slot-style sampler. Two high-volume sample pumps were attached to the slot-style sampler using 2.5 inch galvanized metal tubing. The pumps generated a negative pressure within the slot sampler to ensure the sampling took place under isokinetic conditions. The pressure within the sampler was adjusted until pressure equalized between the outside wind flow and directly within the slot sampler. Four pressure measurements were taken from static pressure tubes located at equal heights both inside and outside of the sampler during all tests.

Total suspended particulate matter was collected on 8 x 10 inch glass fiber filters located near the inlet of the sample pumps. Filters were weighed before and after testing for a gravimetric determination of total suspended particulate material emitted during testing. The filters used were humidity conditioned in a chamber calibrated to 40% relative humidity that was maintained with a solution of fuming sulfuric acid. Filters were conditioned for a minimum of 24 hours before taking initial weights as well as for another 24-hour minimum period before taking final mass readings. The concept for this type of sampling system was adopted from a design described in a study by Stetler (1997). **Figure A-5** shows a scaled three dimensional model of the sampling system used within the wind tunnel.

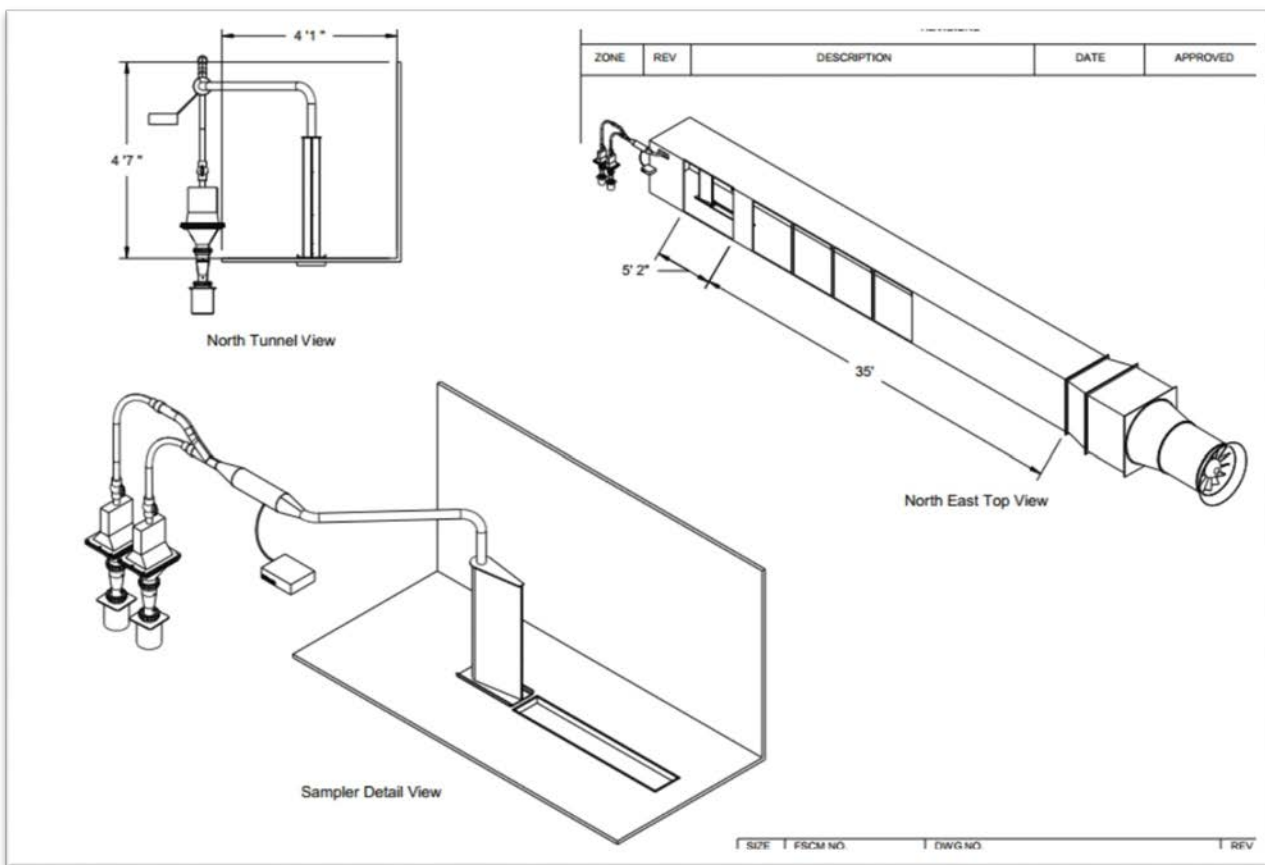


Figure A-5. Schematic of wind tunnel experimental setup.

A sub-sample of the sampler air stream was also obtained for analysis of PM emissions by a GRIMM 1.108 optical spectrometer (GRIMM Aerosol Technik GmbH & Co). The sub-sample allowed for a real-time view of the particulate emission concentrations during testing. The subsample also allowed for determining the particle size distribution of the emissions from each tray. The GRIMM 1.108 has the capability of measuring 15 distinct sampling size ranges from >0.3 micrometers to >20 micrometers in aerodynamic diameter. This instrument uses an internal positive displacement pump to draw in sample air at 1.2 L min^{-1} .

During wind tunnel testing it is important to monitor the centerline wind velocity with the wind tunnel. In order to accomplish this, a pitot-tube was used in conjunction with a variable voltage differential pressure transducer (Setra Systems, Inc., Model 264). The transducers were supplied with factory calibration curves in order to correlate the output voltage to actual pressure drop. The figure below shows a calibration curve used to develop an equation relating output voltage to observed pressure differential (**Figure A-6**).

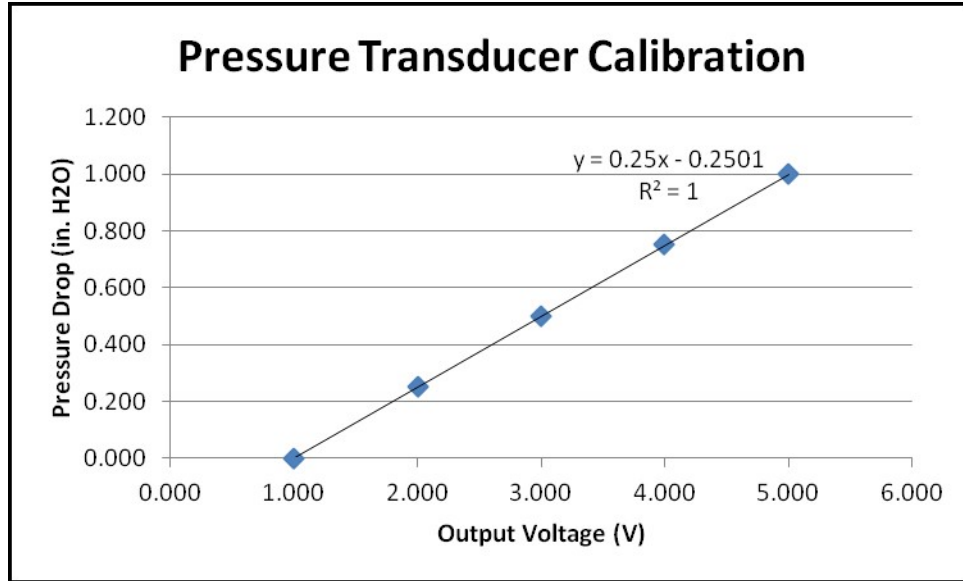


Figure A-6. Pressure transducer calibration curve.

The voltage reading from the pressure transducer was connected to a PC-based data acquisition card (Measurement Computing, DAS-6036) where analog to digital signal conversion took place. This card allowed the data from the pressure transducers to be read into a specially designed software program developed with National Instruments' LabVIEW 2011 software. Pitot-tubes were also used during an initial calibration period to develop a velocity profile within the tunnel. The model 264 used during testing had a pressure measurement range of 0 to 1 inches of water column with a corresponding voltage output of 1 to 5 VDC.

Temperature and relative humidity were collected and recorded using a capacitive-type electronic humidity sensor (Vaisala HUMICAP HMP 110). Additionally, barometric pressure was measured and recorded using a micromechanical electronic pressure sensor (Vaisala BAROCAP PTB110). These values were used for determining the air density at the time of testing. The air density value were calculated in real-time and used in conjunction with the differential pressure measured across the pitot-tubes to determine air velocity at various heights throughout the entire wind tunnel testing procedure. Equation A-1 was used for calculating air velocity is an adaptation of Bernoulli's equation, shown below.

$$V = \sqrt{\left[\frac{2(P_2 - P_1)}{\rho} \right]} \quad (\text{A-1})$$

Where:

- V = wind velocity (m/s)
- $P_2 - P_1$ = differential pressure across pitot-tube (Pa)
- ρ = air density ((kg/m³))

Because the wind tunnel is located in an outdoor environment, the temperature and humidity conditions can vary greatly throughout the testing procedure. Because of this, it was not feasible to assume a constant density of air. To overcome this limitation, humidity and temperature were measured at one second intervals throughout each test. The data acquired from the sensors were input directly into a specially developed software program which then used this data for calculating the air velocity equation in real-time. This allowed a real-time, temperature and humidity compensated wind velocity to be displayed directly on screen without a need for post-processing. Equation A-2 was used for developing the software program, which is an adaptation of the Ideal Gas Law, is shown below.

$$\rho = \left[\frac{P_d}{R_d * T} + \frac{P_v}{R_v * T} \right] = \left[\frac{(P_t - \phi * P_{sat})}{R_d * T} + \frac{\phi * P_{sat}}{R_v * T} \right] \quad (A-2)$$

Where:

- P_{sat} = saturation vapor pressure of water (Pa) = $\left\{ 6.1078 * 10^2 * 10^{\left(\frac{7.5 * T - 2048.625}{T - 35.85} \right)} \right\}$
- ρ = air density ((kg/m³))
- R_d = gas constant for dry air = 287.05 [J/(kg*K)]
- R_v = gas constant for water vapor = 461.495 [J/(kg*K)]
- T = temperature (K)
- P_v = partial pressure of water vapor in air (Pa)
- P_d = partial pressure of dry air (Pa)
- Φ = relative humidity (%)

All data were acquired by a program developed specifically for this testing procedure. The environmental sensors used during experiments interfaced with a 100-pin analog-to-digital terminal board that is connected to a PC through a PCI interface data acquisition card (PCI-DAS 6036, Measurement Computing). This board is capable of acquiring data from up to 16 separate analog input channels at approximately 10,000 Hz per channel. The converted digital data values were input into the specially designed program developed in National Instruments' LabVIEW 2011 software.

This software eliminated the need for data loggers that have traditionally been used in wind tunnel studies. The graphical interface allowed for sensor readings to be viewed in real-time to detect errors and make any required adjustments quickly. Using a data logger requires the user to run experiments without knowledge of the accuracy of incoming data values until after testing is complete. When using a data logger, the user is required to download the raw data after running experiments and perform post-processing calculations prior to being able to interpret the results. However, with this software, these limitations have been greatly overcome. The LabVIEW interface allows computations to be calculated in real-time as opposed to converting

raw values with post-processing analysis. This enabled the ability for wind dynamics, static pressure drop across the slot-sampler and many other variables to be viewed on screen in meaningful units, and in real-time, without relying on post-processing analysis. **Table A-1** shows a summary of the instruments used during wind tunnel testing.

Table A-1. Wind tunnel testing instruments used. PM is particulate matter.

Variable Tested	Instrument Used	Sampling Frequency
PM Concentration/Size Distribution*	GRIMM Model 1.108	6 Seconds
Relative Humidity	Vaisala HMP 110	1 second
Air Temperature	Vaisala HMP 110	1 second
Barometric Pressure	Vaisala PTB 110	1 second
Wind Speed	Setra Model 264	1 second
PM Emissions	Isokinetic Slot Sampler**	Continuous***

*The Grimm subsampled from the isokinetic slot sampler train

**Isokinetic slot sampler train, including filters obtained total emissions from the tray

***One sample per tray

Wind Tunnel Tray Test Preparation

All wind tunnel trays were initially laser scanned to determine their initial surface roughness (**Figure A-7**).



Figure A-7. Laser system used to scan surface roughness of wind tunnel trays.

The soils collected at the Ft. Riley site were high in clay content and were highly aggregated, and thus are not considered to be highly susceptible to wind erosion. This is in contrast to the soils collected from the other two sites which had very little aggregation and a much higher fraction of erodible material. Because of the soil texture, the Ft. Riley trays were subject to breakage of the surface as the samples were collected. A solution was devised to fill in the cracks caused by the

sampling to attempt to replicate a more uniform and natural surface that would not trap saltation particles, especially during sand abrasion testing.

To fill the Ft Riley soil cracks, a sample of each soil was oven-dried and mechanically pulverized into less than 0.42 mm size. Distilled water was then gradually added to the pulverized soil to fully saturate the mixture. A thick paste consistency was desired with no free liquid present. This paste was used to fill in large cracks in the tray samples with a caulking gun. Large cracks to be filled were defined as those at least 1cm in width. The soil paste mixture was then carefully inserted into the large cracks within the sample tray through a small orifice. This soil paste was then allowed to solidify to create a more uniform surface comparable to actual field conditions. The main objective of this procedure was to prevent trapping saltation-sized particles during sand abrasion testing.

This hardened soil paste technique was shown during tests, to be non-erodible compared to the natural surface. This testing confirmed that the soil paste mixture only served to fill in cracks to more closely represent the natural surface and to prevent trapping of saltating particles. The solution did not contribute significantly to any emissions during the tests. Additionally, the surface area taken up by the soil paste is very small in comparison with the tray, and never exceeded 5% as determined by image analysis.

All wind tunnel trays were weighed immediately before any testing. Additionally, trays were scanned with a laser scanning setup to determine surface roughness of each tray. After weighing and scanning, the trays were placed level with the wind tunnel floor directly upwind of the vertically integrated slot sampler. The wind tunnel floor had a cutout of the same dimension as the trays in which the trays were lowered. Additionally, floor mounted hydraulic jacks were located directly underneath the cutout to allow for the trays to be inserted and raised or lowered to an even level with the wind tunnel floor gravel surface.

Because surface roughness plays an important role in erodibility of soils, it was necessary to not only consider the wind velocity but also the friction velocity. This measurement gives a sense of the physical interaction between the moving air mass and the soil surface. In general, a flat smooth surface will experience more friction for a given wind speed than a rough surface. This is due to the boundary layer between the fluid and solid surfaces. To account for this, wind profiles were developed at free stream velocities of 4 and 5 m/s using pitot tube measurements at heights of 1, 2, 3, 5, 7.5 and 10 cm above the tray. The collected wind speed data were used to determine friction velocity and aerodynamic roughness using a best fit to the Prandtl equation.

Wind Tunnel Tray LEM Testing Procedure

After the threshold testing was completed for a given tray, the wind speed was increased to a higher free stream velocity of approximately 14 m/s Kohake, et al (2010) determined that this velocity was significant enough to ensure all loose erodible material is fully removed. This speed is also near the maximum wind speed of the current laboratory wind tunnel being used; therefore, it would require an alternate wind-tunnel configuration in order to achieve higher wind speeds. The goal of this testing procedure was to determine the amount of loose erodible material removed from the surface of the trays. In order to determine this, two high volume sampling pumps were connected to a specially designed slot-style sampler. The slot sampler is outfitted with 4 static pressure tubes at equal heights both inside and outside the sampler in order to monitor pressure differential during testing to ensure isokinetic operations. Pressure differential

between the wind tunnel and inside the sampler was able to be maintained at or very near 0 during all testing. **Figure A-8** shows a schematic of the sampling train configuration.

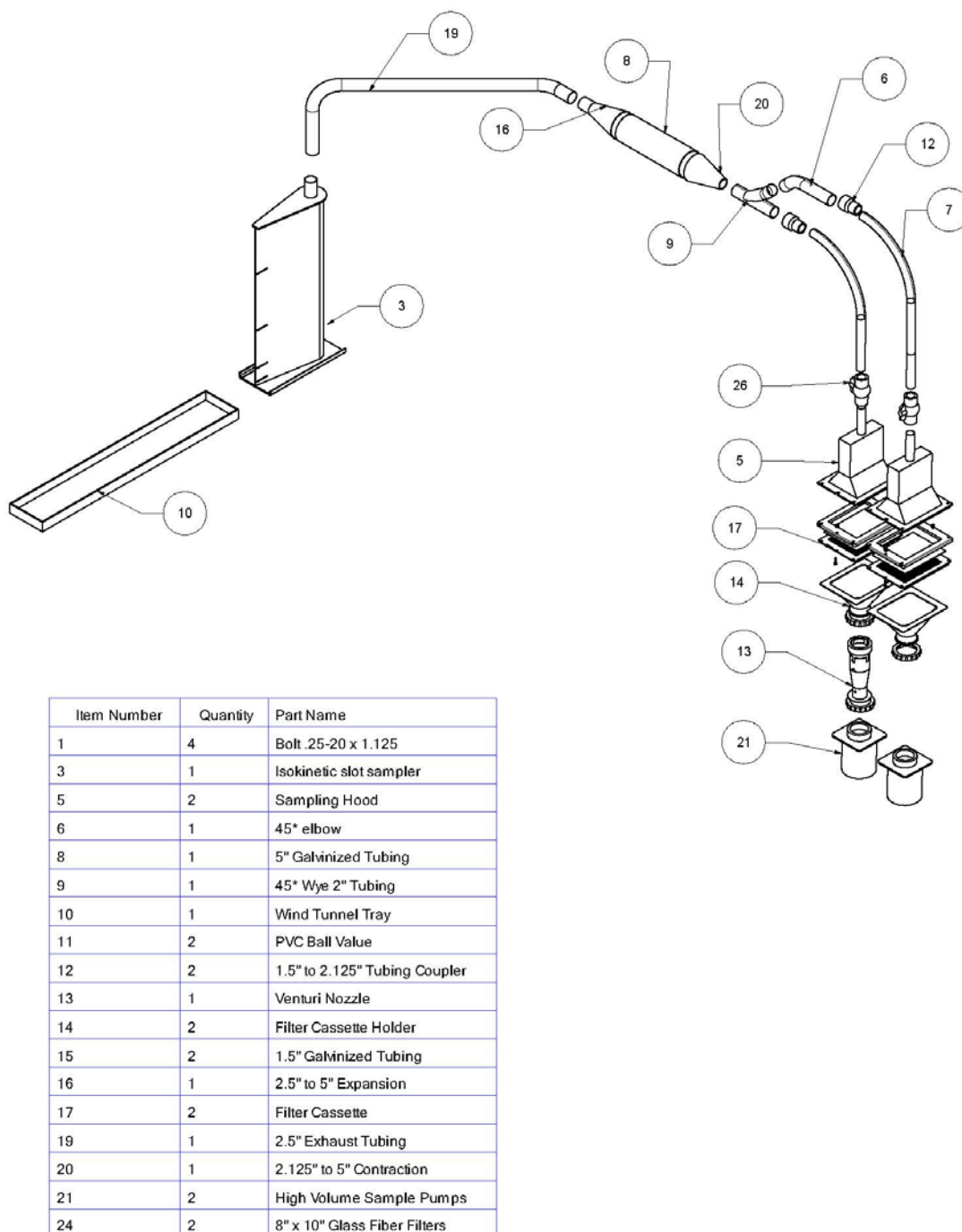


Figure A-8. Sampling train configuration for wind tunnel testing.

When sampling particulate matter in a moving fluid it is important to maintain isokinetic operating conditions. Very small particles are subject to Brownian motion effects over the entire

moving stream. The goal of an isokinetic system is to sample from the center line of a flow to minimize wall effects (Tyree & Allen, 2004). The system developed for the wind tunnel tray testing is designed to maintain nearly isokinetic conditions for sampling soil emissions in a moving air stream within a wind tunnel.

Two high volume sample pumps were used to generate a negative pressure within the sampling system in order to equalize pressure with the moving wind stream. The pressure was monitored at 4 locations along the sampler, both inside and out, to ensure isokinetic sampling conditions were achieved. The pumps were initiated for 60 seconds prior to engaging the wind-tunnel to allow a settling period for the sub-sample system as well as to obtain background suspended particulate levels. The total particulate emissions collected from each test tray were collected on 2 glass fiber filters. The mass of the filters was obtained prior to each experimental run. The filters were humidity conditioned for a minimum of 24 hours before and after testing to eliminate inaccuracies caused by water weight fluctuations on the filters. Humidity was maintained constant at 40% by a solution of fuming sulfuric acid.

A sub-sample was obtained by the GRIMM optical aerosol monitor from within the ducting of the isokinetic sampling train. This sample was obtained through a sample inlet of 4 mm diameter. This will allow a sample of the suspended particulate matter to be collected and analyzed from within the slot sampler system. The ducting connecting the high volume sample pumps is expanded to a diameter of 13 cm for a 50 cm length. This allows for the velocity in the duct to match the velocity of the GRIMM sample inlet resulting in isokinetic sampling conditions. **Figure A-9** shows an image of the inside of the ducting as well as an external view.



Figure A-9. Sub-sample expansion section inside (right) and outside view (left).

The sub-sample measurement will provide data for determination of individual size fractions of the suspended PM. This will allow for the determination of the PM₁₀ and PM_{2.5} components, which are regulated air quality health hazards. In addition, this sample will also allow the geometric mean diameter and standard deviation of the emissions to be determined.

Wind Tunnel Tray Sand Abrader Testing Procedure

In addition to determining the loose erodible material, the amount of suspension generated by aggregation destruction from abrasion is also of significant interest. Because of the relatively

short length of the trays samples in comparison to an actual field, a method to simulate saltation was used. After running tests for loose erodible material, tests were conducted using a known amount of silica sand abrader flux across the trays. This method has been well studied and is proven to be a good representation of the physics of crust and aggregate abrasion that occurs in actual field conditions (Hagen, 1999). Silica sand has been used for several primary reasons. This method will allow for correlation with previously accepted and published results. Additionally, silica sand is relatively easy to sieve to the correct size fraction and easier to control within boundary layer conditions.

5 kg of saltation sized (0.29 to 0.42 mm) silica sand was placed evenly at the upwind portion of the wind tunnel floor. Wind velocity was maintained at 11 m/s across the trays in order to keep most of the saltation sand material in the lower portion of the boundary layer. The blowing sand particles acted as an abrasion agent on the soil trays to simulate effects closely to actual field conditions.

The primary emissions results from the abrasion testing came from the GRIMM subsample. Due to heavy loading of sand onto the filter medium, it was decided not to pursue the use of glass fiber filters for this experimentation phase. Additionally, due to the accumulation of some sand particles on the tray surface, the mass difference of the trays before and after testing was of little use.

Wind Tunnel Data Analysis

With a laboratory scale wind tunnel, conditions for generating wind erosion events can be simulated and controlled. Soil tray samples collected at field sites were subjected to shearing by a 13 m/s wind velocity for 5 minutes. Fugitive particulate emissions were collected through a vertically integrated slot-sampler. The slot sampler was connected by 2.5 inch ducting to 2 high volume sampling pumps. Directly above the 2 sampling pumps, glass fiber filters were attached above each of the sampling pumps. A new filter was used for each tray sample, with the filter being weighed before and after testing. Because of the relatively low mass difference being measured, the filters were humidity conditioned before and after testing to eliminate the effects of water weight on the filters. The weight difference of these filters was used to determine the TSP resulting from each tray and was analyzed to determine differences among the treatments. Additionally, an aerosol spectrometer was used to obtain a sub sample from each tray test. Both data sets were used as dependent variables of dust emissions in statistical analysis.

Multiple linear stepwise regressions were used to determine independent variables that were most important to predicting dust emissions from off road military vehicle maneuvering. Many dependent variables were identified during testing that may be significant in determining the effects of dust emissions. Sand content of the soil and vehicle type/weight were generally the best predictors for determining dust emissions. **Table A-2** shows the parameters used in statistical testing.

Table A-2. Variables used in statistical analysis. TSP is total suspended particulates, PM10 and PM2.5 are particulate matter less than 10 and 2,5 microns respectively in aerodynamic diameter.

Dependent Variables	Method	Units	Independent Variables	Units
TSP	Gravimetric	mg m ⁻²	Vehicle Type	Wheeled or Tracked
PM10	GRIMM Spectrometer	mg m ⁻²	Vehicle Weight	lbs
	PI-SWERL	mg m ⁻²	Soil Sand Content	%
PM2.5	GRIMM Spectrometer	mg m ⁻²	Soil Silt Content	%
Total Soil Loss	Gravimetric	g m ⁻²	Soil Clay Content	%
Saltation Loss	Gravimetric	mg m ⁻²	Track Location	Curve or Straight

PI-SWERL Instrument Description

The Portable In-Situ Wind Erosion Laboratory (PI-SWERL) is a device developed and patented by researchers at the Desert Research Institute (DRI) (**Figure A-10**). It is a potential alternative to the traditional straight-line field wind tunnel traditionally used for wind erosion research. This method provides a much more portable and economical means of collecting wind erosion data without the cumbersome task of setting up a large, full-scale wind tunnel, however it does have several limitations.

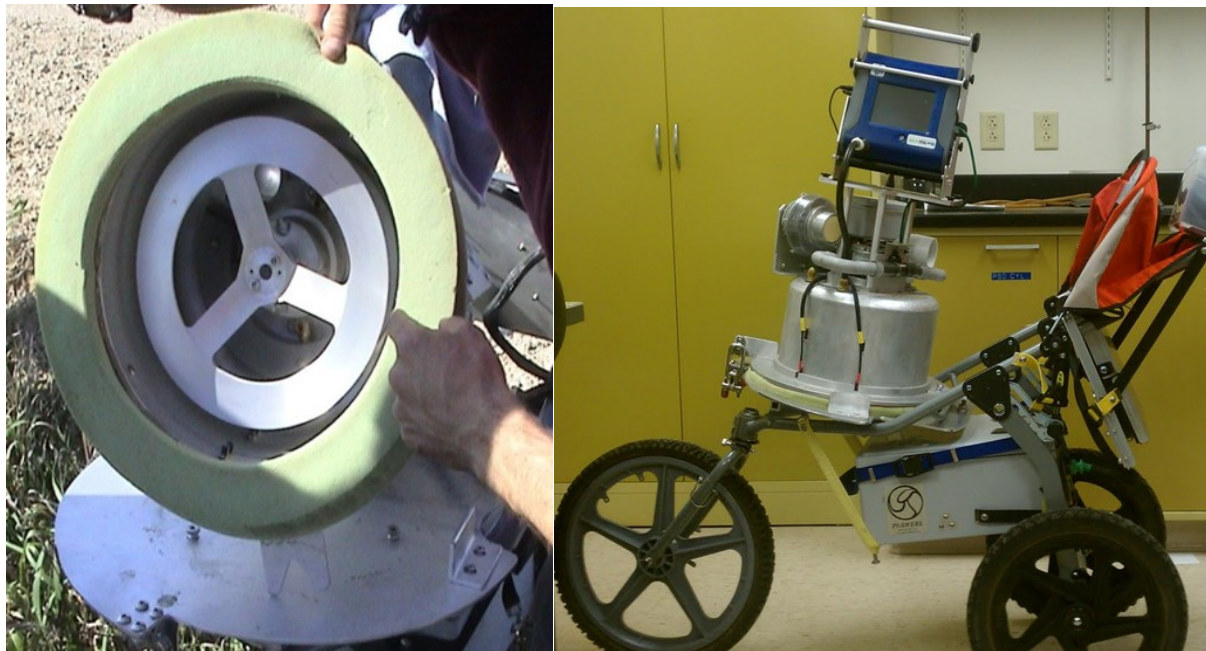


Figure A-10. Portable In-Situ Wind Erosion Laboratory (PI-SWERL).

The PI-SWERL uses a spinning annular ring to generate a shear stress over a small surface area of soil (Etyemezian et al., 2007). This type of shear stress is designed to mimic the physical action of blowing wind. The shear stress results in any erodible particulate matter being suspended within the device. **Figure A-10** shows an image of the annular ring and a full view of the PI-SWERL instrument. The suspended PM is then measured with the attached light-scattering laser photometer (DustTrak II Model 8531, TSI, Inc.) which gives real-time aerosol concentration readings.

The DustTrak II-8531 (**Figure A-11**) is an optical aerosol that uses 90-degree light scattering technology to determine particle concentration in ambient air. This instrument is used as part of the PI-SWERL to provide a portable means to measure particulate matter concentration in a field setting. Several different selective size inlets are provided to measure distinct size ranges of particles. During the field testing, the PM10 inlet was used to ensure only particles less than 10 μm were included in the sampling analysis.



Figure A-11. DustTrak II 8531 portable aerosol spectrometer (TSI, Inc.).

Although a correlation has been shown between the PI-SWERL and straight-line field wind tunnels, several major limitations have been identified with this instrument. The most prevalent error comes about with use on very rough surfaces such as a gravel-packed bed. Because the instrument uses the principle of Couette flow, which is the shearing force developed between two infinitely flat plates, the calculated friction is likely an underestimate of the actual friction developed on a rough surface (Sweeney, et al., 2008).

Another major limitation of this system is that it does not actually generate a velocity profile and boundary layer conditions as observed in nature. This will affect the way that saltation sized particles are suspended and measured. Because of this limitation, it has been identified that this system is not ideal for a detailed investigation of the principle mechanics of wind erosion. Despite the mentioned limitations, the PI-SWERL has been shown to be a sufficient instrument for measurement of non-abrader dust emissions potential over a wide range of surface conditions. **Figure A-12** shows a representative diagram of the RPM profile as well as a sample of data collected with the PI-SWERL.

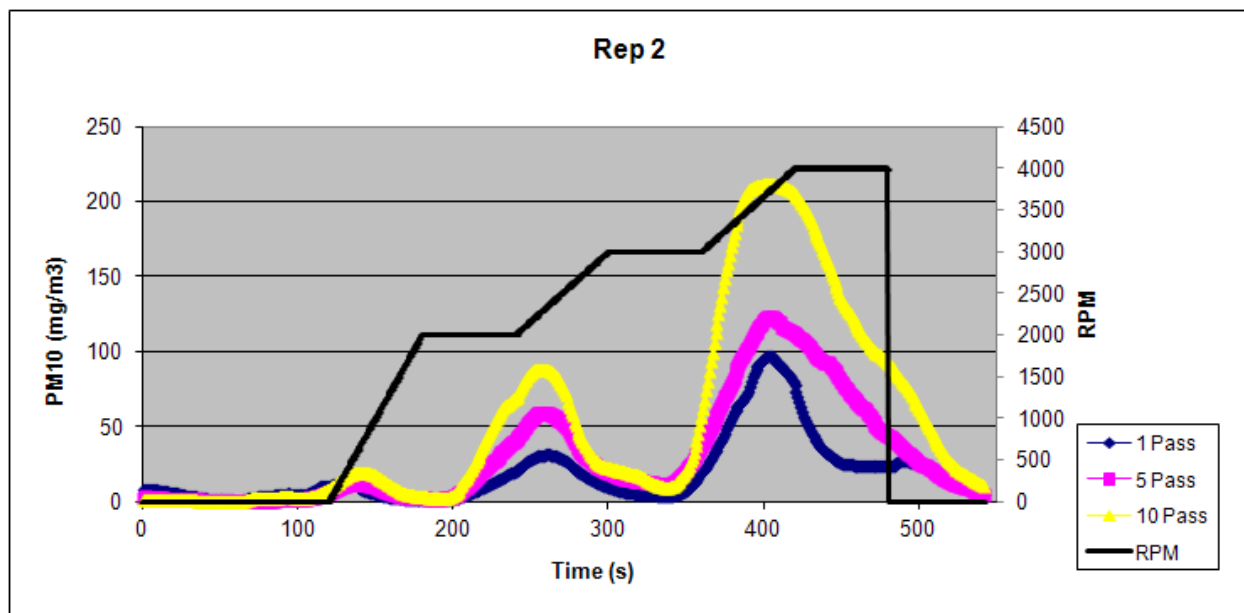


Figure A-12. Example of test data from PI-SWERL.

The PI-SWERL instrument has been evaluated as a method for measuring dust emissions potential from wind erosion events and results have been published in several refereed journal publications (Kavouras et al., 2009; Etyemezian et al., 2007; Sweeny, et al., 2008). These studies have demonstrated that this instrument provides data comparable with a portable straight-line wind tunnel on a wide range of surface conditions.

Appendix B: CELiS Design Schematics and Photos

These figures are a collection of photos and design information generated during the development of CELiS.

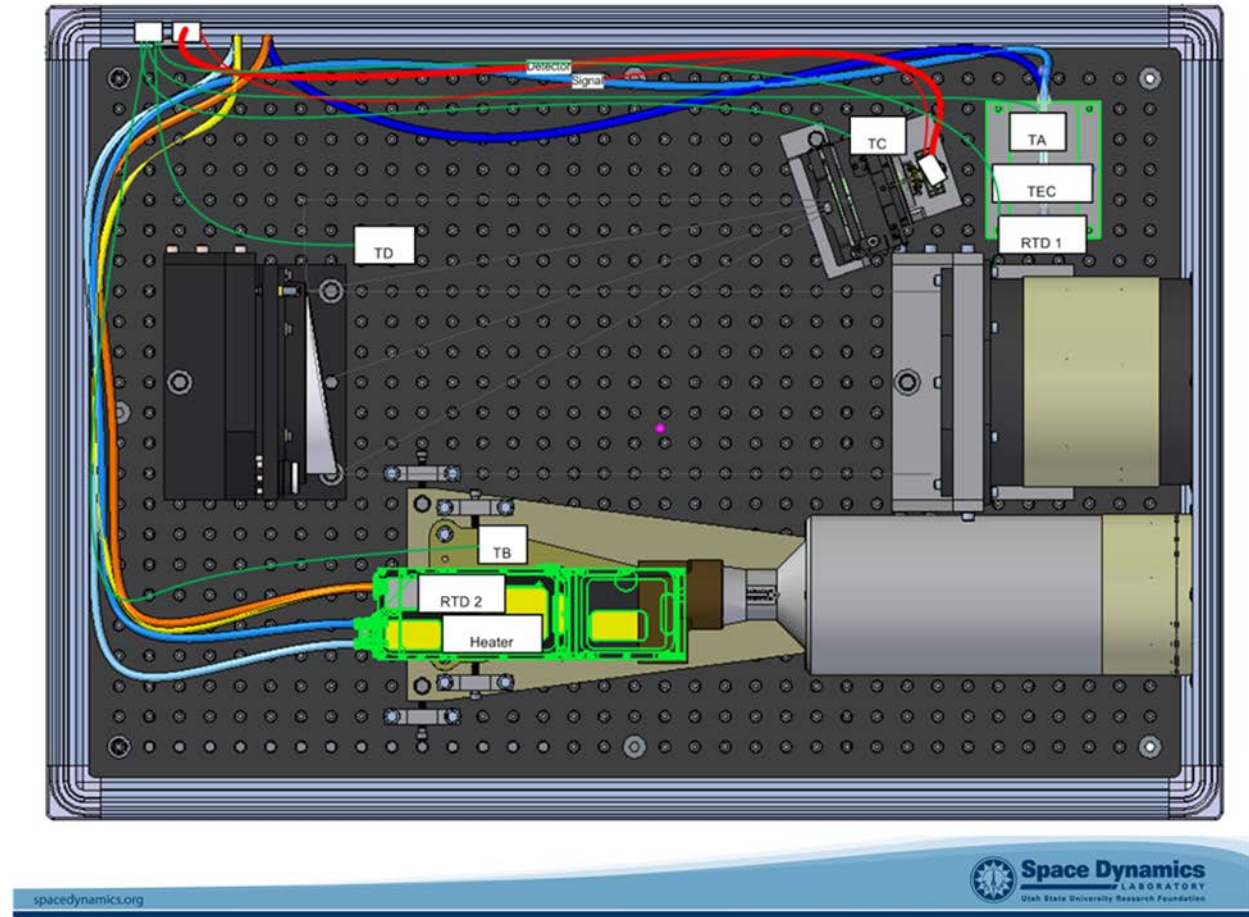


Figure B- 1. Top level solid model of CELiS. Showing the electrical cable routing, cooling line routing, hermetic enclosure and optomechanics.



Figure B- 2. Two different views of the actual CELiS assembly. The optical breadboard is carbon fiber, chosen for light weight and low coefficient of thermal expansion.



Figure B- 3. The hermetic enclosure for CELiS, prior to machining the penetrations for the cabling and the windows. The breadboard assembly drops directly inside this enclosure.



Figure B- 4. Cable fabrication materials and National Instruments data acquisition hardware.



Figure B- 5. MetOne E-Sampler to be used for calibrating CELiS. E-Sampler subjected to 30 day trial run to assess its reliability.



Figure B- 6. E-Sampler radio link tested at distances up to 1 mile and shown here communicating via the yagi antenna to SDL (white building shown in the distance).

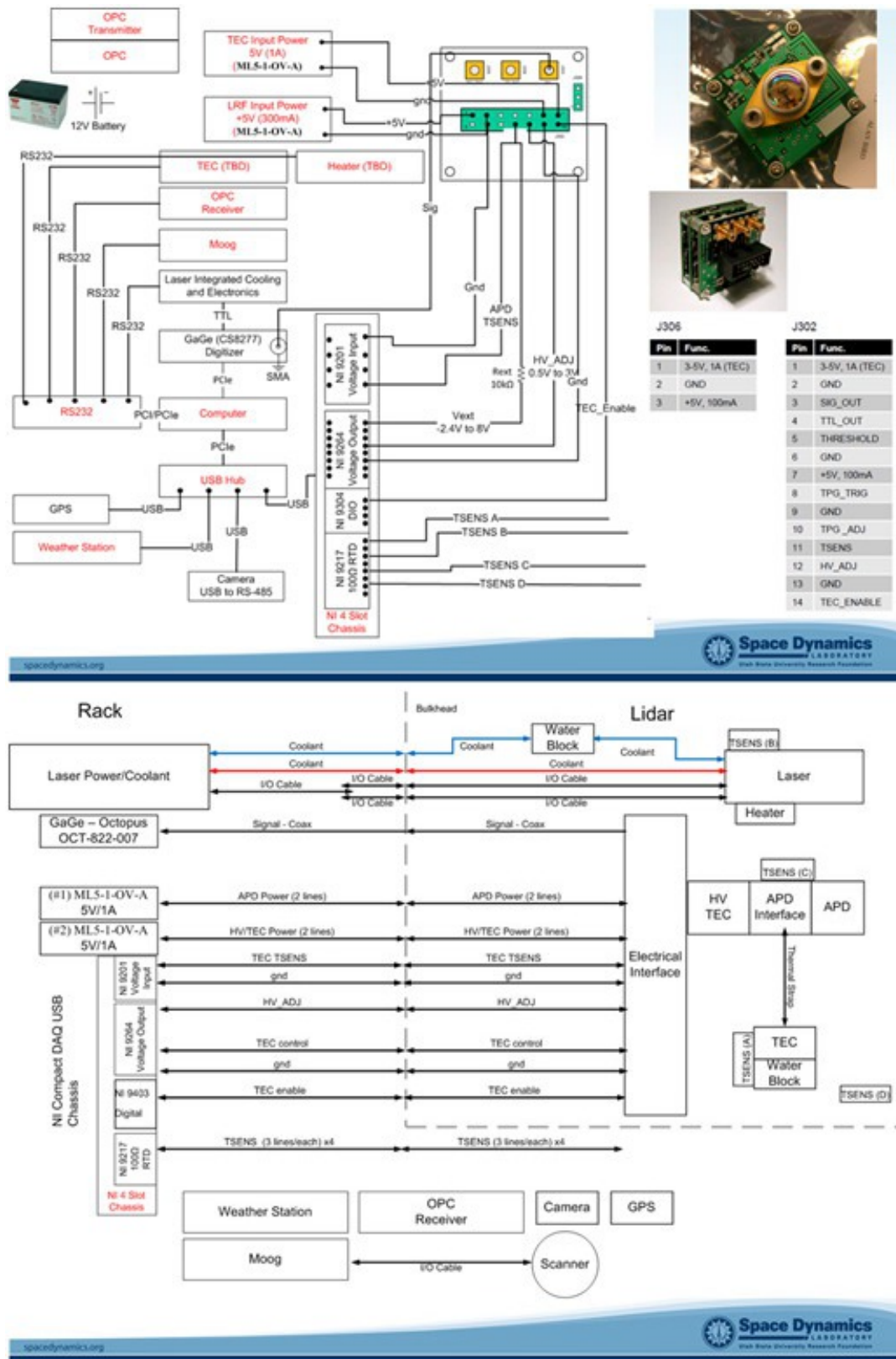
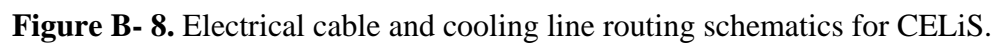


Figure B- 7. Electrical wiring schematics for CELiS.



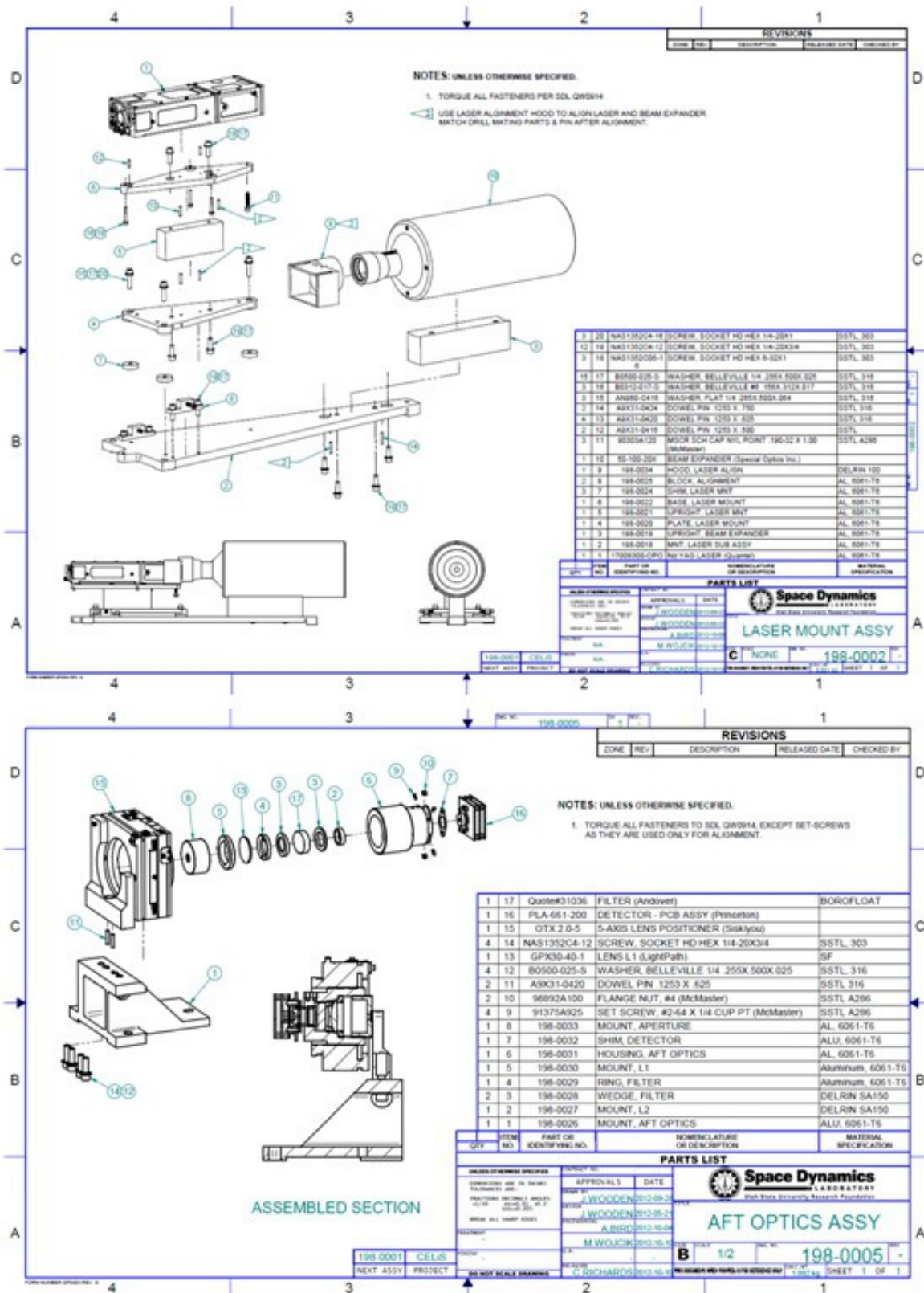


Figure B- 9. Several mechanical drawings used for assembly of CELiS.

Appendix C: Comparison of Technologies for Fence Line Monitoring

Project Title: Measurement and Modeling of Fugitive Dust from Off-Road DoD Activities

Project Number: RC-1767

Principle Investigator: Dr. Larry Wagner (USDA-ARS)

Date: 15 June 2012

Action Item:

In a **white paper** due 15 June 2012, provide a comparison of the currently available monitoring technologies and your proposed fence line monitoring technology in terms of advantages, disadvantages, projected costs to deploy, and feasibility to use in a mobile context.

PI Response:

The purpose of SERDP project RS-1767 is to demonstrate a remote sensing instrument capable of measuring ambient PM concentration over large distances with fine spatial and temporal resolution that is also field rugged and can be operated by an unskilled technician.

There are very few available commercial off the shelf (COTS) remote sensing instruments which are suitable for quantitative fence line monitoring of ambient airborne particulate matter (PM) concentrations. The small suite of available COTS instruments generate data products that are relative measures of PM concentration or are designed for weather and visibility monitoring.

There is a wide variety of COTS *in situ* point sensors which have been used with limited success to provide accurate fence line emissions monitoring for spatially inhomogeneous and temporally intermittent emission behavior over long fence lines. The primary reason that point sensors do not work well for this kind of fence line measurement is that the individual plumes must pass over the point sensor inlet, and the inherent time/space inhomogeneity is not representative of the entire emission source. To some extent the variability of the emission source can be captured by using a large array of point sensors, but large arrays of point sensors come with a distinct set of logistical and operational challenges. It is the belief of the author that a comprehensive review of point sensors is not the purpose of this white paper, therefore point sensors will not be discussed in this paper.

Below is a summary of the available remote techniques which are suitable for fence line PM concentration measurement.

US EPA Method 9- Passive Optical Detection

US EPA Method 9 is, quite literally, a trained human observer. The trained observer attends a “smoke school” where they are trained to interpret the relative opacity of different types of standard plumes. There are specific requirements for angle of viewing relative to the plume and lighting conditions. The observer reports a “percent visibility” in regard to concentration of the plume; there is no quantitative aspect about the measurement nor is the reported opacity able to be corrected for humidity, water content of the plume or wind speed.

Advantages: Low cost

Disadvantages: Subjective measurement, visible opacity is not rigorously linked to PM concentration. May only be used during daylight hours.

Projected Costs to Deploy: Costs are determined by the travel/per diem costs of the trained observer. There observer must recertify every 6 months at a cost of roughly \$200/certification period.

Feasibility for Use in a Mobile Context: Method 9 is a very portable insomuch as the method follows the human who is making the opacity assessment.

Digital Opacity Compliance System (DOCS)- Passive Optical Detection

In order to address the subjective nature of Method 9, various efforts have been made to use digital image analysis to estimate plume opacity. The most successful of these is called Digital Opacity Compliance System (DOCS) and has been successfully demonstrated at EPA sponsored Method-9 “smoke schools” as well as at a number of government and commercially operated industrial facilities.

The idea is to compare the digital information from “background” and “plume” regions of a digital photograph to calculate visible opacity. In general, DOCS performs quite well when nonzero visible opacity levels. For opacity values of 5-40 %---the region of regulatory interest---the DOCS software operated with two of the newer camera models gave readings that were slightly more precise and slightly lower on average than the readers, and statistical analysis showed each camera gave results equivalent—at a 99% confidence level--to those reported by the readers.

Example of a DOCS analysis screen, the yellow box is the analysis area.



Advantages: Low cost, provides a permanent record of the conditions, non-subjective (when compared to Method 9), it is able to be operated by an untrained user.

Disadvantages: Visible opacity is not rigorously linked to PM concentration. May only be used during daylight hours.

Projected Costs to Deploy: Low. Required hardware is a small digital camera, tripod, and a laptop to run the analysis software.

Feasibility for Use in a Mobile Context: DOCS is very portable, the required equipment can fit into a small backpack and be set up in a matter of minutes.

Transmissometer – Active Optical Detection

A transmissometer is an instrument for measuring the extinction coefficient of the atmosphere, and for the determination of visual range. It operates by sending a narrow, collimated beam of energy (usually a laser) through a fixed length of the atmosphere. A narrow field of view receiver at the designated measurement distance determines how much energy arrives at the detector, from which the atmospheric extinction coefficient can be derived.

Atmospheric extinction is wavelength dependent phenomenon, and since transmissometers are often used for visibility measurements at airports, so transmissometers typically use 550 nm lasers, 660 nm lasers or white LEDs. The optical path length for a transmissometer can range from 10-10,000 meters and are typically used with a 2-5 km range. Because of the narrow field of view for the receiver (usually a few mrad), transmissometers are somewhat vibration sensitive and require very stable mounting. This usually leads them to be permanently mounted or mounted upon heavy tripods. Because of all the supporting electronics, transmissometers require AC power at both the transmitter and the receiver, making it difficult for them to operate unattended for long periods of time in remote locations. In the image shown below, the mounting height is 2.7 m above the ground.



Advantages: Very rugged, long product heritage, fully automated software, remotely operable. Most accurate measure of atmospheric visibility.

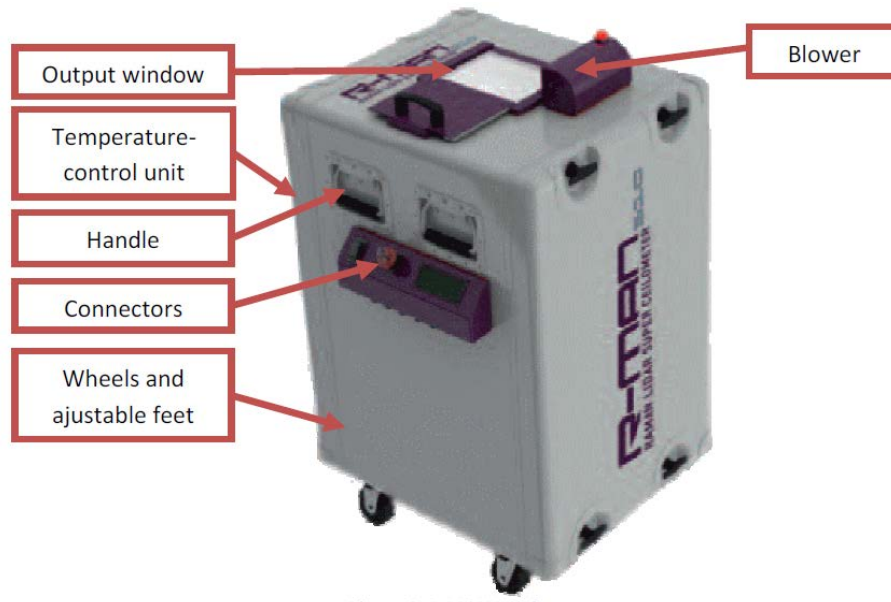
Disadvantages: Requires wall plug power, susceptible to vibration (requires permanent or semi-permanent installation). Requires periodic service to clean optical windows.

Projected Costs to Deploy: High. Unit cost is \$50,000. Installation costs are substantial due to low vibration mounting requirements.

Feasibility for Use in a Mobile Context: Not particularly mobile. Large, heavy tripods and gasoline powered generators are required (at both transmitter and receiver locations). Several days of setup are required. Must be installed by a trained user.

Leosphere R-510 – Active Optical Detection

A French company named Leosphere makes a product line of small lidar systems that are designed for sensing of boundary layer studies and meteorology research which can be used to measure optical aerosol depth, and with some assumption be used to estimate aerosol particle concentration. The full technical specifications of the LeoSphere R-510 lidar instrument are listed in the following table.



Advantages: Commercial product.

Disadvantages: Foreign (France) manufactured. Software does not generate PM concentration as a data product. Not eye safe at all distances. High unit cost, \$200,000.

Projected Costs to Deploy: High. Requires a 1 kW AC power source.

Feasibility for Use in a Mobile Context: Feasible. Its size weight and power are not prohibitive for a vehicle-based deployment. Must be operated by a trained user.

PERFORMANCES		COMMENTS
Measurement range	7.5 m – 20,000 m / 15 ft – 65,000 ft	Data acquisition First measurement point @ 7.5 m Full overlap @ 400 m
Averaging time	Minimum: 1 s Standard: 30 s to 10 min	Fully programmable
Vertical range resolution	Minimum : 4.5m / 15 ft Standard : 15m to 60m / 49 ft to 200 ft	Fully programmable
Cloud layers report	9 layers reported, up to 15,000 m / 49,200 ft 3 types (low, middle, high), Ice/water discrimination	
Aerosol layers report	2 main gradients detection in the low troposphere (planetary boundary layer) Non-spherical particles detection in the free troposphere (ash, dust)	
Relative attenuated backscatter (parallel polarization)	Molecular measurement range (day/night): 0 – 13,000 / >15,000 m* (10 min averaging time)	Range corrected data Performances estimated for SNR=1 with: - Aerosol optical depth = 0.2** - Averaging time: 30s / 10mn - Vertical resolution: 15m
Basic particle shape information (Depolarization ratio)	Molecular measurement range (day/night): 0 – 6,000m/9,000m* Aerosol/cloud measurement range (day/night): 0 – 13,000m* (10 min averaging time)	Range corrected data Performances estimated for SNR=1 with: - Aerosol optical depth = 0.2** - Averaging time: 30s / 10mn - Vertical resolution: 30m
Nitrogen Raman vertical profile @387nm	Measurement range (day/night): 0 – 1,000 / 3,000 m* (10 min averaging time)	Range corrected data Performances estimated for SNR=1 with: - Aerosol optical depth = 0.2** - Averaging time: 10min - Vertical resolution: 60m
Retrieved atmospheric parameters	Backscatter and extinction coefficients Structure layer reports (clouds, aerosol, PBL) and heights AOD (Aerosol Optical Depth) Depolarization ratio (particle asphericity information) Lidar ratio	
HARDWARE		COMMENTS
Laser source	Nd:Yag 355 nm – diode pumped	
Detection channels	- Parallel-polarized channel @ 355 nm - Cross-polarized channel @ 355 nm - Nitrogen Raman channel @ 387 nm	
Acquisition type	Analog & photon-counting on each channel	
Power supply	100-240V AC / 50-60 Hz	
Electrical consumption	300W to 600W (in maximum heating mode)	
Dimensions and weight	Dimensions (mm): H1000 x L700 x W600 Weight (kg): 60	
Tilt position	Vertical to 5° tilted	
ENVIRONMENTAL		COMMENTS
Vibration	FEDEX 6B	
EMC	IEC 61326-1	
Electrical safety	IEC 61010-1	
Eye safety	IEC/EN 60825-1 / ANSI-Z136.1-2007 compliant	
Housing classification	IP65	
Operating conditions	- Temperature range: -20°C to +45°C - Operating humidity: 10% to 100% - Air conditioning / heating modules	Transportable by 2 people
Ice/Rain protection	Automatic window blower	

*Upper or lower range can be reached according to atmospheric conditions and averaging time

**Typical for relatively polluted urban areas. Optical depth of 0.2 corresponds to a clear weather without rain

SOFTWARE/DATA		COMMENTS
Data format	ASCII / HDF	
Data transfer	Ethernet / LAN	
Software features	- Full instrument control, - Data automatic processing (parallel and cross polarizations, Nitrogen channels) - Signal calibration, noise filtering - Alarm, system status - Data storage and edition	
SERVICES		COMMENTS
Technical support	Hotline	LEOSPHERE engineers are available from 10 am to 5 pm, from Monday to Friday (GMT+1).
Warranty	1 year (parts & labour)	

LSA-2C Smoke Lidar – Active Optical Detection

A Russian company called Photonics Technology Obninsk manufactures several models of lidar units designed to detect particulate emissions. The smallest and most portable of their lidar systems is the LSA-2C which is meant for early warning of forest fires. These systems are advertised as small and easy to use. It operates at 20 Hz pulse repetition rate and emits two wavelengths, 1064 nm and 532 nm. The unit cost is ~\$150,000.

SDL owns and has tried to use a LSA-2C. It is anything but easy to use. It does not operate of 120V/60Hz AC, it only runs of 240V/50Hz so a large transformer is required. The mechanical design is sloppy making the internal optics require frequent realignment. It is made from steel (instead of aluminum) and it is therefore very heavy. The software is buggy. The operation manual is written in Russian. The software is terrible, and several of the instrument cables were incorrectly wired. This lidar is nowhere near eye-safe (the NOHZ is 12 km), it is in fact dangerous because of the high pulse energies (100 mJ/pulse) and visible wavelengths. The manufacturer is impossible to contact so there is no customer support.

We have abandoned the use of the LSA-2C, it is an enormous time and money sink. Avoid this instrument.



Advantages: None.

Disadvantages: Russian manufactured. Too many to name.

Projected Costs to Deploy: High.

Feasibility for Use in a Mobile Context: Even if you could get the LSA-2C to operate reliably, it would not be feasible due to eye safety concerns.

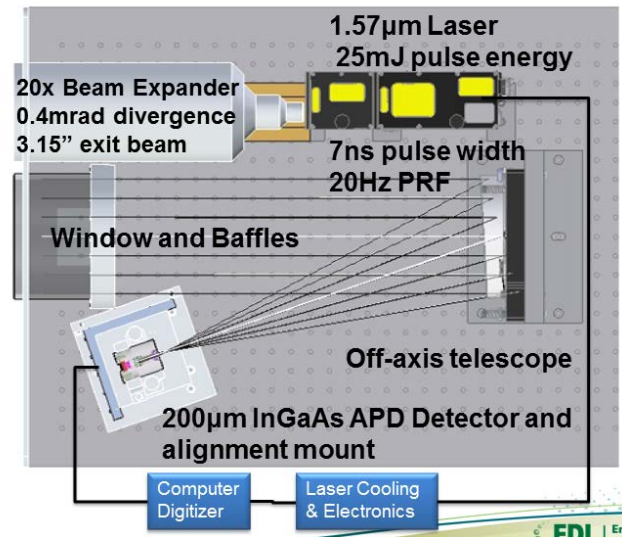
Compact Eyesafe Lidar System (CELiS) – Active Optical Detection

One of the purposes of SERDP project RS-1767 is to demonstrate a remote sensing instrument capable of measuring ambient PM concentration over large distances with fine spatial and temporal resolution that is also field rugged and can be operated by an unskilled technician.

CELiS uses a 1.57 μm wavelength laser, has a pulse energy of <25 mJ/pulse, and operates at 20 Hz pulse repetition rate. Taken together, CELiS is eye-safe (according to ANSI Z136.1-2008) at the laser aperture which means it can operate unrestricted in any environment regardless of the proximity of personnel or wildlife.

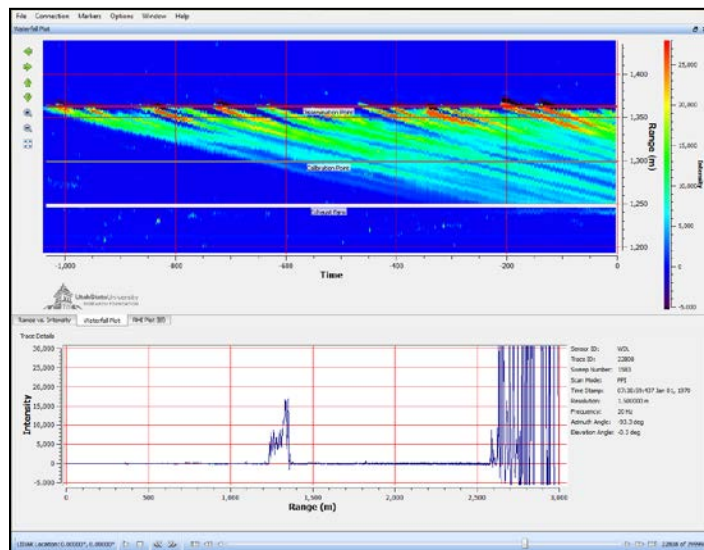
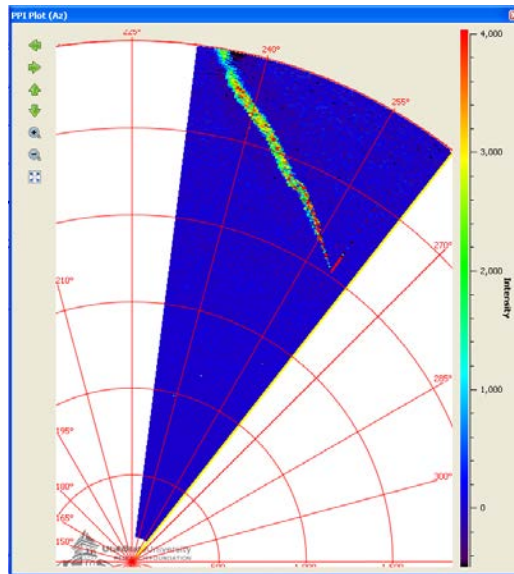
The size, weight and power (SWaP) footprint of CELiS will be 300 lbs and, 1 m^3 and 1 kW of 120VAC/60Hz power for the combined lidar system and control electronics. This is slightly larger than the advertised footprint of the Leosphere system.

CELiS has been designed to provide a PM measurement on every laser shot (20 Hz) but in practice will utilize 20-shot averaging yielding a 1 Hz data rate. CELiS has maximum range of 2.5 km in clean air environment, though system performance improves with heavier ambient PM loading. The range resolution of CELiS is 6 m. Below is the optical layout of the CELiS lidar instrument.



The key advantages of CELiS does not lie in the hardware, the main advantage CELiS has as a fence line monitor is that the laser system works in tandem with an *in situ* point sensor that acts as a transfer standard for PM concentration such that the lidar data is not directly tied to high reliability, long heritage PM point sensor (e.g., MetOne E-Sampler). In this way, CELiS not only provides experimental atmospheric extinction values it can directly convert those extinction values into PM concentration.

The conversion of lidar signal into PM concentration is done real time using a software package called LidarView. SDL has developed LidarView over several years of ongoing collaboration with the US Army Dugway Proving Ground (DPG, Dugway, UT) and the USDA-ARS Laboratory for Agriculture and the Environment (Ames, IA). LidarView has been in operational use on the DPG test grid for over three years. Below are some screenshots of LidarView displaying a plume of PM.



Below is a summary of the CELiS instrument performance.

CELiS Instrument Summary	
Transmitter	
Wavelength	1.547 μ m
Pulse Energy	25mJ
Pulse Rate	20Hz
Beam Diameter	3.3" (84mm)

Beam Divergence	0.5mrad
Receiver	
Telescope Diameter	6" (152.4mm)
Full Field of View	1.2mrad
Detector	200 μ m InGaAs APD
Digitizer	
Dynamics Range	14bit
Rate	200MS/s to 1kS/s
Input Voltage Range	± 100 mV, ± 200 mV, ± 500 mV
Performance Predictions	
Sensing Range	>2km
Range Bin (25MS/s)	6m

Advantages: Completely eye-safe, even at the laser aperture. Generates true calibrated lidar imagery of PM concentration. Manufactured in the United States from domestically available components.

Disadvantages: 1 kW of 120VAC/60Hz power required.

Projected Costs to Deploy: Projected unit cost is high, \$200,000. Operational costs will be low since a non-skilled operator may be used and power can be obtained from a small generator if line power is not available.

Feasibility for Use in a Mobile Context: Feasible after the initial operational/logistical process is established.

Comments:

The most obvious comparison to draw is between CELiS and the LeoSphere R-510. At first glance, it may seem that this SON could have been met by simply coupling an optical particle counter with an R-510. This simple solution does not adequately address the SON for several reasons, as will be described below.

The LeoSphere product line has been designed primarily as a high-altitude cloud sensor and under certain circumstances can be used for air quality purposes. By way of comparison, CELiS has been designed specifically for the SON to meet the specific science and technology goals of SERDP.

User Interface

This is by far the biggest driver and cannot be underestimated. Arguably, more than the hardware, the software is the primary deliverable for RC-1767 because it is what creates meaning from the hardware measurement. From an operational standpoint, a useful management tool the fence line emission monitor must produce meaningful data in a very short period of time and can also be used by a very unskilled operator (equivalent of two years of high school education). From a scientific standpoint, the raw lidar data (photons/range bin) needs to be directly accessible in order to meaningfully couple an *in situ* optical particle counter for calibration.

The R-510 falls short of both counts. LeoSphere does not allow for access to the raw photons, LeoSphere only reports “extinction” values and couple atmospheric extinction to concentration via a look-up table of known aerosol types. This method does not provide sufficient EPA traceability for defensible emissions reporting. Furthermore, the display software is optimized for atmospheric layer identification and seems not to be adequate for small and transient plume identification (such as will be relevant to fugitive emissions). The required averaging time for LeoSphere particle data product is reported to be somewhere either 30 and 60 seconds. Fugitive dust plumes from wheeled and tracked vehicles can easily enter and exit the field of regard of the LeoSphere in less time.

CELiS, by contrast, has been designed to collect data with sufficient signal to background in a single laser shot ($1/10^{\text{th}}$ of a second), though in most cases it will report data at 1 Hz. In addition, the CELiS software interface (described above), can directly report the physical concentration (g/m^3) of fugitive emissions in real time (updated every second).

If the raw instrument response could be extracted from the LeoSphere device it may well be possible to interface the R-510 with LidarView. However, every indication is that obtaining that level of instrument communication is a low probability event.

Unnecessary instrument complexity

The R-510 has been designed as a research instrument while the CELiS has been designed to be a ruggedized, field hardened, and operationally transparent device. The LeoSphere offers far more data products than are required to meet the specifications of the SON; it has three detection channels and offers a particulate depolarization ratio and a Raman channel. The design of CELiS has been focused on achieving a highly reliable PM measurement while stripping away any unnecessary opto-mechanical or signal processing components.

By way of example, CELiS has been designed for to be isothermal over an 80°C temperature range and requires no active cooling or even a fan. It is completely hermetically sealed and can operate in any weather conditions without the use of blowers or heaters.

Instrument pointing

The LeoSphere cannot be actively pointed outside the range of 0° (zenith) to 5° . The mission requires the ability to point anywhere within a full hemisphere. It is unknown (and unlikely) that the LeoSphere would perform to specification if its housing was not sitting upright. LeoSphere,

Inc. would not comment on this matter when asked (personal communication). This greatly limits the potential conops for which the R-510 may be employed. CELiS, however, has a motorized pan-tilt head and may be operated in either a staring (fixed pointing) or nodding (angular scanning) mode.

Wavelength

Both the R-510 and CELiS are specified as eye-safe instruments. However, the R-510 operates at 355 nm is a UV wavelength (primarily for enhanced efficiency of the Raman channel) which strongly attracts insects – especially at night. Our experience with UV lidar systems (e.g., Aglite operates at 355 nm) is that since interference from insects flying into the optics are a profound operational nuisance; and at a predictable frequency (roughly every several hundred hours of operation) cause an instrument failure.

For these reasons, we feel that the investment in the CELiS hardware development is justified as the operational performance of CELiS differentiates itself from its closest competitor, the LeoShere R-510.

Appendix D: CELiS QA/QC Procedures

Measurement and Modeling of Fugitive Dust from Off-road DoD Activities

RC-1767

Dr. Larry Wagner

April 15, 2011

Action Items: Please provide a white paper, due 15 April 2011, that:

- a. outlines how you intend to document your fence-line monitoring technology/methodology
- b. begins the process of ensuring methodology documentation and data management for the project meets appropriate Quality Assurance/Quality Control (QA/QC) standards (experimental protocols such as the development of the fence-line monitoring technology/methodology need to meet at least Quality Assurance Project Plan [QAPP] and Quality Management Plan [QMP] Category 4 requirements)
- c. can be used to initiate a dialogue with the appropriate offices within the Environmental Protection Agency (EPA) to facilitate ultimate acceptance by the EPA of project products.

The above action items were given in response to the presentation and from discussions at the February 2011 SERDP/ESTCP In-Progress Review.

PI Response: The Energy Dynamics Laboratory (EDL), the subcontracting organization for development of the fence line monitoring technology/methodology portion of this project, is committed to meeting appropriate QA/QC standards. EDL is currently using the USURF ISO 9001:2008 registered QMS and undergoing preparations to certify for registration to ISO 9001:2008 in June 2011 to assist in meeting both project QA/QC requirements and organizational QA/QC objectives, with plans to continue meeting compliance requirements into the foreseeable future. The Utah State University Research Foundation (USURF), EDL's parent company, and the Space Dynamics Laboratory (SDL), EDL's sister company, are both currently registered to the ISO 9001:2008 standard. USURF personnel experienced in its ISO 9001 registered QMS are/will be key participants in EDL's application process.

Compliance with ISO 9001 requires QA/QC policies and procedures be documented at organizational and project levels. The organizational level QA/QC protocols are given in the Utah State University Research Foundation Quality Manual, QM0201, Revision J document and QA/QC protocols for individual projects are outlined in Project Implementation Plan documents (PIPs). The EPA's QMP (organizational level) and QAPP (project level) requirements and guidelines are based on the ANSI/ASQ E4 (2004) document. The ISO 9000 series QA/QC management system is stated as one of several acceptable alternatives to the QA/QC

management and project plan systems recommended by the EPA (EPA, 2001a, 2001b). Through compliance with the ISO 9001 standards, EDL will meet the EPA QA/QC requirements for this project.

The ANSI/ASQ E4, QMP, and QAPP documents all state that a “graded approach” should be applied to the QA/QC documentation requirements, meaning “the components and tools of a quality system are applied according to the scope and nature of an organization, program, or project and the intended use of its products or services” (EPA, 2001a). Based on Table 1 in Appendix C of the EPA QA Handbook, Vol. II (2008), it is anticipated EDL’s technology/methodology development would qualify as a Category 3 effort. The appropriate level of detail and information to meet at least the Category 3 QMP and QAPP requirements will be included in the QM0201 and PIP EDL prepares for ISO 9001 (2008) compliance.

Dr. Larry Wagner, SERDP contact persons will be notified of the results of EDL’s ISO 9001 compliance application. Further information about and final copies of the relevant QM0201 and PIP upon completion can be obtained by contacting the EDL PI, Michael Wojcik.

Regarding initiating dialogue with EPA, Dr. Larry Wagner, PI will also be contacting Eben Thomas via email to discuss QA/QC documentation required with respect to possibly including our approach to determining residual risk to wind erosion subsequent to ground disturbance by military activities.

References:

- ANSI. 2004. Quality Systems for Environmental Data and Technology Programs – Requirements with Guidance for Use. ANSI/ASQ E4. American National Standard Institute.
- EPA. 2001a. EPA Requirements for Quality Management Plans, EPA QA/R-2, March 2001. EPA/240/B-01/002. Government Printing Office.
- EPA. 2001b. EPA Requirements for Quality Assurance Project Plans, EPA QA/R-5, March 2001. EPA/240/B-01/003. Government Printing Office.
- EPA. 2008. Quality Assurance Handbook for Air Pollution Measurement Systems, Vol. II: Ambient Air Quality Monitoring Program. EPA-454/B-08-003. Government Printing Office.

Appendix E: List of Scientific/Technical Publications

Conference Proceedings

- Bird, A.W., K.D Moore, M. Wojcik, and R. Lemon. 2015 Single Wavelength Lidar Retrieval Algorithm of Particulate Matter Concentration using CELiS (Compact Eyesafe Lidar System), a 1.5 μm Elastic Lidar System. Proceedings of the SPIE Defense and Security Symposium. Baltimore, MD.
- Meeks, J., L. Wagner, J. Tatarko, and R. Maghirang. 2013. Fugitive dust emissions from off-road vehicle maneuvers on military training lands. ASABE 2013 Annual International Meeting. July 21-24, 2013. Kansas City, MO Paper no: 131598778
- Moore, K., A. Bird, M. Wojcik, and R. Lemon. 2015. Compact Eyesafe Lidar System (CELiS), Rapid Detection and Quantification of Fugitive Particulate Emissions using a 1.5 μm Wavelength Lidar. Proceedings of the A&WMA ACE Meeting. Raleigh, NC.
- Retta, A., L.E. Wagner, and J. Tatarko. 2013. Military vehicle trafficking impacts vegetation and soil bulk density at Fort Benning, Georgia. ASABE 2013 Annual International Meeting. July 21-24, 2013. Kansas City, MO Paper no: 131599028
- Wojcik, M. and A. Bird. 2012. CELiS (Compact Eye safe Lidar System): A Portable 1.5 μm Elastic Lidar System for Rapid Aerosol Concentration Measurement. SPIE, Defense and Security Sensing, April 23-27, 2012. Baltimore, MD. Published in: SPIE Proceedings Vol. 8366. Advanced Environmental, Chemical, and Biological Sensing Technologies IX, Tuan Vo-Dinh; Robert A. Lieberman; Günter Gauglitz, Editors, 83660K. DOI: 10.1117/12.919260
- Wojcik, M. and A. Bird. 2012. CELiS (Compact Eye safe Lidar System): A Portable 1.5 μm Elastic Lidar System for Rapid Aerosol Concentration Measurement. Optical Society of America, Conference on Optical Instrumentation for Energy and the Environment, November 11-14, 2012. Eindhoven, Netherlands. (In press)

Posters

- Bird, A., M.D. Wojcik, K.D. Moore, R. Lemon, A. Weibe. 2014. "CELiS (Compact Eyesafe Lidar System), a portable 1.5 μm elastic lidar system for rapid aerosol concentration measurement: Part 1, instrument design and operation," poster # A21D-3061, presented at the 2014 AGU Fall Meeting, San Francisco, CA, December 2014.
- Meeks, J., L. Wagner, J. Tatarko, and R. Maghirang. 2013. Fugitive dust emissions from off-road vehicle maneuvers on military training lands. ASABE 2013 Annual International Meeting. July 21-24, 2013. Kansas City, MO
- Moore, K., A. Bird, M.D. Wojcik, R. Lemon, J. Hatfield. 2014. CELiS (Compact Eyesafe Lidar System), a portable 1.5 μm elastic lidar system for rapid aerosol concentration measurement: Part 2, retrieval of particulate matter concentration. poster #A21D-3062, presented at the 2014 AGU Fall Meeting, San Francisco, CA, December 2014.

Retta, A., L.E. Wagner, and J. Tatarko. 2013. Military vehicle trafficking impacts vegetation and soil bulk density at Fort Benning, Georgia. ASABE 2013 Annual International Meeting. July 21-24, 2013. Kansas City, MO

Patent

Marchant, A., J.C. Peterson, A. Bird, J. Simmons. Compact Robust Lidar Receiver.. App No.: 61/846,972 Docket Number: PSDL12-02.01

Journal Articles

Meeks, J.C., L.E. Wagner, R.G. Maghirang and J. Tatarko. 2015. Fugitive Dust Emissions from Off-road Vehicle Maneuvers on Military Training Lands. Trans. of ASABE 58(1): 49-60

Retta, A., L.E. Wagner, J. Tatarko and T.C. Todd. 2013. Evaluation of Bulk Density and Vegetation as affected by Military Vehicle Traffic at Fort Riley, Kansas. Trans. of ASABE 56(1):653-665.

Retta, A., L.E. Wagner and J. Tatarko. 2014. Military Vehicle Trafficking Impacts Vegetation and Soil Bulk Density at Fort Benning, Georgia. Trans. of ASABE 57(4):1043-1055

Theses

Meeks, Jeremy C. 2013. Fugitive Dust Emissions from Off-Road Vehicle Maneuvers on Military Training Lands. MS Thesis, Kansas State University, Master of Science, Department of Biological and Agricultural Engineering. <http://hdl.handle.net/2097/15607>

Moore, Kori. PhD Thesis. Utah State University. 2016 expected. "Measurement of Agriculture-Related Air Pollutant Emissions using Point and Remote Sensors"

Xu, Youjie. 2014. Dust Emissions from Undisturbed and Disturbed Soils: Effects of Off-Road Military Vehicles. MS Thesis, Kansas State University, Master of Science, Department of Biological and Agricultural Engineering. <http://hdl.handle.net/2097/18726>

Additional Peer-reviewed Manuscripts

Additional peer-reviewed manuscripts are anticipated from the multi-pass trafficking study. They include: a) complete analysis and discussion of the after-trafficking measurements obtained from all sites; b) a complete analysis and discussion of the abrader wind tunnel tray experiments; c) a comprehensive description of the soil bulk density normalization procedure results, possibly including additional published and unpublished data including the development of a compaction routine that would be useful over a wide range of soil types and applicable to most vehicles; and d) completing the analysis on additional data that were not a part of the primary objectives in this study, such as the vacuum samples collected and laser surface roughness scans.